ON

The Histochemical Labelling and Quantitative Stereological Assessment of

Synaptic Puncta Within the Dorsal Horn:

With a Focus on Synaptic Remodelling Following a Lesion to the Peripheral Nerve

By Steven J. West, B.Sc

Doctor of Philosophy

Trinity 2015

This Thesis is submitted for the award of Doctor of Philosophy (DPhil) in Clinical Neurosciences in the Nuffield Department of Clinical Neurosciences, Trinity 2015.

This Thesis was set in LaTeX by the author in the LyX document processor. Printed and bound in Oxford, UK.

Preface

Neural circuitry remains one of the key challenges to overcome in understanding the link between brain structure and cognition. A number of recent advances in methodology have made this realisation ever closer. The overall aim of this Thesis was to generate and validate a method to take a holistic view on connectivity within the dorsal horn. It is hoped such a method may prove useful for other neuroscientific endeavours in understanding the structure of the brain and its relation to cognitive processes.

To develop such an approach, I had to merge two key technologies widely used in the neuroscience community: computing and histology. Histological preparations have traditionally been manually processed and analysed. Therefore, a key aim of this new approach was to utilise the increasing computing power available to process and analyse the resulting images. A great deal of research effort has been focussed on bringing such approaches to histology, and I hope my endeavour will contribute in some way to a growing scientific field determined to achieve this goal.

Throughout my DPhil I have been stretched in many ways, and expanded my skills and knowledge in many dimensions. This includes practical skills such as dissection & histological preparation, computer programming and lab organisation; and the development of essential scientific skills such as the appreciation and development of technique, understanding the different ways of approaching a scientific question, logic and problem solving in the laboratory, experimental design & the importance of keeping a detailed record of work.

Overall, I have enjoyed my experience as a DPhil student, and I am excited to move to the next step as a post-doctoral researcher, and continue to expand and use the skills I have developed throughout my DPhil.

Acknowledgements

This work would not have been possible without the constant guidance and support from my supervisor, Prof. David Bennett. Thank you so much for advising and guiding me through this arduous process, your thoughtful input and kind words at times of alarm have been very helpful and comforting, and I look forward to further scientific exploration in your laboratory.

My DPhil was conducted under the auspices of the London Pain Consortium, a consortium of scientists and clinical academics focussed on research into chronic pain states. My first year was spent at a number of different laboratories, and I would like to thank the London Pain Consortium (LPC) for its support, especially Prof. Tony Dickenson at UCL for his support during my first year, giving me a home at his lab throughout that time and providing me with a fantastic second-rotation project, as well as his ongoing support with research. I am grateful to Prof. John Wood at UCL for providing me with an excellent first rotation project, and Dr. Line Loken for providing me with a great final rotation at the University of Oxford. A special mention for Prof. Steve McMahon for

his support and guidance throughout my time in the LPC, and to Vivien Cheah for her administrative support in the LPC. A big thank you to all the members of the LPC who have helped and encouraged me through this time, although too many to mention every individual, you all have made this journey special, and I thank you all dearly for that.

My DPhil was split between Kings College London, where Prof. Bennett's lab began, and the University of Oxford, where we were relocated during my DPhil project. Firstly, I want to thank all the members of the Wolfson Centre for Age Related Diseases, KCL, for creating such an integrative environment for research. It really was a home-from-home, and everyone really contributed to such a great atmosphere there, so a big thank you to you all. Specifically, I want to thank Mr. Carl Hobbs for encouraging and training me with histological technique, and for some thoughtful discussion on that topic; Mr. John Grist for assisting me with surgeries and providing me with very helpful advice with *in vivo* work; Margarita Calvo for her support with *in vivo* work; and finally another special mention of Prof. Steve McMahon for his support for me at that time.

Upon our arrival at Oxford, we have been blessed with a fantastic new department, the Nuffield Department of Clinical Neuroscience, and I want to thank all the groups for making us feel very welcome. A special thanks to the administrative team, with a special mention of Ms. Marion Greenleaves, all of whom have always been incredibly helpful, especially with any difficulties I encountered during my transfer to the University of Oxford. My college at Oxford provided me with accommodation upon arrival, and have been very supportive over the past 3 years, and a special thanks to Dr. Arthur Lipstein, my academic advisor at Green Templeton College, Dr. Chris Sauer, the head tutor who has provided me with helpful advice and insightful discussions, and Ms. Alison Franklin for administrative support.

Prof. David Bennett has built a fantastic lab full of bright and talented post doctoral researchers and DPhil students, and I would like to extend my sincere gratitude for their constant support in the lab, their insightful input to discussions, and their eagerness for a relaxing beer down the pub! John Dawes, Alex Clark, Jorge Gallino, Sanam Sikander, Ilaria Cervellini, Rose Fricker, Juan Ramirez, Annina Schmid, Ning Zhu, Malte Kaller, Lucy McDermott, Andy Themistocleous & Greg Weir, thank you all, every one! Kinan Muhammed & Trevor Chong, researchers who share our office, have always been a delight to be around, and thank you for your interesting discussions.

None of this work would be possible without the financial support of the Wellcome Trust, so I wish to extend my thanks to them for their constant support of British Science.

Finally, a big thank you to my Mum and Dad for their constant support and love during this tough time. Thank you for all your guidance throughout my life, and I hope I have made you proud with this work. To my Sister, Hayley Atkinson, and Harry and Bryan, I want to thank you all for your moral support, and for all the fun times we have had together. And last, but by no means least, I want to thank my partner in life, best friend, and all round most awesome person I know (!), Emma James. Thank you so much for always supporting me through the tough times, giving helpful guidance and insightful input to any geeky conversation we engage, and for your incredible ability to put up with me all this time! I truly treasure every moment we get to spend together, and am over the moon we have now managed to find and move into a place of our own. I love you dearly, and hope I have made you proud.

Steven J. West, Oxford, 2015.

Abstract

On the Histochemical Labelling and Quantitative Stereological Assessment of Synaptic Puncta Within the Dorsal Horn: With a Focus on Synaptic Remodelling Following a Lesion to the Peripheral Nerve.

Steven J. West, Green Templeton College. DPhil Clinical Neurosciences. Trinity 2015.

Peripheral nerve injury often results in neuropathic pain, which is chronic, maladaptive, and hard to treat. Accompanying the injury to the peripheral nerve are a series of changes within the central nervous system. Understanding these changes and how they relate to the neuropathic condition is vital in driving evidence-based treatment strategies. Neuronal connectivity is widely believed to underlie many cognitive processes, and altered connectivity may underlie the development and maintenance of neuropathic pain. Here, a tractable method of analysing connectivity, via the histological marking and fluorescence imaging of synaptic puncta, was developed. This method utilised automated image processing methods, and developed a stereological filter for unbiased object measurement. Using this approach, different synaptic markers were analysed in the superficial dorsal horn of rodents, a key component in the reception and processing of somatosensory information. Analysing PSD95 and SynaptoPhysin fluorescent puncta in naive adult rodents revealed distinct puncta distributions in the dorsal horn, reflecting gross circuit formation throughout this region. Peripheral nerve lesion to aspects of the sciatic nerve of rodents resulted in a selective loss at 21 days post injury of PSD95 puncta from lamina II inner of the superficial dorsal horn, with Synaptophysin puncta remaining unchanged. These experiments were complemented by a transgenic approach, where eGFP was expressed exclusively and permanently in sensory neurons, which also revealed no loss of sensory neuron afferent input to the dorsal horn after nerve lesion up to 21 days post injury. Finally, the hypothesis that microglial cells may be driving this synapse loss was explored by treating animals with minocycline following peripheral nerve lesion, which did not interfere with the PSD95 puncta loss observed at 21 days post injury.

Contents

List of Figures

Abbreviations

2D 2-dimensional

3D 3-dimensional

5HT 5-hydroxytryptamine

AMPA Alpha-amino3-hydroxy-5-methyl-4-isoxazoleproprionic acid

ATP Adenosine triphosphate

BDNF Brain-derived neurotrophic factor

CNS Central nervous system

CVLM Caudal ventrolateral medulla

DH Dorsal horn

DRG Dorsal root ganglion

EDTA Ethylenediaminetetraacetic acid

FWHM Full Width Half-Maximum

GABA Gamma-aminobutyric acid

GFAP Glial fabrilliary acidic protein

HIER Heat Induced Epitope Retrieval

Iba1 Ionized calcium binding adaptor molecule 1

KCC2 Potassium-chloride cotransporter 2

LC Locus coeruleus

LDCV Large dense-core vesicle

LTP Long-term potentiation

NA Noradrenaline

NGF Nerve growth factor

NK1 Neurokinin 1

NKCC1 Sodium-potassium-chloride cotransporter 1

NMDA N-Methyl-D-Aspartate

NS Nociceptive specific

OCT Optimal Cutting Temperature compound

PAD Primary afferent depolarisation

PAG Periaqueductal grey

PBS Phosphate buffered saline

PBSTx Phosphate Buffered Saline with 0.3

PFA Paraformaldehyde

PSD Post synaptic density

PSD95 Postsynaptic Density Protein 95

PSF Point spread function

ROI Region of interest

RVM Rostroventral medulla

SNI Spinal Nerve Injury

SNL Spinal Nerve Ligation

SRS Systematic random sampling

SV Synaptic vesicle

WDR Wide dynamic range

Chapter 1

General Introduction: The Synapse, Neuropathic Pain & Quantitative Anatomical Methods

1.1 Introduction

The study of neuroscience has a rich and inspiring history, one that has shaped our view of the world, and the nature of our existence within it (Kandel, 2013). Although only formally recognised as a subject in its own right relatively recently (Cowan et al., 2000), it has dramatically affected our philosophy of the mind (Churchland, 2008), has had profound effects on the development of information technology, the understanding & treatment of disease, and has illuminated our comprehension of the modern world (Green et al., 2001; Churchland, 2008; Shepherd, 2009; Gordon and Koslow, 2010).

A review of the impact of neuroscience on our philosophical and scientific development is far beyond the scope of this Thesis, but a key concept in neuroscience research which has strongly influenced our understanding of the brain and its relation to the mind is

that of the synapse; highlighting its important place in neural circuitry, central nervous system (CNS) information processing and the emergence of cognitive processes (Cowan et al., 2001; Mandler, 2002; Miller, 2003; Bliss et al., 2004; Takeuchi et al., 2014).

This Thesis begins with a brief overview of the anatomy, physiology and molecular biology of synapses, the key interacting element between neuronal components within the CNS, highlighting their diversity. Synaptic connectivity and signalling is important throughout the CNS, including the dorsal horn of the spinal cord; the principle region in the reception and initial processing of somatosensory information from the body. Understanding how synaptic connectivity and signalling influences this region is thus vital for understanding somatosensory processing. Therefore, a detailed review of the physiology and anatomy of the dorsal horn, focussing on its four major neuronal elements, is given.

A key disease associated with the dorsal horn and its processing of somatosensory inputs is neuropathic pain, defined as a lesion or disease to the somatosensory nervous system. An overview of neuropathic pain is presented, followed by a critical review of known mechanisms driving neuropathic pain states, with the mechanisms leading to synaptic plasticity and alterations in neuropathic pain given special emphasis.

Finally, neuroanatomical techniques have seen a plethora of interesting discoveries and advances recently. Insights into the progress in quantitative neuroanatomical approaches are highlighted, stressing the array of tools available which allow detailed quantitative analysis of the synaptome within CNS, which is concluded with the goals & aims of this Thesis.

1.2 The Synapse and its Plasticity

1.2.1 An Historical View of the Synapse & its Plasticity

The beginning of the epoch of the synapse could be considered to have begun when, in 1897, Sherrington propounded the following: "So far as our present knowledge goes, we are led to think that the tip of a twig of the arborescence is not continuous with but merely in contact with the substance of the dendrite or cell body on which it impinges. Such a special connection of one nerve cell with another might be called '*synapsis*'." (Foster and CS, 1897; Cowan and Kandel, 2001). This statement, driven by the overwhelming anatomical evidence for discreet yet contiguous networks of neurons largely adduced by Cajal, His, Forel and Waldeyer, is considered the defining point where the neuron theory of the nervous system became a widely accepted fact, and the interest and study of synapses began (Ramon y Cajal, 1989; Bennett, 2001; Cowan and Kandel, 2001).

Although a large body of research developed on synapses from this point, culminating in the 'soup versus spark' controversy, a time when a great deal of information concerning the pharmacological and physiological properties of synapses were discovered (including: the discovery of the traditional neurotransmitters, the electrical potential of neurons, quantal release at synapses, electrical transmission, and the action potential; see Eccles, 1982; Hodgkin and Huxley, 1990; Davenport, 1991; Cowan and Kandel, 2001; Valenstein, 2006, for reviews), it wasn't until the 1950s and the implementation of electron microscopy to neural tissue that direct visualisations of the structural discontinuity between pre- and post- synaptic cells was observed (De Robertis and Bennett, 1955; Palay, 1956; Pappas and Waxman, 1972). It was during this period that seminal discoveries on synapse structure were made, including the identification of synaptic vesicles (Gray and Whittaker, 1962; Palay, 1967), the synaptic cleft (Gray and Whittaker, 1962), and the realisation of two

predominant types of synapses based on the post synaptic density (Gray, 1959): the axo-somatic symmetric synapse, and the axo-dendritic asymmetric synapse.

The diversity of synapses was also being realised, with the identification of presynaptic inhibition in the spinal cord, first electrophysiologically (Eccles et al., 1961, 1962), and then anatomically (Gray, 1962, 1963), providing one example of many diverse synaptic structures (see Peters et al., 1976; Cowan and Kandel, 2001, for reviews). Concomitant with the discovery of a plethora of different synapse types was the realisation that a number of different neurotransmitter substances were also utilised by the nervous system, including acetylcholine, noradrenaline, gamma-aminobutyric acid (GABA) & glycine, glutamate, dopamine, serotonin and an expanding array of neuropeptides (historically reviewed in Cowan and Kandel, 2001).

An understanding of the complexity of synaptic transmission was also being appreciated. As far back as 1894, Santiago Ramon y Cajal, giving the prestigious Croonian Lecture at the Royal Society in London, postulated the possibility of synaptic plasticity as a means of acquiring and storing information by stating [translated from French] '... pre-existing connection between groups of cells could be reinforced by multiplication of the terminal branches of protoplasmic processes and nervous collaterals. But the pre-existing connections could also be reinforced by the formation of new collaterals and protoplasmic expansions.' (Cajal, 1894; Jones, 1994).

A landmark theory which provided a framework for understanding synaptic alterations came when Donald Hebb proposed the concept of synaptic plasticity, later referred to as Hebbian Plasticity, as a means of modifying neuronal circuits in an associative manner such that information storage exists as a complex web of tiny alterations to existing synaptic contacts, being recalled through the precise spread of parallel impulses through this primed network (Hebb, 1949).

A fundamental discovery in this regard was the observation that stimulation of the CA3-CA1 pathway in the hippocampus led to a dramatic and prolonged increase in neuronal excitability in the CA1 region, a phenomenon referred to as long-term potentiation (LTP; Bliss and Gardner-Medwin, 1973; Lomo, 2003; Bliss et al., 2004). This phenomenon, as well as its counter part long-term depression, has been explored in depth in the modern era of neuroscientific research to uncover its molecular characteristics, as well as its importance in influencing neuronal circuit input-output functions, behavioural responses, and understanding fundamental questions in neuroscience such as the basis of memory, learning, decision making and other cognitive tasks (Bliss et al., 2004; Kandel, 2012; Takeuchi et al., 2014; Tonegawa et al., 2015).

These seminal discoveries have laid the foundations for moderns neuroscience. Next, a modern purview on the synapse is given, including an overview of synapse structure and function.

1.2.2 The Structure & Molecular Biology of the Synapse

Although synapses can be generally divided into chemical and electrical, based on their transmission medium, chemical synapses are by far the most numerous and most intensely studied. Thus, this overview will deal exclusively with chemical synapses. Briefly, electrical synapses allow direct electrical-coupling between cells via gap junctions, which allows bipolar communication that integrates with chemical synaptic transmission to influence the neuronal membrane potential and firing characteristics. For a more detailed discussion of electrical synapses, see Hormuzdi et al. (2004); Pereda (2014).

The chemical synapse (from now referred to simply as the 'synapse') is a polarised intercellular junction between pre- and post- synaptic cells, which provides (mostly) unidirectional communication between the two cells (see Figure 1.1). This signal is propa-

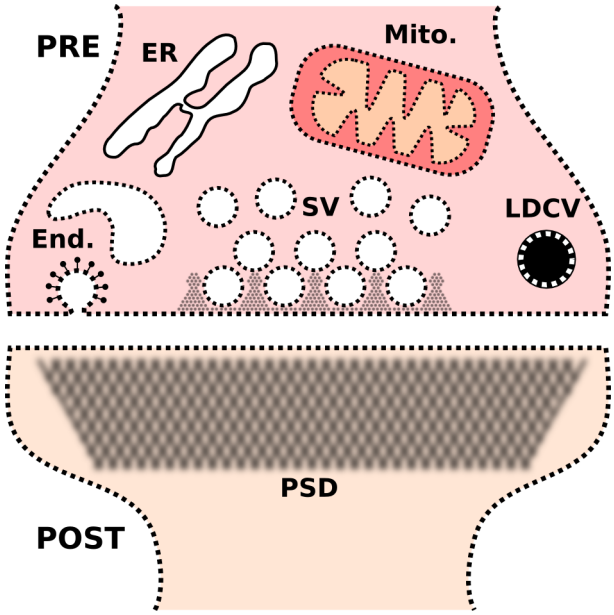

Figure 1.1: **An overview of synapse structure.** Both the presynaptic (PRE) and postsynaptic (POST) specialisations have unique ultrastructure. The presynaptic compartment contains numerous synaptic vesicles (SV), some which are docked and ready for release. Large electron-dense vesicles (LDCV) can also be observed. Occasionally, clathrin coated pits and endosomes (End.) can be observed. Mitochondria (Mito.) and endoplasmic reticuli are often found presynaptically. The postsynaptic compartment of the synapse is distinguished ultrastructurally by the presence of a postsynaptic density (PSD), which is well developed in excitatory synapses, but less developed in inhibitory synapses.

gated from an electrical, to a chemical, and back to an electrical medium, which integrates within the postsynaptic cell to influence its firing characteristics & activation state.

Despite the increasingly realised diversity amongst sub-populations of synapses, they all share some common structural and functional characteristics, indicating the general functions implemented by all synapses. Each component of the synapse has a rich array of proteins which bestow it with its relevant functions, and subserve the overarching aim of transmitting information within neural networks. Here a review of synapse structure and its molecular machinery is given with respect to synaptic transmission, including an overview of the presynaptic terminal, synaptic cleft, and postsynaptic density.

1.2.2.1 The Presynaptic Terminal

The presynaptic terminal consists of a number of components vital for the reception and conversion of action potentials into chemical intermediate signals for propagation across the synapse (Sudhof, 2004; Südhof, 2012, 2014; Kononenko and Haucke, 2015). The most conspicuous of these components are the numerous synaptic vesicles present in close apposition to the presynaptic membrane. Generally two vesicle types have been described based on their appearance in electron micrographs: small electron-lucent vesicles between 35-50nm (although some small vesicles do contain an electron-dense core, it is believed these are the aminergic subtype of small vesicle, see Winkler (1997); Stjärne (1999)), and large electron-dense vesicles between 70-200nm in diameter (often referred to as large dense-core vesicles [LDCVs]) which contain neuropeptides substances, are abundant in specialised neurons, and are released with strong pre-synaptic activation (Thureson-Klein and Klein, 1990; Schoch and Gundelfinger, 2006).

Small electron-lucent vesicles (synaptic vesicles, SVs) have been thoroughly characterised, due to the ease of isolating them with subcellular fractionation techniques. All SVs contain neurotransmitter and an array of membrane-bound proteins, which can generally be divided into two groups: a set which are important for neurotransmitter filling (including the proton pump), and a set which are important for trafficking of SVs (including the synapsins, synaptophysins, synaptotagmins, synaptobrevins amongst others). The vesicles are known to cluster into three distinct pools in the pre-synaptic terminal: docked vesicles primed for release at the pre-synaptic membrane, the ready-releasable pool connected to the pre-synaptic grid (an electron-dense framework connected to the pre-synaptic membrane), and finally a reserve pool of SVs present posterior to the pre-synaptic grid (Rizzoli and Betz, 2005; Südhof, 2012; Rizzoli, 2014).

As well as SVs, often mitochondria, smooth endoplasmic reticuli and endocytotic ap-

paratus can be found in the presynaptic terminal. Endocytotic apparatus consist of clathrin-coated pits on the presynaptic membrane, and various membrane compartments such as vacuoles and cisternae, which are typically located external to synaptic vesicle clusters (Heuser and Reese, 1973; Miller and Heuser, 1984; Takei et al., 1996; De Camilli et al., 2001).

Smooth endoplasmic reticuli are occasionally present in electron microscopy sections of presynaptic terminals, are important for calcium regulation (Pozzan et al., 1994), and whilst not important for SV exocytosis at synapses (Smith and Augustine, 1988), they may play other important roles such as the exocytosis of LDCVs (Nicholls, 1998). Mitochondria are often present in the presynaptic compartment, indicating the high ATP requirement for neurotransmission and its associated mechanisms. Their size and distributions are affected by synapse usage - where tonically active synapses contain more numerous and larger mitochondria than phasically active synapses (Brodin et al., 1999).

The cytoskeleton around the presynaptic terminal is unique from the rest of the axon, as it is composed of actin filaments as opposed to microtubules and intermediate filaments (Hirokawa et al., 1989; De Camilli et al., 2001). This actin-based cytoskeleton likely plays an important role in vesicle clustering and dynamics, and vesicle-associated proteins such as synapsin appear to bind SVs to polymerised actin in the reserve pool (Hirokawa et al., 1989; Shupliakov et al., 2011).

The presynaptic membrane is defined as the membrane area in close apposition with the post-synaptic membrane, and by the presence of docked vesicles lying between portions of the presynaptic grid. It is often oval in shape, although in larger synapses the continuity of the docked vesicles and presynaptic grid can be interrupted, in so called "perforated synapses". The perforations can create ring-shaped presynaptic membranes with one perforation, or more complex patterns with several perforations present (Andres, 1975;

De Camilli et al., 2001). These may reflect either clathrin-coated pits, important in the recovery via endocytosis of plasma membrane for vesicle formation (De Camilli et al., 2001), or the presence of synaptic spinules, which are projections from the post-synaptic membrane which invaginate into presynaptic terminals (Spacek and Harris, 2004; Petralia et al., 2015).

1.2.2.2 The Vesicle Cycle

The frequency of SV exocytosis for neurotransmission requires a local mechanism to replenish SVs, which is accomplished in presynaptic terminals via the synaptic vesicle cycle. This cycle comprises the exocytosis of SVs, balanced with the endocytosis of presynaptic plasma membrane, and the subsequent re-formation of newly-formed pleiotropic membranous structures into synaptic vesicles ready for neurotransmission (Rizzoli, 2014).

SV exocytosis is well described, and is driven by the SNARE complex of proteins. In essence, SVs contain the SNARE proteins synaptobrevin/vamp, which bind to the SNARE complex located within the presynaptic membrane, consisting of SNAP-25 and syntaxin-1. With the influx of extracellular calcium, synaptotagmin and complexin act to initiate this binding, and this induces exocytosis of neurotransmitter via SM proteins, leading to the release of neurotransmitter (Südhof and Rothman, 2009).

Concomitant with this process, endocytotic processes are required to prevent presynaptic membrane inflation and to recover plasma membrane for the re-formation of synaptic vesicles. The first step is the formation of clathrin-coated pits for the retrieval of plasma membrane. This is followed by the endocytosis of membrane, and uncoating of the vacuole. The re-formation of SVs is poorly understood, but is believed to occur via mechanisms similar to the Golgi apparatus vesicle formation. Finally, SVs are filled with neurotransmitter, which is preceded by the filling of the SV with hydrogen ions via the proton

pump, to drive the influx of neurotransmitter. The currently known molecular details of this process are expertly reviewed by Rizzoli (2014).

The reformed vesicles are then required to re-dock. Proteins important in the docking of vesicles include bassoon, piccolo and the RIM molecules - key components of the presynaptic grid (Dani et al., 2010; Hallermann et al., 2010; Rizzoli, 2014). Once re-docked, the vesicles are available for exocytosis, and thus the cycle is complete.

1.2.2.3 The Synaptic Cleft

The synaptic cleft is 20-30nm wide, displays a thickened membrane, and consists of a number of scaffold proteins, linked across the pre- and post- synaptic elements, which keep the elements aligned, and are intimately involved in the development and breakdown in synaptic connections. These include the well-described neurexin and neuroligin families, but may include other cell adhesion molecules (Sudhof, 2001; Craig and Kang, 2007; Bemben et al., 2015).

1.2.2.4 The Post-Synaptic Density

The post-synaptic component is specialised for the reception of neurotransmitters, and the conversion of this chemical signal ultimately into an electrical signal. The post-synaptic density achieves this by containing specific receptors for the neurotransmitter released; signal cascade molecules for the conversion of neurotransmitter signal to intracellular messages; adhesion molecules extending across the synaptic cleft; and cytoskeletal elements to arrange these components for appropriate signal transduction (Sheng, 2001).

The appearance of the post-synaptic density (PSD) in electron micrographs is used to distinguish two broad categories of synapse: the excitatory (glutamatergic) asymmetric synapse, and the inhibitory (GABAergic & glycinergic) symmetric synapse (Gray, 1959). The asymmetric PSDs display an intense electron-dense region below the post-synaptic

membrane, are present on distal dendritic branches, and are often located on small protrusions from the post-synaptic cell dendrites referred to as dendritic spines. Whereas, symmetric PSDs display a weaker electron-dense region below the post-synaptic membrane, and are located on proximal dendrites and the cell soma, including the axon hillock, suggesting their importance lies in generally controlling cell excitability (Sheng and Kim, 2011).

The excitatory asymmetric PSD consists of a large array of proteins, many of which have been characterised by mass spectrometry. Abundant proteins such as PSD95, SynGAP, CaM Kinases and Shank have well characterised interactions within the PSD, yet recent work puts the number of molecules associated with the asymmetric PSD at approximately 1,500 different proteins (Bayés et al., 2011, 2012). Relative abundance of different PSD proteins has been measured, which has revealed that many of the well characterised proteins are highly abundant, including PSD95, CaM Kinase proteins, and SynGAP. Many of these proteins are susceptible to post-translational modifications, such as phosphorylation, which can underpin plastic changes to the synaptic response (Kim and Sheng, 2004).

PSD95 plays a central role in asymmetric PSDs via multiple protein-protein interactions. PSD95 is known to anchor glutamatergic receptors such as the alpha-amino3-hydroxy-5-methyl-4-isoxazoleproprionic acid (AMPA) and n-methyl-d-aspartate (NMDA) receptors to the post-synaptic membrane, as well as connect with signalling molecules such as CaM Kinases and shaker-type potassium channels, bind to cell adhesion molecules including neuroligins, and interact with deeper scaffold proteins such as GKAP, which in turn connects with other scaffold proteins such as Homer and Shank. Many of these proteins also associate with other signalling molecules, ion channels, receptors and enzymes to comprise the whole PSD, and current research is still focussed on unravelling this com-

plex subcellular structure (Kim and Sheng, 2004; Sheng and Kim, 2011; O'Rourke et al., 2012).

The inhibitory symmetric PSD is less well understood, principally due to the inability to isolate the smaller PSD for biochemical analysis (Sheng, 2001; Sheng and Kim, 2011). However, some information concerning symmetric PSD molecular content has been acquired, through analysis of proteins which interact with $GABA_A$and glycine receptors, inhibitory ionotropic receptors present at inhibitory synapses.

The key scaffolding molecule present at symmetric synapses is gephyrin, which can interact with both $GABA_A$ and glycine receptors, and anchors them to the post-synaptic site via the actin cytoskeleton (Sheng and Kim, 2011; Tyagarajan and Fritschy, 2014). Gephyrin helps to bind post- and pre-synaptic components via interactions with neuroligins, and a number of other signalling molecules have been identified to interact with gephyrin, which may mediate post-synaptic modifications at these sites. Understanding the complexities of the symmetric PSD is still an area of intense research (for review, see Tyagarajan and Fritschy, 2014).

1.2.3 Activity at the Synapse and its Plasticity

Research into synaptic activity has been heavily influenced by the work of Katz and colleagues, who identified three key variables that characterise quantal release of neurotransmitter: the size of the quantal response, the probability of quantal release, and the number of release sites. This landmark work led to the formulation of the quantal theory of synaptic transmission, and this conceptual framework provides an excellent foundation to understand synaptic transmission and its plasticity (Katz, 1969; Regehr and Stevens, 2001). A great deal of research has attempted to understand what morphological correlates and molecular mechanisms constitute the three key variables in synaptic

transmission, which is briefly overviewed here.

From a morphological perspective, the quantum is accepted to consist of the release of a single presynaptic vesicle (Regehr and Stevens, 2001). Thus, the quantal size is determined by the signal induced by a single presynaptic vesicle on the post-synaptic component. The size of the quantal response at individual CNS synapses is highly variable (Bekkers et al., 1990; Liu and Tsien, 1995; Forti et al., 1997), and this has been attributed to the variation in synaptic vesicle filling with neurotransmitter (Bekkers et al., 1990; Frerking et al., 1995), and to alterations in post-synaptic receptor number (Edwards et al., 1990).

The release site has been associated with the active zone. Whilst it was originally believed that only one release site existed per active zone (Stevens and Wang, 1995; Dobrunz and Stevens, 1997; Regehr and Stevens, 2001), it remains controversial, with some researchers arguing that multiple vesicular release is common across CNS synapses (for review see Rudolph et al., 2015). This issue has profound implications for alterations in synapse strength, as multi-vesicular release with each nerve impulse could provide a mechanism for altered synaptic signalling.

The probability of quantal release is highly variable, and is typically low at CNS synapses (Branco and Staras, 2009; Borst, 2010). The release probability is determined by the number of vesicles available for release (Dobrunz and Stevens, 1997; Murthy et al., 1997), and changes in this probability underlie synaptic strength regulation (Regehr and Stevens, 2001; Branco and Staras, 2009; Borst, 2010).

1.2.3.1 Short-Term Plasticity

Synaptic strength is subject to constant short-term changes in a use-dependent manner, and this exhibits significant variation across different synapses. For example, some synapses such as the climbing fibre synapse, are depressed with repetitive activation;

whereas other synapses such as the parallel fibre synapse, are facilitated with repetitive activation (Dobrunz and Stevens, 1997; Dittman et al., 2000; Regehr and Stevens, 2001). These responses reflect pre-synaptic mechanisms leading to altered calcium channels and currents, vesicle pool properties and release, and ultimately changes in quantal release probability and quantal response size (Fioravante and Regehr, 2011; Regehr, 2012; de Jong and Fioravante, 2014).

The diversity seen in synaptic responses is driven by the identity of both the pre-synaptic and post-synaptic cells (Blackman et al., 2013), and simulations of synaptic integration in cerebellar granule cells indicate profound non-linear changes in neuronal output with slight alterations to synaptic release probability and response size (Arleo et al., 2010). These observations indicate the complexities of the modulation of synaptic transmission throughout the CNS and its consequences for neural network function, and highlights the importance in understanding the diversity of this response across different synapses.

1.2.3.2 Long-Term Plasticity

Long-term changes in synaptic activity, on the contrary, is believed to reflect predominantly post-synaptic mechanisms. At excitatory synapses, NMDA receptor activation, and AMPA receptor insertion or removal, leads to a prolonged increase in synaptic strength (Lüscher and Malenka, 2012). At inhibitory synapses, which are less studied, insertion and removal of post-synaptic receptors is also believed to drive long-term changes in synapse strength (Vogels et al., 2013).

The induction of long-term potentiation or depression occurs with different pre- and post-synaptic activity patterns, and is well described. Long-term potentiation occurs with concomitant pre- and post-synaptic activation, whereas long-term depression is observed

with low-frequency post-synaptic activation only (Bliss et al., 2004; Lüscher and Malenka, 2012). These observations fit with the principles of Hebbian plasticity, as previously outlined by Donald Hebb (Hebb, 1949). Long-term plasticity results in changes in synapse size, and its maintenance has been shown to be dependent on protein synthesis (Lüscher and Malenka, 2012).

Long-term plasticity is also affected by the pre-existing molecular differences present at distinct synapses throughout the CNS (O'Rourke et al., 2012), and understanding this diversity is essential in understanding how different synapses will respond to different inputs, and ultimately how neural networks are sculpted in the CNS long-term.

1.2.4 Summary

This Section has given a brief and broad overview of the current understanding of synaptic structure and function. It has highlighted that although a considerable degree of knowledge has been obtained concerning the molecular mechanisms and morphological correlates of synaptic function, the vast molecular diversity present across synapses throughout the CNS remains elusive (O'Rourke et al., 2012; Burette et al., 2015).

Understanding the deep molecular diversity of synapses remains a significant challenge in neuroscience. Techniques which can illuminate the distribution of molecules across large samples of synapses in different regions of the CNS will provide a wealth of information to aid in this endeavour. This diversity across synapses will ultimately need to be linked to synaptic function, including synaptic responses as well as short- and long-term plastic changes; which could provide a comprehensive framework that links certain molecules to specific synaptic mechanisms of function and plasticity, and contribute to understanding neural network function. It therefore can provide fundamental information in understanding the link between networks, their function and cognitive processes.

Research on synapse diversity and its link to synapse plasticity and network function is important across all areas of neuroscience. One area where its effects have wide-ranging consequences in terms of quality of life is neuropathic pain, a condition characterised by a lesion or disease to the somatosensory nervous system. Studying plasticity in neuropathic pain is important, as it is not only widely believed to drive the neuropathic phenotype, but most currently licensed drugs for neuropathic pain affect synaptic signalling, plasticity or integration in some way, and it is hoped further understanding can help to drive more efficacious treatment. The dorsal horn is given special attention when attempting to understand plasticity in neuropathic pain states, since it is the first relay and processing point in the somatosensory neuraxis, and thus displays a wide degree of plastic changes following the onset and maintenance of neuropathic pain.

Below is given a review of the anatomy and physiology of the dorsal horn, followed by an overview of alterations observed following peripheral nerve injury, a common driver of neuropathic pain, with special emphasis given to synaptic plasticity, connectivity, and alterations in neuronal excitability.

1.3 The Dorsal Horn

The dorsal horn (DH) is divided into 6 parallel laminae based on cytoarchitectonics, originally described by Rexed (Rexed, 1952), and later extended to the rodent (Molander et al., 1984) (Figure 1.2A). It is composed principally of four major neuronal components: primary afferent input, intrinsic neurons, projection neurons, and descending input from higher centres (Todd, 2010). These four components interact in complex ways to receive, process, modulate and forward incoming somatosensory information, as outlined below.

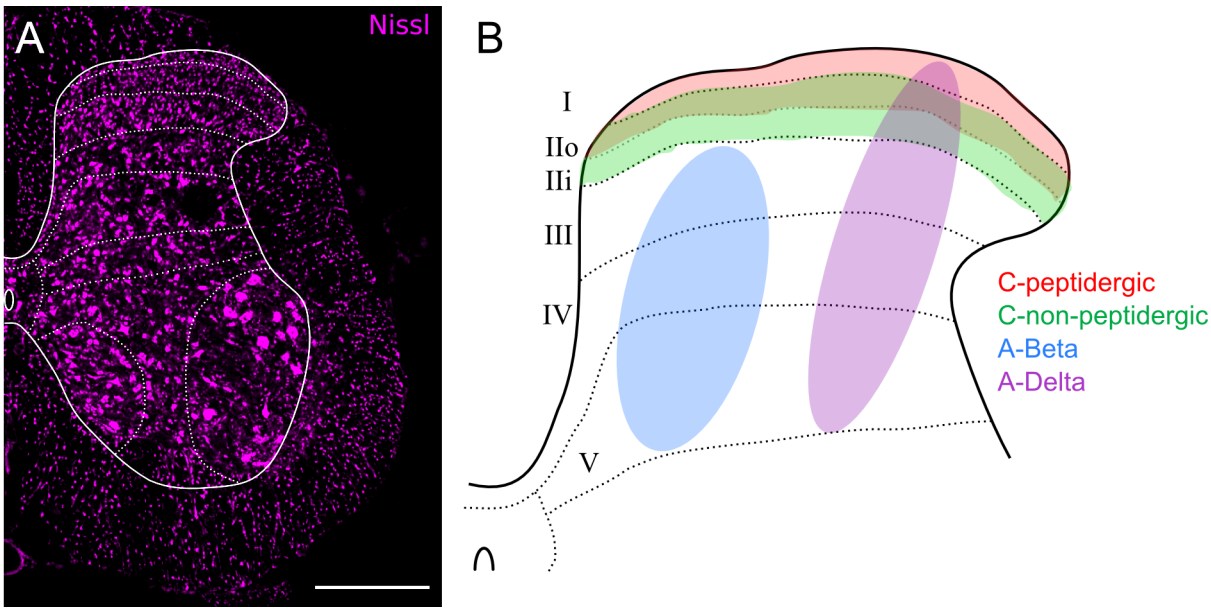

Figure 1.2: **Different primary afferent classes terminate in distinct regions of the dorsal horn. A:** The dorsal horn is divided into six separate laminae based on cytoarchitectonics. **B:** Primary afferents terminate in the dorsal horn into specific laminae, with C fibres innervating superficial (I/II) laminae, whereas A fibres tend to innervate deeper (III/IV) laminae.

1.3.1 Dorsal Horn Input: Primary Afferent Neurons

The dorsal horn (DH) receives sensory information from primary afferent neurons, whose cell bodies are located in the dorsal root ganglion (DRG). These neurons form a pseudounipolar morphology, sending one projection towards the periphery, and the second towards the CNS. The majority of research conducted in neuropathic pain is focussed on the lumbosacral plexus, and specifically the sciatic nerve and its peripheral and central innervation territories, and so a brief overview of the anatomy of this plexus is given (Figure 1.3). The sciatic nerve receives input from between two and three lumbar DRGs, which varies across species and strain of rodent (Rigaud et al., 2008). The sciatic nerve then branches into three separate nerves: the tibial, common peroneal, and sural nerves. These nerves then innervate the hindpaw in stereotypical ways (Takahashi et al., 1994). The general outline of the gross anatomy in the rat is overviewed in Figure 1.3.

The most commonly used scheme to classify primary afferent neurons has been by their myelination, diameter and conduction velocity, which are inherently linked, and

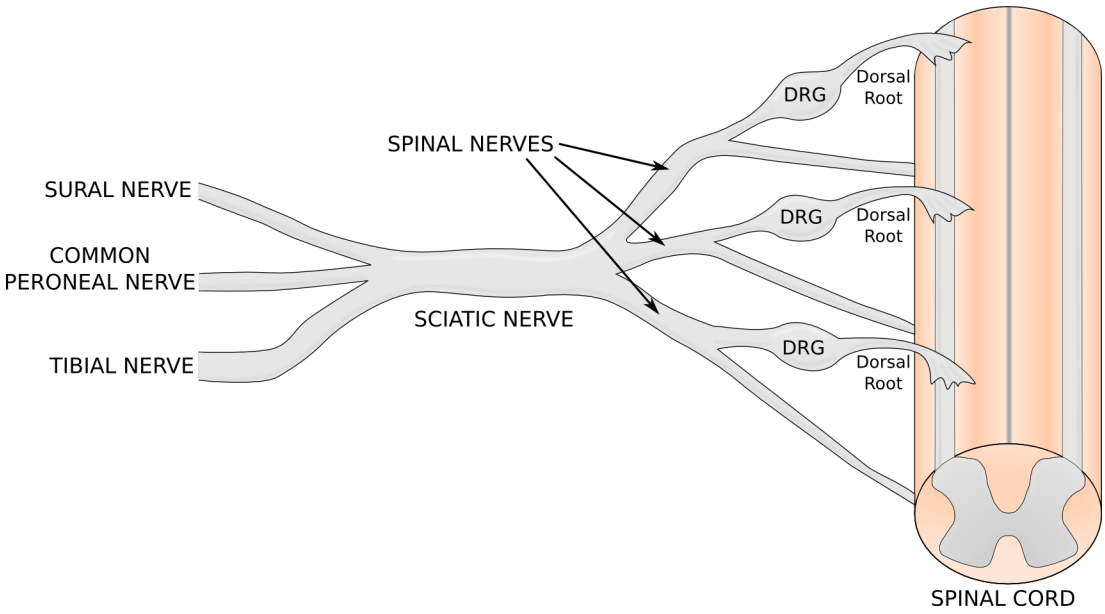

Figure 1.3: **The sciatic nerve and its connections.** The sciatic nerve receives input from the spinal nerves derived from 2-3 Lumbar dorsal root ganglia (DRGs) which innervate the lumbar spinal cord. The sciatic nerve then branches into three separate nerves: the sural, common peroneal and tibial nerves.

have been classically divided into two types: the large myelineated and fast A-fibres, and the small unmyelinated and slow C-fibres. Histochemical markers have also been used to delineate primary afferent neurons. All A-fibre neurons appear to selectively express the heavy chain neurofilament (NF200, Lawson et al., 1984), and a subset of A-fibres which also express parvalbumin & calbindin appear to mark proprioceptive primary afferent neurons (Carr et al., 1989; Szabolcs et al., 1989; Ernfors et al., 1994). C fibres can be split broadly into three groups based on their expression of calcitonin gene related peptide (CGRP; peptidergic C-fibres), and binding of isolectin B4 (IB4; non-peptidergic C-fibres) (Snider and McMahon, 1998), as well as expression of tyrosine hydroxylase (which mark C-fibre low threshold mechanoreceptors) (Li et al., 2011); such divisions are practically helpful, however recent unbiased molecular analysis indicates that the situation is clearly more complex than these gross subdivisions, with 11 subtypes of primary afferent neuron identified (Usoskin et al., 2014).

Primary afferent neurons produce distinct termination patterns within the DH that

is based on the class of neuron. Broadly, a graded pattern of termination is seen, where C fibres synapse in the superficial laminae (I/II), Aδ fibres synapse in the superficial as well as deeper laminae, and Aβ fibres are more restricted to deeper laminae (IIi-V, Figure 1.2B) (Millan, 1999). Upon entering the dorsal horn, A fibres bifurcate, sending collaterals into the somatotopically-relevant region of the dorsal horn, as well as ascending the dorsal columns to connect with the dorsal column nuclei (Giuffrida and Rustioni, 1992).

All primary afferent fibres use the neurotransmitter glutamate. Glutamate has been shown to be released after electrical and noxious stimulation, and its uptake and release are decreased after dorsal rhizotomy (De Biasi and Rustioni, 1988). Glutamate is found in many primary afferent terminals, both large and small (Battaglia and Rustioni, 1988; De Biasi and Rustioni, 1988). Additionally, glutamate has also been shown to be co-localised with peptides such as substance P and CGRP (Battaglia and Rustioni, 1988; De Biasi and Rustioni, 1988), and the release of such transmitters after a noxious stimulus appears to demonstrate that they play a role in nociception. Glutamate actions are exerted through its ionotropic receptors kainate, the AMPA receptor and NMDA receptor and its metabotropic receptors (Watkins and Evans, 1981; Woodruff et al., 1987; Dickenson, 1995).

Primary afferents form complex synaptic structures within the DH. Synaptic glomeruli are complex arrangements of synaptic contacts between primary afferent fibres and DH neurons. These structures show multiple connectivity patterns, including axo-dendritic, axo-axonic and dendro-axonic synapses (Ribeiro-da Silva and Coimbra, 1982; Ribeiro-da Silva et al., 1985). Two types are recognised: type 1, which are formed from IB4+ primary afferent fibres; and type 2, that are formed by Aδ hair follicle axons (Ribeiro-da Silva and Coimbra, 1982; Ribeiro-da Silva et al., 1985; Ribeiro-Da-Silva et al., 1986). Peptide-containing C-fibres may rarely form glomeruli within the DH, although most have

been observed to form simple synaptic contacts (Ribeiro-da Silva et al., 1989).

These glomerular structures are important in primary afferent depolarisation (PAD), a form of primary afferent pre-synaptic inhibition mediated through GABA by GABAergic interneurons (Rudomin and Schmidt, 1999). The mechanisms underlying PAD and pre-synaptic inhibition are well understood. Primary afferents possess a high intracellular chloride concentration due to high sodium-potassium-chloride cotransporter 1 (NKCC1) and low potassium-chloride cotransporter 2 (KCC2) expression levels (Coull et al., 2003; Price et al., 2009). GABAergic interneurons, acting via $GABA_A$ receptors (Eccles et al., 1963; Gallagher et al., 1978), cause an efflux of chloride ions, and thus depolarise the primary afferent fibre. Crucially, this is not sufficient to release synaptic vesicles, but does result in inactivation of sodium and calcium channels (Graham and Redman, 1994), therefore preventing action potentials from initiating synaptic transmission – a process referred to as shunting. Suprathreshold excitation of this mechanism, either via increased efficacy of GABA on primary afferents, or alterations in the chloride gradient within primary afferents, has been suggested to cause direct excitation of primary afferent terminals, and may play a role in neurogenic inflammation and hypersensitivity (Willis, 1999; Bardoni et al., 2013).

1.3.2 Dorsal Horn Processing

The DH comprises two basic neuronal subtypes: local interneurons and projection neurons, which form complex circuits within the DH (Todd, 2010; Petkó and Antal, 2012). Plasticity within such circuits following repetitive nociceptive input (Ikeda et al., 2006; Latremoliere and Woolf, 2009; Sandkühler, 2009) can act to facilitate or amplify incoming somatosensory inputs, and ultimately modifying the processing and propagation of somatosensory information to higher centres.

An early and still influential theory postulating the importance of circuits involving DH interneurons was the 'gate control' theory of pain proposed by Melzack and Wall (Melzack and Wall, 1965). Melzack and Wall argued that spinal projection neurons transmitting nociceptive information received input not only from nociceptors, but also from low threshold Aβ afferents. This low threshold input is, however, gated by feed-forward activation of inhibitory interneurons. Disinhibition would therefore lead to these low threshold inputs activating the transmission neurons and the development of allodynia. Whilst being subject to some criticism, this theory has strongly influenced research efforts and thinking of the dorsal horn and its processing of incoming somatosensory information, and it is generally regarded that understanding the function of dorsal horn interneurons and how they integrate somatosensory information will help in recognising how the dorsal horn contributes to various chronic pain states.

1.3.2.1 The Dorsal Horn is Subject to Activity-Dependent Plasticity

A number of discoveries have led to the understanding that activity-dependent plasticity in DH neurons plays a key role in the generation of hypersensitivity. The first process describes a progressive increase in DH output with repetitive low-frequency stimulation of C-fibres, an electrophysiological phenomenon referred to as wind up (Mendell and Wall, 1965; Mendell, 1966). Later, it was recognised that repeated C-fibre input following intense and sustained noxious stimulation generated increased excitability in flexor motorneurons, causing a reduced threshold for reflex withdrawal, an increase in receptive field size and novel responses to normally innocuous Aβ fibre inputs. This effect proved to be driven by plasticity in the spinal cord, and was thus named central sensitisation (Woolf, 1983; Latremoliere and Woolf, 2009).

This work was extended by experiments which looked at C-fibre induced DH field

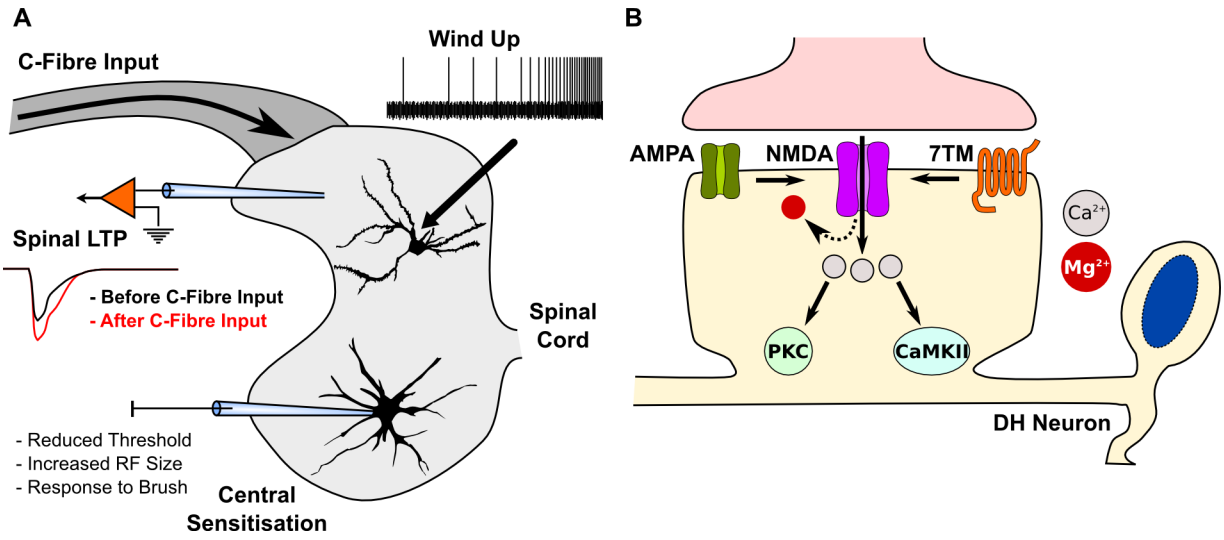

Figure 1.4: **Activity-dependent plasticity in the dorsal horn. A:** An overview of the three historical accounts of activity-dependent plasticity: Wind up describes an activity-dependent increase in WDR neuron output with continuous input, spinal LTP was identified as increased dorsal horn field potentials following C-fibre input, central sensitisation was initially described as changes in flexor motor neuron output following prolonged noxious or C-fibre stimulation. **B:** Overview of the molecular mechanisms involved in activity-dependent plasticity within the dorsal horn. AMPA and neuropeptide (GPCR receptors, 7TM) receptors depolarise the post-synaptic neurons sufficiently to release the NMDA receptor of its magnesium block, allowing calcium ions to enter the cell. Calcium activates a number of down-stream pathways (including protein kinase C and Calcium/Calmodulin-dependent protein kinase II), which leads to altered synaptic and cellular responses to inputs. LTP, long-term potentiation; AMPA, alpha-amino3-hydroxy-5-methyl-4-isoxazoleproprionic acid; NMDA, n-methyl d-aspartate receptor; 7-TM, 7-trans membrane G-protein coupled receptor; DH, dorsal horn.

potentials, which showed that high frequency C-fibre input was capable of significantly increasing the amplitude of DH field potentials, reminiscent of long term potentiation (LTP), and was thus called spinal LTP (Liu and Sandkühler, 1995; Drdla and Sandkuhler, 2009) (Figure 1.4A). These experiments were later broadened by showing that neurons which project to the periaqueductal grey (PAG) responded specifically to low-frequency (2Hz) C-fibre inputs with a prolonged increase in excitatory postsynaptic potentials, that DH field potentials are significantly increased with natural low-frequency afferent barrages (Ikeda et al., 2006), and that spinal LTP is heterosynaptic through induction of C-fibre induced LTP between intrinsic DH neuronal connections (Fenselau et al., 2011).

These phenomena all demonstrate that activity-dependent plasticity in the DH re-

quires C-fibre input. It has been previously demonstrated, using *in vitro* spinal cord slices, that Aδ- and C- fibre strength stimulation produces prolonged excitatory post-synaptic potentials in recorded DH (Yoshimura and Jessell, 1989) and ventral horn (Thompson et al., 1990) neurons. Some C-fibre terminals contain glutamate and neuropeptides such as substance P and CGRP (Merighi et al., 1991), and some DH neuron C-fibre potentials contain both a glutamate (Thompson et al., 1990) and neuropeptide (Nagy et al., 1993) component. Prolonged potentials driven by glutamate and neuropeptides allow pronounced temporal summation to occur, even at low frequencies, leading to cumulative depolarisation of dorsal and ventral horn neurons (Sivilotti et al., 1993). The summation is not linear, but progressively increases with continued input. A large body of work now reveals that activity-dependent plasticity comprises multiple distinct phases, each associated with specific mechanisms. Below a brief review of these mechanisms is given, although more detailed accounts can be found in the literature (Drdla and Sandkuhler, 2009; Latremoliere and Woolf, 2009; Sandkühler, 2009).

It is well established that the NMDA receptor plays an integral role in activity-dependent plasticity in the DH, since inhibition of NMDA currents can inhibit activity-dependent plasticity (Dickenson and Sullivan, 1987; Woolf and Thompson, 1991; Liu and Sandkühler, 1995). Its role in the progressive output of DH neurons with continued C-fibre input is dependent on its ligand- and voltage-gated behaviour (Dickenson, 1990). At resting membrane potentials, the NMDA receptor is under Mg^{2+} blockade. This is lifted following depolarisation (Mayer et al., 1984), which then allows glutamate to activate the NMDA receptor, and results in an increased input of Na^{+} and Ca^{2+} ions into the DH neuron. Much of the acute response to nociceptive input in DH neurons can be explained using this model, as neuropeptide blockade and morphine administration may inhibit the C-fibre evoked slow synaptic potentials sufficiently to prevent NMDA receptor activation

and thus stop amplification of the C-fibre input (Ma and Woolf, 1995; Sivilotti et al., 1995). Depolarisation sufficient to induce NMDA receptor activation occurs through glutamate acting on AMPA, kainate receptors, and through neuropeptides such as substance P (Afrah et al., 2002; Khasabov et al., 2002), CGRP (Woolf and Wiesenfeld-Hallin, 1986; Sun et al., 2003) and brain-derived neurotrophic factor (BDNF) (Lever et al., 2001). mGlu Type I are also important for the induction of DH activity-dependent plasticity (Azkue et al., 2003; Derjean et al., 2003).

The rise in intracellular Ca^{2+} is considered a key trigger for subsequent plasticity of synapses within the DH. This rise results from activation of NMDA- and Ca^{2+}-permeable AMPA-receptors, as well as voltage-gated Ca^{2+} channels and intracellular stores (Coderre and Melzack, 1992; Morisset and Nagy, 1999). This influx of Ca^{2+} ions results in the activation of a number of second messenger systems, including protein kinase A and protein kinase C Calcium/Calmodulin-dependent protein kinase II, phosphatidylinositol-3-kinase and mitogen-activated protein kinase (Figure 1.4B). The net effect of these pathways is phosphorylation of postsynaptic receptors, recruitment of new receptors, and the expression of novel genes. These in turn result in altered synaptic and cellular responses to inputs, and are believed to underlie, at least in part, the hypersensitivity seen in different pain states (Latremoliere and Woolf, 2009; Sandkühler, 2009).

1.3.2.2 Interneuron Subtypes in the Dorsal Horn

The DH contains numerous interneurons, exceeding 95% in each lamina (Burstein et al., 1990; Todd et al., 2000; Todd, 2010), which is indicative of their important role in DH processing. Understanding the function of these neurons and how they relate to pain perception can help to recognise how this system breaks down in various chronic pain states. Reviewed here are the physiological and anatomical properties of this diverse

collection of cells.

Interneurons within the DH are often sub-divided into morphological subtypes. Lamina I neurons have been divided into four morphological subtypes: fusiform, flattened, multipolar and pyramidal cells (Lima and Coimbra, 1983, 1986). In lamina II a similar scheme exists, consisting of central, islet, radial and vertical cells (Grudt and Perl, 2002). However, a significant proportion of cells continue to remain unclassified (Yasaka et al., 2010). Fewer studies have looked at neurons in deeper laminae, however one scheme used to divide lamina III-V neurons into two subtypes based on axonal branching has been proposed (Schneider, 1992).

Lamina II has been interrogated in detail by pain researchers due to its important role in pain transmission. Recent work has highlighted the distribution of excitatory and inhibitory neurons of distinct morphologies within lamina II (Heinke et al., 2004; Punnakkal et al., 2014). Approximately 60% of GABAergic neurons were islet cells, 5% vertical cells, and the rest remained unclassified (Heinke et al., 2004). An even distribution of glutamatergic neurons displayed vertical, central, radial and unclassified cell morphologies, but no excitatory neurons displayed islet morphology (Punnakkal et al., 2014). These results suggest that neuronal morphology is at least partially related to neuronal phenotype and function.

Approximately 25, 30 & 40% of neurons in laminae I, II & III/IV are GABAergic (Todd and Sullivan, 1990; Polgár et al., 2003). Recent work showed the importance of dynorphin-expressing inhibitory interneurons in the DH for gating mechanical pain. Ablation of the dynorphin lineage of GABAergic interneurons resulted in spontaneous mechanical hypersensitivity (Duan et al., 2014). Furthermore, this study demonstrated the function of somatostain positive glutamatergic neurons in mechanical pain, by demonstrating that loss of this neuronal subtype resulted in loss of noxious mechanical sensations (Duan et al.,

2014).

Another recent study demonstrated the importance of glutamatergic DH neurons in mechanical nociception and itch sensation. Ablation of a subset of excitatory DH neurons expressing the testicular orphan nuclear receptor 4 resulted in the complete absence of mechanical pain and itch behavioural measures, as well as loss of a formalin test response (Wang et al., 2013). Interestingly, a rewiring of primary afferent C-fibre input to the medial inner lamina II region of the DH was seen, where IB4 positive afferents were reduced and replaced with substance P afferent arborisations, suggesting the loss of these excitatory DH neurons led to altered input and circuitry.

Glutamate uncaging within DH slice preparations has been used to understand properties of inhibitory and excitatory DH neurons (Grudt and Perl, 2002; Kato et al., 2007, 2009, 2013). One consistent finding was the localised input of inhibitory interneurons versus the diffuse input of excitatory interneurons. The extent of dendrites in different planes of orientation was found to be predictive of the degree of excitatory input in that plane across all laminae. This was shown in the dorsoventral axis to result in translaminar inputs (Kato et al., 2007, 2009, 2013), which bears relevance for the processing of information from deep to superficial laminae, and vice versa.

1.3.2.3 Projection Neurons in the Dorsal Horn

Neurons projecting from the DH carry somatosensory signals in ascending tracts to specific brain centres such as the midbrain, cortical structures and the thalamus (Todd, 2002; D'Mello and Dickenson, 2008). Many of these neurons express the neurokinin 1 (NK1) receptor; the highest concentration of which is found in lamina I (Nakaya et al., 1994; Todd, 2002). Pathways through which second order neurons can transmit pain-related signals from the spinal cord include the spinothalamic, spinomedullary and spinobulbar

tracts (Dostrovsky and Craig, 2013). Most supraspinal projections from the spinal cord originate either in lamina I, and III-VI, with no observed projections from lamina II in lumbar DH (Todd, 2010).

Projections from the spinal cord innervate different supra-spinal structures including the parabrachial area, nucleus of the solitary tract, the PAG, caudal ventrolateral medulla (CVLM), and thalamic nuclei, which are believed to code for specific dimensions of the pain experience. In particular, the parabrachial area has been linked to the affective and autonomic components of pain, owing to its projections to forebrain structures such as the amygdala and hypothalamus, and the thalamus has been associated with the sensory-discriminative components of pain due to its projection to primary and secondary somatosensory cortical regions. The PAG and the CVLM communicate with other brainstem regions (notably the rostral ventromedial medulla and nucleus raphe magnus), and can influence descending controls that engage DH circuits (Tracey and Mantyh, 2007; Todd, 2010; Dostrovsky and Craig, 2013).

Within the DH of the spinal cord there are two main groups of projection neuron involved in pain processing, as defined by their receptive field characteristics: nociceptive specific (NS) and wide dynamic range (WDR) neurons. Whilst NS neurons respond on the whole to high intensity input, WDR neurons respond to a much broader range of stimuli and code stimulus intensity and wind up (Dubner et al., 1989; Simone et al., 1991; Dougherty and Willis, 1992). A recent study by Sikandar and colleagues clearly demonstrated using lamina V WDR neuron recordings along with human quantitative sensory testing and electroencephalography, that the response characteristics of these DH neurons parallels psychophysical responses in humans (Sikandar et al., 2013).

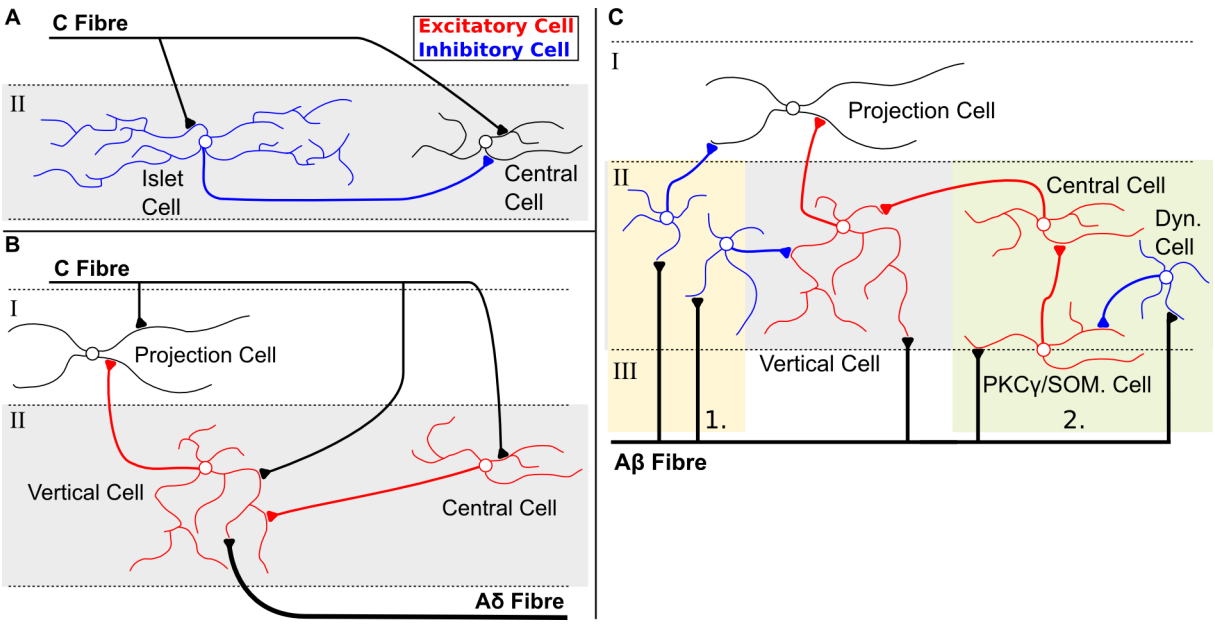

Figure 1.5: **Dorsal horn circuitry.** A number of consistent connectivity motifs between interneurons identified within the superficial dorsal horn. **A:** Inhibitory islet cells were found to consistently contact central interneurons in lamina II, and both received C-fibre input. **B:** Excitatory connectivity motif connecting lamina II excitatory central cells, to excitatory vertical cells leading to lamina I projection neurons, all received C-fibre input, and vertical cells received Aδ input. **C:** Two major pathways that gate Aβ input to lamina I projection neurons. 1. Excitatory vertical cells receive Aβ input, which is gated by inhibitory interneurons. Aβ input can also directly inhibit lamina I projection neurons. 2. A complex excitatory circuit from Protein Kinase C/somatostatin cells to central to vertical cells, that can stimulate lamina I projection neurons is gated by dynorphin-expressing inhibitory interneurons.

1.3.2.4 The Dorsal Horn Forms Local Circuits

A set of studies using paired recordings revealed a number of connectivity motifs within the DH (Lu and Perl, 2003, 2005). Approximately 10% of randomly selected superficial DH interneurons showed connectivity, indicating selective connectivity motifs within this region. Lu et al have proposed two canonical circuits: an inhibitory connection between lamina II islet interneurons and central interneurons (both which received C-fibre inputs) (Lu and Perl, 2003)(Figure 1.5A); and an excitatory connectivity motif between central neurons (receiving C-fibre input) to vertical interneurons (receiving Aδ fibre input), and vertical interneurons to putative lamina I projection neurons (which received C fibre inputs) (Lu and Perl, 2005) (Figure 1.5B).

Yasaka et al. revealed a diverse set of inputs to all morphologically defined lamina II interneurons (Yasaka et al., 2007). Consistent with the paired recording studies, islet and central cells showed exclusively monosynaptic C fibre input only; however, vertical and radial interneurons received monosynaptic inputs from both C and Aδ fibres. Furthermore, islet interneurons showed inhibitory synaptic inputs following Aδ fibre stimulation, and central, vertical and radial cells all showed inhibitory synaptic input following both C and Aδ fibre stimulation (Yasaka et al., 2007). These data suggest that many more connectivity patterns exist within the DH.

Circuitry involved in Aβ primary afferent processing has been revealed in recent work. Miraucourt et al. demonstrated that, following removal of glycine inhibition in the DH, NS lamina I neurons could respond synaptically to innocuous Aβ fibre input, and was suggested to occur through the protein kinase C gamma (PKCγ)-expressing excitatory interneuron (Miraucourt et al., 2007, 2009). These results suggest that PKCγ interneurons are usually inhibited from activating lamina I NS neurons through a glycinergic inhibitory pathway. This work was extended by Lu et al., who demonstrated a polysynaptic pathway between Aβ input and lamina I projection neurons, via a bridge of excitatory interneurons, including PKCγ positive, central and vertical neurons (Lu et al., 2013). The PKCγ interneuron, which received monosynaptic Aβ input, was inhibited by a glycinergic interneuron, which also received Aβ input, thus producing a feedforward inhibitory circuit (Lu et al., 2013).

Further experiments have highlighted the parallel nature of this circuit, by showing that the larger somatostatin subset of excitatory neurons present in lamina II forms a network that transfers Aβ input through lamina II to lamina I, which included lamina II cells that were PKCγ positive (present on lamina II/III border), and other cells with central and vertical morphologies (Duan et al., 2014; Yasaka et al., 2014). Interestingly,

monosynaptic Aβ input was present on both somatostain/PKCγ positive interneurons on the lamina II/III border and on the somatostatin positive vertical neurons, indicating two pathways for Aβ input to reach lamina I. Furthermore, at each successive step through the circuitry, inhibitory interneurons, some of which received Aβ input, formed a feedforward synaptic gate with the somatostatin-positive neurons (Duan et al., 2014) (Figure 1.5C). This circuitry was shown to relate functionally to mechanical allodynia, as ablation of somatostatin positive neurons resulted in loss of mechanical pain sensation in these mice, whereas dynorphin cell ablation resulted in spontaneous mechanical hypersensitivity (Duan et al., 2014).

Finally, a recent study has shown that lamina I projection neurons themselves are directly subject to low-threshold, primary afferent driven inhibitory input (Luz et al., 2014) (Figure 1.5C). These inhibitory inputs were found to temporally precede high-threshold Aδ fibre inputs, and acted to shunt excitatory post-synaptic potentials generated from these fibres.

1.3.3 The Dorsal Horn Receives Input from the Brainstem

Descending pathways from the brainstem play a pivotal role in the modulation of pain processing. Inputs driving circuits in the amygdala, hypothalamus, frontal lobe and anterior cingulate cortex activate areas of the PAG and this in turn feeds into the rostroventral medulla (RVM). The RVM also has reciprocal innervations from the dorsal lateral pontine tegmentum, which sits rostrally to this and contains clusters of noradrenergic nuclei of the A5, A7 and the locus coeruleus (LC) cell groups. From the RVM neurons project bilaterally via the dorsolateral and ventrolateral funiculi to the DH, giving rise to descending facilitatory and inhibitory pathways (Basbaum and Fields, 1979).

Such pathways have been identified as key players in the complex synergistic pain

processing system, where the release of 5-hydroxytryptamine (5HT) from the RVM and noradrenaline (NA) from the LC play overriding pro-nociceptive and anti-nociceptive roles respectively (Heinricher et al., 1992; Bannister et al., 2011). In particular, the descending control system is thought to be activated by a spinal-bulbo-spinal loop whereby activated NK1 receptor expressing lamina I/III projection neurons send signals to the parabrachial area and onto the limbic system (Suzuki et al., 2002).

A small population of dopaminergic neurons in the PAG mediates anti-nociception via participation in supraspinal nociceptive responses after opiates; this dopaminergic system is another network within the PAG involved in opiate induced anti-nociception (Flores et al., 2004). The inhibitory PAG-RVM-DH descending pathway is well characterized but the RVM is also involved in descending facilitation of nociceptive processing (Porreca et al., 2002). The monoamine neurotransmitters NA and 5HT and are released from neurons in the brain and the peripheral nervous system and are known to have a crucial influence on mood and behaviour. They are also proposed to play complex, often overlapping, modulatory roles in pain signaling.

1.3.4 Summary

The dorsal horn contains neural elements which interact and affect one another in complex ways. This manifests as the modifiability and plasticity imposed upon incoming somatosensory information, exerted through local and supraspinal circuits, which ultimately motivates an appropriate behavioural response from the organism given the stimulus and the context (Craig, 2003; Tracey and Mantyh, 2007; Tracey, 2010). However, this complex signalling can occasionally break down, with the most striking example seen in neuropathic pain: chronic pain resulting from a disease or lesion to the somatosensory nervous system. Below, an overview of neuropathic pain and its mechanisms is given.

1.4 Neuropathic pain

Neuropathic pain is a type of chronic pain which occurs as a consequence of a lesion or disease to the somatosensory nervous system (Jensen et al., 2011). In contrast to acute pain, which serves to warn the organism of impending tissue damage, and furthermore to protect an injured region during the healing process (a hypersensitive state driven by inflammatory mechanisms), neuropathic pain serves no useful purpose, and due to its chronic nature, can be severely debilitating (Millan, 1999).

A plethora of nerve damaging stimuli can result in neuropathic pain, including trauma, metabolic syndromes, drug- or toxin-induced injury, hereditary disorders, malignancy and infective or post-infective nerve damage. The sensory manifestations expressed by patients are complex, including lesion-induced reductions in somatosensation combined with paradoxical sensory perceptions, manifesting as spontaneous or ongoing sensations with pain as the dominating positive symptom. Furthermore, evoked somatosensory stimulation often induces amplified painful responses following noxious or non-noxious stimuli (Baron et al., 2010).

Neuropathic pain is common, affecting 6-8% of the population, and in many cases treatment is inadequate, leading to significant disability and suffering (Jensen et al., 2007; Smith et al., 2007; Smith and Torrance, 2012). In a typical randomised control trial, less than 50% of neuropathic pain patients experience satisfactory pain relief, with side-effects a common problem (O'Connor and Dworkin, 2009; Dworkin et al., 2010); and in the community setting it has been found that neuropathic pain patients, on average, suffer with moderate pain intensity, even though they are receiving the recommended treatment for their condition (O'Connor and Dworkin, 2009).

Poor selection of treatment for individual patients (O'Connor and Dworkin, 2009), and suboptimal pharmacological agents (Finnerup et al., 2010) have been suggested to

contribute to this lack of efficacy. This ultimately stems from a lack of understanding of not only the systems in which neuropathic pain manifests, but also in how these systems change as a result of a lesion or disease to the somatosensory nervous system. Thus, in order to identify new treatments, an accurate model which brings together a high-level understanding of the physiological function of the neuraxis involved in nociception and somatosensation, combined with the alterations to these pathways which occur following the onset and maintenance of neuropathic pain, is essential.

A key region involved in nociceptive and somatosensory processing is the dorsal horn, and thus this region has been subject to intense study to understand the mechanisms relating to neuropathic pain. Following on from the overview of the physiology and anatomy of the dorsal horn given above, here a review of literature relating to mechanisms found within the dorsal horn to contribute to the neuropathic pain phenotype is given.

This discussion is complicated by the myriad disease states which can cause neuropathic pain. Since the majority of the literature uses traumatic nerve injury models, most of our understanding of pathophysiological mechanisms stems from neuropathic pain resulting from traumatic nerve injury, and this will therefore be given special emphasis. However, where appropriate, literature relating to models of other types of neuropathic pain will be addressed.

1.5 Mechanisms of Neuropathic Pain

Mechanisms relating to the neuropathic pain phenotype can be generally divided into four key areas: changes peripheral drive and input, altered dorsal horn excitability, descending control changes, and glial activation. These will be reviewed in turn.

1.5.1 Initial Injury Reactions: Primary Afferent Signals

Given that peripheral neuropathic pain develops following injury to the axons of DRG cells, the early events in these neurons must have a key role in the initiation of neuropathic pain. Ultimately, axotomy results in profound phenotypic changes in injured DRG cells, and depending on the threshold used, altered expression in up to a quarter of known genes (Perkins et al., 2014), including: growth factor receptors, axon guidance molecules, neurotransmitters and ion channels which will have important consequences for DH function (Costigan et al., 2002; Xiao et al., 2002; Michaelevski et al., 2010; Perkins et al., 2014).

In traumatic injury, initial transection of a nerve results in a small burst of neuronal activity (Adrian, 1930; Wall et al., 1974), which quickly subsides, and is followed by 'positive' and 'negative' molecular signals as a consequence of calcium flux and altered retrograde signalling within the axon. The initial reaction to traumatic nerve injury involves the propagation of calcium waves from the site of injury towards the cell soma, and which are important for the two dominant retrograde signalling complexes that form following nerve injury: mitogen-activated protein kinases (Zrouri et al., 2004), including JNK (Lindwall and Kanje, 2005); and nuclear localisation signalling molecules such as importins (Hanz et al., 2003; Hanz and Fainzilber, 2006). These signals are retrogradely transported via dynein motors to the soma, where they induce profound changes in gene transcription (Michaelevski et al., 2010; Perkins et al., 2014).

Concurrent with injury-evoked retrograde signalling, the ongoing flux of neurotrophin support that is derived from peripheral targets is altered in injured axons, which is important for the DRG transcription profile. Treating uninjured nerves with antibodies against nerve growth factor (NGF) replicates some of the axotomy-related changes to DRG protein expression (Shadiack et al., 2001). Following nerve injury, levels of NGF appear to fall rapidly, with nerve transection exhibiting a stronger reduction (Raivich et al., 1991).

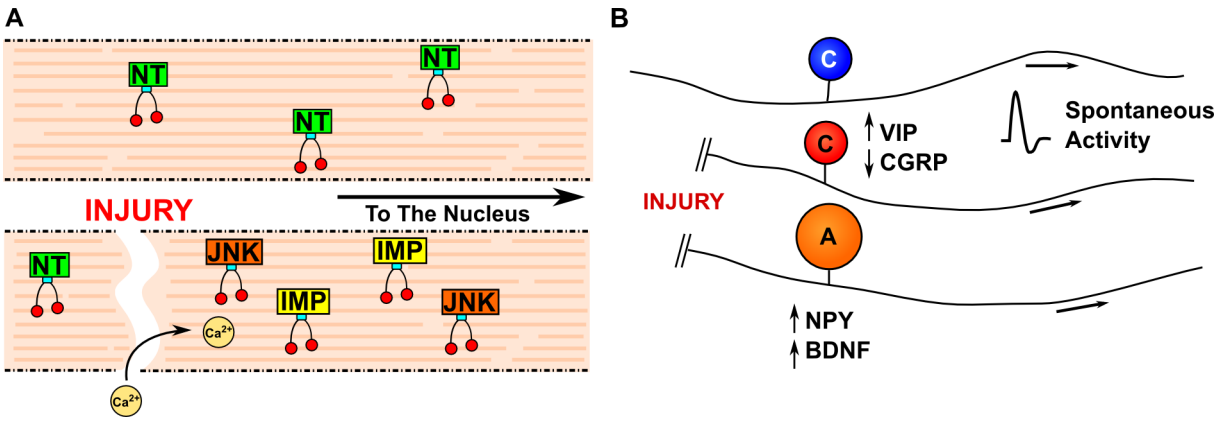

Figure 1.6: **Primary afferent fibres show changes after nerve injury. A:** Following nerve transection, regular retrograde transport of trophic signals is disrupted, leading to a rise in intracellular calcium, as well as the initiation of axonal transport of injury-related signals. **B:** Primary afferent neurons show changes in expression and activity. Injured C-fibres show increased VIP and reduced CGRP expression, and injured A-fibres display increased NPY and BDNF expression. Injured A- and C-fibres as well as uninjured C-fibres show spontaneous activity. NT, neurotrophic factor; IMP, importin; JNK, c-Jun N-terminal Kinase; VIP, vasoactive intestinal peptide; CGRP, calcitonin gene related peptide; NPY, neuropeptide Y; BDNF, brain-derived neurotrophic factor.

Consistent with loss of NGF signalling, intrathecal injection of NGF after nerve crush delays the neuronal responses of nerve injury (Gold, 1997). Furthermore, supplementation of a synthetic peptide mimicking NGF, as well as NGF itself, reduces pain behaviour associated with nerve injury (Colangelo et al., 2008; Cirillo et al., 2010). These data in general support a role for a loss of neurotrophic signalling in the onset of the neuropathic pain phenotype, which is likely to be important for central terminals of primary afferents following nerve injury (Figure 1.6A).

1.5.2 Changes in Primary Afferent Input and Projections

1.5.2.1 Spontaneous Activity

Spontaneous activity in injured sensory neurons has been observed in both animal models and in patients following nerve injury, and is believed to play an important role in the initiation and maintenance of neuropathic pain. Since the original description by Wall and Gutnick (1974), it has been shown that 1-3 days following nerve injury a significant

proportion of A-fibres demonstrate spontaneous activity, peaking at a 1-2 weeks and then declining (Govrin-Lippmann and Devor, 1978; Liu et al., 2000a). Interestingly, there is evidence to suggest this ongoing activity is a result of proprioceptors innervating muscle tissue, since transection of nerves which innervate skin resulted in no spontaneous activity, whereas nerves innervating muscles did produce spontaneous activity following lesion (Michaelis et al., 2000).

C-fibres can also develop spontaneous activity at a lower frequency, and importantly, spontaneous activity is not restricted to injured afferents, but is also observed in neighbouring un-injured afferents, probably as a consequence of the shared inflammatory environment with injured axons (Hulse et al., 2010). Spontaneous activity in primary afferents has also been observed in rodent models of chemotherapy (Xiao and Bennett, 2008), and painful diabetic neuropathy (Khan et al., 2002) and crucially in neuropathic pain states in humans (Orstavik and Jørum, 2010). A recent clinical study highlights the importance of ectopic activity in maintaining peripheral neuropathic pain as peripheral nerve blocks using local anaesthetic were highly efficacious in reducing ongoing pain (Haroutounian et al., 2014). In animal models, the behavioural consequences of spontaneous activity have been investigated. Giving brief and high intensity C-fibre input results in mechanical hypersensitivity in adult rats (Hathway et al., 2009), suggesting continuous inputs can sensitise central circuitry.

1.5.2.2 Expression Changes in Primary Afferents Following Nerve Injury

Traumatic nerve injury alters the pattern of expression of neurotransmitters/neuromodulators within sensory neurons. For instance C-fibres reduce their expression of CGRP as well as show increased expression of vasoactive intestinal polypeptide (Shehab and Atkinson, 1986) (Figure 1.6B). These effects seem to be driven, at least in part, by altered

neurotrophic support, as inhibition of axonal transport with vinka alkaloids results in a similar phenotype (Leranth et al., 1984; Knyihár-Csillik et al., 1991). A-fibres begin to express neuropeptide Y and BDNF following traumatic nerve injury paradigms (Wakisaka et al., 1992; Obata et al., 2006) (Figure 1.6B). Interestingly some of these changes are likely to be adaptive. For instance, intrathecal administration (Intondi et al., 2008) and conditional deletion (Solway et al., 2011) following nerve injury suggests that neuropeptide Y actually suppresses pain related hypersensitivity within the DH.

The α2δ-1 calcium channel subunit is upregulated on primary afferent terminals after nerve injury (Li et al., 2004), and appears to contribute to mechanical hypersensitivity seen after nerve injury (Li et al., 2004, 2014). Upregulation of the α2δ-1 subunit has been linked with enhanced neurotransmission of primary afferents as an apparent increase in pre-synaptic terminals (Li et al., 2014).

PAD has been hypothesised to be dysregulated after nerve injury, via modified chloride ion gradients within primary afferents, which could increase excitability in primary afferent terminals, or even reach sufficient intensity to excite these fibres (Cervero et al., 2003). Alterations in the chloride ion potential in primary afferents after nerve injury has been reported in spinal cord slices (Pieraut et al., 2007), where the investigators observed a shift in the $GABA_A$ receptor reversal potential towards depolarised potentials in injured neurons.

Recently, this shift has been shown to occur in the DH in vivo (Wei et al., 2013; Chen et al., 2014). Primary afferent neurons in culture showed a shift in the GABA A receptor reversal potential, as well as a loss in GABA-mediated conductance, which were due to increased NKCC1 activity and reduced GABA receptor, respectively (Chen et al., 2014). NKCC1 has been shown to be specifically upregulated following trigeminal nerve injury in primary afferent neurons (Wei et al., 2013), and using fluorescent voltage-

sensitive dyes to record pre-synaptic activity in trigeminal nuclear complexes, $GABA_A$ agonists failed to reduce primary afferent terminal discharge in injured animals compared to sham treated animals, and this was reversed by the application of bumetanide, an NKCC1 inhibitor (Wei et al., 2013). Importantly, a conditional knock out of the β-3 subunit of the $GABA_A$ receptor in the voltage-gated sodium channel 1.8 expressing primary afferent population showed spontaneous mechanical and heat hypersensitivity, which was not further altered by nerve injury (Chen et al., 2014), which implies that the hypersensitivity seen following nerve injury is at least partially dependent on a loss of pre-synaptic inhibition. These effects were recapitulated with the application of BDNF, and inhibition of BDNF signalling following nerve injury prevented the change in GABA conductance, $GABA_A$ receptor potential, and behavioural sensitivity, suggesting BDNF plays an important role in regulating pre-synaptic inhibition in the DH after nerve injury (Chen et al., 2014). Taken together, these data indicate an important role for pre-synaptic inhibition in the generation of hypersensitivity following peripheral nerve injury.

1.5.2.3 Sprouting of A Fibre Terminals

The sprouting of A-fibres from deep to superficial laminae one week following traumatic nerve injury has been proposed to drive hypersensitivity after peripheral nerve injury (Woolf et al., 1992). Here, Woolf et al. demonstrated that exogenous cholera toxin β subunit transported by A-fibres, began to occupy the superficial DH following injury. Single axon tracing was also performed which suggested A fibres began to sprout terminals into superficial laminae. This sprouting was suggested to contribute to allodynia following nerve injury, as A-fibre sprouting into lamina I could potentially allow innocuous signals to gain access to nociceptive projection pathways.

However, this study is now controversial and the consensus is that, although this is

an attractive hypothesis, such sprouting of low threshold A fibre mechanoreceptors does not occur. Firstly, the tracing method used is not specific to A-fibres following nerve injury (Shehab et al., 2003, 2004). Secondly, the findings of individual axon fills could not be replicated. Following axotomy, low threshold A fibres were not found to sprout into lamina II, and the only A-fibres found to project into this region were Aδ fibre nociceptors which are known to project to lamina II in the intact DH (Woodbury et al., 2008).

1.5.2.4 Loss of C Fibre Terminals

Transganglionic degenerative atrophy, which involves the degeneration of primary afferent C fibres within lamina II of the DH, has been reported following nerve lesions (Csillik and Knyihár-Csillik, 1981; Tajti et al., 1988), which is reported to occur and recover following a crush injury (Csillik and Knyihár-Csillik, 1981) as well as local administration of vinka alkaloids (Csillik and Knyihár-Csillik, 1982). Analysis of synapses from glomeruli derived from C-fibres reveals a loss of synapses progressively over the course of two weeks in transection (Castro-Lopes et al., 1990) and a loss followed by recovery in constriction injury (Bailey and Ribeiro-da Silva, 2006).

This data supports the view that blockade of neurotrophic signals, by nerve lesion or blockade of axonal transport, leads to a loss of C-fibre synapses within the DH. Is it possible to reconcile this loss of input with the gain-of-function associated with neuropathic pain states? The non-peptidergic population of C-fibres appear to be most vulnerable in terms of terminal loss/withdrawal. This population is important in mediating noxious mechanosensation (Cavanaugh et al., 2009), as shown by targeted ablation. However, their terminals express prostate acid phosphatase (Zylka et al., 2008), an enzyme that generates adenosine, which acts to suppress nociceptive signalling within the DH; in which respect the loss of such terminals would be maladaptive. The loss of C-fibre input may also help

to facilitate A-fibre access to nociceptive pathways, through homeostatic adaptation of DH circuitry, which has lost input (see Section 1.5.3.3).

Furthermore, a distinction between the injured region itself, and adjacent regions which contain intact afferent input and drive the evoked behaviours, should be made. Whereas C fibres in the locus of injury may break synaptic contact with the dorsal horn, the effects of this loss on adjacent uninjured afferents through homeostatic plasticity may influence subsequent signalling in these circuits.

1.5.3 Peripheral Nerve Injury: Effects on the Dorsal Horn

It is well acknowledged that central plasticity plays a role in the hypersensitivity seen following peripheral nerve injury (Woolf and Salter, 2000; Ji et al., 2003; Drdla and Sandkuhler, 2009). Understanding which molecules, cells and circuits are affected by neuropathic pain states is important in defining the functional consequences of nerve injury, as well as indicating potential targets for therapy. Below is a review of the evidence of dorsal horn alterations following peripheral nerve injury.

1.5.3.1 Altered Excitatory and Inhibitory Processing Following Neuropathy

As previously reviewed, primary afferents display spontaneous activity after peripheral nerve injury, and this input is believed to contribute to activity-dependent plasticity between primary afferent terminals and DH neurons (Drdla and Sandkuhler, 2009; Latremoliere and Woolf, 2009; Sandkühler, 2009). Another important observation is the reduction in GABA and glutamic acid decarboxylase following traumatic nerve injury (Castro-Lopes et al., 1993; Moore et al., 2002), which results in a reduction in inhibitory tone.

Previous work has investigated the loss of inhibitory tone, with electrophysiological studies of lamina II neurons showing reduced inhibitory post-synaptic potentials in magnitude, incidence and duration following partial peripheral nerve injuries (Moore et al., 2002; Scholz et al., 2005) (Figure 1.7A). Analysis of the inhibitory post-synaptic potentials (Moore et al., 2002) suggested a reduction in GABA release, and other studies have found a reduction in GABA secretion from stimulated spinal cord sections (Lever et al., 2003), and significant reductions in GABA immunoreactivity within the dorsal horn (Castro-Lopes et al., 1993; Ibuki et al., 1997). This evidence suggests a loss of GABAergic neurons, which has been demonstrated in some studies (Castro-Lopes et al., 1993; Scholz et al., 2005), and some evidence suggests that apoptosis drives the loss of inhibitory interneurons (Moore et al., 2002; Scholz et al., 2005) following peripheral nerve injury (Figure 1.7B).

Recent work has highlighted the loss of putative inhibitory terminals following peripheral nerve injury, that mirrors the temporal and spatial alterations in presumed IB4+ primary afferent synapses (Lorenzo et al., 2014). GAD65 immunoreactive puncta, representing terminals of inhibitory interneurons, were found to be significantly reduced 3-4 weeks after nerve injury in the superficial DH (Figure 1.7B). Whether this reflects a dying back of primary afferent fibres in this region, and the subsequent loss of pre-synaptic inhibitory control on these terminals or represents reorganisation of other circuits within the DH remains unknown.

The exact nature of the loss of inhibitory tone remains controversial, as other studies have suggested no loss of GABAergic boutons or $GABA_A$ $\beta 3$ subunits in denervated dorsal horn following nerve injury (Polgár and Todd, 2008), and no loss in the proportion of GABAergic neurons (Polgár et al., 2003), nor the total number of neurons in lamina I-III (Polgár et al., 2004, 2005). Furthermore, in these studies markers for apoptosis were

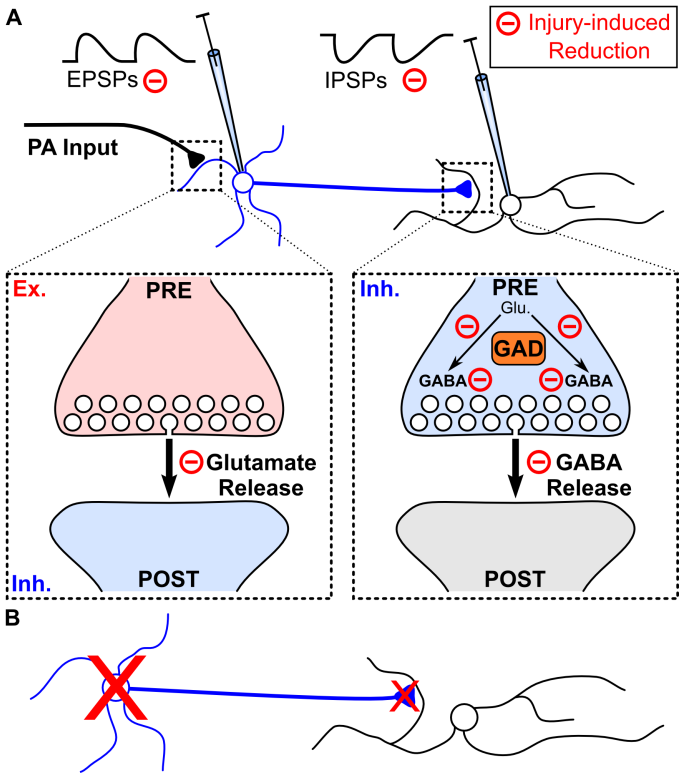

Figure 1.7: **Loss of inhibitory tone after peripheral nerve injury. A:** Electrophysiological studies have demonstrated a reduction in excitatory and inhibitory post-synaptic potentials (EPSPs & IPSPs) measured on inhibitory interneurons or superficial dorsal horn neurons, respectively. These have been related to reduced transmitter release, and with reductions in GAD and GABA levels in inhibitory terminals. **B:** Some studies have indicated a loss of inhibitory terminals as well as inhibitory interneurons in the dorsal horn after nerve injury. EPSP, excitatory post-synaptic potential; IPSP, inhibitory post-synaptic potential.

not co-localised with neuronal cells, but instead found in microglia (Polgár et al., 2005).

A different mechanism that may account for inhibitory tone reduction without the frank loss of inhibitory interneurons was recently described. Measurement of miniature excitatory post-synaptic potentials were shown to be reduced in GABAergic neurons of neuropathic animals (Figure 1.7A), and measurement of paired-pulse ratios suggested a reduction in primary afferent transmitter release may explain the decline in inhibitory tone (Leitner et al., 2013). This study did not find any changes in the density or morphology of dendritic spines or the number of excitatory synapses on inhibitory neurons, consistent with a pre-synaptic effect on primary afferent neurotransmitter release (Figure 1.7A).

A further promising mechanism that may account for reduced inhibitory tone without a loss of GABAergic neurons relates to the down-regulation of KCC2. This ion pump, along with NKCC1, regulates the chloride concentrations within neurons, and thus regulates neuronal responses to $GABA_A$ receptor activation. Following nerve injury, a reduction in KCC2 leads to impaired chloride homeostasis resulting in reduced inhibitory tone (Coull et al., 2003). Further work has demonstrated that enhancing KCC2 activity after nerve injury can restore normal response characteristics of spinothalamic tract NS neurons (Lavertu et al., 2014), and normalise behavioural hypersensitivity seen following peripheral nerve injury (Gagnon et al., 2013).

1.5.3.2 Altered Structure and Function of Projection Neurons

Anatomical evidence has revealed alterations in dendritic spines on deep DH WDR projection neurons, as determined by anatomical characteristics, following traumatic nerve injury, and these effects correlated with electrophysiological alterations of WDR neurons showing hyper-excitability to a range of stimuli (Tan et al., 2011) (Figure 1.8A). Crucially, administration of a drug that selectively inhibited Ras-related C3 botulinum toxin sub-

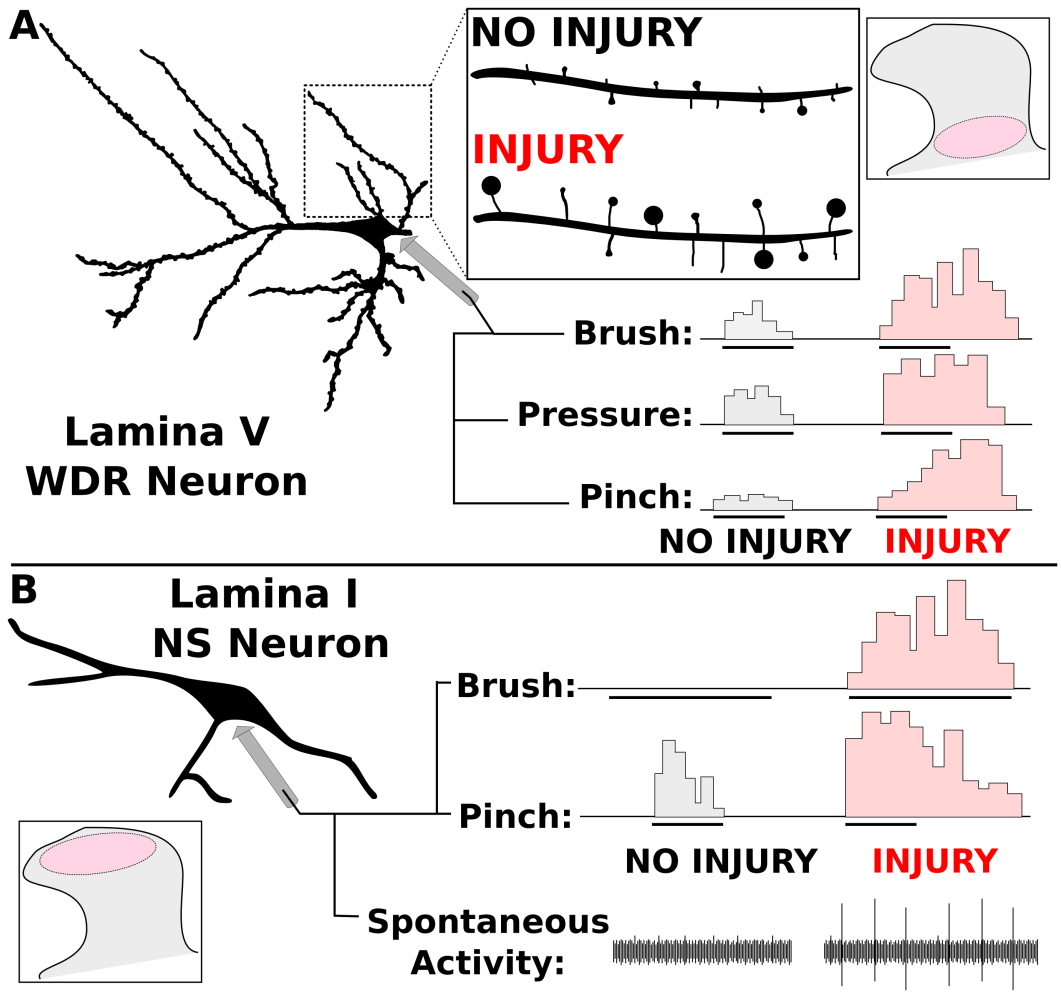

Figure 1.8: **Deep and superficial projection neuron structure and function changes. A:** Lamina V neurons display altered dendritic spine dynamics, with increased average length and spine head size. Responses to brush, pressure and pinch are amplified, with longer after-discharges. **B:** Lamina I neurons show novel responses to brush inputs after injury, and exaggerated responses to noxious mechanical pinch stimuli. These neurons also show higher levels of spontaneous activity.

strate 1 (known as Rac1), a key molecule involved in dendritic spine plasticity, resulted in attenuation of behaviour sensitivity, dendritic spine remodelling, and WDR neuronal hyper-excitability. Further work from this group has shown a similar response to WDR neurons to diabetic-induced neuropathy (Tan et al., 2012). Thus, dendritic spine remodelling on WDR neurons may contribute in general to the neuropathic pain phenotype. Electrophysiological changes to WDR neurons that have been observed include increased spontaneous activity, enlargement of receptive field size, and reduced C-fibre threshold with increased C-fibre responses (Liu et al., 2011; Tan et al., 2011).

Lamina I projection neurons appear to respond to innocuous inputs after nerve injury, which may contribute to mechanical allodynia in neuropathic pain states. Using extracellular recording, lamina I projection neurons of the spino-parabrachial pathway have been shown to generate spontaneous activity, respond to innocuous inputs, and produce an amplified response to nociceptive inputs following peripheral nerve constriction (Keller et al., 2007) (Figure 1.8B). Further work has indicated the ability for C-fibre input onto lamina I projection neurons to induce long term potentiation, even at physiologically active levels in the intact cord (Ikeda et al., 2006), which can sensitise other inputs (Fenselau et al., 2011), implying that spontaneous C-fibre input, as is seen after peripheral nerve injury (Liu et al., 2000a), may sensitise this projection pathway.

Consistent with this idea, ablation of NK1 receptor-expressing cells in the DH, many of which are lamina 1 projection neurons (Todd et al., 2000), reduces the mechanical hypersensitivity seen following nerve injury (Nichols et al., 1999). Considered with the evidence of rewiring of specific elements within the DH to gate innocuous inputs to these projection neurons (see Section 1.5.3.3), the lamina I projection pathway appears to play an important role in the production of neuropathic pain symptoms.

1.5.3.3 Dorsal Horn Rewiring

Many of the dorsal horn circuits previously reviewed have been shown to be affected by nerve injury. Lu et al. demonstrated a circuit between PKCγ excitatory interneurons in lamina II inner and glycinergic neurons in lamina III, which produced a feed forward inhibitory gate of Aβ input, preventing Aβ potentials reaching lamina I projection neurons (Lu et al., 2013). Following peripheral nerve injury, Lu et al. showed that the glycinergic inhibitory interneuron connection to the PKCγ excitatory interneuron became weaker, which thus allowed the PKCγ interneuron to excite lamina I projection neurons with

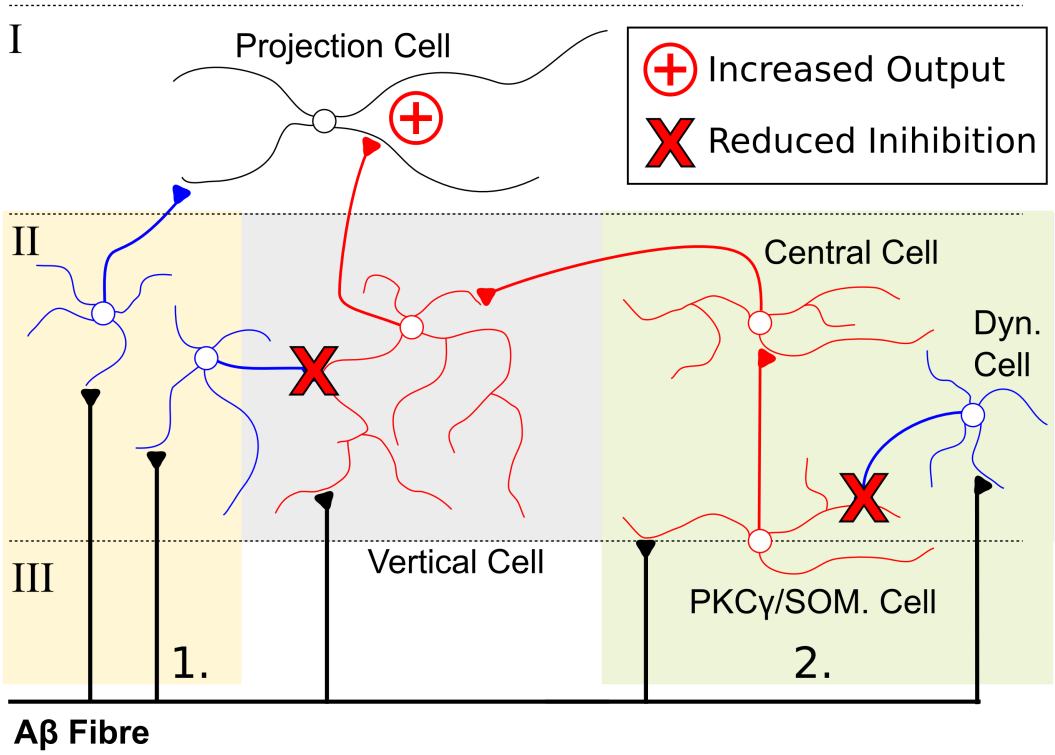

Figure 1.9: **Aβ fibres gain access to lamina I projection neurons after nerve injury.** Both identified pathways that can potentially lead Aβ input to projection neurons are affected. 1. Inhibitory Vertical Cells show reduced inhibitory drive to excitatory vertical cells, removing the inhibitory gate and allowing Aβ stimulation to evoke activity in lamina I neurons. 2. The dynorphin inhibitory interneurons show reduced inhibitory tone, resulting in increased access of Ab input to excitatory neurons in lamina II, resulting in increased lamina I projection neuron activation.

Aβ input. Therefore, under neuropathic pain conditions, the gate had been removed, allowing innocuous input to gain access to nociceptive-specific projection pathways (Lu et al., 2013) (Figure 1.9).

Elaborating on this work, Duan et al. showed that ablation of somatostatin-positive neuron results in complete loss of mechanical hypersensitivity following peripheral nerve injury, with no effect on heat hyperalgesia (Duan et al., 2014). Ablation of the dynorphin-positive inhibitory neurons did not change the mechanical hypersensitivity after nerve injury (Figure 1.9). These results indicate that Aβ fibres can gain access to lamina I projection neurons after nerve injury, and that this may be mediated through two parallel pathways.

Whilst it has been shown that the feedforward inhibition has been reduced in these

studies, allowing Aβ input to reach lamina I, these studies did not explore why inhibition is reduced. This may reflect many of the changes to inhibitory tone previous reviewed (see Section 1.5.3.1), however another possibility could relate to the observed loss of C-fibre terminals (Bailey and Ribeiro-da Silva, 2006), which may interfere with these circuits.

1.5.4 Plasticity in Descending Controls Following Peripheral Nerve Injury

Plasticity of descending modulation from the brainstem is involved in central sensitisation in abnormal pain states and acts alongside the spinal events. Descending pain facilitation can promote a chronic pain state that persists long after the initial lesion has healed. Prolonged noxious stimulation also causes pronounced changes in the activity of nociceptive modulatory neurons in the RVM (Morgan and Fields, 1994), which is implicated in the development of central sensitisation and secondary hyperalgesia following noxious stimulation (Urban and Gebhart, 1997, 1999).

Descending facilitatory influences are also enhanced in neuropathy, possibly contributing to allodynia and hyperalgesia (Millan, 2002; Suzuki et al., 2004) and are purported to be involved in the maintenance of nerve-injury induced pain (Burgess et al., 2002; Vera-Portocarrero et al., 2006). DH neuronal responses to noxious stimuli are reduced in normal injury-free animals after lidocaine injection into the RVM and a greater effect is observed in nerve injured animals (Bee and Dickenson, 2007). Here, descending modulation from the RVM influences neuronal responses to non-noxious tactile stimulation, suggesting a possible mechanism for mechanical allodynia.

Nerve injury is associated with enhanced descending 5HT excitatory drive, and specifically the $5HT_3$ receptor is implicated (Porreca et al., 2002; Suzuki et al., 2004; Ossipov et al., 2010). The contribution of descending serotonergic facilitation in neuropathic pain

states is further confirmed by experiments showing a significantly enhanced ability of $5HT_3$ antagonist ondansetron to suppress spinal responses to mechanical punctate stimulation in spinal nerve ligated animals (Suzuki et al., 2005). In osteoarthritic rats there is evidence of an adaptive change in the excitatory serotonergic drive (Rahman et al., 2009).

Many drugs that have efficacy in neuropathic pain take advantage of descending control systems. The state-dependency of pregabalin and gabapentin is reliant on upregulation of $5HT_3$ receptor mediated descending facilitation (Suzuki et al., 2005). Peripheral nerve injury can cause a loss of neurons in the RVM (Leong et al., 2011). While 5HT actions are enhanced in some chronic pain states, descending inhibitory noradrenergic pathways may also undergo plastic changes and become down regulated.

In nerve-injured animals, the efficacy of atipamezole, an α2 adrenoceptor antagonist, is shown reduced in specific sensory modalities. In contrast, low intensity mechanical stimulation in sham-operated rats was shown significantly enhanced (Rahman et al., 2008). These results suggested a lack or suppression of descending inhibition of DH neurons via spinal α2 adrenoceptors for low intensity mechanical stimuli. Enhanced efficacy of spinally administered α2 adrenoceptor agonists (Mansikka and Pertovaara, 1995; Tsuruoka et al., 2003), increased noradrenergic innervation to DH (Ma and Eisenach, 2003) and upregulation of spinal α2 adrenoceptors and increased spinal cord NA content (Satoh and Omote, 1996) all indicate profound alterations to descending adrenergic inputs to the dorsal horn in neuropathic pain.

A recent paper addressed the clinically relevant question of why only a minority of patients develop chronic neuropathic pain following the same nerve lesion (De Felice et al., 2011). The suggestion from the authors that a descending noradrenergic mechanism could actually protect from pain put brain to spinal cord pathways once again at the forefront of pain modulation, and implies that neuropathic pain could ultimately depend on altered

descending input.

1.5.5 Glial Cells React to Peripheral Nerve Injury

Concomitant to the multitude of mechanisms relating to neuronal connectivity and synaptic plasticity following nerve lesion reviewed above, glial cells present within the dorsal horn also show substantial changes as a result of peripheral nerve injury (Cao and Zhang, 2008; Nakagawa and Kaneko, 2010). The glial reaction ("gliosis") seen after peripheral nerve injury is characterised by cell proliferation, hypertrophy, and increased expression of various markers within microglia and astrocytes within and adjacent to the central innervation territories of injured primary afferent neurons (O'Callaghan and Miller, 2010; Nakagawa and Kaneko, 2010). These two cell types and their contribution to the neuropathic pain phenotype will be considered in turn.

1.5.5.1 Microglia Respond to Peripheral Nerve Injury

Microglial cells constitute 10% of all cells within the CNS (Greter and Merad, 2013; Salter and Beggs, 2014), and whilst widely referred to as the macrophages of the brain, microglia show a distinct developmental progression from primitive erythromyeloid progenitors in ectodermal tissues (Ginhoux et al., 2010; Schulz et al., 2012; Greter and Merad, 2013; Kierdorf et al., 2013), and appear to populate the brain during development and then maintain this population through self-renewal, persisting independently of hematopoietic stem cell replenishment, unlike macrophages (Ajami et al., 2007; Schulz et al., 2012; Salter and Beggs, 2014). Microglia also depend on different developmental signals to macrophages (Erblich et al., 2011; Schulz et al., 2012; Kierdorf et al., 2013), and possess a unique transcriptome relative to circulating macrophages (Hickman et al., 2013; Butovsky et al., 2014). Given these differences with the principle immune cells of the body, questions

relating to non-inflammatory functions of resident microglia within the CNS have been raised (Salter and Beggs, 2014).

The possible roles of microglia independent of inflammatory processes has received greater interest following the important discovery that microglial processes in "resting" microglia were found to be highly motile, and appear to continuously assess and scan their surroundings (Nimmerjahn et al., 2005; Davalos et al., 2005). This constant surveillance brings microglial processes into close apposition with dendritic spines, synaptic contacts, and astrocytic perisynaptic contacts; and thus microglia are well positioned to respond to neuronal activity (Wake et al., 2009; Tremblay et al., 2010). Microglia possess a multitude of neurotransmitter receptors (Kettenmann et al., 2011), and more recent evidence has shown these cells can phagocytose synapses and dendritic spines via a complement-mediated signaling pathway (Stevens et al., 2007; Wake et al., 2009; Tremblay et al., 2010; Schafer et al., 2012; Kettenmann et al., 2013). The functions of microglia are now being recognised as important for synapse maturation, synaptic plasticity, and for a multitude of CNS diseases (Salter and Beggs, 2014).

Concomitant with these functions of resident microglia in the CNS in the absence of injury, an important development within the dorsal horn after peripheral nerve lesion is the subsequent microgliosis within and around the central territories of injured afferents (Eriksson et al., 1993; Beggs and Salter, 2007, 2013). A number of observations suggest that this response is intimately linked to the hypersensitivity associated with peripheral nerve injury: administration of lipopolysaccharide, a potential activator of microglia, spinally results in hypersensitivity (Clark et al., 2009, 2010), and injection of stimulated microglial cells intrathecally results in hypersensitivity within the relevant peripheral dermatomes (Tsuda et al., 2003; Coull et al., 2005). Furthermore, a number of signalling cascades have been identified in microglia which are essential for the microgliosis, as well

as the hypersensitivity, seen after peripheral nerve injury.

$P2X_4$ receptors respond to adenosine triphosphate (ATP), and are upregulated on microglia following peripheral nerve lesions (Tsuda et al., 2003). These receptors have been shown to be essential for the mechanical hypersensitivity seen following peripheral nerve lesion, as removal of $P2X_4$ eliminates mechanical hypersensitivity seen after peripheral nerve lesion (Ulmann et al., 2008; Tsuda et al., 2009). Following stimulation of microglia by ATP, a signalling cascade culminating in the release of BDNF from microglia is initiated (Trang et al., 2009), with BDNF release ultimately affecting dorsal horn neuron excitability (Ulmann et al., 2008), through reduction of KCC2 (Coull et al., 2005) and altered dorsal horn projection neuron output (Keller et al., 2007).

Fractalkine and it receptor CX3CR1 is another crucial signalling cascade important in microglial responses after peripheral nerve injury (Clark and Malcangio, 2014). Fractalkine is present on dorsal horn neurons in the spinal cord, whereas CX3CR1 is present on microglial cells (Jung et al., 2000; Verge et al., 2004; Lindia et al., 2005; Clark et al., 2009). Intrathecal administration of the chemokine domain of fractalkine results in thermal and mechanical hypersensitivity, which is dependent on CX3CR1 (Milligan et al., 2004; Clark et al., 2007; Zhuang et al., 2007). CX3CR1 stimulation results in p38 phosphorylation in microglia (Clark et al., 2007; Zhuang et al., 2007), and subsequently the release of pro-inflammatory mediators such as interleukin-1β, interleukin-6 and nitric oxide (Milligan et al., 2005).

This pathway is important in the hypersensitivity seen after peripheral nerve injury. CX3CR1 is strongly upregulated in the dorsal horn on microglia following peripheral nerve lesion (Verge et al., 2004; Lindia et al., 2005; Zhuang et al., 2007), and soluble fractalkine levels in the cerebrospinal fluid of the dorsal horn is highly elevated (Clark et al., 2009). Administration of sequestering antibodies targeted towards fractalkine or CX3CR1 can

ameliorate hypersensitivity due to nerve injury (Milligan et al., 2004; Clark et al., 2007; Zhuang et al., 2007), and this behavioural phenotype is related to reduce phosphoylation of p38 within microglia (Zhuang et al., 2007). Consistent with these observations, knock out of the CX3CR1 receptor displays reduced thermal and mechanical hyperalgesia following peripheral nerve injury (Staniland et al., 2010), and this correlated to reduce microgliosis in these knock out mice.

To understand the effects of stimulation of CX3CR1 and the subsequent release of pro-inflammatory cytokines, further work has shown that interleukin-1β enhances primary afferent glutamate release via presynaptic NMDA receptors (Yan and Weng, 2013), as well as lead to the down-regulation of glial glutamate transporters (Yan et al., 2014), both resulting in enhanced excitability of the dorsal horn.

Finally, the mechanism leading to fractalkine liberation has been recently explored. Cathepsin S is upregulated in microglia in the dorsal horn following peripheral nerve injury, which can cleave fractalkine on dorsal horn neurons (Clark et al., 2007), which occurs in a $P2X_7$ receptor-dependent manner (Clark et al., 2010). Cathepsin S has been shown to be an essential step in this process, as intrathecal or systemic administration of cathepsin S inhibitors has shown efficacy in reversing established neuropathic pain hypersensitivity to varying degrees (Barclay et al., 2007; Clark et al., 2007; Irie et al., 2008; Zhang et al., 2014a).

In summary, microglia respond to peripheral nerve injury in the dorsal horn, and are intimately related to the development of neuropathic hyperalgesia through two key intracellular signals, $P2X_4$-dependent and $P2X_7$/Fractalkine dependent pathways, which result in the release of various signalling molecules and ultimately, an increase in dorsal horn excitability.

1.5.5.2 Astrocytes React to Peripheral Nerve Injury

Astrocytes have traditionally been viewed as passive support cells in the CNS, where they aid neuronal function passively through roles in energy metabolism, potassium buffering, blood brain barrier formation and maintenance, and neurotransmitter recycling; however, increasingly these cells are being seen as active players in neuronal function, including roles in synaptogenesis, regulating neurotransmission, and synapse elimination (Seth and Koul, 2008; Wang and Bordey, 2008). Astrocytes share a common neuroepithelial origin to neurons and oligodendrocytes, emerging from the neuroectoderm (Sloan and Barres, 2014; Molofsky and Deneen, 2015). However, recent transcriptome analysis has revealed these cells possess a unique gene profile from both neurons and oligodendrocytes, underlining their specific role within the CNS (Cahoy et al., 2008; Zhang et al., 2014b).

Astrocytic function in the healthy brain has been radically reviewed following a series of illuminating observations, placing astrocytes as star players in the role of CNS processing (Seth and Koul, 2008; Wang and Bordey, 2008; Svensson and Brodin, 2010). Astrocytes can sense neuronal activity by a multitude of receptors, which can lead to calcium mobilisation (Fiacco and McCarthy, 2006; Wang and Bordey, 2008; Volterra et al., 2014). Calcium transients within astrocytes have been shown *in vivo* to correspond tightly with neuronal activity (Hirase et al., 2004; Wang et al., 2006; Winship et al., 2007; Schummers et al., 2008), and astrocytic depolarisations have been shown to be selective and exhibit some form of short-term plasticity (Linden, 1997; Pasti et al., 1997), and can signal to other neurons in the CNS (Perea and Araque, 2005), implying an important role for astrocytes in information processing in the brain.

Alongside these vital functions, astrocytes react to peripheral nerve injury in the corresponding central terminal region of injured afferents within the dorsal horn (McMahon and Malcangio, 2009; Svensson and Brodin, 2010). This gliosis presents as a slowly gen-

erating yet persistent increase in astrocytic cell processes, the cell marker glial fibrillary acidic protein (GFAP), and cell hypertrophy (Ma and Quirion, 2002; Guo et al., 2007; Hald et al., 2009; Svensson and Brodin, 2010). Mitogen-activated protein kinases have been implicated in astrocytic activation, and appear to play a critical role in pain sensitisation after peripheral nerve injury (Ma and Quirion, 2002; Zhuang et al., 2006; Ji et al., 2009). Both extracellular signal-regulated kinase and c-Jun N-terminal kinase were shown to co-localise to GFAP in the dorsal horn after peripheral nerve injury (Ma and Quirion, 2002), and inhibition of c-Jun N-terminal kinase pharmacologically was able to reverse and prevent the hypersensitivity seen after peripheral nerve lesion (Zhuang et al., 2006). These data suggest mitogen-activated protein kinases play an important role in astrocytic responses to peripheral nerve injury.

Two key mechanisms by which astrocytes impinge on neuronal function after peripheral nerve injury include the dys-regulation of glial glutamate transporters, and the release of glutamate from astrocytes (Binns et al., 2005; Tawfik et al., 2008; Xin et al., 2009; Bardoni et al., 2010). Glial glutamate transporters are downregulated on astrocytes following nerve injury (Binns et al., 2005; Xin et al., 2009), and reversal in this downregulation by propentofylline can reverse the hypersensitivity seen after axotomy (Tawfik et al., 2008). Further evidence indicates that astrocytes can actively release glutamate within the CNS (Jourdain et al., 2007; Perea and Araque, 2007), and in the dorsal horn this mechanism has been suggested to underlie slow inward currents detected in substantia gelatinosa (lamina II) neurons, which are also present after injury that induced hypersensitivity (Bardoni et al., 2010).

1.5.6 Summary

In summary, neuropathic pain presents with a multitude of complex interacting mechanisms, of which the general consequence is increased neuronal excitability, potentiation of synaptic contacts, and a reduction in inhibitory tone, at either a local level or from descending supraspinal centres. A great deal of knowledge has been gained from studying the molecules, cells and circuits within the dorsal horn; yet translation of these findings to clinical treatments remains frustrated (Percie du Sert and Rice, 2014; Baron, 2009). Although a vast volume of data has been acquired on the molecular, cellular and circuit-level basis for hypersensitivity seen after neuropathic pain, it appears further insights are required to build a more holistic picture of the complex changes which are occurring after nerve lesion. A key aspect affecting progress in research is exploiting the development of new techniques which allow us to observe the system, in this case the dorsal horn, and the complex inter-relationships between its components with greater clarity than before, which may help connect previous work, or indeed open new avenues of discovery.

In terms of developing a deeper understanding of the consequences of neuropathic pain, finding new approaches to observing synapses and synaptic plasticity may provide novel insights into its mechanisms. Thus, next is reviewed methods for studying connectivity, specifically synaptic contacts, with an emphasis on quantitative anatomical techniques.

1.6 Analysis of Synapses using Anatomical Methods

1.6.1 The Development of Histological and Light Microscopical Approaches to Synapse Research

The observation of the ultrastructure of the synapse with electron microscopy has provided important insights into synaptic structure and function (see Section 1.2), and helped to

shape the current view of the synapse. Electron microscopy has also contributed to the development of subcellular fractionation of synaptic PSDs (Cotman et al., 1974; Cohen et al., 1977; Matus and Taff-Jones, 1978; Carlin et al., 1980), which helped to visualise the synaptosome and synaptic vesicle preparations and confirm their purity prior to any biochemical analyses. The development of subcellular methodologies to isolate synaptic PSDs (Cotman et al., 1974) was crucial in analysing the diversity of synaptic proteins, and has laid a solid foundation for our understanding of synapses at the molecular level.

These analyses also allowed the first antibodies to be developed against synaptic proteins (Cho et al., 1992; Hunt et al., 1996), which introduced the possibility of visualising synapses at the light-microscope level with immunohistochemistry. Visualisation of synaptic proteins in this manner proved difficult (Hunt et al., 1996; Kim et al., 1996; Bassand et al., 1999; Valtschanoff et al., 1999), until the development of antigen retrieval methods to allow antibody access to the synaptic protein cluster (Watanabe et al., 1998; Fukaya and Watanabe, 2000). Pepsin treatment provided a key method by which adequately fixed tissue could be stained for synaptic proteins.

Electron microscopists have been wary of the use of light microscopical methods to study synapses, with the principle criticisms concerning the limited resolution and the inability to confirm whether fluorescent puncta really are functional synapses (Bolam, 1992; Briggman and Denk, 2006; Kuwajima et al., 2013). Whilst these criticisms are legitimate, they do not negate the study of synapses at the level of light microscopy.

Developments in imaging methods over the past few decades have greatly enhanced the resolution attainable with light microscopy. First, the development of the confocal (Davidovits and Egger, 1969; Conchello and Lichtman, 2005), and then the two-photon (Denk et al., 1990; Helmchen and Denk, 2005), microscope greatly improved resolution in the axial plane. These methods allowed the labour-free 3D reconstruction of fluorescent

objects in histological preparations (Conchello and Lichtman, 2005), and have been used to analyse synapses and dendritic spines, which have dimensions close to the resolution limit of the system (Briggman and Denk, 2006). More recently, the development of super-resolution imaging methodologies have extended this resolution improvement for light microscopy (Tønnesen and Nägerl, 2013), which can now achieve true nanoscale resolution.

Post-image processing also has the capacity to further improve the resolution of fluorescent images. Deconvolution is a post-image processing method which aims to re-assign the blur associated with high-resolution imaging back to the original fluorescent object, which can produce an improvement in resolution up to two times in the lateral planes, and four times in the axial plane (Sibarita, 2005). More recently these methods have been applied to confocal (Cannell et al., 2006), and even two-photon (Noakes et al., 2001), microscopy.

Thus, the resolution limit for light microscopy is able to be improved using either computational techniques or new imaging methodologies.

Furthermore, these methods offer an advantage over traditional electron microscopical study: reconstructing the synapse in 3-dimensions using electron microscopy is very labour-intensive and time consuming (Harris and Stevens, 1989; Chklovskii et al., 2010; Kuwajima et al., 2013), whereas reconstructing entire synapses with the confocal microscope is a simple procedure (Conchello and Lichtman, 2005). Thus, 3D reconstruction is feasible for large numbers of synapses using laser-scanning imaging methods.

Due to the limited resolution, light microscopy cannot stain and observe the ultrastructure of synapses, such as individual vesicles or docking sites, which can make it difficult to confirm whether synapses have been observed, or staining is indicating the localisation of the marker used to other structures. However, the specificity of certain

markers such as synapsin, synaptophysin, PSD-95, gephyrin and other important structural proteins at the synapse; both by their apposition as pre- and post-synaptic proteins on confocal images (Kirsch and Betz, 1993; Watanabe et al., 1998; Fukaya and Watanabe, 2000; Choii and Ko, 2015), and by confirmation of staining at the ultrastructural level (Micheva et al., 2010; Kay et al., 2013; Collman et al., 2015) have provided important evidence that suggests these markers are specific for synapses. Previous work has aimed to utilise synapse-specific proteins to highlight synaptic contacts between histologically labelled cells with success (Wouterlood et al., 2003).

Once again, the immunofluorescence method reveals an advantage in this regard over electron microscopy. Since fluorescence signals naturally produce a distinct signal against a dark background (with sufficient signal:noise), fluorescence immunohistochemical images obtained on the confocal microscope are well suited for automated image analysis methodologies, which in theory could greatly increase the sampling of synapses, and dramatically reduce the degree of manual intervention during image processing. Electron microscopy has struggled in this regard, although some efforts in automating synapse analysis at the electron microscopy level have been previously described (Helmstaedter et al., 2013; Navlakha et al., 2013; Kim et al., 2014).

Thus, whereas electron microscopy is well suited to studying the ultrastructure of a small number of synapses in great detail, histological and light microscopical methods provide an ability to reconstruct large numbers of synapses in 3 dimensions, which can be interrogated to understand the synapse at a population level (Burette et al., 2015). This level of analysis moves away from the descriptive studies commonly performed at light- and electron- microscopy levels, and into the realm of quantitative understanding of the synaptome. Understanding the diversity of synapses across different brain regions will be vital to understand how they function and respond to activity, as described in Section

1.2.4.

1.6.2 Automated Image Processing Methods

Fluorescence immunohistochemical interrogation of synaptic populations is well suited to automated image analysis methods, due to the clear delineation between object signal and background ascertained with such preparations. Here an overview of appropriate methods for such an analysis paradigm are reviewed.

Computer vision and artificial intelligence research has attempted to endow a computer, via algorithmic implementations, with the capacity to interpret and understand images; and whilst progress on this important problem has been made, the abilities for machines to perform this task effectively across different types of images is very limited. Interpretation can be considered a mapping from the raw image data to a model which allows the extraction of the semantic meaning of the image. This distinction between the raw image pixel values, and the final model used to interpret the images is defined as the Semantic Gap, and defines the central problem in automated image processing (Gonzalez and Romero, 2010; Sonka et al., 2013).

Although the Semantic Gap and its solutions for different imaging problems are well described in the image analysis literature, real-world implementations of these workflows are often case-specific, and no universal workflow, or a method to automatically determine the optimal workflow, is available (Sonka et al., 2013). The task of developing an image analysis workflow is left to a human operator, which also requires significant work towards optimisation and verification of this process. Fluorescence images are unique as, in an ideal image, a strong fluorescent signal is present on objects of interest, with low background signal, and a generalised workflow in moving from this raw pixel data towards a model to extract the relevant information is presented below.

A common and flexible way of mapping fluorescence images to an appropriate model is to move from the raw pixel data to a model which isolates individual objects within the image for further analysis. This processing can be divided into steps summarised as low-level image processing, and methods designed to extract high-level image understanding (Gonzalez and Romero, 2010; Prodanov and Verstreken, 2012; Sonka et al., 2013).

Low-level image processing steps include methods designed to improve image quality, including noise filtering, deconvolution methods and image sharpening, and methods to isolate the objects of interest. The isolation of regions in the image of interest is typically achieved with segmentation methods, where pixels determined to consist of objects are isolated from pixels determined to be background. This segmentation can be achieved by edge-detection, histogram shape, or object attributes, and results in a binary image (Sezgin and Sankur, 2004; Prodanov and Verstreken, 2012).

Once the images have been processed to yield segmented objects against background, the next step is to extract the high-level image data. This is generally achieved through object labelling (Burger and Burge, 2008; Gonzalez and Romero, 2010), which allows the isolation and identification of each object within the image. Once the objects are labelled uniquely, each object can be isolated and measured in the desired manner.

Image processing utilising such a workflow has been previously described for nuclei (Russell et al., 2009; Ollion et al., 2013; Gul-Mohammed et al., 2014), gene and chromosome territories within nuclei (Gué et al., 2005; Iannuccelli et al., 2010), dendritic spines (Dumitriu et al., 2012), and pre-synaptic terminals illuminated with transgenic approaches (Heck et al., 2014). However, the success of this process is highly dependent on the signals obtained from the histological preparation under analysis.

1.6.3 Stereological Methods for Unbiased Sampling

Object measurement of a sample derived from a population of irregularly shaped objects can become biased due to the size, shape, orientation or distribution of these objects within the region they occupy. To overcome these issues, stereology emerged as a methodology, initially as an *ad hoc* method to compensate for 2-dimensional profile measurement in relation to 3-dimensional object measurement (so called assumption-based stereology, Abercrombie, 1946; Hedreen, 1998), but later extended to design-based methods that remove any assumptions of object size, shape or orientation (Sterio, 1984; Gundersen, 1986; Gundersen et al., 1988; Mayhew and Gundersen, 1996; West, 1999; Schmitz and Hof, 2005). These methods have proved important in establishing unbiased estimates of object number, but also of obtaining an unbiased sample for further measurement. Stereological methods thus ensure measurements made from a sample is representative of the population they come from, subject to sufficient sampling. Here a review of stereological methods is given, outlining the key advancements in this technique.

Stereology can be defined as a series of methods to allow the unbiased estimation of object measurements, principally inferring 3D object structure from 2D tissue sections. Original methods considered stereological, which are now referred to as assumption-based stereology, made inferences of 3D object number based on assumptions of the relation between 2D object profiles in tissue sections to the 3D object size (Abercrombie, 1946). These calculations provided a means of moving from 2D profile counts to 3D object counts.

However, these methods are not unbiased, which can lead to inaccurate data collection. Thus, assumption-based methods were superseded with design-based stereology, driven by the development of the Di-Sector probe (Sterio, 1984; Gundersen et al., 1988), which eliminated biases introduced during object analysis due to object size, shape or orientation.

The methods employed in stereology can be divided into two important categories:

1. Systematic random sampling.

2. Counting frames (such as the Di-Sector).

1.6.3.1 Systematic Random Sampling

Systematic Random Sampling (SRS) is a method of sampling which ensures an adequate spread of samples are obtained across the tissue section, whilst also maintaining the potential for any part of the tissue to be sampled. SRS is performed by initially selecting a starting point in the region to be sampled at random, and then systematically moving through the region by a pre-defined length to generate an array of samples that are evenly spaced throughout the region (West, 1999; Schmitz and Hof, 2005; West, 2013), see Figure 1.10.

This contrasts with simple random sampling, where samples are randomly selected from the region to be sampled. SRS has been demonstrated to reduce the coefficient of error (the error due to sampling) from a value proportional to $1/\sqrt{n}$ to $1/n$ when compared to simple random sampling (West, 1993), which implies that SRS provides a less variable and therefore more precise estimate of object measurements.

1.6.3.2 Counting Frames

For quantification, objects must be selected in an unbiased manner from sampled regions. This is achieved with a counting frame. By far the most popular counting frame in stereology is the Di-Sector, and on dedicated stereological workstations (where users quantify objects on the fluorescence widefield microscope, see the Stereo Investigator system by MBF Biosciences), a variant called the Optical Di-Sector is often employed.

Counting frames achieved an unbiased sample by only including objects according to

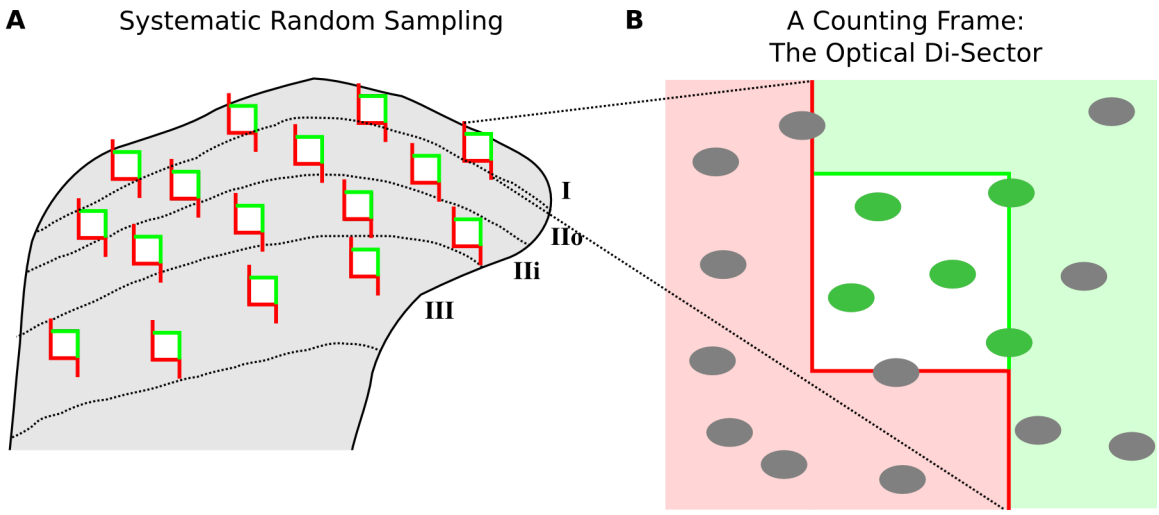

Figure 1.10: **Systematic random sampling and the counting frame. A:** An example of systematic randoms sampling over multiple regions of interest (here, laminae I-III of the dorsal horn). A random start position is selected, followed by a systematic shift in this position to place the desired number of counting frames. B: A counting frame used to quantify objects in an unbiased manner. The box contains two acceptance lines and two rejection lines. Objects within the counting frame and/or touching an acceptance line are counted (green objects); whereas any object outside the counting frame or touching a rejection line are rejected (grey objects).

specific rules. In the case of the Di-Sector rules, a series of rejection lines and inclusion lines are set up around the counting frame area in the lateral planes. Objects which touch a rejection line are automatically eliminated, whereas objects which are within the counting frame or cross an acceptance line are still counted (Sterio, 1984; West, 1993, 1999; Schmitz and Hof, 2005), see Figure 1.10. A similar rule is applied in the axial plane, where objects present in the first slice (the Reference Slice, which can be thought of as a rejection line in the Z-plane) are rejected, and only new objects which emerge as the image stack is traversed are quantified. This will include objects which are within the counting frame volume, but extend out of the bottom of the counting frame (which is where the inclusion line would reside).

By applying these rules, the counting frame volume is sampled in an unbiased manner, meaning objects of different sizes, shapes and orientations have the same chance of being quantified.

1.6.3.3 Automation in Stereology

Stereological methods have traditionally been applied via manual quantification methods. Indeed a recent study has highlighted the difficulties in attaining histological preparations and images of sufficient quality to perform stereological analyses with sufficient accuracy in an automated fashion (Schmitz et al., 2014). Although the authors reject the ability for current 3D detection methods to perform robust stereological analysis, improvements in histological processing, image acquisition and processing may provide the conditions for automated stereological methods to flourish.

Automation would provide a significant improvement to current stereological implementations, as it will allow the assessment of many thousands of objects, such as synapses, in a practical time frame. Given the huge numbers of synapses in any region of the CNS, the application of automation in a stereological fashion is well suited to this task.

A recent study delineating a methodology for the ultrastructural assessment of synapses on neurons labelled via the juxtacellular labelling method highlights this issue. This method offers the ability to correlate synaptic distributions across a cell of known morphology with its *in vivo* electrophysiological activity signature, which can provide the opportunity to link structure with activity (Henny et al., 2013). This approach will dramatically aid in understanding the computations performed by individual neurons, but the manual stereological assessment of synapses becomes impractical when attempting to analyse the synaptome of a whole brain region, due to the sheer number of synapses to be analysed.

1.6.4 Anatomical Methods Overview

The analysis of synaptic puncta has expanded from the detailed observations obtained using electron microscopy methods, and the biochemical procedures to isolate and study

proteins present at synaptic structures (research which continues to this day, Chklovskii et al., 2010; Bayés et al., 2011, 2012; Helmstaedter et al., 2013), to more recent developments utilising antigen retrieval methods with immunofluorescence, and modern imaging methodologies such as confocal, two-photon or super-resolution microscopy. These methods offer the ability to assess large numbers of synaptic puncta, which can contribute to understanding how synaptic distributions and phenotypes change in different conditions.

These datasets have the potential to benefit from automated image processing and analysis to extract relevant measures of synaptic objects. Through automation, increasingly larger samples can be processed, producing an more detailed level of understanding of synaptic populations across broader regions of the CNS. Some researchers have made some progress in this area. Array Tomography, which allows detailed fluorescence and electron microscopical analysis of CNS tissue is one methodology (Micheva et al., 2010; Kay et al., 2013; Collman et al., 2015), although the image analysis methods utilised remain labour intensive.

Finally, ensuring unbiased sampling via stereological methods is an essential aspect to quantitative anatomical analysis methodologies, and it would be desirable for any system designed to perform automated analysis to do so in a stereological manner. Although stereology is traditionally performed in a manual fashion, and current opinion states automated methods are not well suited for stereological analysis (Schmitz et al., 2014), one study does claim to perform automated stereological analysis of synaptic puncta using fluorescence microscopy (Dumitriu et al., 2012).

This paper would represent an important connection between histological methods, automated image analysis and stereological principles outlined above, which as yet has remained elusive. Critically, contrary to the authors claims (Dumitriu et al., 2012), this paper does not implement stereological methods, but is subject to a strong bias in size,

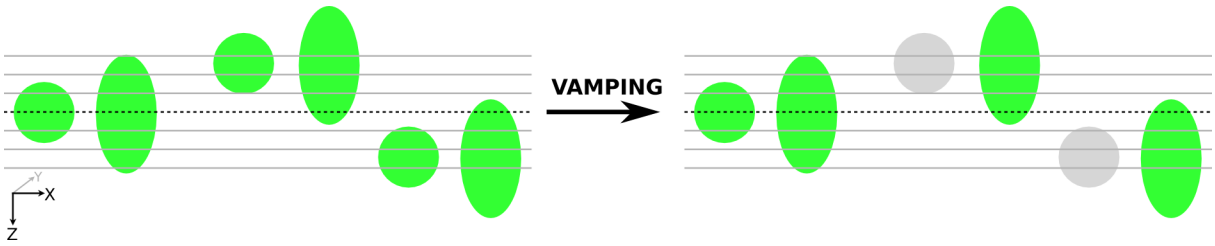

Figure 1.11: **Systematic bias in stereological assessment of objects derived from the Vamping method.** An X-Z projection of six objects is shown on the left. Vamping selects objects based on whether they are transected by a single selected Z slice (dashed black line). This is shown for the six example objects on the right, where two objects (grey) were rejected. This example indicates the bias introduced by vamping, where objects elongated in the Z plane have a higher chance of selection. Thus, the vamping method is biased towards selecting objects which are larger in the Z plane, have shapes which bias towards Z plane enlargement, or have their longest aspect oriented in the Z plane, and it is therefore not unbiased.

due to the implementation of the described vamping method (see Figure 1.11). Surprisingly, this method does not utilise the well-described antigen retrieval methods for the effective labelling of synaptic proteins, and little use is made of automated image analysis methodologies (for example, thresholding and much of the rest of the image processing is performed in a manual fashion). Thus, it falls far short of the promise of automated or stereological analysis, and it is unclear how reliable the staining, image processing methodology, or the resulting data is with this method.

It therefore appears apparent that a method which performs the detailed analysis of synaptic puncta at the light microscopical level, which utilises both automated approaches and implements stereological principles is not presently available, and such a method would be highly desirable for studying synaptic populations, and their modification throughout development, ageing, disease states and different environmental and genetic environments. The method should ideally produce robust synaptic fluorescence signal suitable for automated methods, and an optimised automated image analysis workflow which is capable of delivering unbiased, stereologically-relevant data without the need for manual quantification.

This method would serve as a great tool to investigate structural plasticity in synaptic

populations within the CNS, including the dorsal horn, and the effects to these populations following peripheral nerve injury. This method could also be used to investigate how known mechanisms relate to changes in synapse populations after peripheral nerve injury. For example, microglia have recently been implicated in synaptic alterations during development (Schafer et al., 2012), and are known to play an important role after peripheral nerve injury, and thus an investigation into their role in any alterations in synapse populations could be performed.

1.7 Aims

The principle aims of this Thesis are:

- To develop a workflow consisting of the marking, imaging, processing and analysis of samples of the synapse populations in the superficial dorsal horn.
- To analyse the synapse samples derived from the dorsal horn to discern any patterns within the synaptome of this region of the CNS.
- To compare synapses sampled from animals which have received a peripheral nerve injury to a SHAM surgery control group, to discern any anatomical neuroplastic changes as a result of peripheral nerve injury.
- To test the hypothesis that microglia may impact on putative changes in synaptic properties following peripheral nerve injury.

Chapter 2

Synapse Histology, Imaging & Analysis in the Dorsal Horn

2.1 Introduction

The dorsal horn provides the first step in somatosensory information processing, and is responsible for integrating information concerning submodalities of the somatosensory experience, via dorsal root ganglion neurons, with reflex circuitry in the ventral horn, as well as the organisms expectations, via descending control circuits, before transmission of this information to higher CNS centres. These processes all require synaptic integration of information, and so studying synapses within this region can provide important information concerning these processes. As previously outlined (see Section 1.6), a histological strategy may provide a novel approach to understanding large numbers of synapses, and yield useful data on the synaptic population. This Chapter therefore aims to establish the methodology to enable the visualisation, image acquisition, data processing and analysis of synaptic puncta using an unbiased approach.

First, the histological procedures used to visualise synaptic puncta are described. This

process includes the implementation of antigen retrieval methods, which aid in unveiling synaptic epitopes to subsequently applied antibodies. An important step involves the acquisition of confocal image stacks for accurate 3-dimensional (3D) representations, as well as sufficient sampling, of synaptic puncta. The optimised image acquisition method is given, which ensures images are in the required format for the subsequent image processing steps. Image processing consists of a number of steps with the principle aim of producing accurate binary representations of the image objects. These steps are detailed and the optimised process outlined. Next, a description of image analysis methods which derive counts of 3D objects is given.

To demonstrate each component within the workflow, a set of sections are taken through the entire process as an exemplar. This workflow has been largely automated, and a suite of new algorithms has been written as extensions to the open-source image processing package, ImageJ. This suite of algorithms implements the image processing within the workflow, and has been named StereoMate.

2.2 Histological Preparation of Tissue for Synaptic Visualisation

Visualisation of synaptic puncta using immunohistochemical methods was revolutionised following the demonstration that tissue treated with pepsin unveiled different post-synaptic proteins, which had previously been difficult to label with antibodies (Watanabe et al., 1998; Fukaya and Watanabe, 2000). This method resulted in a dramatic change in staining pattern, from a somatodendritic staining distribution, to a tiny punctate distribution throughout the neuropil. The authors showed that this method was appropriate for unveiling PSD95 as well as NMDA receptor subunits, and importantly, that the antibody

against PSD95 was confirmed to specifically label asymmetric synapses by postembedding immunogold electron microscopy (Watanabe et al., 1998; Fukaya and Watanabe, 2000). This work also demonstrated the ability to illuminate both pre- and post- synaptic components by showing double labelling with PSD95 and synaptophysin. This method has been used to visualise synaptic puncta throughout the nervous system, including the dorsal horn (Yamada et al., 2001; Nagy et al., 2004a; Somogyi et al., 2004; Yasaka et al., 2009).

The initial aim was to replicate this antigen retrieval methodology in order to visualise synapses within the dorsal horn.

2.2.1 Tissue Preparation and Staining Procedure

To test this histological procedure on spinal cord tissue, standard histological procedures were followed. Briefly, adult FVB/N mouse lumbar spinal cord tissue was used for all histological preparations. Animals were sacrificed using pentobarbitone, followed by exposure of the heart, and perfused with PBS followed by 4% PFA (See Gage et al., 2012, for details). A laminectomy was performed, and the lumbar enlargement removed. Tissue was post fixed overnight in 4% formaldehyde at 4ºC. Tissue underwent cryoprotection (submersion in 30% sucrose at 4ºC, ~24 hours), was embedded and frozen into OCT, and cut on the cryostat ($30\mu m$ transverse sections). Sections were left to dry overnight, and stored at -80ºC.

The following antibodies were used: rabbit anti-PSD95 (PSD95-Rb-Af628) and guinea pig anti-Synaptophysin (Syn-GP-Af300) both from The Frontier Institute, Japan (see Figure 2.1). These two antibodies have been extensively characterised for specificity: both antibodies display intense punctate staining throughout the neuropil of the CNS, and were closely apposed to each other, consistent with synaptic labelling; the overall staining

Antibody	Species	Dilution	Source	Catalog Number
PSD95	Rabbit	1:200	Frontier Institute	PSD95-Rb-Af628
SynaptoPhysin	Guinea Pig	1:200	Frontier Institute	Syn-GP-Af300

Figure 2.1: Antibodies used to mark pre- and post- synaptic structures.

distributions match their mRNA distributions; and the labelling performed with these antibodies overlapped with other synaptic markers (see Watanabe et al., 1998; Fukaya and Watanabe, 2000). Isolectin B4 isolated from *Bandeiraea simplificifolia* (Sigma, L2140) was used to mark the non-peptidergic C fibres, as shown previously (Streit et al., 1985; Molliver et al., 1995; Snider and McMahon, 1998).

Tissue staining was performed as follows (except where indicated): Thawing from -80°C and re-hydration of tissue sections in PBS for 10 minutes, incubation in 50% ethanol for 30 minutes to enhance antibody penetration (Llewellyn-Smith and Minson, 1992), antigen retrieval (see Section 2.2.2), primary antibody incubation in PBS containing triton-X 100 (0.3%) for 3 days at room temperature, a wash step in PBS containing triton-X 100 (0.3%), secondary antibody incubation conjugated to a fluorophore in PBS containing triton-X 100 (0.3%) (occasionally DAPI (D8417, Sigma) was added in the secondary antibody mixture [1:50,000]), a final wash step in PBS containing triton-X 100 (0.3%). Tissue was mounted using Vectashield (Vector Labs, H-1000) and No. 1.5 coverglasses (±0.01mm, Hecht-Assistent 1014/4024).

A Zeiss LSM 700 confocal microscope was used for all imaging. Where comparisons of relative intensity of staining was made, imaging was always performed in the same session, and with identical imaging conditions (laser power, gain settings, identical objective lens, pinhole diameter, and image dimensions). Where comparisons were made, a minimum of 3 sections were measured per slide, and a minimum N number of 3 slides were used for

quantification. Images for deconvolution were acquired at 16-bit depth, whereas all other images were taken at 8-bit depth.

2.2.2 Antigen retrieval

Different antigen retrieval methods have been employed here to visualise synaptic puncta. Generally, antigen retrieval is reserved for formalin fixed-paraffin embedded tissue, due to the tissue's robustness against the harsh antigen retrieval methods available. The general consensus is that these methods are of limited use in fixed-frozen tissue specimens due to their delicate nature (Ramos-Vara, 2005; D'Amico et al., 2009), although some protocols have been published (for example Jiao et al., 1999; Fukaya and Watanabe, 2000). These studies demonstrate that harsh antigen retrieval protocols usually applied to formalin fixed-paraffin embedded tissues can be modified to induce similar gains in antigenicity in formalin fixed-frozen sections, whilst controlling for potential tissue damage. Antigen retrieval methods used here on formalin fixed-frozen tissue include:

Pepsin Antigen Retrieval: Pepsin is a non-selective & strong protease found in the stomach (Fruton, 2002). Originally used to isolate DNA (Dahm, 2005), it has been used for retrieval of synaptic epitopes for almost 20 years (Watanabe et al., 1998; Fukaya and Watanabe, 2000). The method involves diluting pepsin to 1mg/mL in 0.2M HCl at 37°C. Tissue slides are carefully introduced to the solution and incubated for 10 minutes. The reaction is inhibited quickly by gently removing the slide, and carefully adding PBS to the tissue sections.

Heat Induced Epitope Retrieval (HIER): The discovery that heat could retrieve antigens in the 1990s revolutionised histology (Ramos-Vara, 2005; D'Amico et al., 2009). However, this method is usually restricted to formalin fixed paraffin embedded tissue, since the delicate nature of Formalin fixed-frozen tissue means heat-

treatment invariably causes significant tissue damage. To overcome this limitation, a milder methodology has been developed, where tissue is incubated in 10mM citrate buffer containing 2mM EDTA (pH 6.2) for 5 minutes at room temperature. A second measure of citrate buffer is heated to its boiling point using a microwave, and the tissue slides are gently introduced once boiling had stopped. The tissue is incubated in high temperature buffer for 10 minutes, before transferring to PBS at room temperature. This method is similar to Jiao et al. (1999).

Proteinase K Antigen Retrieval (ProK): Proteinase K is a serine protease with broad specificity (Ebeling et al., 1974; Morihara and Tsuzuki, 1975), which has been used for enhancing penetration of *in situ* hybridisation probes with whole-mount specimens (Lécuyer et al., 2008; Piette et al., 2008), and more recently for immunostaining of large blocks of neural tissue (Gleave et al., 2013). Here, Proteinase K digestion was tested for use in retrieving synaptic epitopes, which has previously shown promising results (see Watanabe et al., 1998). Proteinase K was diluted to 1-10μg in PBS containing Triton X-100 (0.3%) and applied to the tissue for 10 minutes at room temperature.

2.2.3 Pepsin Retrieves Synaptic Puncta in the Dorsal Horn

In order to study the synaptome using immunohistochemical labelling of synaptic puncta, initial experiments focussed on utilising the pepsin antigen retrieval method previously described (Watanabe et al., 1998; Fukaya and Watanabe, 2000). Using the same antibodies from the original papers (PSD95: PSD95-Rb-Af628, Synaptophysin: Syn-GP-Af300; The Frontier Institute, Japan, see Figure), the first experiment aimed to replicate the staining seen in the literature (for example see Fukaya and Watanabe, 2000; Nagy et al., 2004a; Yasaka et al., 2009).

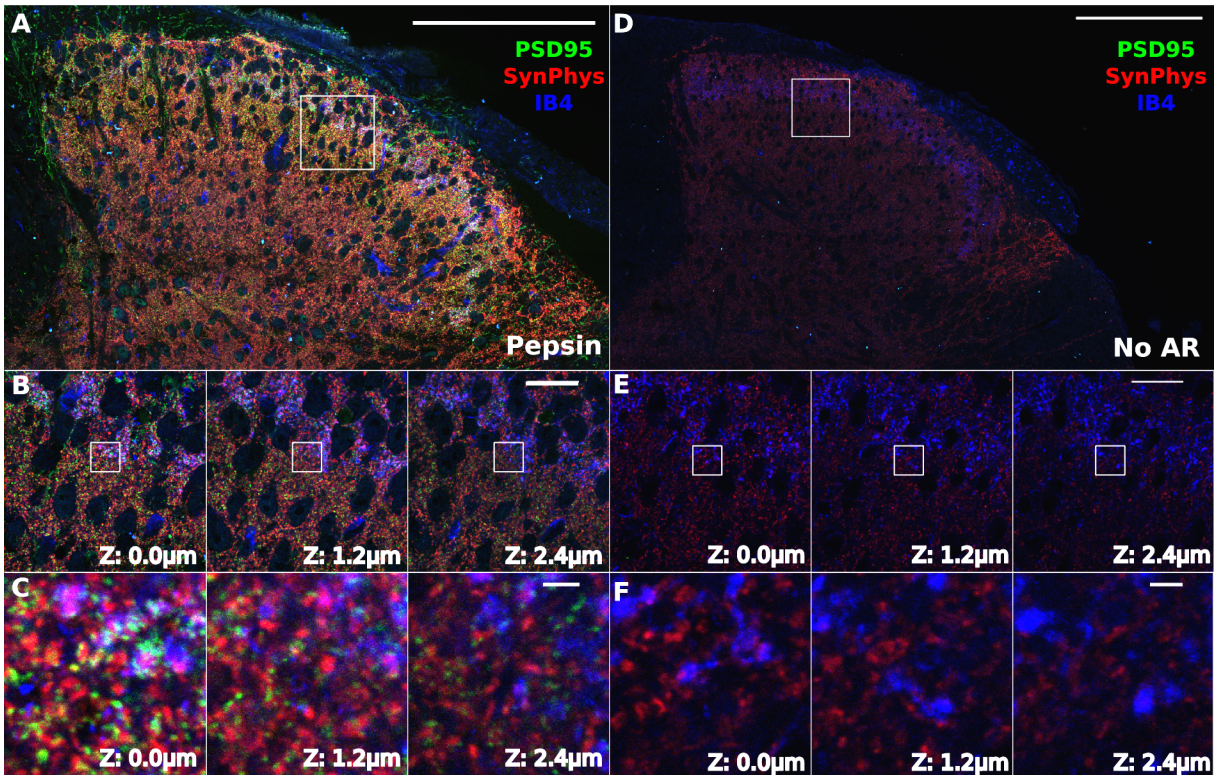

Figure 2.2: **PSD95 & SynaptoPhysin are effectively retrieved by pepsin pre-treatment. A-C:** Pepsin antigen retrieval unveils both SynaptoPhysin and PSD95 epitopes which results in strong antibody labelling and fluorescence signals within the grey matter of the dorsal horn. **A:** Single Z slice overview of the dorsal horn reveals extensive labelling throughout the grey matter. **B:** Magnification of highlighted region from A, within the superficial dorsal horn, reveals sharp punctate staining for both SynaptoPhysin and PSD95 on single Z slices at various Z depths. **C:** Magnification of highlighted region from B, revealing individual pre- and post- synaptic staining for Synaptophysin and PSD95, respectively on single Z slices at various Z depths. **D-F:** Single Z slice of tissue not treated with pepsin pre-treatment abolishes PSD95 labelling and significantly reduces SynaptoPhysin labelling intensity. **D:** Overview of the dorsal horn shows reduced SynaptoPhysin and absent PSD95 labelling throughout the grey matter. **E:** Magnification of highlighted region in D, revealing a lack of PSD95 staining on single Z slices at various Z depths. **F:** Magnification of highlighted region in E showing SynaptoPhysin labelling is reduced intensity relative to pepsin-treated tissue (see C), and a complete absence of PSD95 puncta on single Z slices at various Z depths. All Z slices taken at 1 AU, Z thickness: $0.56\mu m$. Scale bars: A & D: $200\mu m$; B & E: $20\mu m$; C & F: $2\mu m$. SynPhys, SynaptoPhysin; IB4, Isolectin B4; AR, antigen retrieval.

Double labelling for SynaptoPhysin and PSD95 were performed as described (see Section 2.2.1 & 2.2.2). As can be seen from Figure 2.2, pre-treatment with pepsin increases SynaptoPhysin staining intensity as well as unveils the PSD95 epitope for fluorescence labelling. The labelling achieved with pepsin pre-treatment results in labelling reaching several micrometers into the tissue (up to $2.4\mu m$, see Figure 2.2C).

However, pepsin pre-treatment also leads to suboptimal staining and limited staining penetration. As is shown in Figure 2.3, PSD95 antibody labelling also marks neurites following pepsin pre-treatment, and the penetration of both PSD95 and SynaptoPhysin labelling is limited. Both of these factors limit the utility of this antigen retrieval method for automated image analysis. Thus, in order to attempt to improve the labelling selectivity and penetration, pepsin pre-treatment was combined with other antigen retrieval methods.

2.2.4 HIER and Proteinase K Improve Antibody Penetration and Synapse Staining Specificity

In order to investigate the possible improvement of synapse labelling with other antigen retrieval methods, slides were labelled for PSD95, SynaptoPhysin and IB4 which were pre-treated with pepsin; HIER & pepsin; or HIER, proteinase K & pepsin. This followed the rationale that pre-treatment with different antigen retrieval methodologies might help pepsin to penetrate deeper into the tissue, and thus retrieve synaptic antigens deeper within the tissue, since other antigen retrieval methods are known to aid penetration of other proteins, such as antibodies (Hayat, 2002; Gleave et al., 2013).

Initially, these sections were imaged to observe the effects of each set of antigen retrieval methods on synaptic labelling. Figure 2.4 shows a representative dorsal horn section stained for PSD95, SynaptoPhysin and IB4 following pepsin pre-treatment. As can be

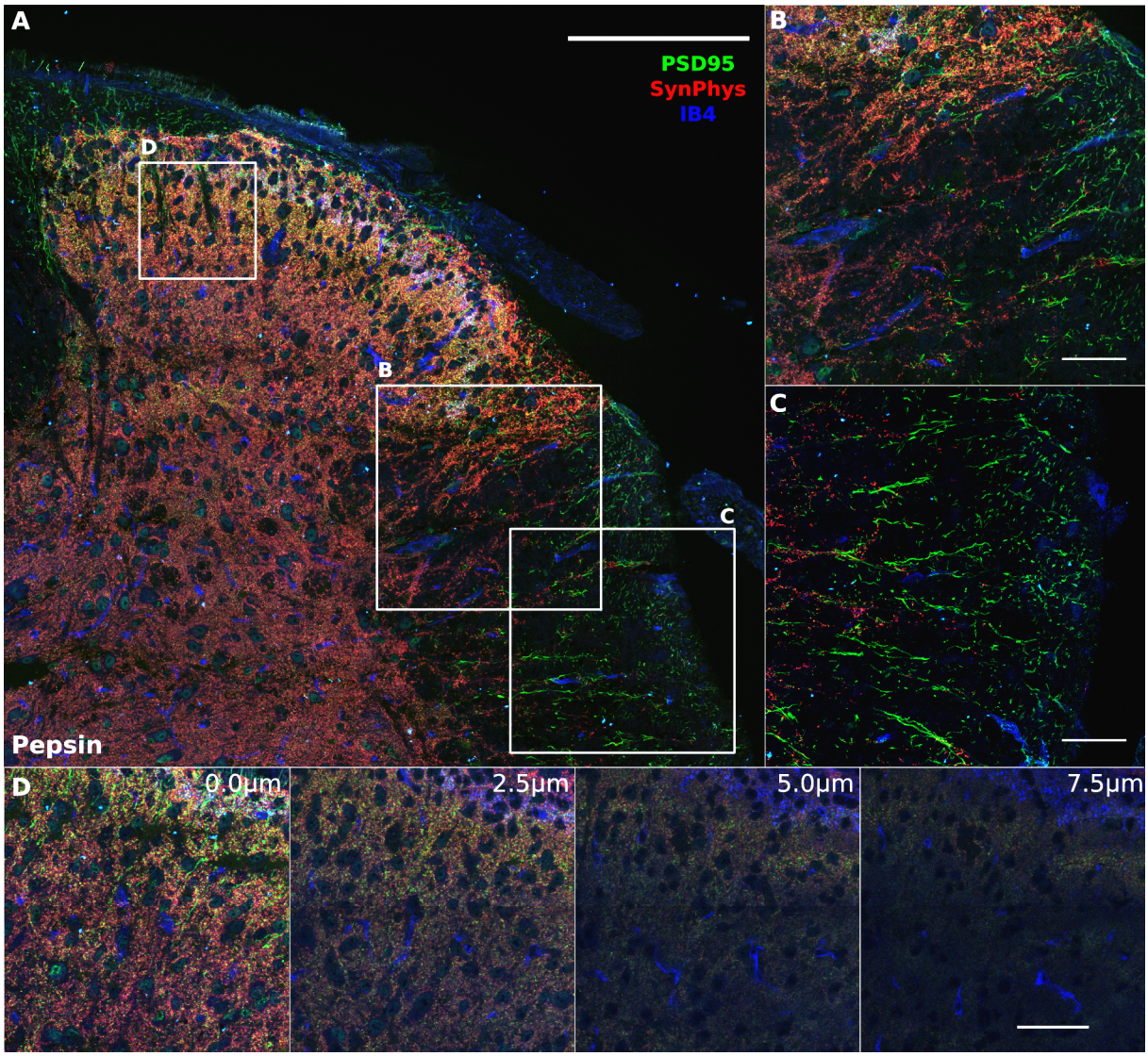

Figure 2.3: **Pepsin pre-treatment retrieves synaptic epotopes to a shallow depth and results in neurite labelling for PSD95. A:** Overview image of dorsal horn section pre-treated with pepsin and labelled with PSD95, SynaptoPhysin antibodies and IB4. **B & C:** Magnification of regions highlighted in A indicating labelling of dendritic elements by the PSD95 antibody within the white matter of the dorsal horn. **D:** Magnified Z stack of region highlighted in A which shows the progressive loss of PSD95 and SynaptoPhysin signal as the tissue is traversed in the Z plane. Scale bars: A: 200μm; B & C: 50μm; D: 20μm. SynPhys, SynaptoPhysin; IB4, Isolectin B4.

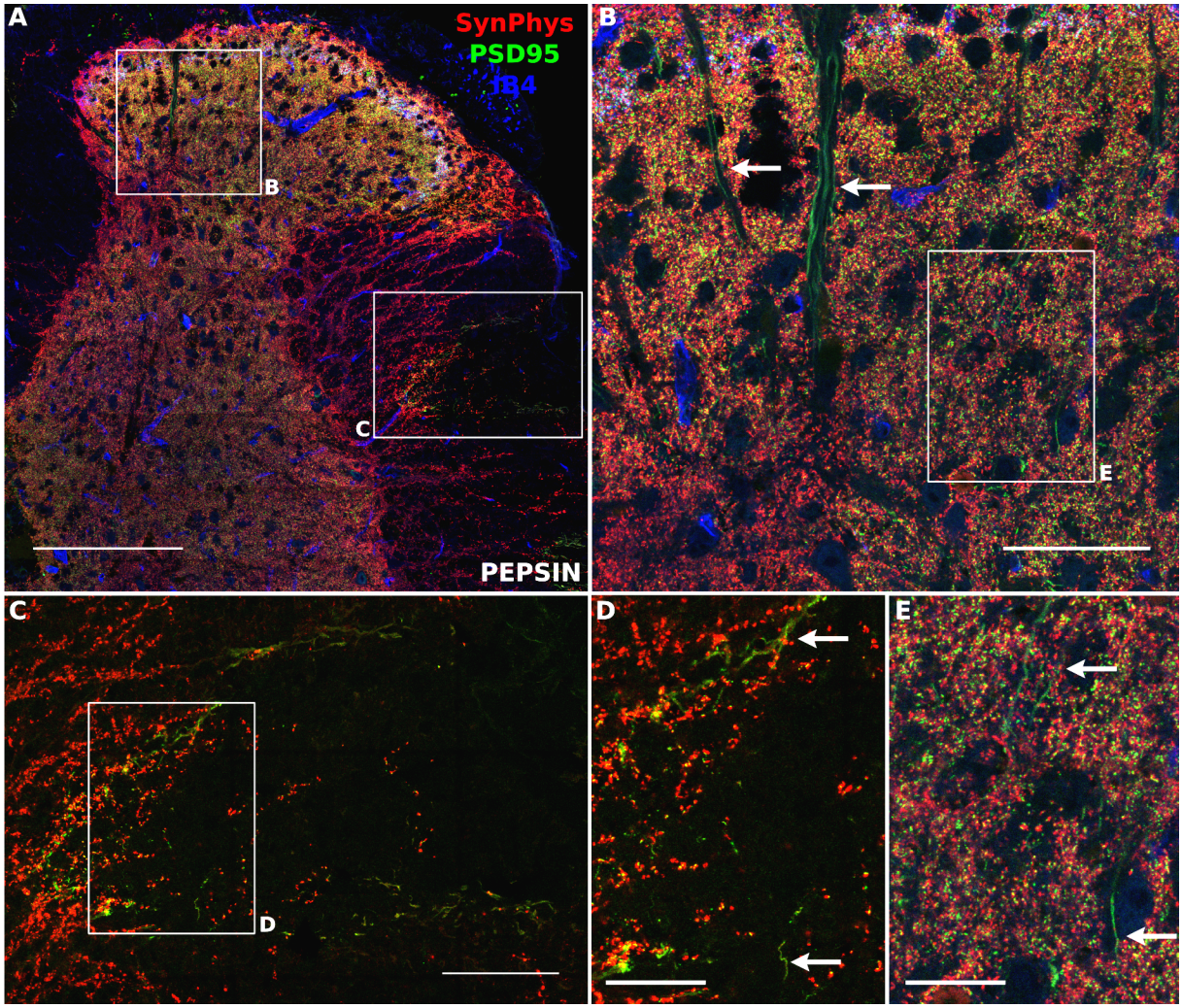

Figure 2.4: **Pepsin pre-treatment results in PSD95 antibody labelling of neurites. A:** Overview single Z slice image of representative dorsal horn. **B:** Magnified view of highlighted region in A indicating neurite labelling in the medial dorsal horn (horizontal arrows). **C:** Magnification of region highlighted in A, showing neurite labelling in lateral white matter. **D:** Magnified view of region highlighted in C showing extensive neurite labelling in lateral white matter (horizontal arrows). **E:** Magnified view of highlighted region in B showing neurite labelling within the neuropil of the dorsal horn (horizontal arrows). All images taken at tissue surface. All Z slices taken at 1 AU, Z thickness: $0.56\mu m$. Scale bars: A: $200\mu m$; B & C: $50\mu m$; D & E: $20\mu m$. SynPhys, SynaptoPhysin; IB4, Isolectin B4.

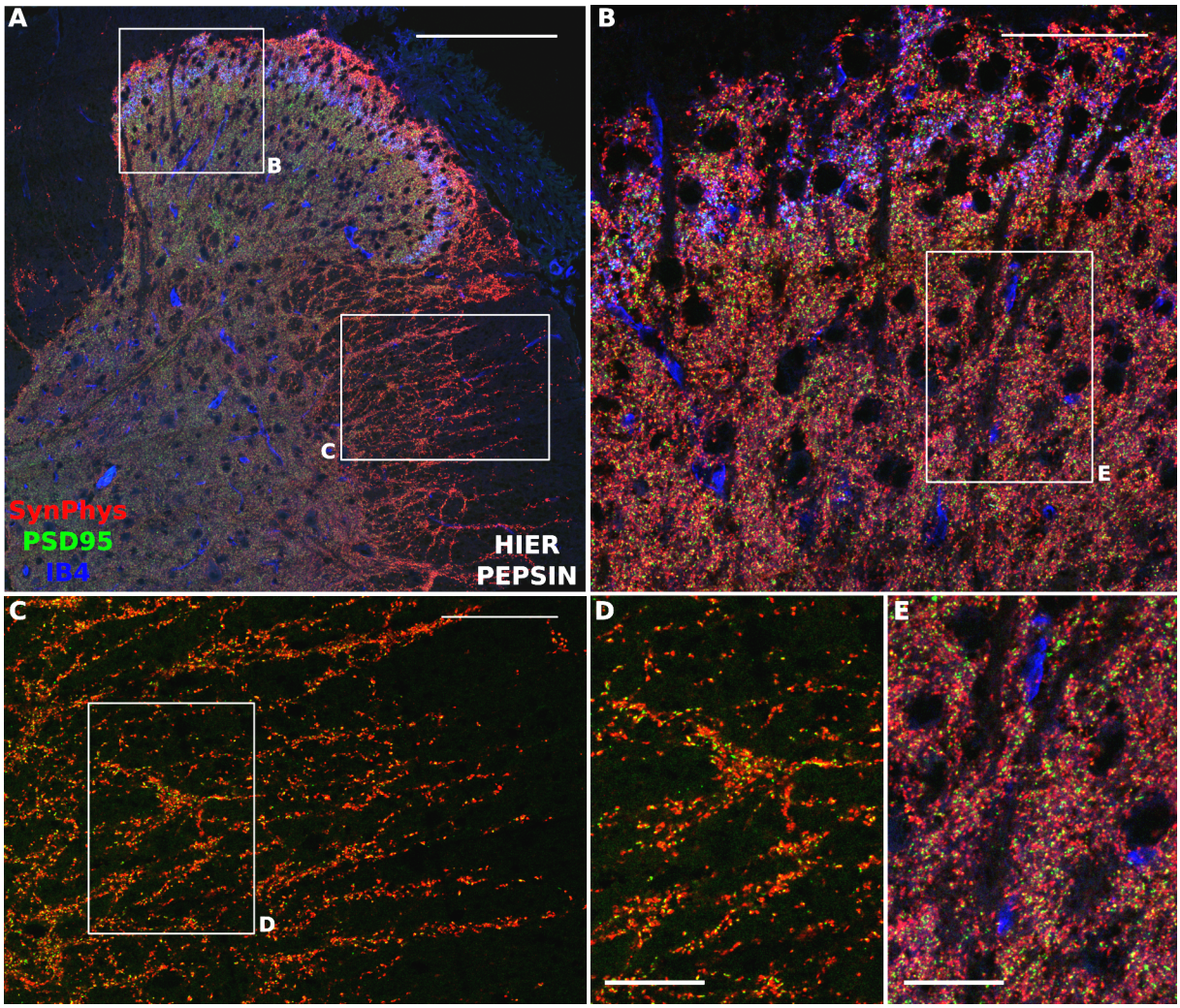

Figure 2.5: **Heat induced epitope retrieval prior to pepsin eliminates PSD95 antibody neurite staining. A:** Overview single Z slice image of representative dorsal horn. **B:** Magnified view of highlighted region in A, note the lack of neurite labelling. **C:** Magnification of region highlighted in A, indicating no neurite labelling in lateral white matter. **D:** Magnified view of region highlighted in C showing extensive punctate PSD95 labelling in lateral white matter. **E:** Magnified view of highlighted region in B showing punctate PSD95 labelling within the neuropil of the dorsal horn. All Z slices taken at 1 AU, Z thickness: 0.56μm. Scale bars: A: 200μm; B & C: 50μm; D & E: 20μm. SynPhys, SynaptoPhysin; IB4, Isolectin B4.

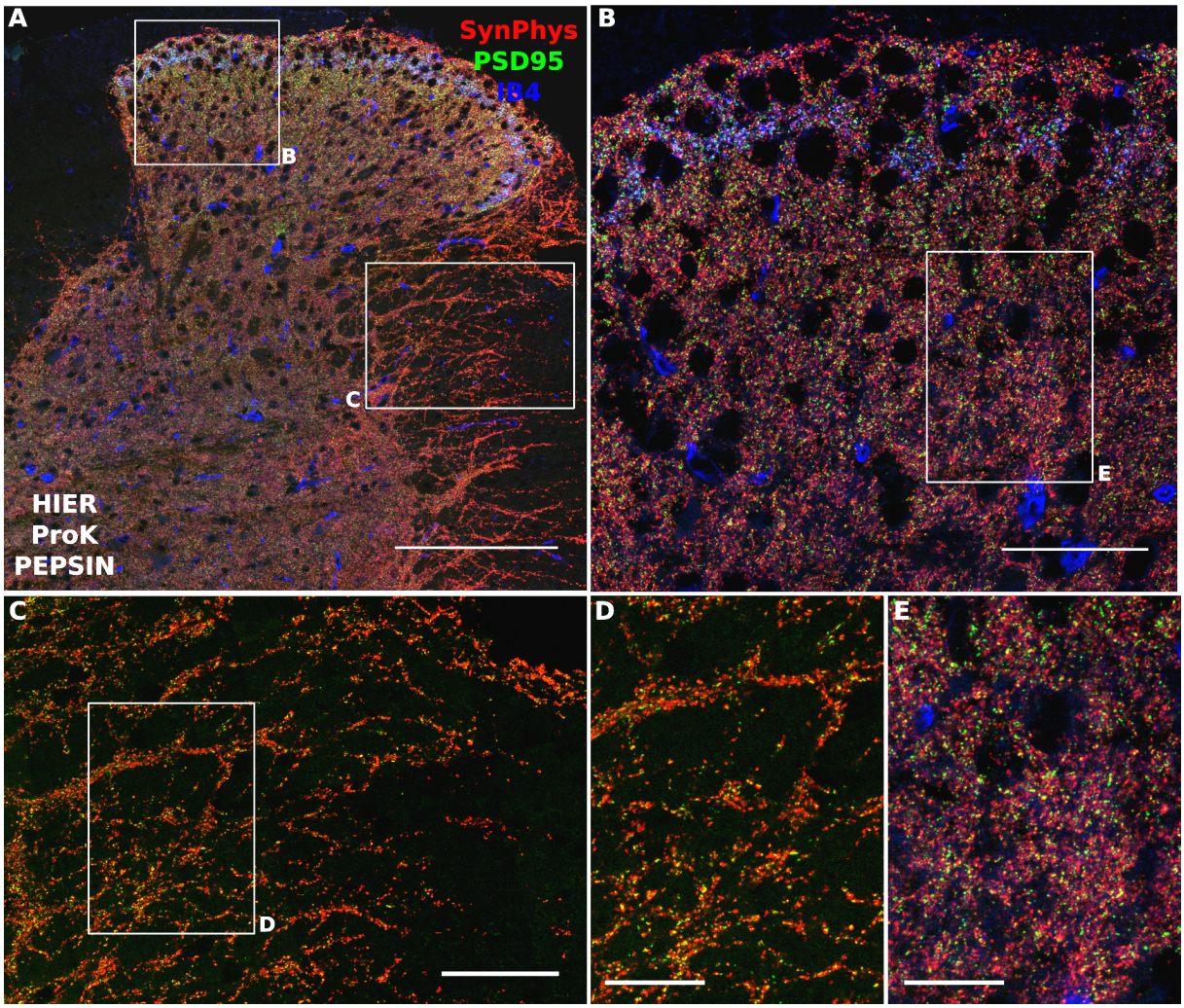

Figure 2.6: **Heat induced epitope retrieval & Proteinase K treatment prior to pepsin eliminates PSD95 antibody neurite labelling. A:** Overview single Z slice image of representative dorsal horn. **B:** Magnified view of highlighted region in A, note the lack of neurite labelling. **C:** Magnification of region highlighted in A, indicating no neurite labelling in lateral white matter. **D:** Magnified view of region highlighted in C showing extensive punctate PSD95 labelling in lateral white matter. **E:** Magnified view of highlighted region in B showing punctate PSD95 labelling within the neuropil of the dorsal horn. All Z slices taken at 1 AU, Z thickness: 0.56μm. Scale bars: A: 200μm; B & C: 50μm; D & E: 20μm. SynPhys, SynaptoPhysin; IB4, Isolectin B4.

seen, and consistent with the first set of staining (see Figure 2.3), pepsin alone results in significant labelling of neurites, especially apparent in the medial dorsal horn (where myelinated A fibres enter the dorsal grey matter, Figure 2.4B&E), and in the white matter lateral to the dorsal horn (Figure 2.4C&D). Surprisingly, preceding pepsin pre-treatment with HIER or HIER and proteinase K eliminated this aberrant neurite staining (see Figures 2.5 & 2.6).

Applying extra antigen retrieval methods could potentially eliminate or alter the synaptic antigens, resulting in loss of signal. However, punctate PSD95 labelling remained with both HIER and HIER with Proteinase K treatments. This PSD95 labelling was closely apposed to SynaptoPhysin puncta, consistent with these antigen retrieval methods retaining PSD95 synaptic labelling. On closer inspection, no apparent changes to the appearance or density of synaptic labelling were evident (see Figures 2.7 & 2.8).

To investigate the effects of the different antigen retrieval regimens on staining depth, Z stack images were taken through the middle aspect superficial dorsal horn and compared across different antigen retrieval treatments. Figure 2.9A-C shows representative Z stacks through pepsin, HIER-pepsin and HIER-Proteinase K-pepsin treated tissue, indicating a progressive loss of staining intensity for PSD95 and SynaptoPhysin labelling for all antigen retrieval methods.

Figure 2.9D-E has quantified the average pixel intensity in the middle aspect of the superficial dorsal horn at $2\mu m$ intervals. Figure 2.9D shows that PSD95 staining intensity is retained at greater depths by both HIER and HIER-Proteinase K treatments, indicating these treatments are effective in improving the antigen retrieval produced by pepsin. Figure 2.9E shows a reduction in SynaptoPhysin average fluorescence intensity throughout the Z stack with HIER treatment, which is recovered by combined HIER-Proteinase K treatment.

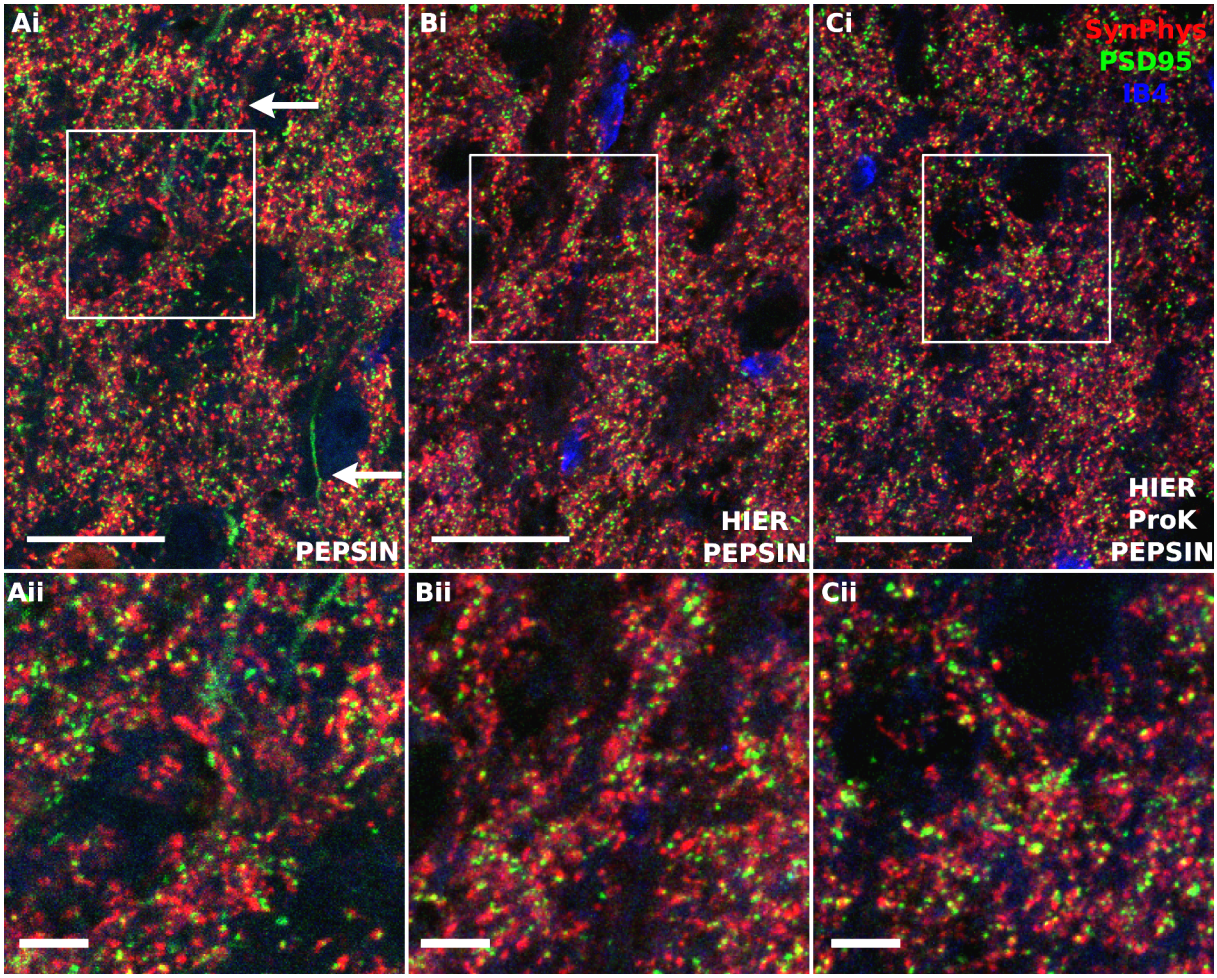

Figure 2.7: **HIER and Proteinase K do not reduce PSD95 or SynaptoPhysin Labelling in medial dorsal horn. Ai:** High resolution single Z slice image of the medial dorsal horn of pepsin treated tissue. **Aii:** Magnified view of highlighted region in A, note the punctate synaptic staining and neurite staining in green. **Bi:** High resolution single Z slice image of the medial dorsal horn of HIER-pepsin treated tissue. **Bii:** Magnified view of highlighted region in A, note only punctate synaptic labelling in green. **Ci:** High resolution single Z slice image of the medial dorsal horn of HIER-ProK-pepsin treated tissue. **Cii:** Magnified view of highlighted region in A, note only punctate synaptic labelling in green. All Z slices taken at 1 AU, Z thickness: $0.56\mu m$. Scale bars: Ai, Bi, Ci: $20\mu m$; Aii, Bii, Cii: $5\mu m$. SynPhys, SynaptoPhysin; IB4, Isolectin B4; HIER, heat induced epitope retrieval; ProK, proteinase K.

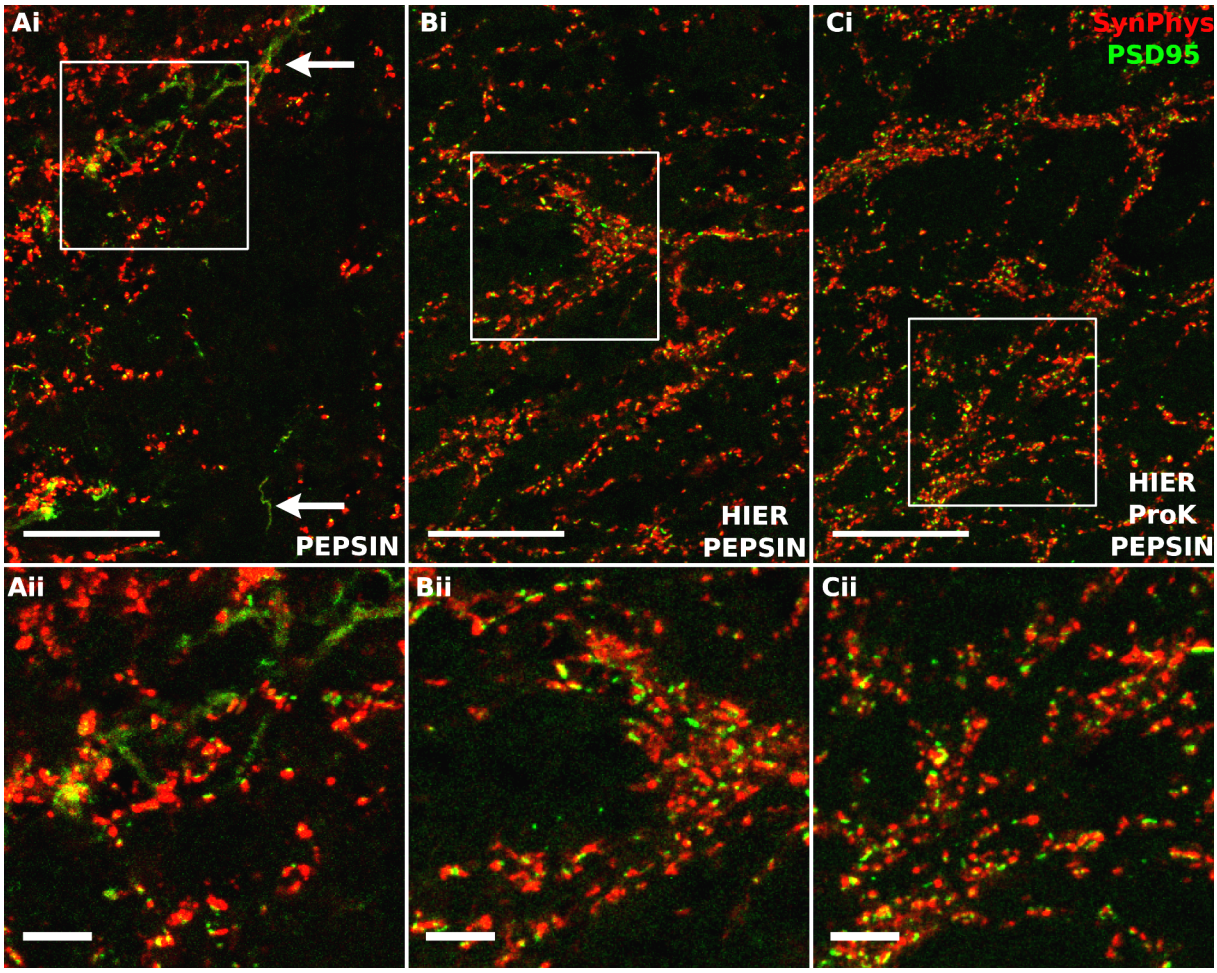

Figure 2.8: **HIER and Proteinase K do not reduce PSD95 or SynaptoPhysin Labelling in the lateral white matter. Ai:** High resolution single Z slice image of the lateral white matter of pepsin treated tissue. **Aii:** Magnified view of highlighted region in A, note the punctate synaptic staining and neurite staining in green. **Bi:** High resolution single Z slice image of the lateral white matter of HIER-pepsin treated tissue. **Bii:** Magnified view of highlighted region in A, note only punctate synaptic labelling in green. **Ci:** High resolution single Z slice image of the lateral white matter of HIER-ProK-pepsin treated tissue. **Cii:** Magnified view of highlighted region in A, note only punctate synaptic labelling in green. All Z slices taken at 1 AU, Z thickness: $0.56\mu m$. Scale bars: Ai, Bi, Ci: $20\mu m$; Aii, Bii, Cii: $5\mu m$. SynPhys, SynaptoPhysin; HIER, heat induced epitope retrieval; ProK, proteinase K.

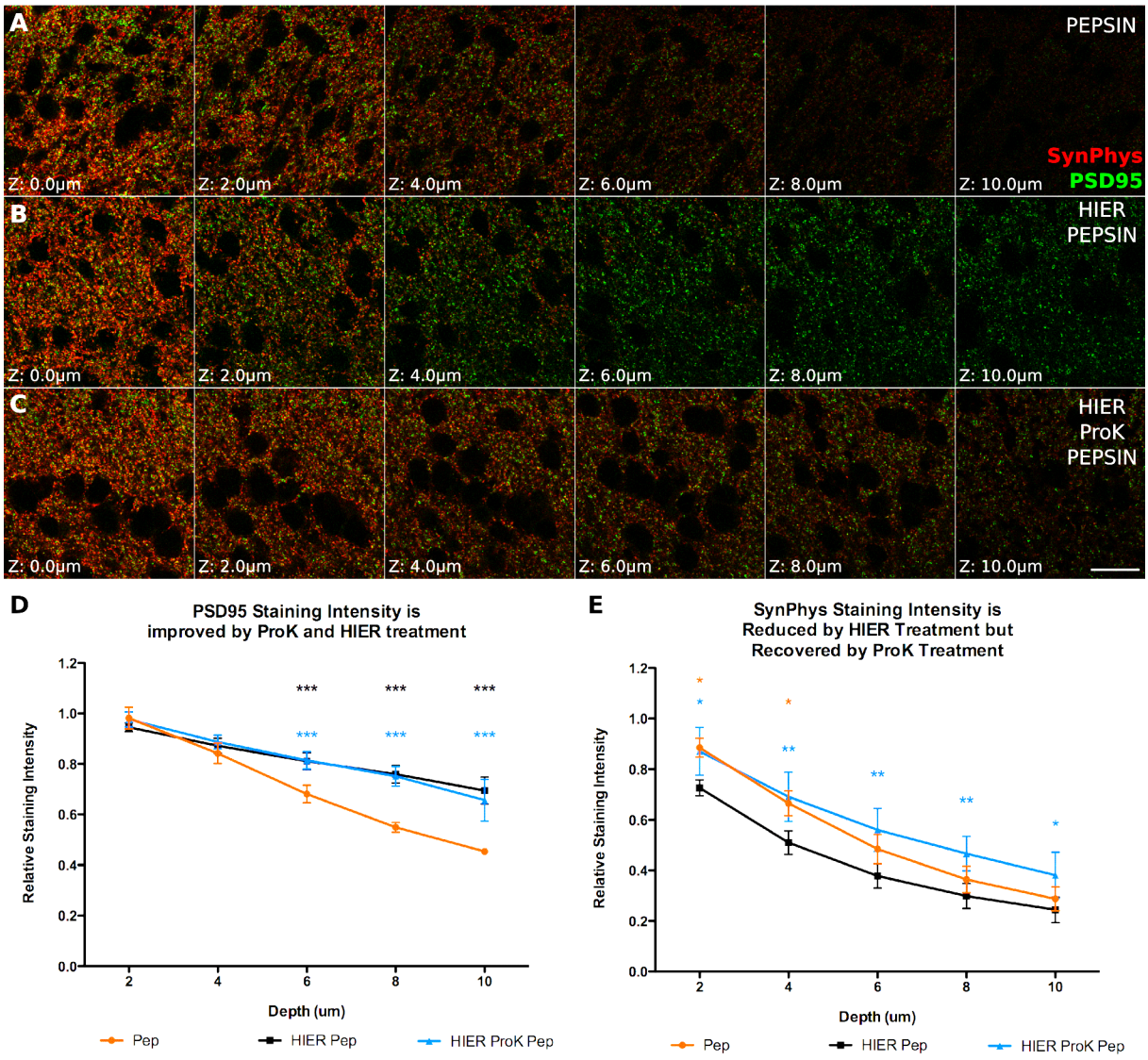

Figure 2.9: **HIER and Proteinase K improve PSD95 and SynaptoPhysin Labelling staining penetration. A, B, C:** Representative Z slices taken at $2\mu m$ intervals showing the reduction in staining intensity as the Z stack is traversed (All Z slices taken at 1 AU, Z thickness: $0.56\mu m$). **A:** Pepsin treated tissue. **B:** HIER-Pepsin treated tissue. **C:** HIER-ProK-Pepsin treated tissue. **D:** Quantification of normalised Average Pixel Intensity of each Z slice for PSD95 labelling across multiple sections (6 sections per slide, n = 3 slides per group). HIER and HIER-ProK treatment both significantly maintained PSD95 labelling from 6-10μm (two-way ANOVA, bonferonni post-hoc test; ***, $p<0.001$, Blue - HIER ProK Pep compared to Pep, Black - HIER Pep compared to Pep). **E:** Quantification of normalised Average Pixel Intensity of each Z slice for SynaptoPhysin labelling across multiple sections (6 sections per slide, n = 3 slides per group). HIER and HIER-ProK treatment both significantly maintained PSD95 labelling from 6-10μm (two-way ANOVA, bonferonni post-hoc test; *, $p<0.05$; **, $p<0.01$. Red - Pep compared to HIER-Pep, Blue - HIER ProK Pep compared to HIER-Pep). Scale bar: A,B,C: $20\mu m$. SynPhys, SynaptoPhysin; HIER, heat induced epitope retrieval; ProK, proteinase K; Pep, pepsin.

Taken together, these results suggest the combination of HIER-Proteinase K-Pepsin treatment gives the best representation of pre- and post- synaptic structure with SynaptoPhysin & PSD95 immunohistochemistry, respectively. This antigen retrieval regimen results in the eradication of PSD95 neurite labelling, and improved penetration of both PSD95 & SynaptoPhysin staining, both essential improvements to allow automated synaptome analysis of regions within the dorsal horn.

In order to reduce the loss of signal seen as the tissue section is traversed (see Figure 2.9), the application of a laser power and gain correction was tested. The sections pretreated with HIER, Proteinase K & Pepsin were re-imaged, and the laser and gain settings adjusted at the start-point, mid-point and end-point of the Z stack to correct for the loss of signal.

As can be seen in Figure 2.10, application of a laser power and gain correction resulted in a significant improvement in signal throughout the Z stack, which completely eliminated any reduction in average pixel intensity. Crucially, although increasing laser and gain settings may result in increased noise as well as signal, the signal:noise was well maintained throughout the Z stack (see Figure 2.10Bi & ii). This is likely attributed to the fact that antibody binding is excessively high at the tissue surface, which requires very low laser and gain settings, and that a lower but still significant level of antibody binding occurs at deeper tissue sites. This level of binding is almost undetectable with very low laser and gain settings, but is effectively revealed with an appropriate correction to laser and gain settings without contributing to extra noise.

Applying a correction of pepsin-retrieved tissue does not produce the same level of signal:noise, due to the patchy loss of pepsin antigen retrieval as the tissue is traversed (see Figure 2.11). Thus, application of HIER and Proteinase K helps pepsin act throughout the depth of the tissue to retrieve PSD95 and SynaptoPhysin antigens which pepsin alone

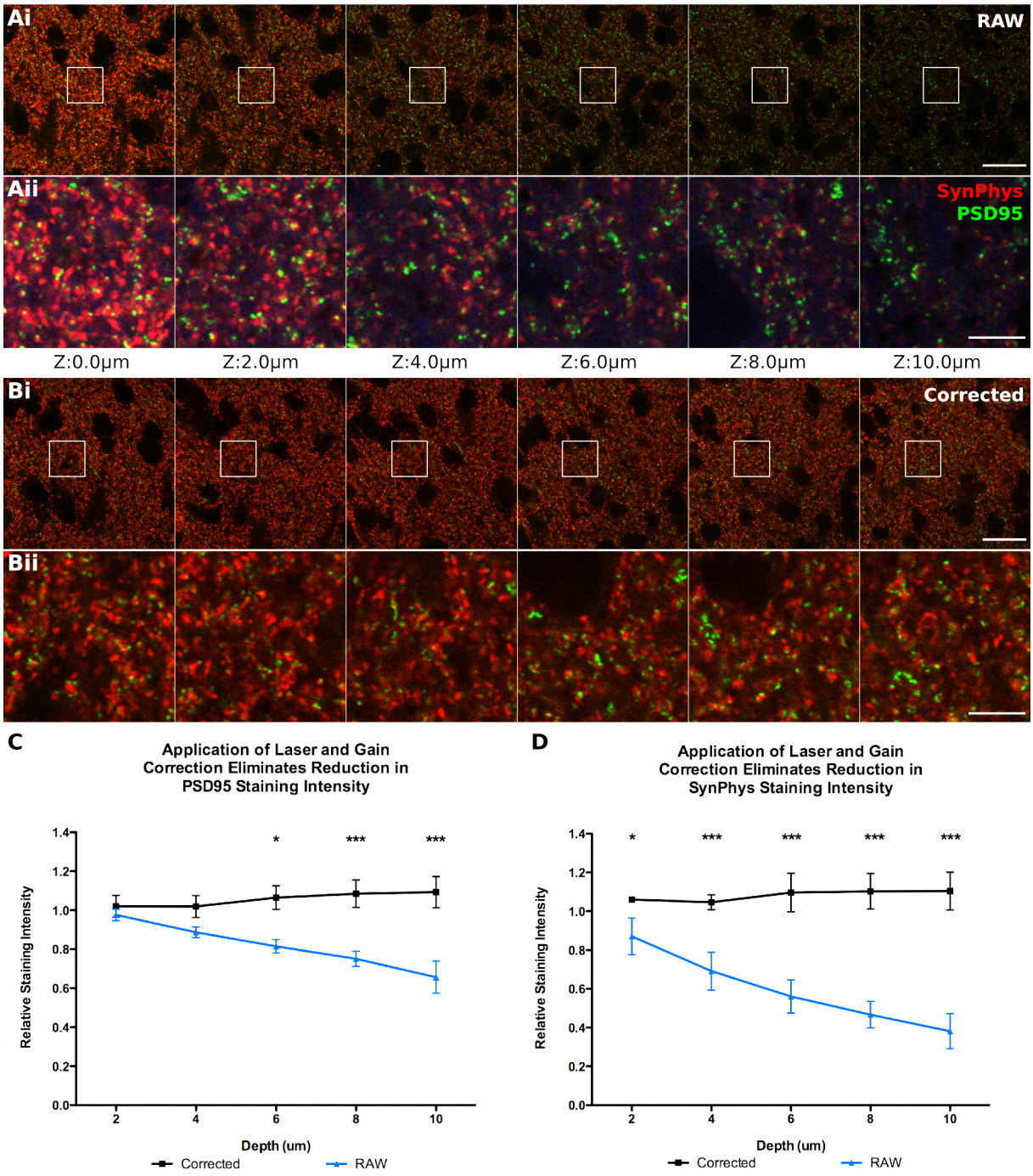

Figure 2.10: **Laser and gain correction enables retention of fluorescent signal throughout the tissue. A, B:** Representative Z slices taken at 2μm intervals showing raw and corrected images (All Z slices taken at 1 AU, Z thickness: 0.56μm). **Ai,ii:** Uncorrected Z slices showing loss of signal as the tissue is traversed. **Bi,ii:** Corrected Z slices showing maintained signal as the tissue is traversed. **C:** Quantification of normalised Average Pixel Intensity of each Z slice for PSD95 labelling across multiple sections (6 sections per slide, n = 3 slides per group). Corrected images significantly maintained PSD95 labelling from 6-10μm (two-way ANOVA, bonferonni post-hoc test; *, $p<0.05$; ***, $p<0.001$). **E:** Quantification of normalised Average Pixel Intensity of each Z slice for SynaptoPhysin labelling across multiple sections (6 sections per slide, n = 3 slides per group). Corrected images significantly maintained PSD95 labelling throughout the Z stack (two-way ANOVA, bonferonni post-hoc test; *, $p<0.05$; ***, $p<0.001$). Scale bars: Ai, Bi, Ci: 20μm; Aii, Bii, Cii: 5μm. SynPhys, SynaptoPhysin.

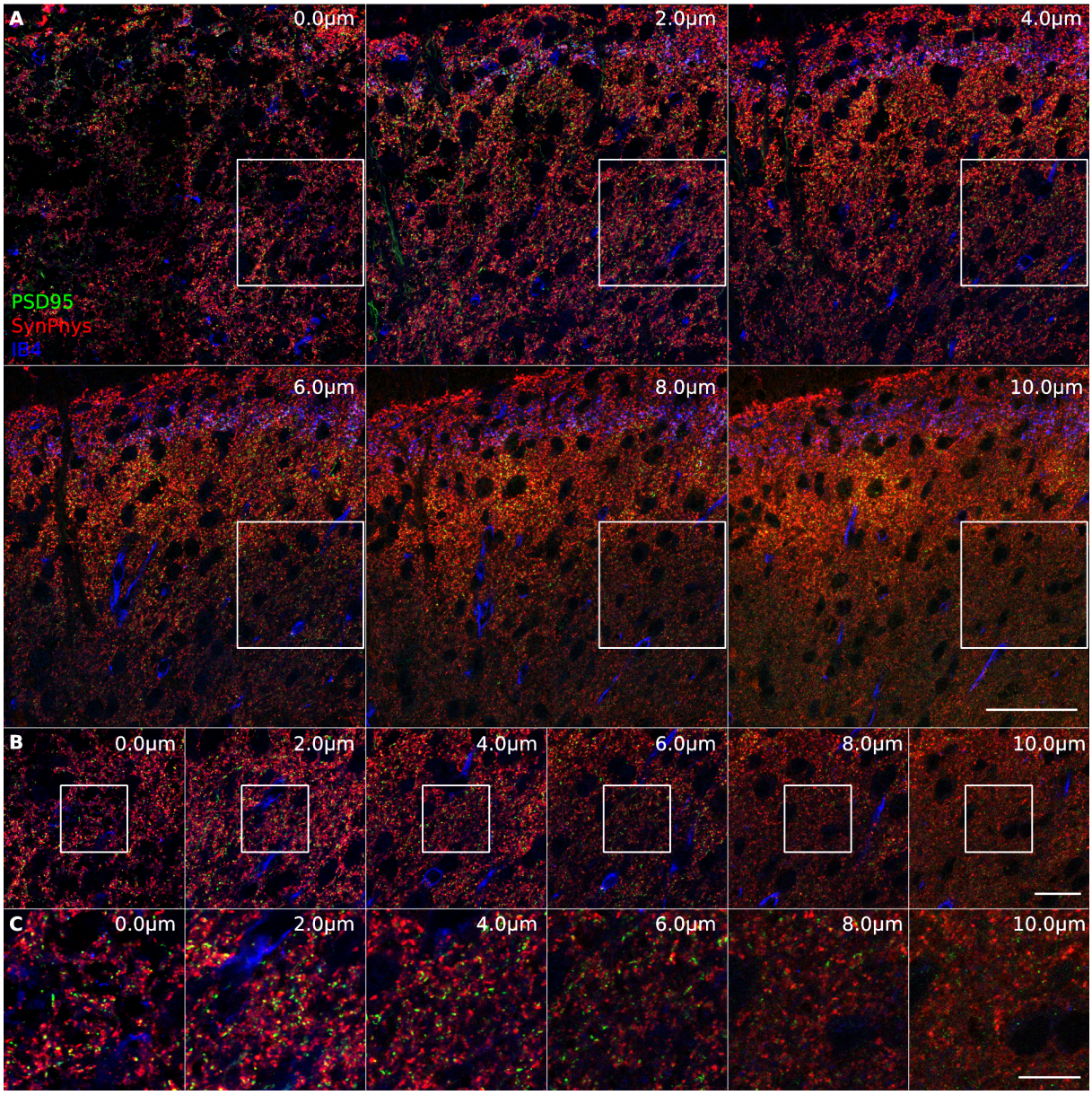

Figure 2.11: **Laser and gain correction applied to pepsin-only treated tissue reveals uneven PSD95 and SynaptoPhysin staining. A:** Single Z slices of superficial dorsal horn shows reduced SynaptoPhysin & PSD95 in certain patches as the Z stack is traversed. **B:** Magnified view of highlighted region in A, note a significant loss in SynaptoPhysin and PSD95 staining as the tissue is traversed. **C:** Magnified view of highlighted region in B, both PSD95 and SynaptoPhysin signals are significantly dampened even with laser and gain correction applied. All Z slices taken at 1 AU, Z thickness: 0.56μm. Scale bars: A, 50μm; B, 20μm; C, 10μm. SynPhys, SynaptoPhysin; IB4, Isolectin B4.

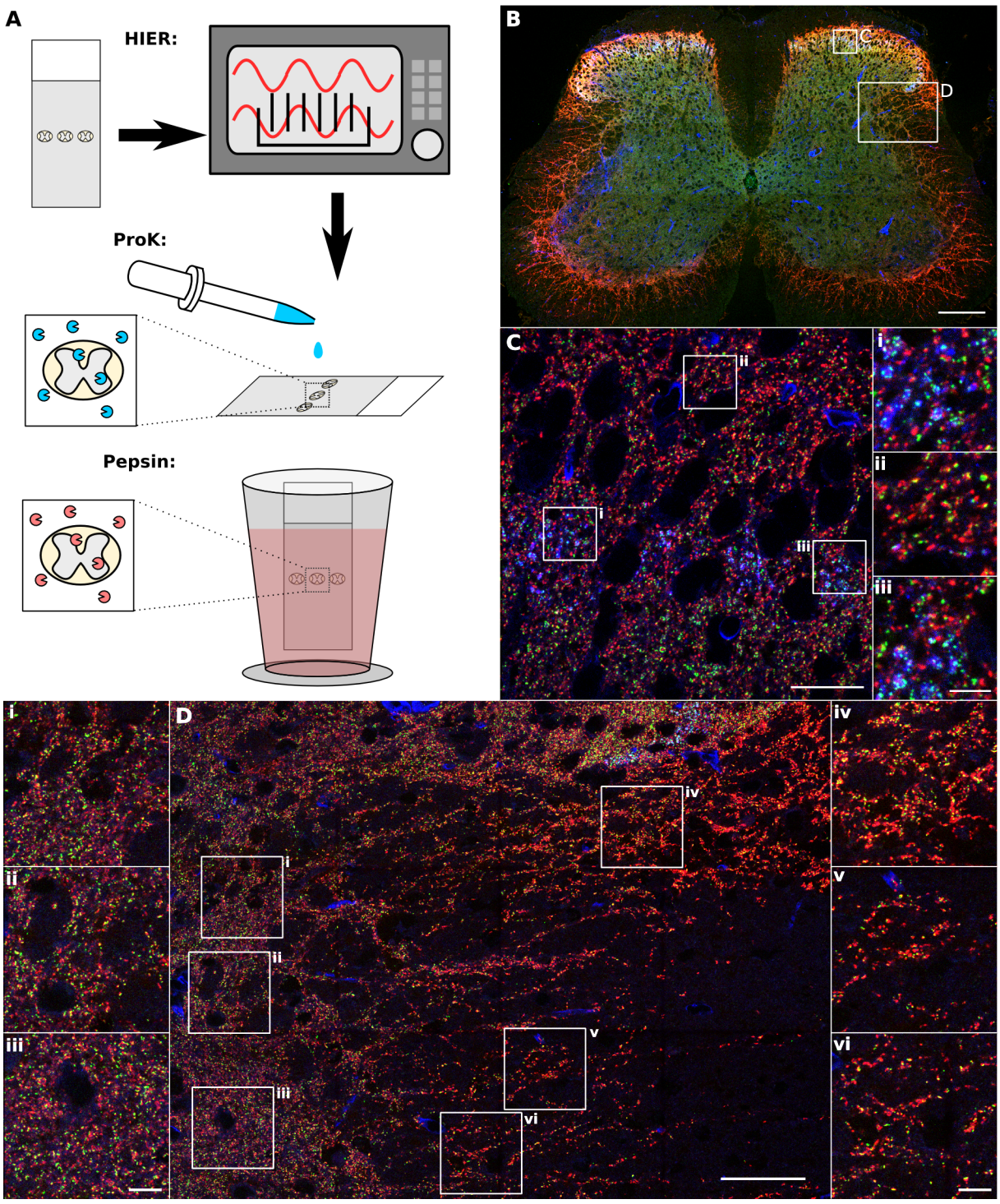

Figure 2.12: **The histochemical staining of three spinal cord sections. A:** A graphic summary of the antigen retrieval regimen applied to three spinal cord sections. **B-D:** Imaging of PSD95-SynaptoPhysin and IB4 histochemical labelling of one spinal cord section. **B:** Overview image of one spinal cord section (Maximum Intensity Projection of 4 Z slices taken with 2 AU [4um depth]). **C:** Single Z slice image of the superficial dorsal horn showing punctate PSD95 and SynaptoPhysin labelling. **D:** Single Z slice image of the lateral white matter showing punctate PSD95 and SynaptoPhysin labelling throughout the lateral dorsal horn. All Z slices taken at 1 AU, Z thickness: 0.56μm. Scale bars: B, 200μm; C, 20μm, i-iii, 5μm; D, 50μm, i-iv, 10μm.

is unable to achieve.

These observations have culminated in a staining workflow which produces vivid and robust synaptic labelling throughout a spinal cord section. This work is summarised in Figure 2.12, which represents the histochemical staining of three spinal cord test sections that will be taken through the remainder of the image processing and analysis workflow presented in this Chapter. The tissue was prepared and stained as described (see Sections 2.2.1 & 2.2.2), using the established HIER - Proteinase K - Pepsin antigen retrieval regimen (shown graphically in Figure 2.12A, see Section 2.2.2). Figure 2.12B-D show the PSD95-SynaptoPhysin labelling seen in one of these spinal cord sections (2.12B), in the superficial dorsal horn (2.12C), and in the lateral white matter (2.12D).

2.3 Stereological Image Processing

Stereology is a methodology originally developed to overcome the biases associated with interpretting 3D anatomical structures and objects from 2D image profiles (Schmitz and Hof, 2005; West, 2012). These biases include object size, shape and orientation, and thus stereology aims to quantify objects independent of their size, shape and orientation. This is achieved through two important concepts: systematic random sampling (SRS), and application of a counting frame.

In order to obtain unbiased estimates of the properties of synapses throughout the dorsal horn, these stereological principles have been implemented throughout the image acquisition, processing and analysis workflow. However, as described below, some extensions to these principles have been made to combine the unbiased estimates achieved with stereological methods with the 3D image sampling and high signal-to-noise ratios achievable with confocal microscopy, including full automation of object quantification and application of the stereological methods, and an improvement on the counting frame

to allow its application to entire 3D regions of interest (ROIs) in an efficient manner.

Below is described the sample image acquisition and processing to study the synaptome of the dorsal horn. Each step is detailed followed by a demonstration of the step on the tissue stained for PSD95 and synaptophysin shown in section 2.2.4 (see Figure 2.12).

2.3.1 Sample Image Acquisition

Once an adequate histological preparation to highlight the biological structures of interest has been obtained (see Section 2.2), the first step is sample image acquisition. This process requires some careful fore-thought, as the sampling will shape the ensuing image processing and analysis. First, a description of two different means of acquiring sample images for stereological analysis is given, drawing attention to the benefits and disadvantages that each method conveys, followed by an overview of required image resolution for the subsequent image processing.

2.3.1.1 Optical Sampling

One of the pillars of stereology is Systematic Random Sampling; a method designed to obtain a set of random and representative samples from the tissue of interest. In order to meet the demands of SRS, both histological sections and image samples obtained from them must be selected in a systematic and random manner (West, 1999, 2012).

Systematic random sampling of histological sections is achieved through serial sectioning of tissue onto a number of slides, which starts at a random point rostral to the region of interest, in this case the dorsal horn, and is systematically cut such that each subsequent section taken is the same distance from the previous section on any slide (see Figure 2.13). Thus, staining of any one of these slides provides a collection of sections which are systematically and randomly sampled from the tissue of interest.

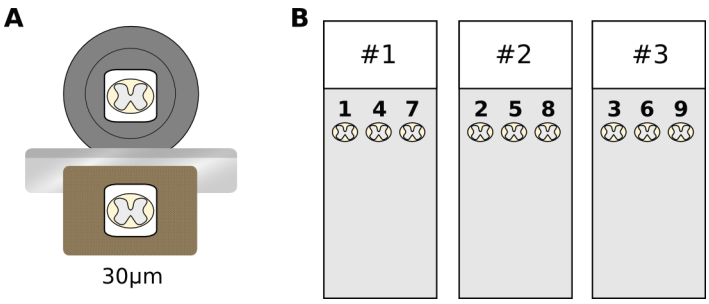

Figure 2.13: **Systematic random sampling of histological sections. A:** Tissue sections are cut on a cryostat at $30\mu m$, which begins at a random starting point rostral to the region of interest. **B:** Tissue sections are taken caudally and systematically distributed across several slides using a serial sectioning paradigm. This ensures an even distribution of tissue sections across all slides. Combined with the random starting point, this method produces an array of slides consistent with SRS and suitable for stereological image analysis.

Systematic random sampling on each tissue section is dependent on the process of image acquisition. Imaging can be performed via two distinct methods:

1. Small sample images can be obtained in a systematic random manner throughout each region of interest (ROI), and each image is processed and analysed separately (here on referred to as SRS Sample Imaging, see Figure 2.14A).

2. One large sample image can be taken, ROIs are delineated onto this sample image post-acquisition and SRS applied to these ROIs for subsequent image processing and analysis (here on referred to as Large Sample Imaging, see Figure 2.14B).

SRS Sample Imaging requires a map of the region to be sampled, in order to locate the positions of image samples. This is achieved by taking a low-resolution overview image which displays the ROI borders, delineating the ROIs onto this image, and calculating a random start position in the vertical and horizontal plane for each ROI to locate the first sample position. This is followed by a systematic shift of this position through the ROI to obtain the positions for the pre-selected number of samples for each ROI. This acquisition method has the benefit of producing 3D image stacks which can have a stereological counting frame applied directly to them, but has the disadvantage of being very labour

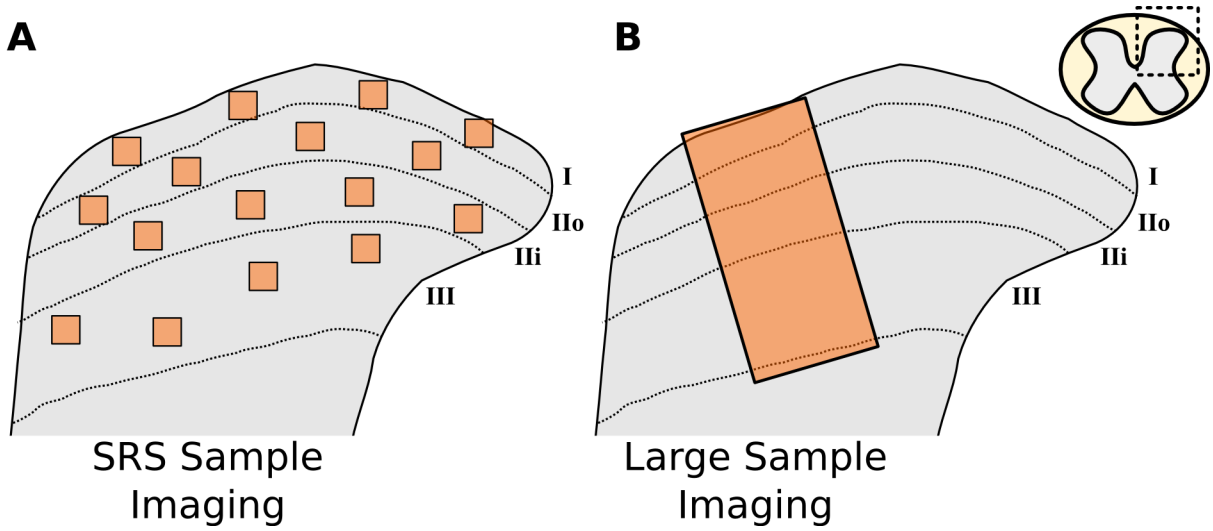

Figure 2.14: **Image acquisition methods. A:** SRS Sample Imaging derives numerous small sample images throughout each region of interest (here, lamina 1-3 of the dorsal horn). To acquire these images, an anatomical map of the tissue section is required. This method is labour-intensive due to the large number of images acquired. **B:** Large Sample Imaging takes one large image covering all ROIs (lamina 1-3 of the dorsal horn here). This image is acquired by taking a tiled image across the ROIs, and no anatomical map is required (see Text). This method requires less intervention due to the reduced number of images acquired.

intensive, requiring the constant imaging of numerous small image samples. Furthermore, deriving the SRS co-ordinates for each sample in each region of interest adds an extra complication to this method.

Large Sample Imaging consists of selecting a large region for imaging which includes a portion of each ROI, taking a single Z slice containing information of the ROI borders (the Reference Image), followed by the acquisition of a Sample Image Stack (Figure 2.15). Imaging of each Sample Image Stack can have a long acquisition time (dependent on resolution and averaging, see Section 2.3.1.2); however, this time is free from user intervention, making this method less labour intensive. Furthermore, although the dorsal horn is randomly sampled in the rostro-caudal plane (due to the SRS performed at the histological section level, see Figure 2.13), the sampling in the mediolateral plane can be controlled. This results in targeted sampling to a specific mediolateral segment of the superficial dorsal horn, which would reduce any variability in measurement if the dorsal

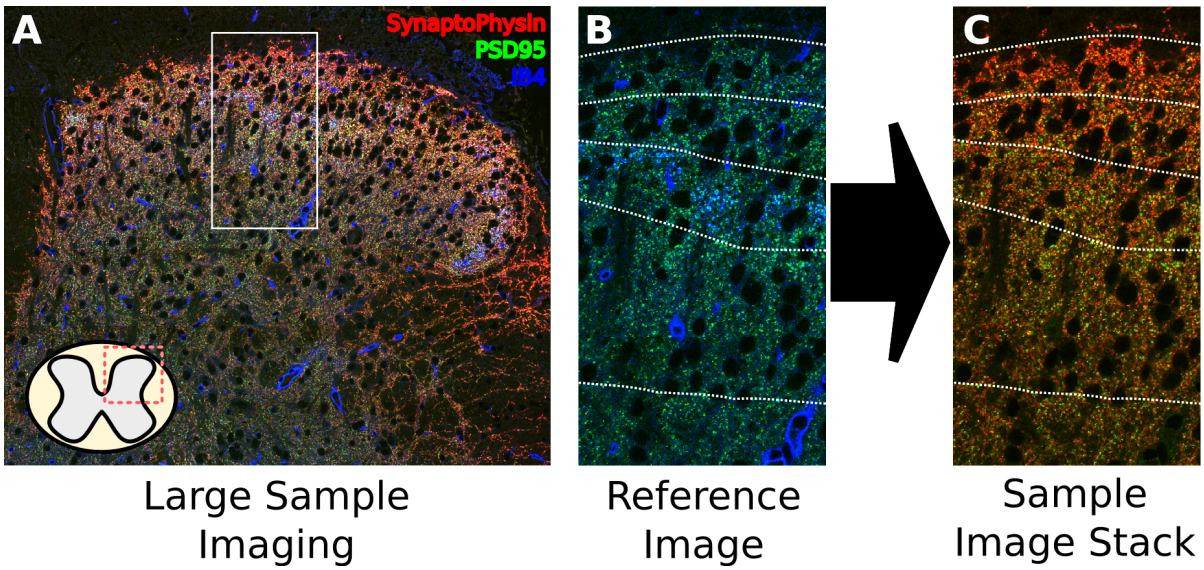

Figure 2.15: **Large Sample Imaging. A:** Large Sample Imaging of the dorsal horn is performed by selecting a region along the mediolateral axis of the superficial dorsal horn for imaging. **B:** Initially, a single Z slice is taken across the ROIs (here, lamina 1-3 of the dorsal horn) of staining that specifies ROI boundaries, producing an Reference Image used to delineate the ROIs. **C:** Next, a Z stack of the sample staining is taken. The ROIs delineated in the Reference Image can be applied to the Sample Image Stack for analysis of the individual ROIs.

horn did not have a homogenous distribution of synapses throughout the mediolateral axis (and there is evidence to suggest at least circuitry varies in the mediolateral plane, see Petkó and Antal (2012) for review). This targeted sampling regimen results essentially in a reduced region for sampling, which can be advantageous. By restricting analysis to only one well defined region, sample variation should be minimised, thus leading to a reduction in error of the estimated synapse count within a given experimental group, which will enhance the statistical power of the experiment.

Once Sample Image Stacks have been obtained for several spinal cord sections, image processing can be applied to each ROI, which can be obtained from the Reference Image (Figure 2.15 B & C).

2.3.1.2 Image Sampling Density & Acquisition

During image acquisition, the sampling density, or resolution, at which to acquire the images must be set. This has an impact on the subsequent image processing steps, and

so deserves special mention. The maximum resolution attainable with a given objective lens is determined by its Numerical Aperture, which is a measure of the range of angles which the lens can accept or detect light. As more light is received, finer detail can be acquired during image acquisition, and thus a higher resolution can be achieved. However, this resolution is ultimately diffraction-limited by the wave-like nature of light, which limits the ability for a given objective lens to differentiate fine detail, and has the effect of distorting small objects with a size near or below the wavelength of the emitted light. Different methods have been developed to overcome this distortion, including newly realised super-resolution methods (Fritzky and Lagunoff, 2013; Tønnesen and Nägerl, 2013), and computational methods such as deconvolution (Sibarita, 2005; Fritzky and Lagunoff, 2013)(reviewed in Section 2.3.2.1), which are applied to conventional imaging methods.

To apply deconvolution to image stacks, a sampling density must be chosen which produces the complete optical coverage of the sample. This rate, known as the Nyquist Rate, ensures the images obtained have been generated by complete sampling of the region (see Figure 2.16) (Sibarita, 2005). This complete coverage is important for accurate deconvolution and for representation of small and diffraction-limited objects.

In order to apply deconvolution to images of sampled synapses, this Nyquist Rate has been calculated for the specific objective lens used throughout this work (Figure 2.16C). This rate is given as the maximal voxel size to meet the Nyquist Rate. Thus, to ensure adequate sampling and to standardise image acquisition, a resolution of 40nmx40nmx100nm in XYZ has been used for all images destined for deconvolution.

Image acquisition was performed with 2x averaging, with a pixel dwell of ~$0.8\mu s$. All images were acquired at 16-bit depth for deconvolution. The acquisition of an image stack of ~78x152μm (sufficient to cover lamina I-III of the superficial DH) to a depth of $5.5\mu m$ was taken for sample image stacks through the middle region of the superficial dorsal horn

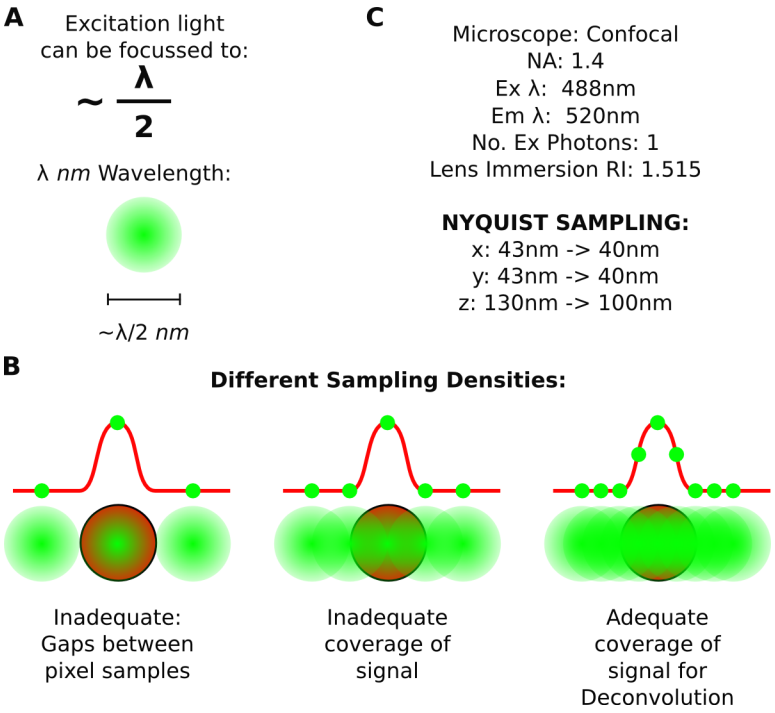

Figure 2.16: **Nyquist Sampling.** **A:** Light is diffraction-limited, which means a light beam can only be focussed to approximately half of its wavelength. **B:** When a diffraction-limited spot of light is used to probe an object, the Sampling Density determines whether complete coverage of the area of interest is achieved. The rate which achieves complete coverage is referred to as the Nyquist Rate, which needs to capture sufficient information to reconstruct the object's signal. **C:** Calculation of the Nyquist Rate for the Confocal Microscope using an oil-immersion 1.4NA lens, and fluorescence from the fluorescent dye Alexa 488. Calculations performed on the Nyquist Calculator from https://svi.nl/NyquistCalculator.

of the three spinal cord test sections stained in the preceding section (see Figure 2.17). This imaging regime took ~12 minutes for acquisition of a single channel.

2.3.2 Image Processing

In order to derive meaningful semantic information from an image, it is necessary to progress from the low-level pixel data to a model that transforms the image into meaningful information (Gonzalez and Romero, 2010; Sonka et al., 2013). After obtaining high-quality image data, image processing enables the extraction of semantic meaning from images. This is generally achieved by attempting to delineate image objects (Sonka et al., 2013). Image processing first attempts to improve object representation through image noise reduction, as well as object feature enhancement. Next, image segmentation is performed, which attempts to separate the image objects from the image background. Finally, the extracted objects are labelled, and relevant measures of these objects are performed. This process allows the derivation of high-level data from the low-level pixel data, and generates knowledge concerning the image content (Gonzalez and Romero, 2010; Sonka et al., 2013).

This methodology of extracting meaningful features from the underlying low-level pixel data has been used to measure the synaptome within the superficial dorsal horn in this Thesis. In order to improve object representation, deconvolution has been employed to reduce image noise and improve object signal:noise. Image segmentation has been achieved by utilising auto-thresholding algorithms, which results in an objective and consistent segmentation of sample images. Extracting data from the isolated objects has been performed with algorithms for object labelling and measurement, which apply a stereological counting frame to ensure measurement from an unbiased sample of objects. These steps are reviewed below.

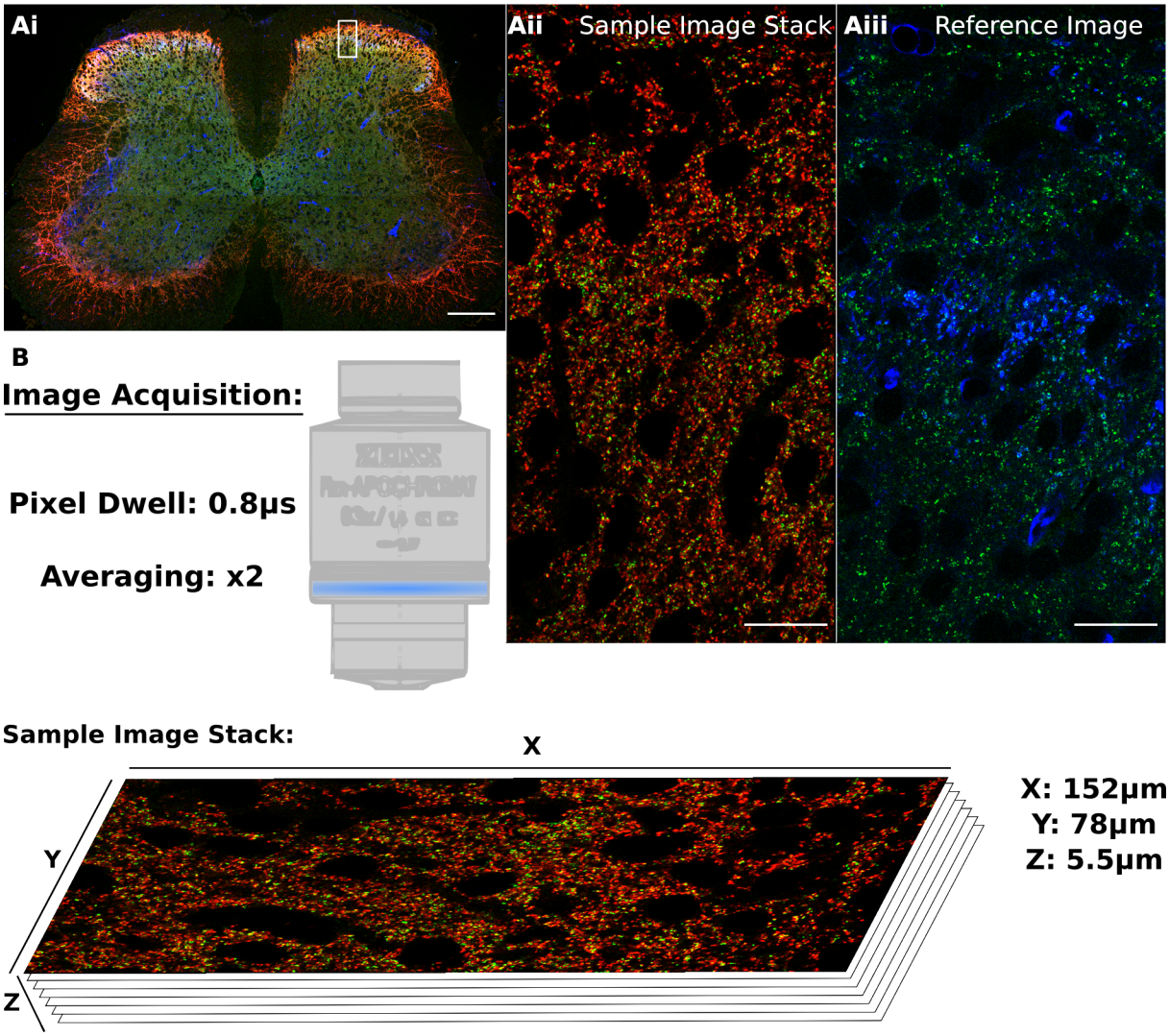

Figure 2.17: **Image Acquisition Settings. A:** Image Acquisition demonstrated on one of the three spinal cord sections, which followed the Large Sample Imaging regime. An overview of the spinal cord section to be imaged (Ai) delineates the area where a large sample will be derived. A Sample Image Stack (Aii) and Reference Image (single Z slice) (Aiii) were acquired from the region highlighted. **B:** An image stack of ~78x152x5.5μm was taken from a pre-selected region of the superficial dorsal horn. Image acquisition was performed with an averaging of 2, a pixel dwell of ~0.8μs, and at 16-bit depth. Scale Bars: Ai, 200μm;Aii & Aiii, 20μm.

2.3.2.1 Deconvolution

Deconvolution is a process which attempts to restore an image which has been distorted during the image formation process (Sibarita, 2005). In microscopy, assuming optimal image acquisition, this distortion results from the diffraction-limited nature of light, and thus results in optical blur. The objective of deconvolution in microscopy is therefore to re-assign this optical blur to its original position, as well as reduce statistical noise. This process results in a representation of each imaged object which is closer to the true underlying object. With an improvement in object representation comes facilitated image segmentation and analysis capabilities.

Deconvolution attempts to reverse the image formation process, which can be modelled as a convolution of the underlying image objects and the optical blur induced by the wave-nature of light & the imaging system (Figure 2.18A). The optical blur can be described visually as the image that would be obtained from an infinitely small point source of light passed through the imaging system (Figure 2.18B). This visual representation is referred to as the Point Spread Function (PSF), and describes the response of the microscope during image acquisition (Sibarita, 2005). Many deconvolution algorithms require the PSF as it illustrates the distortion introduced during image formation.

PSFs can be sourced in two ways:

1. Empirical PSFs can be generated by imaging sub-resolution fluorescent beads.

2. Theoretical PSFs can be generated *in silico* by modelling the image acquisition of the imaging system.

An empirical PSF offers the key advantage of producing an individualised PSF for the specific objective & imaging system under use, encompassing any small variations in the regularity of the objective and light path, which may modify the PSF in unpredictable

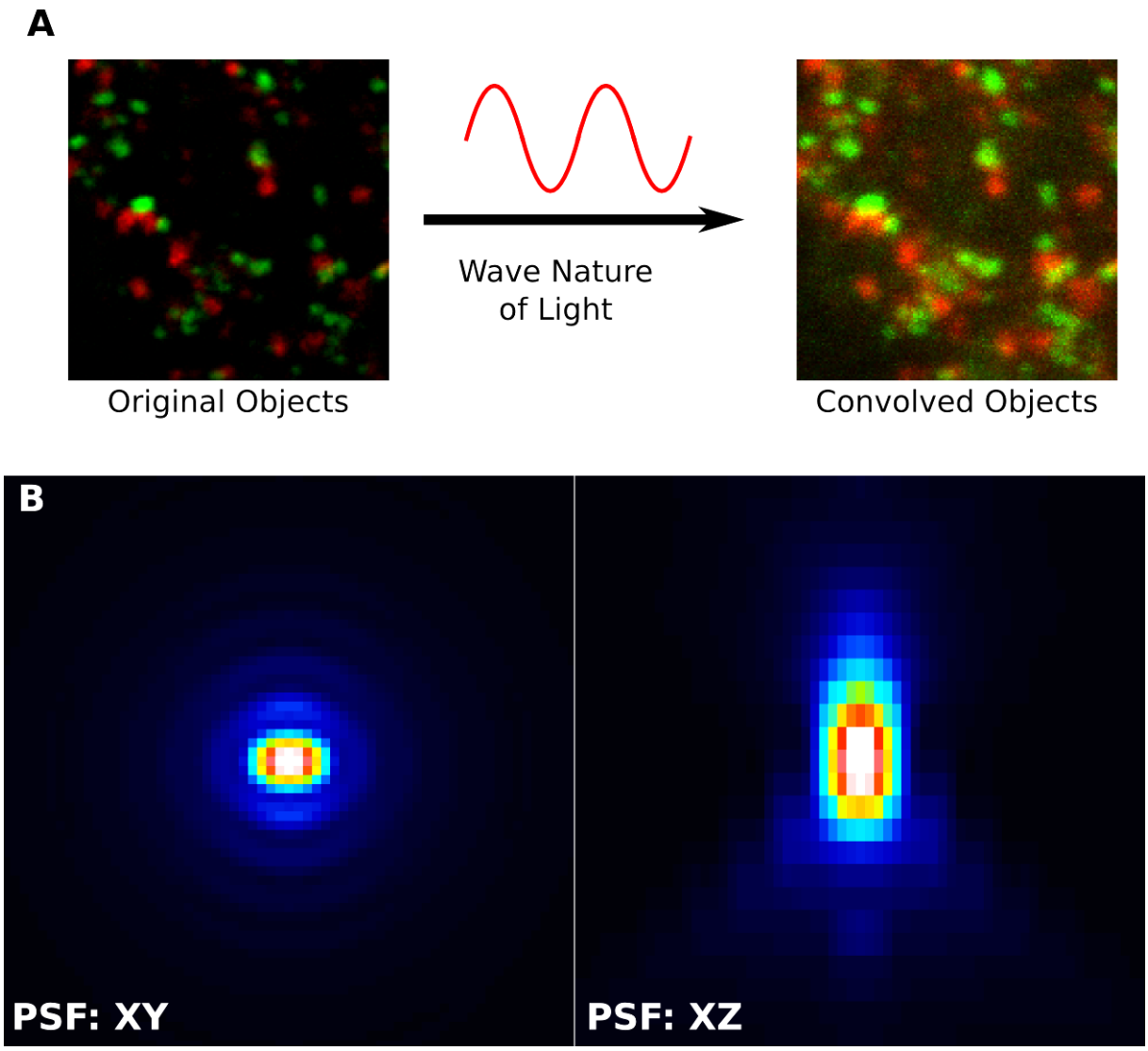

Figure 2.18: **The Image Formation Process & the Point Spread Function. A:** The image formation process can be modelled as a convolution, whereby underlying objects are distorted by the wave-nature of light, and statistical noise. **B:** The Point Spread Function (PSF) represents the modifications to a point-source of light passing through the imaging system. This information is essential for deconvolution.

ways. However, the generation of empirical PSFs is a difficult process involving the careful preparation of sub-resolution fluorescent beads for imaging in the exact conditions of sample imaging. Sub-resolution fluorescent beads often display weak fluorescence intensity and photobleach rapidly, resulting in weak signal:noise. The weak signal:noise is particularly problematic for PSFs as these are designed to describe the blur produced by the optical system, and noise in the PSF can severely hamper deconvolution. Often multiple beads are imaged and registered to give an averaged PSF for image deconvolution (Sibarita, 2005).

The key advantage to a theoretical PSF is the complete absence of noise. This allows an accurate theoretical determination of a 3D PSF both within and far outside the focal plane, which would be degraded with significant noise when measured empirically. Theoretical PSFs are easier to produce, although knowledge of the sample preparation and optical setup are required. These models do not take into account any irregularities which may be present in the specific imaging system in use, and assume a perfect light path free from aberrations, except those induced by RI mismatches between mountant, the glass coverslip and immersion medium (Sibarita, 2005).

A recent model published by Nasse and Woehl (2010), based on high quality 3D experimental PSFs determined using 20nm nanobeads (Nasse et al., 2007), is able to determine theoretical PSFs with accurate correction for spherical aberration due to refractive index mismatching. The model has been released as a software package, PSF Lab, which is freely available from the One Molecule Group (http://onemolecule.chem.uwm.edu/).

Utilising this software package for theoretical PSF generation, two confocal 3D PSFs were generated corresponding to the illumination PSF for the green (488nm) and red (546nm) lasers. PSFs were generated using the voxel size previously determined for Nyquist Sampling (XYZ: 40nm x 40nm x 100nm), and produced in a 3D image stack

$5\mu m$ x $5\mu m$ x $5.5\mu m$ in size (XYZ).

Once a sufficiently accurate PSF has been generated, a high quality deconvolution algorithm is necessary to restore confocal images. Deconvolution is described as an inverse or ill-posed problem (Bertero and Boccacci, 1998), and so multiple different solutions or algorithms have been developed (Sibarita, 2005). Of particular interest are the constrained iterative methods, which provide an approximate solution that is developed with each successive iteration whilst placed under particular constraints (Nagy et al., 2004b).

A number of constrained iterative deconvolution algorithms are provided as plugins for the open-source image processing package, ImageJ. Iterative Deconvolve 3D (Dougherty, 2005) and Parallel Iterative Deconvolution (Nagy et al., 2004b; Wendykier and Nagy, 2010) are two high-quality constrained iterative deconvolution plugins available for ImageJ. Parallel Iterative Deconvolution has the added benefit of taking advantage of the multithreaded nature of current CPUs (Wendykier and Nagy, 2010), resulting in efficient use of computational resources and reduced deconvolution time, and has been used for deconvolution in this work.

2.3.2.2 Fluorescent Bead Deconvolution

To test both the theoretical PSFs and the selected deconvolution algorithm, images were obtained of fluorescent beads of a range of diameters. TetraSpeck Fluorescent Microspheres (T14792, Invitrogen; beads pre-mounted onto a slide), with diameters 175nm, 500nm & 1000nm, were imaged using a LSM 700 Zeiss confocal microscope with the x63/1.4NA apochromat (DIC) objective at the Nyquist Rate (XYZ: 40nm x 40nm x 100nm), using identical image acquisition settings as used for synapse imaging (see Figures 2.17 & 2.19A). Eight beads were imaged of each size in both the green (488nm laser) and red (546nm laser) channels. The laser power, gain, digital offset and digital gain

settings were adjusted for each bead to ensure maximal sampling of the image histogram whilst avoiding over- and under- exposed pixels.

Figure 2.19B shows representative images of 175nm, 500nm & 1000nm beads projected in both the XY and XZ planes. The full width half-maximum (FWHM) was measured for all beads (Figure 2.19C). First, the central pixel was identified on average intensity projections, and measures of X, Y & Z axis profiles through the central pixel were obtained. The X & Y axis profiles were averaged, and the mean(±SEM) lateral (XY) and axial (Z) axis profiles were plotted for eight beads in both 175nm, 500nm & 1000nm beads in both red (546nm) and green (488nm) channels. A gaussian function was fitted to each these plots in GraphPad Prism (GraphPad Software, Inc.) using nonlinear regression with a least-squares fit. The fitted gaussian function was used to calculate the FWHM mean±SEM for each bead size and channel (Figure 2.19C).

In order to determine the effects of deconvolution on bead representation, bead images were subject to deconvolution utilising the previously produced PSFs and the WPL algorithm within the ImageJ plugin Parallel Iterative Deconvolution. Constrained iterative deconvolution algorithms can be run for a pre-selected number of iterations, and to test this parameter, deconvolution was run for 20, 40, 60, 80 & 100 iterations on each bead. Figure 2.20 shows representative beads after 40 and 100 iterations, as well as gaussian plots and FWHM values for each bead size and channel at 40 and 100 iterations.

To compare the FWHM between raw beads and beads subjected to deconvolution, the mean±SEM of FWHM values for each bead type were plotted. As can be seen in Figure 2.21, deconvolution significantly reduces FWHM in both the lateral (XY) and axial (Z) axes. In general, improvements in FWHM are seen up to 40 iterations, with no further improvement seen after this number. This is illustrated in Figure 2.20A & B, where there is no obvious improvement in fluorescent bead representation between 40 and 100

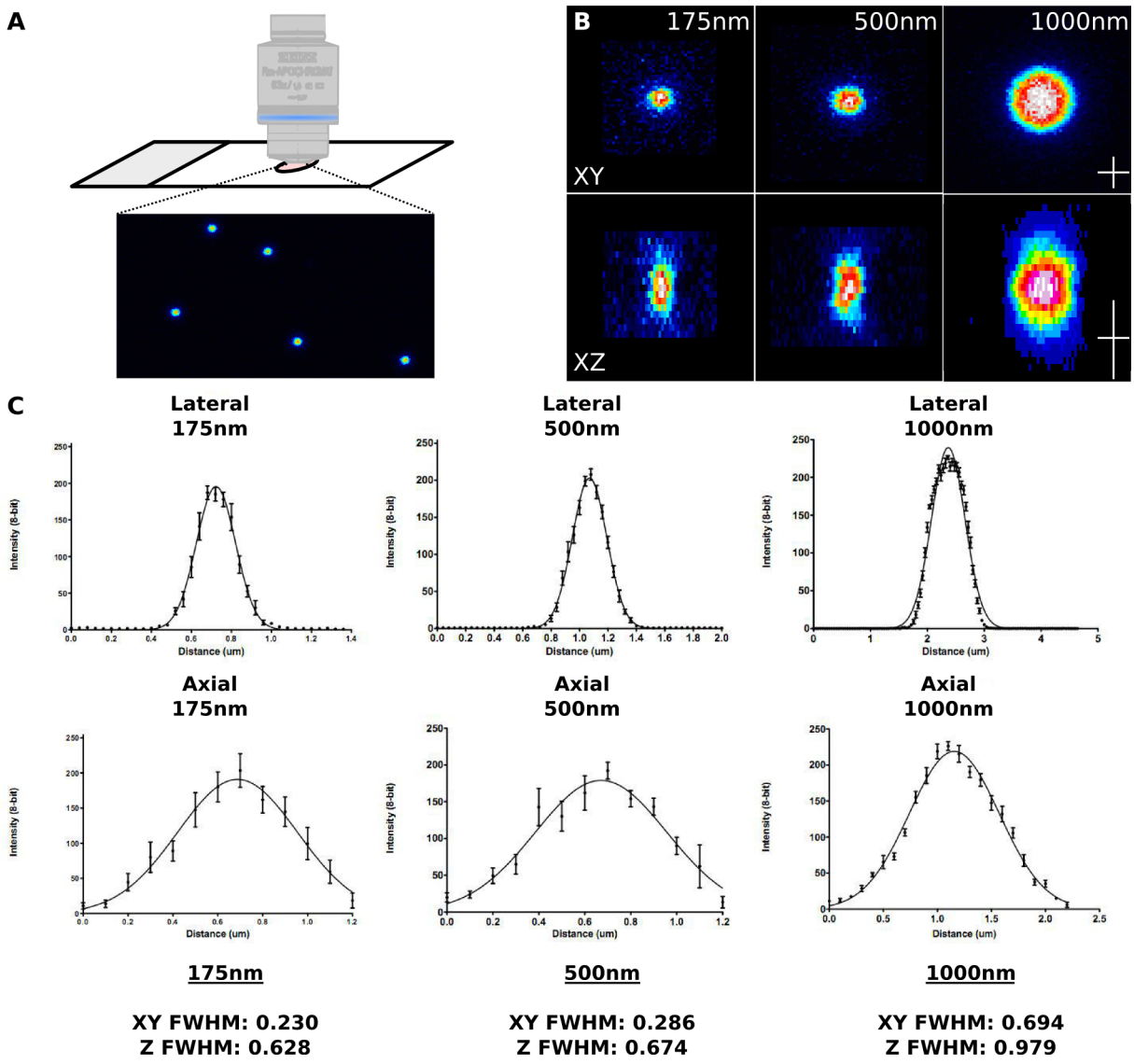

Figure 2.19: **Raw 175nm 500nm and 1000nm bead projections & FWHM measurement. A:** Imaging of fluorescent beads. Tetraspeck (T14792) pre-mounted beads were imaged on a LSM 700 confocal microscope (Zeiss), using the x63 apochromat lens and identical imaging settings as used for synapse imaging (16bit, 40x40x100nm voxel, $0.8\mu s$ pixel dwell with 2x averaging). **B:** Representative images of 175nm, 500nm & 1000nm fluorescent beads, imaged with the 488nm laser. Maximum intensity projections taken from the XY and XZ planes. **C:** Lateral and axial axis-profile plots (mean±SEM) of eight fluorescent beads with gaussian function fitted using least-squares fit. FWHM values determined from gaussian function are given below the graphs. Scale Bars: B, $0.5\mu m$. FWHM, full width half-maximum.

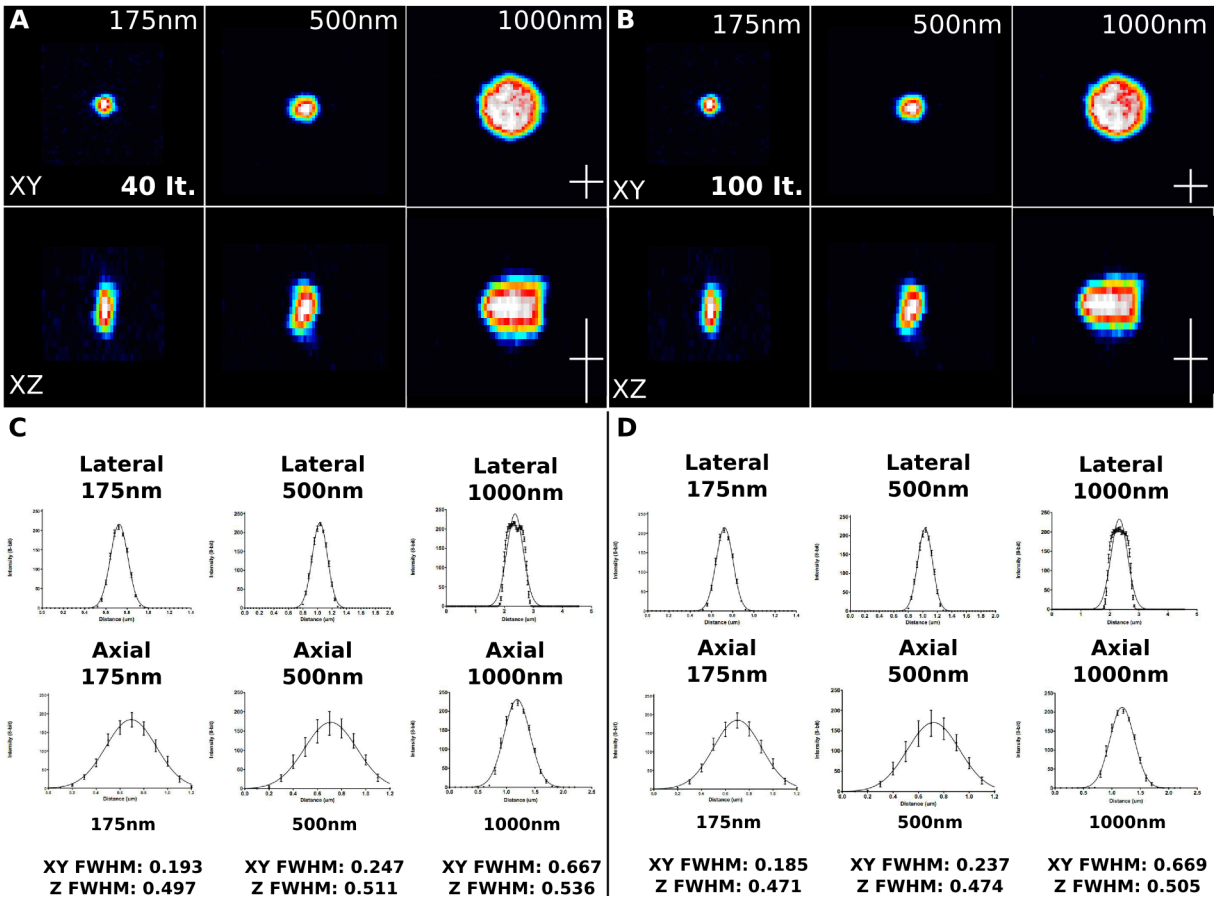

Figure 2.20: **Deconvolved 175nm 500nm and 1000nm bead projections & FWHM measurement. A:** Representative images of 175nm, 500nm & 1000nm fluorescent beads, imaged with the 488nm laser after 40 iterations of deconvolution. Tetraspeck (T14792) bead images were subject to deconvolution using the previously generated PSF & the WPL algorithm within Parallel Iterative Deconvolution. Beads are presented as XY and XZ maximum intensity projections. **B:** Representative images of 175nm, 500nm & 1000nm fluorescent beads, imaged with the 488nm laser after 100 iterations of deconvolution. Tetraspeck (T14792) bead images were subject to deconvolution using the previously generated PSF & the WPL algorithm within Parallel Iterative Deconvolution. Beads are presented as XY and XZ maximum intensity projections. **C:** Lateral and axial axis-profile plots (mean±SEM) of eight fluorescent beads following 40 iterations of deconvolution with gaussian function fitted using least-squares fit. FWHM values determined from gaussian function are given below the graphs. **D:** Lateral and axial axis-profile plots (mean±SEM) of eight fluorescent beads following 100 iterations of deconvolution with gaussian function fitted using least-squares fit. FWHM values determined from gaussian function are given below the graphs. Scale Bars: A & B, 0.5μm. FWHM, full width half-maximum; It., iterations.

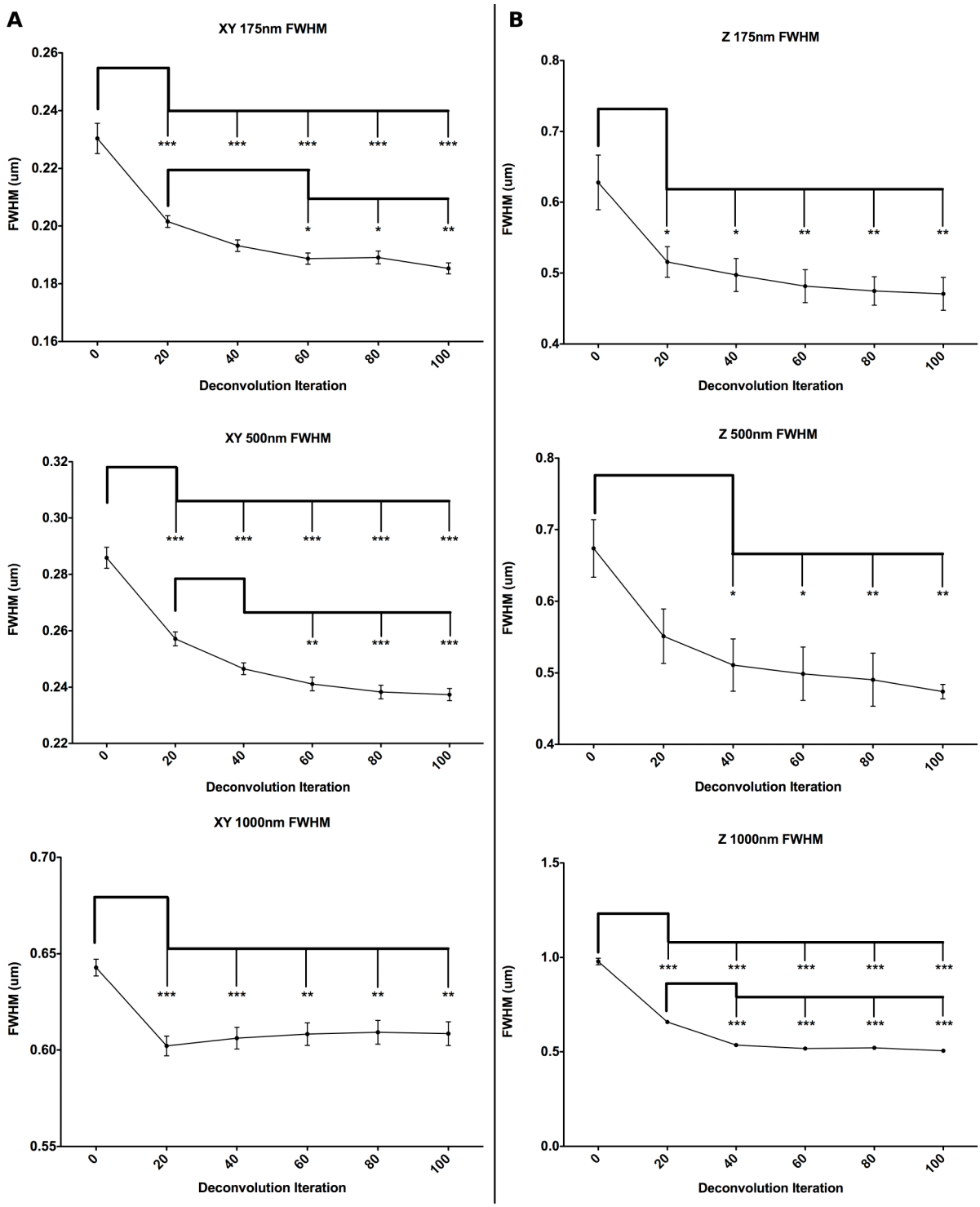

Figure 2.21: **Deconvolution significantly reduces FWHM of fluorescent beads. A:** Lateral FWHM of 175nm, 500nm and 1000nm fluorescent beads are significantly reduced following deconvolution. **B:** Axial FWHM of 175nm, 500nm and 1000nm fluorescent beads are significantly reduced following deconvolution. Analysis: One-Way ANOVA with Tukey post-hoc testing of all pairs. *, $p<0.05$; **, $p<0.01$; ***, $p<0.001$. FWHM, full width half-maximum.

iterations.

Taken together, these results suggests deconvolution up to 40 iterations is sufficient to produce an improvement in object representations, with a particularly significant improvement seen in the Z plane. However, a significant stretch was still apparent in the Z plane (Figure 2.20A&B), most pronounced for 175nm diameter beads, indicating deconvolution did not completely re-assign the blur in the Z plane. This is in line with previous reports, particularly with theoretical PSFs (Sibarita, 2005). Deconvolution does still improve object representation beyond the raw image, and also shows an improvement in signal:noise which is of vital importance for subsequent image processing. Thus, deconvolution at 40 iterations was taken forward to images of synaptic puncta to test deconvolution on the representation of synapses in confocal image stacks.

2.3.2.3 Synapse Sample Deconvolution

Once an improvement in fluorescent beads was shown using the PSF and deconvolution algorithm selected, the process was tested on the images obtained from the three spinal cord test sections. Figure 2.22A shows one sample image stack acquired from one spinal cord test section before and after deconvolution. A clear reduction in the size of synaptic puncta can be observed at this low magnification. Figure 2.22B shows a number of magnified views showing an obvious elimination of optical blur across all synaptic puncta.

Thus, deconvolution appears to improve synapse representation visually, and was taken forward through the remainder of the image processing workflow.

2.3.2.4 Image Segmentation

Image segmentation can be defined as attempting to isolate the objects of interest within an image from the image background, and from each other (Sonka et al., 2013). Image segmentation techniques can be divided into local and global methods, where local thresh-

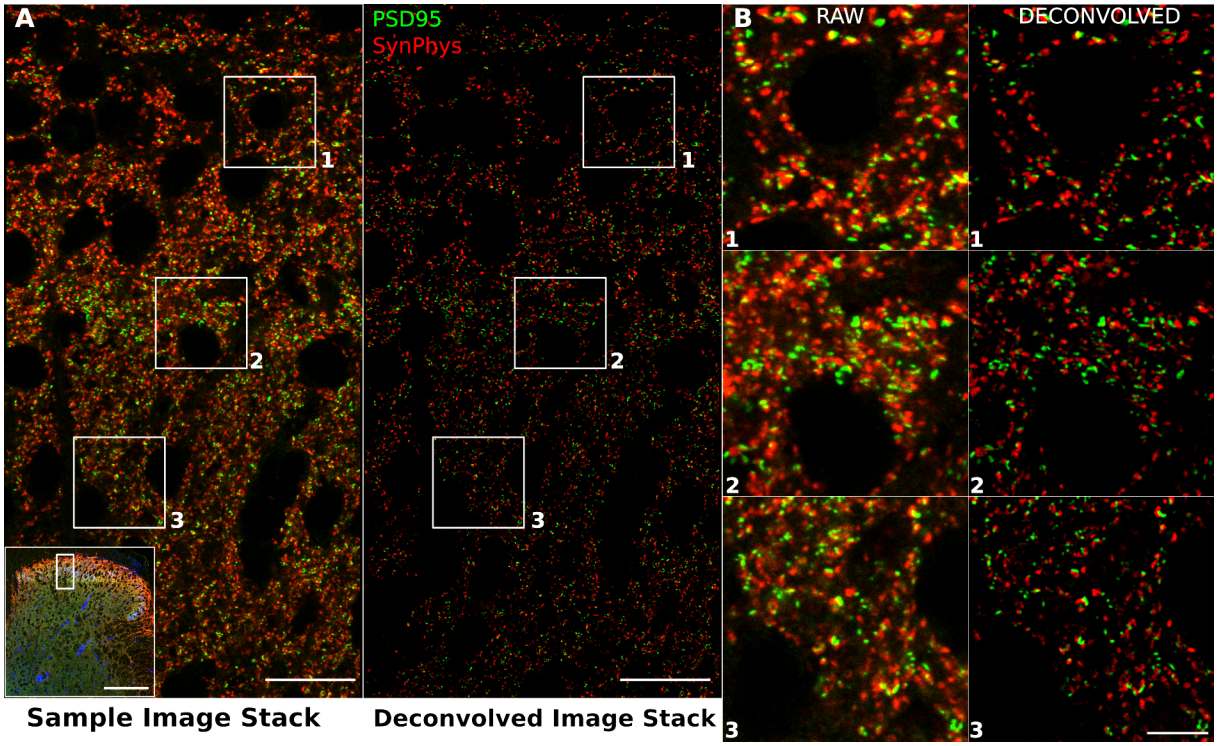

Figure 2.22: **Deconvolution improves synapse representation from confocal image stacks. A:** One Sample Image Stack obtained from the spinal cord test sections before (Sample Image Stack) and after (Deconvolved Image Stack) 40 iterations of deconvolution. **B:** Magnified views of panels 1, 2 & 3 labelled in A. Deconvolution clearly reduces the optical blur seen in the raw image stack. All images are $0.3\mu m$ projections. Scale Bars: A, $20\mu m$ (inset: $200\mu m$); B, $5\mu m$. SynPhys, SynaptoPhysin.

olding partitions an image to calculate local threshold values, whereas global methods determine a single threshold for the entire image (Sahoo et al., 1988; Sezgin and Sankur, 2004). A popular global thresholding method, robust to different levels of contrast and number of object-pixels is the OTSU Method, an algorithm from the cluster-based global thresholding methods (Otsu, 1979; Sezgin and Sankur, 2004).

Prior to thresholding, images often undergo a noise-reduction step to help eliminate statistical noise, and improve the signal:noise (Sonka et al., 2013). A popular method which aims to reduce statistical noise, in the form a abrupt single pixel spikes, is median filtering. This method is often used as a pre-processing method to eliminate statistical noise throughout an image sample, to aid image segmentation.

To test these methods, both raw and deconvolved images obtained from the three spinal cord test samples were processed with a 3x3 median filter (Despeckle), followed by segmentation with the OTSU Method. As can be seen from Figure 2.23, raw images produced a poor segmentation, where objects which appear separate in the raw image become conjoined following thresholding.

In contrast, images subject previously to deconvolution show excellent segmentation. Objects which appear as individual puncta in the original raw image (Figure 2.23A) remain separate after segmentation (Figure 2.23D), and there is a close correspondence between the images. This is further displayed in Figure 2.24, where $0.6\mu m$ projections of synaptic staining has been thresholded before or after deconvolution. Deconvolution clearly isolates individual synaptic puncta, indicating its utility in aiding image thresholding.

These results strongly support the use of deconvolution as a pre-processing step prior to image segmentation. Furthermore, they validate the use of the median filter and cluster-based auto-thresholding method, OTSU. All sample image stacks of the three spinal cord

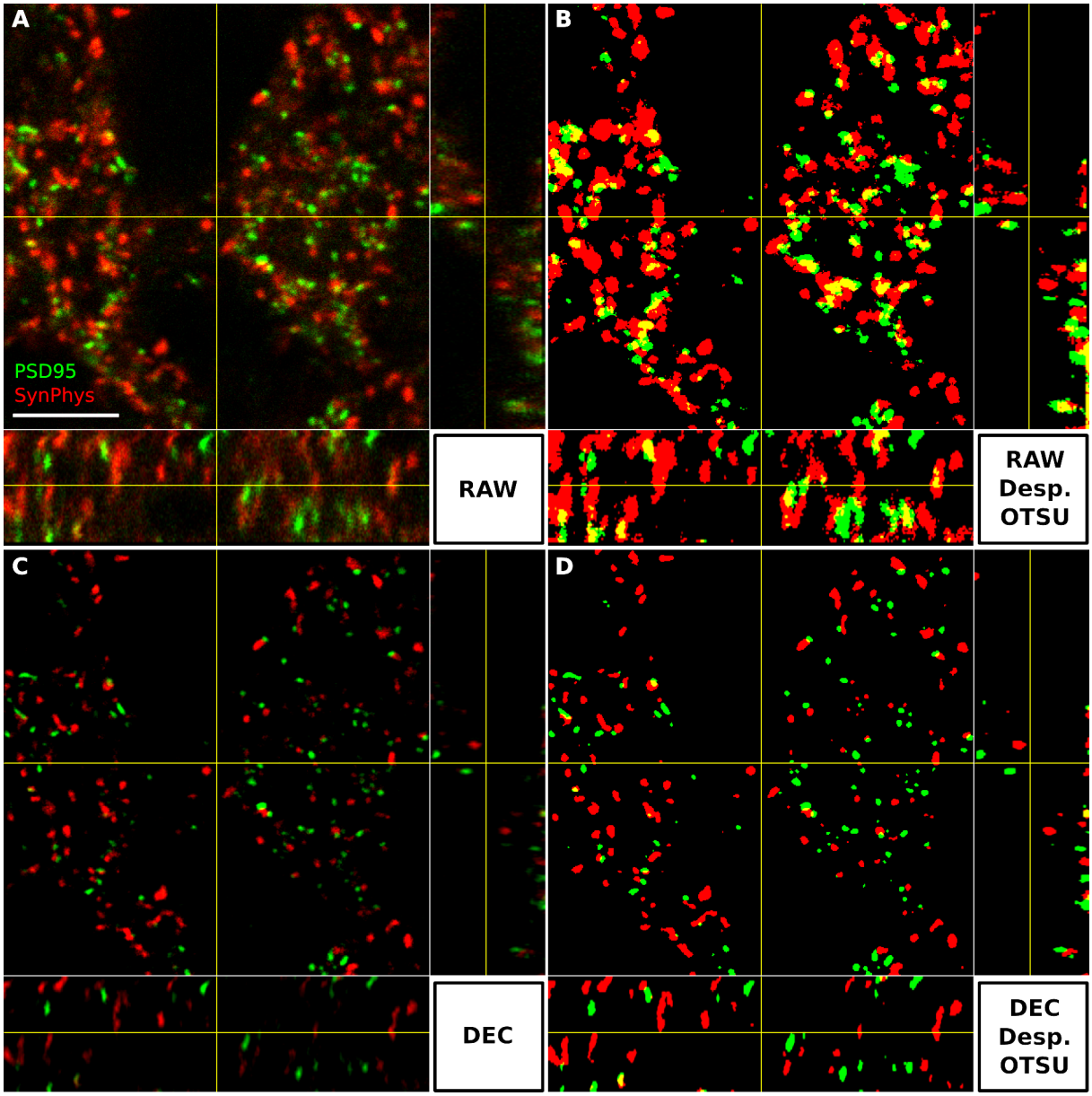

Figure 2.23: **Deconvolution significantly improves automated segmentation.** Images displayed as orthogonal views. **A:** Raw image. **B:** Raw image treated with Despeckle (3x3 median filter) and thresholded using OTSU method. Isolation of synaptic puncta is poor on raw images, with many individual puncta segmented as one structure. **C:** Deconvolved image (40 iterations). **D:** Deconvolved image treated with Despeckle (3x3 median filter) and thresholded using OTSU method. Deconvolution results in thresholded images which keep individual synaptic puncta isolated. The isolated thresholded puncta closely match the observed synaptic puncta in the raw image (A). Scale bar: $5\mu m$. SynPhys, SynaptoPhysin; Desp., Despeckle; DEC, Deconvolved.

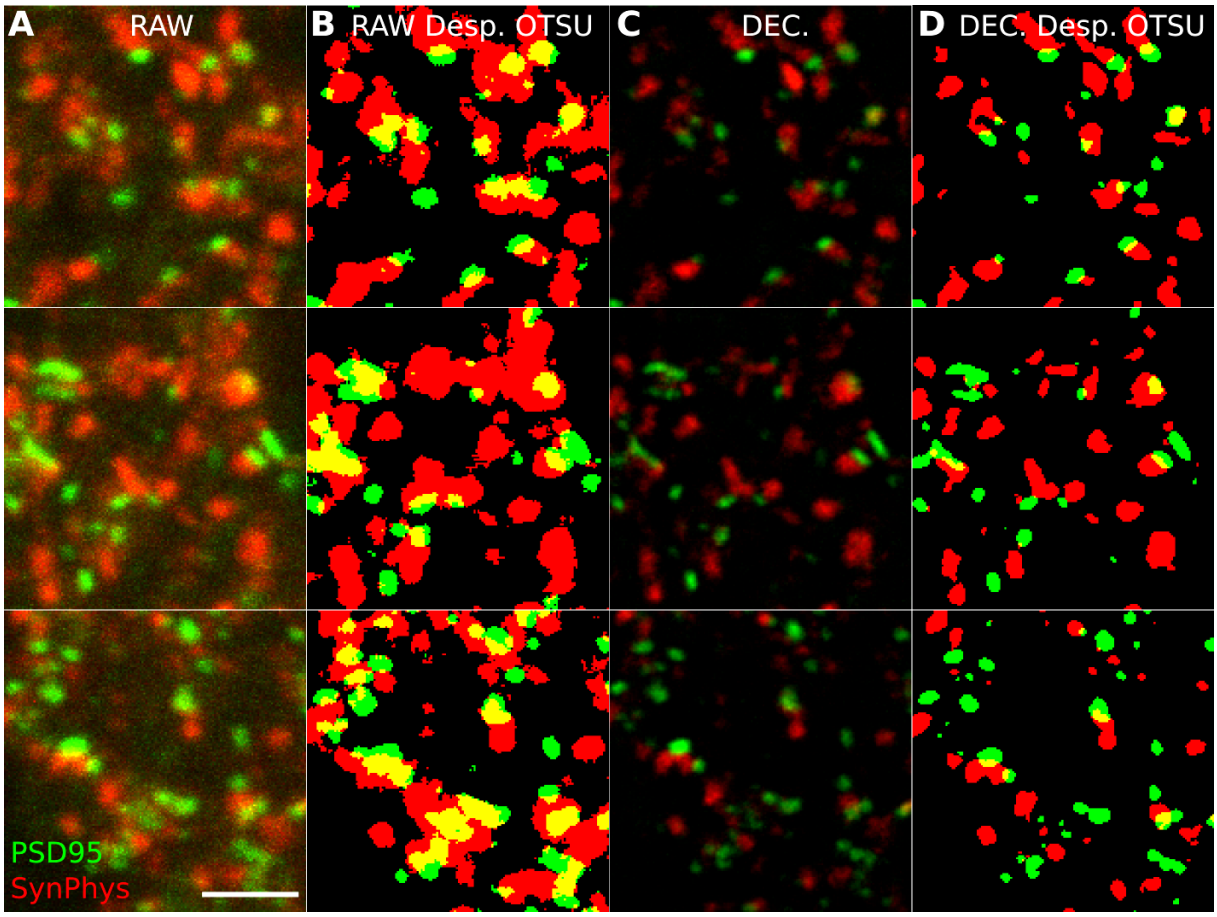

Figure 2.24: **Deconvolution enables isolation of individual synapses.** Three image projections ($0.6\mu m$ deep) isolated from test sample image stacks. A: Raw image. B: Raw image treated with Despeckle (3x3 median filter) and thresholding (OTSU). C: Deconvolved image (40 iterations). D: Deconvolved image treated with Despeckle (3x3 median filter) and thresholding (OTSU). Note synaptic puncta which appear independent in the raw images (A) are often thresholded into a single structure with Despeckle and OTSU (B), whereas following deconvolution, these synaptic puncta remain separate following segmentation (D).Scale bar: $2\mu m$. SynPhys, SynaptoPhysin; Desp., Despeckle; DEC, Deconvolved

test samples have been taken through this image processing to yield thresholded PSD95 and SynaptoPhysin objects for quantification.

2.3.3 Object Quantification

Once a suitable representation of image objects has been generated, object quantification can be performed. The purpose of object quantification is to measure the objects to derive high-level data from low-level pixel data, with the ultimate aim of understanding the image content (Gonzalez and Romero, 2010; Sonka et al., 2013). Object quantification requires object labelling, followed by object measurement. Prior to object measurement, a counting frame can be set up to ensure measurement is performed an on unbiased sample of objects, consistent with stereological methods.

2.3.3.1 Object Labelling

Object labelling converts a binary image so that each isolated object is uniquely identifiable. This is achieved by giving each isolated object a unique greyscale value, which can be used to count and quantify the labelled objects. This algorithm has been well described previously (see Burger and Burge, 2008), and so will not be described further here.

2.3.3.2 Stereological Counting Frame

Accompanying Systematic Random Sampling, the second pillar of stereology is the application of a counting frame. The purpose of the counting frame is to ensure objects are quantified independent of their size, shape and orientation. This means that all objects have an equal chance of being quantified, and no bias in measurement is introduced due to an objects' size, shape or orientation.

When quantifying object number, the counting frame is traditionally applied to an

image in the form of the Optical Di-Sector (see Figure 2.25) (Sterio, 1984; West et al., 1991; West, 1999). The Optical Di-Sector can be envisaged as a cube, which quantifies all objects lying within it according to some basic logical rules. As the cube is transected in any plane, one half is surrounded by Acceptance Lines, and the other half by Rejection Lines (Figure 2.25A). The Optical Di-Sector quantification rules will count objects if they lie entirely within the Counting Region, or if they bisect an Acceptance Line, but not a Rejection Line (Figure 2.25B). (A second method referred to as the Optical Fractionator is a subtle improvement on this method, where a set fraction of an ROI is analysed for objects - see West et al. (1991); Schmitz and Hof (2005) for further information.)

To quantify objects with the Optical Di-Sector and Systematic Random Sampling, a number of systematically and randomly distributed Optical Di-Sectors are placed within the ROIs under analysis (West et al., 1991; West, 1999). This is followed by estimating the total ROI volume. The average object density can be calculated from the measurements obtained from the Optical Di-Sectors, and this density is multiplied by the estimated ROI volume, and thus an estimate of the total number of objects can be attained (the "Nv x vRef" method, see Figure 2.26).

This method is the staple of stereological analysis, and can be readily applied to the ROIs isolated from Sample Image Stacks. Following the acquisition of Sample Image Stacks, each ROI can be isolated and exhaustively sampled to derive sample cubes, with each cube assigned an Optical Di-Sector for object quantification (Figure 2.27). However, this method attempts to impose a rigid array of cubes over what is commonly an irregularly shaped region. This results in an inefficient means of measuring objects, due to the gaps present between Optical Di-Sectors, but may also result in a bias for selection of whole cubes located towards the centre of an ROI rather than the edge, cause problems when attempting to sample narrow ROIs, and result in the potential for Distribution Bias;

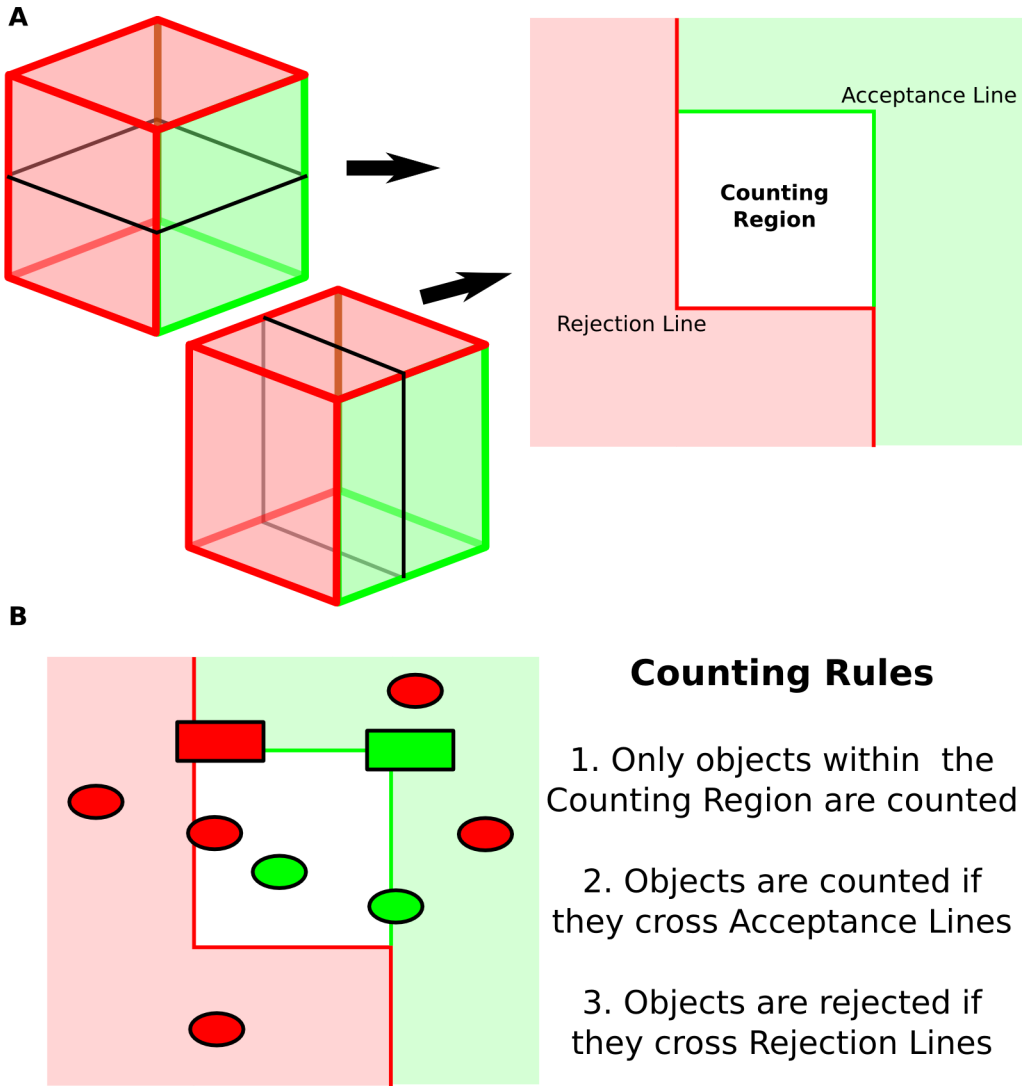

Figure 2.25: **The Optical Di-Sector. A:** The Optical Di-Sector can be envisaged as a 3-dimensional counting cube, possessing Rejection and Acceptance Boundaries. Bisecting this cube (in any dimension), which occurs during image quantification, reveals the more familiar view of the Optical Di-Sector, comprising Acceptance and Rejection Lines. **B:** Demonstration of quantification rules of the Optical Di-Sector. Objects are quantified if they lie within the Counting Region, and if they cross an Acceptance Line, but never a Rejection Line. Objects which are not located within the Counting Region are not quantified.

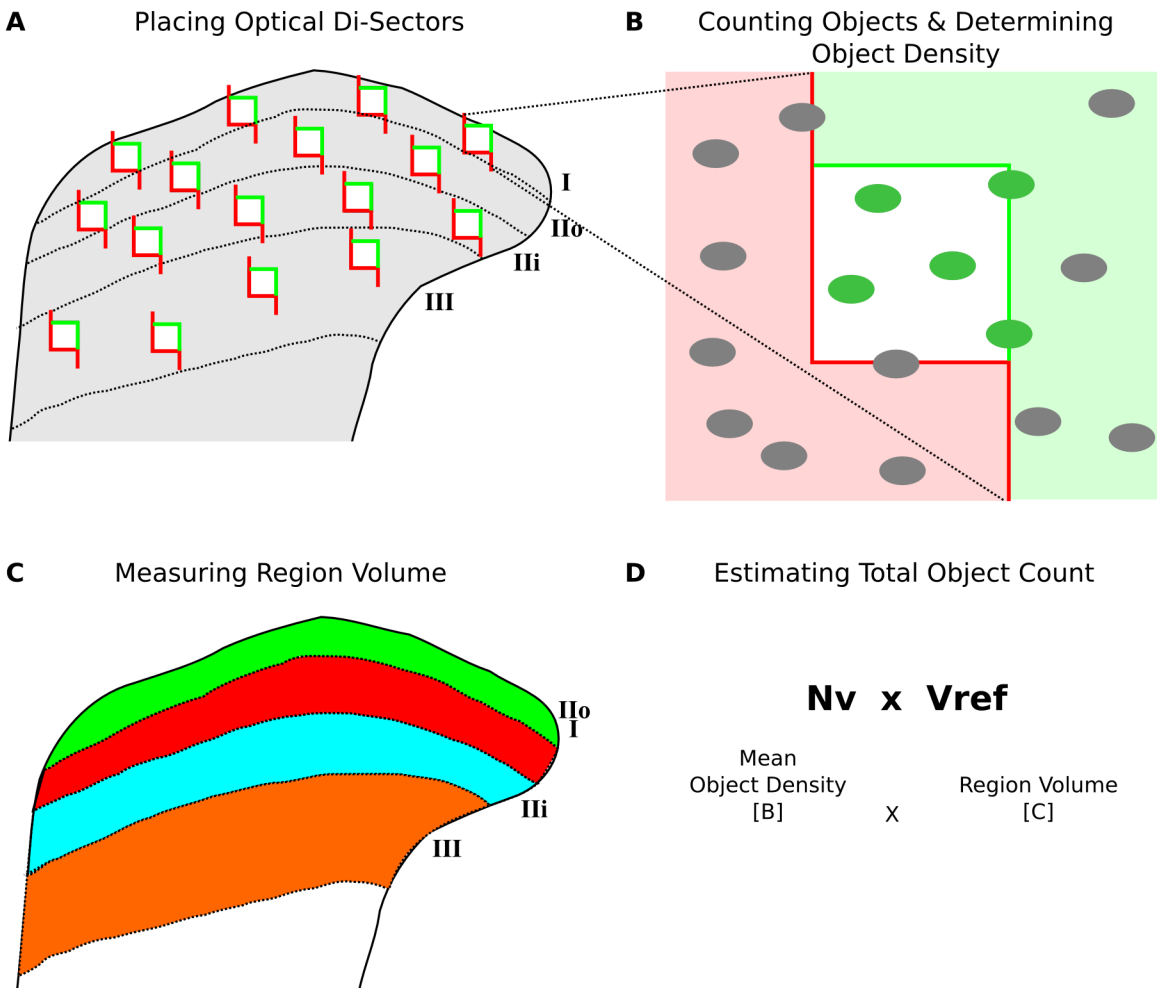

Figure 2.26: **The "Nv x Vref" Method. A:** Optical Di-Sectors are Systematically and Randomly distributed throughout ROIs. **B:** Objects are quantified within each Optical Di-Sector, and object density calculated by dividing object counts by the counting region volume. **C:** Each ROI volume is measured. **D:** An estimate of total object counts is derived by multiplying the mean object density by the measured region volume.

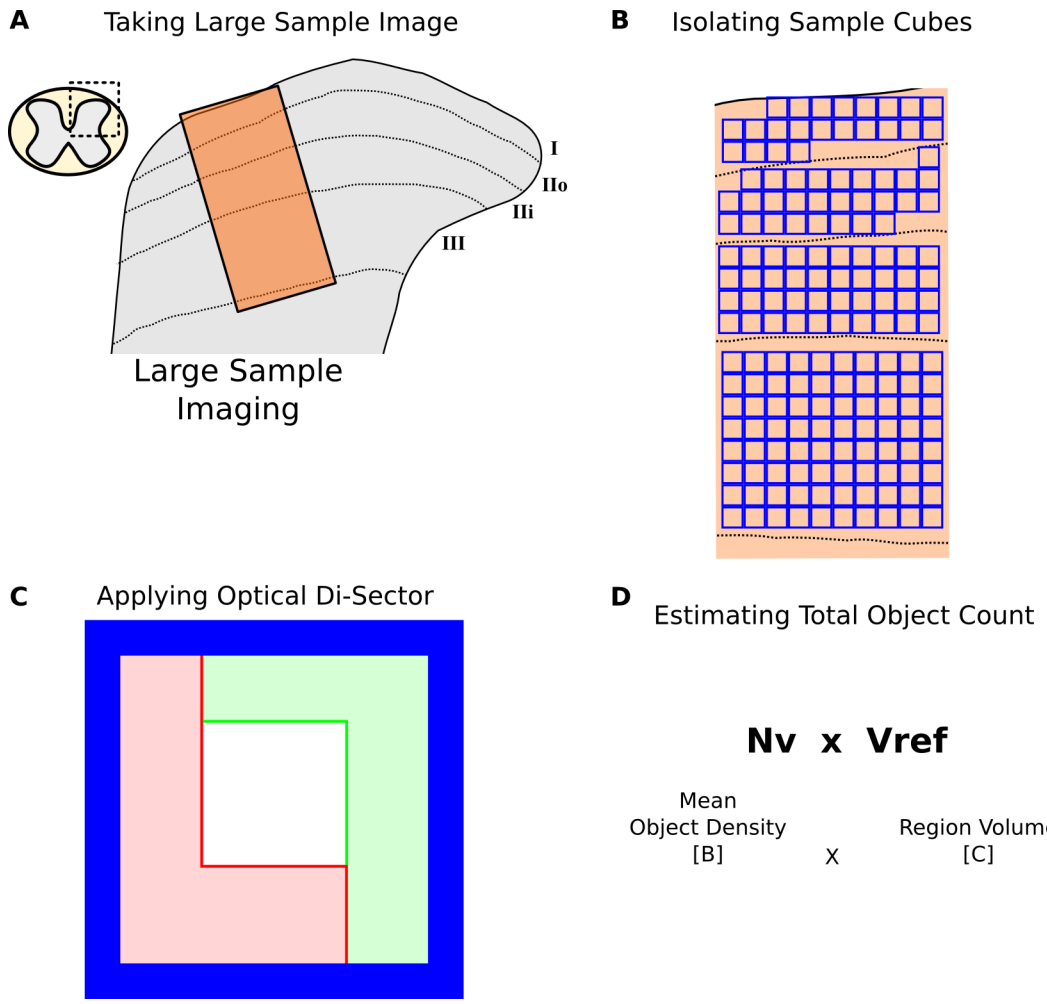

Figure 2.27: **Application of the "Nv x Vref" Method to Large Sample Images. A:** Overview of Large Sample Imaging. **B:** Schematic highlighting the Large Sample with Sample Cubes being isolated from each ROI. **C:** Example image of one Sample Cube, with Optical Di-Sector applied for object quantification. **D:** Estimating total object counts is now performed by multiplying the mean object density by the ROI volume.

thus using an array of Optical Di-Sectors can increase the potential for systematic errors.

Therefore, to overcome the limitation of applying the rigid cuboid counting frame within a naturally undulating ROI, the logic of the Optical Di-Sector has been extended to encompass the irregular shapes often encountered as regions of interest during biological image analysis. In order to achieve this, the underlying quantification rules of the Optical Di-Sector counting frame must be considered.

First, from observing the Optical Di-Sector it is clear that in all three dimensions there is always a Rejection Line paired with an opposing Acceptance Line (Figure 2.28A). The Rejection Line is more accurately described as a boundary imposed upon one edge

in any given dimension of the counting frame, but it appears as a line when the sampling cube is transected during quantification of individual image slices. The volume beyond an Acceptance Line must be sufficient to capture all objects which lie within the counting frame and extend beyond an Acceptance Line, which allows various measurements of the entire object to be performed if desired, and thus the volume beyond the Acceptance line must be at least as long as the largest object. The region lying beyond the Acceptance Line is essential to ensure the entire object is captured during quantification. Applying the counting frame rules, objects lying entirely within this region, and not contacting the counting region, are not within the counting frame, and so are rejected. Thus, this volume extending beyond the Acceptance Line has been named an Exclusion Zone.

Therefore, in practice, an Acceptance Line in any given plane can be converted into an Exclusion Zone which exists between the counting region and the image boundary, with a width equal to the largest object detectable (Figure 2.28B). The Exclusion Zone will extend from the image boundary into the image, and thus, where applied, will eliminate some objects that lie close to the image boundary, due to the Di-Sector counting rules (Figure 2.28C). This ensures an unbiased sampling of objects is performed, and maintains any measurements made on the derived object samples free from systematic biases.

Rejection Boundaries and Exclusion Zones only need to be applied to a given dimension if the whole region under analysis is sampled or cropped in that dimension. For example, taking transverse sections of a spinal cord, the superficial laminae ROIs are not sampled in the mediolateral (horizontal) or dorsolateral (vertical) planes if an image is taken of the entire dorsal horn (see Figure 2.29A). However, inevitably, sampling will be performed in the rostrocaudal (depth) plane, due to thin histological sectioning (Figure 2.29A). In this case, a Rejection Boundary - Exclusion Zone pair would be set up in the Z dimension.

If a sub-section of the superficial dorsal horn were to be imaged, then sampling may

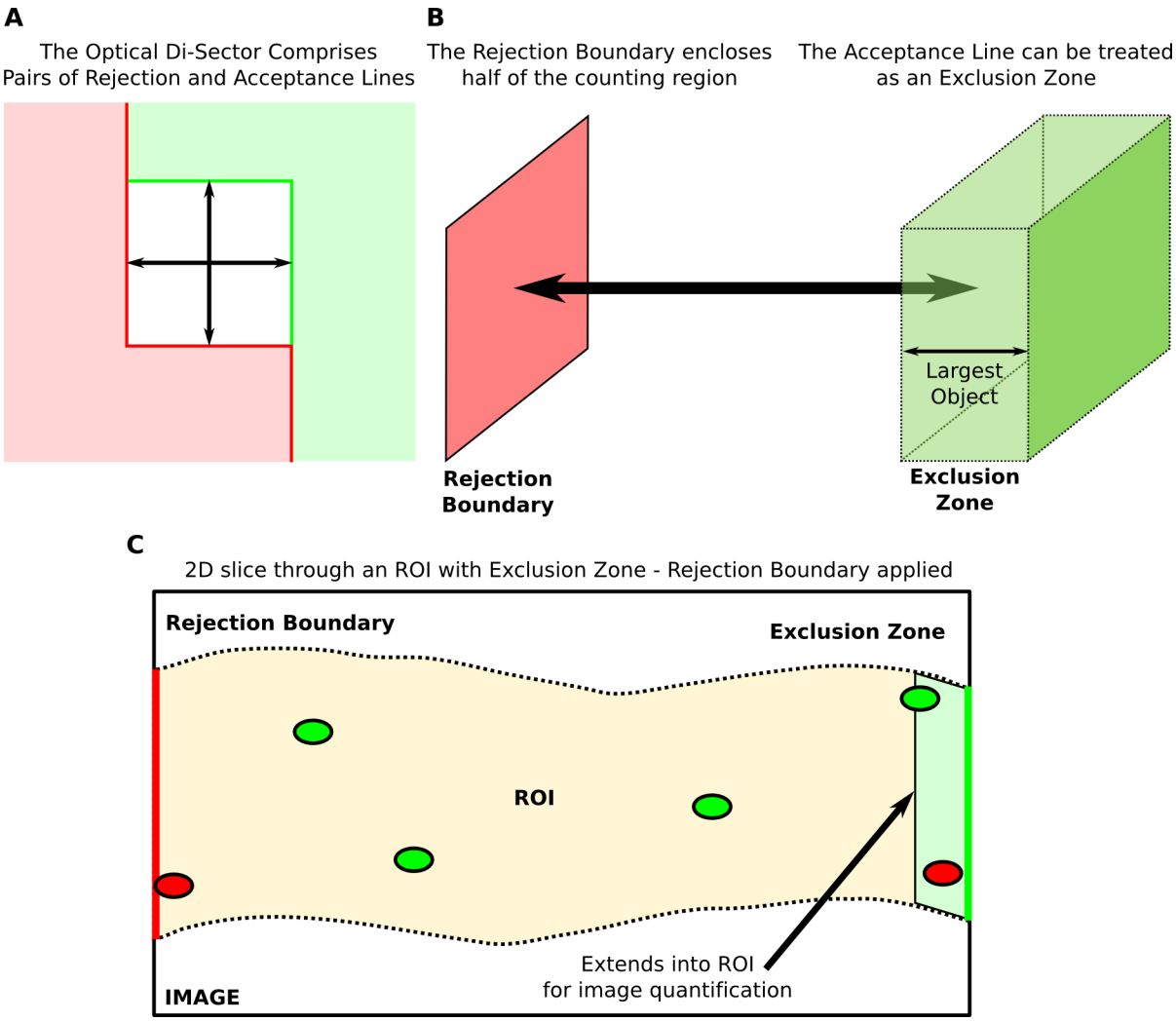

Figure 2.28: **The ROI Di-Sector. A:** The Optical Di-Sector comprises a cube which contains 3 pairs of Rejection and Acceptance Boundaries on opposed surfaces. **B:** The Rejection Boundary can be paired with an Exclusion Zone, which applies the same counting rule as an Acceptance Line, but incorporates a volume which objects may extend into. This volume depends on the size of the objects to be quantified, and must be at least as large as the largest object to prevent bias due to size. **C:** An example of a Rejection Boundary - Exclusion Zone applied to the horizontal dimension of an ROI lying within an image. The Rejection Boundary is placed on one edge of the ROI. The Exclusion Zone is placed on the opposing edge, and extends into the ROI. Objects touching the Rejection Boundary, or entirely within the Exclusion Zone are not quantified.

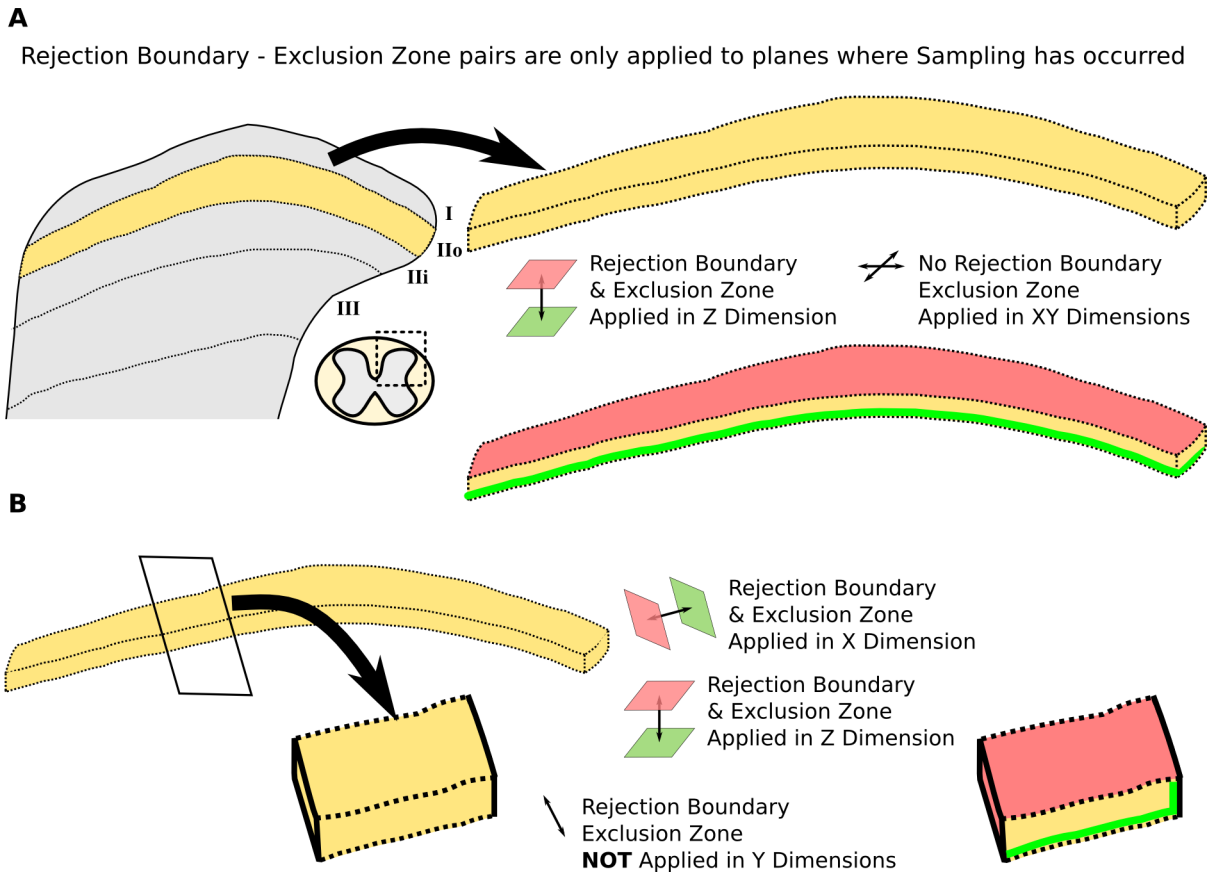

Figure 2.29: **Rejection Boundaries and Exclusion Zones are only applied to planes where sampling has occurred. A:** Rejection Boundary - Exclusion Zone pairs are only applied to dimensions that have been sampled. Here the entire lamina IIo ROI has been captured in the X and Y dimensions, leaving only the Z dimension sampled (i.e lamina IIo has been cropped in the Z dimension and not reconstructed entirely). Thus, a Rejection Boundary - Exclusion Zone pair will be set up in Z, which results in objects touching the first slice being rejected, and an Exclusion Zone set up in the bottom of the Image Stack. **B:** The Lamina IIo region has been further sampled in the mediolateral plane (X dimension), which means in this new sample, Rejection Boundary - Exclusion Zone pairs must be set up in the X and Z dimensions to ensure unbiased quantification of objects.

occur in the mediolateral dimension (Figure 2.29B). In this case, Rejection Boundary - Exclusion Zone pairs would be implemented in both the X and Z dimensions. In dimensions where the ROI boundary exists on both sides, no Rejection Boundary - Exclusion Zone pair needs to be set up, and the ROI boundaries apply a special rule to any objects traversing it, which will include the object if over half of its voxels lie within the ROI in question.

Figure 2.30 shows the ROI Di-Sector applied to Large Sample Images. After the ROIs have been isolated from the Reference Image and applied to the Sample Image Stack, each ROI is sampled in the X and Z (mediolateral and rostrocaudal, respectively) dimensions (because these dimensions crop or sample the entire region of interest), but not in the Y (dorsoventral) dimension (because the entire region of interest is capture in this dimension). Thus, Rejection Boundary - Exclusion Zone pairs will be set up in the X (mediolateral) and Z (rostrocaudal) dimensions, but not in the Y (dorsoventral) dimensions. This specific set-up will be used for all synapse quantification in the dorsal horn throughout this thesis.

These new rules allow the logic of the Optical Di-Sector to be applied to any shaped region, including a cuboid image, or any irregularly shaped ROI. This Di-Sector improves the Optical Di-Sector firstly because it measures, in a very efficient manner, almost all objects which have been acquired in the Sample Image Stack; no sampling has been wasted by imposing a block of cuboid Optical Di-Sectors. Secondly, following the ROI Di-Sector rules also leads to the intuitive conclusion that if the entire region of interest is captured during imaging in all dimensions (and no sampling/cropping occurs in any dimension of the region under analysis, a feat which may be possible with the promise of clearing methodologies, see Chung et al. (2013); Tomer et al. (2014); Yang et al. (2014)), object quantification would measure all of the objects within the region (since the ROI boundaries

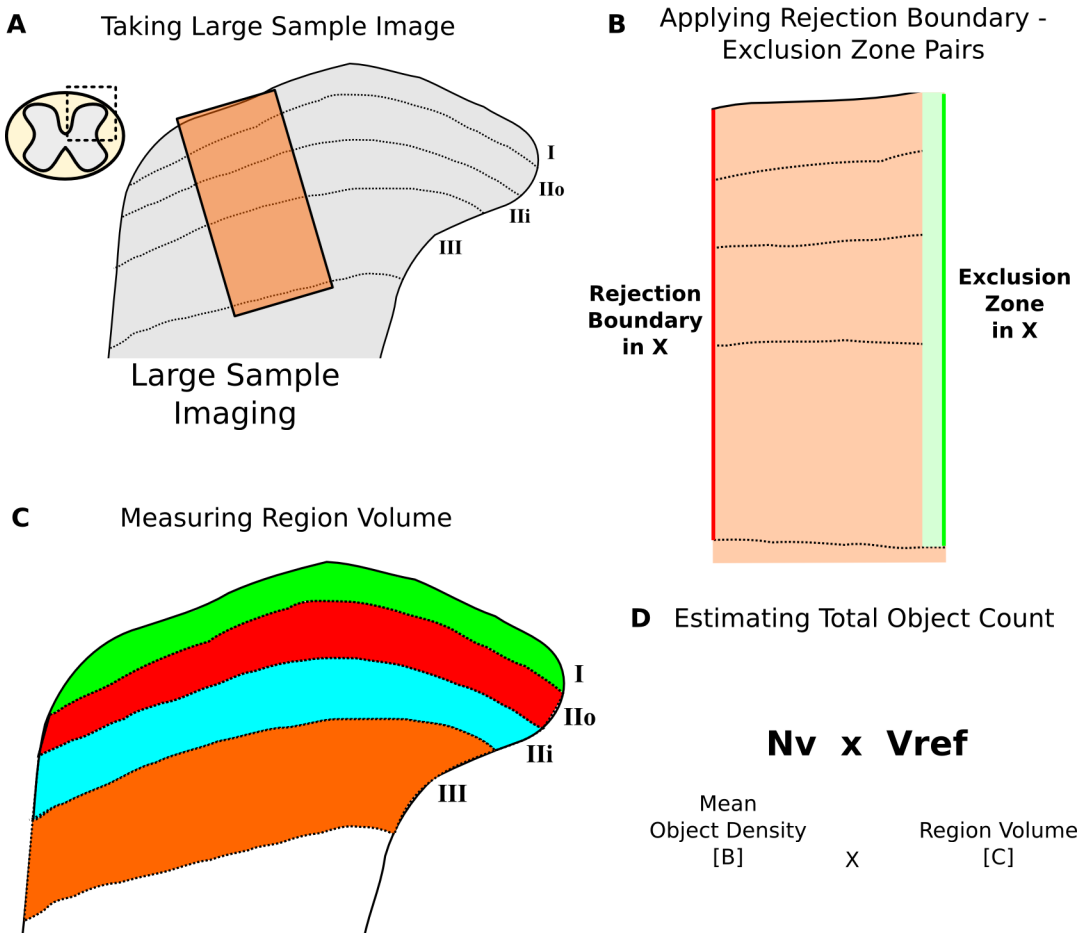

Figure 2.30: **Application of the ROI Di-Sector to Large Sample Imaging. A:** Overview of Large Sample Imaging. **B:** Schematic highlighting the Sample Image Stack with the Rejection Boundaries and Exclusion Zones applied across each ROI in the medi-olateral [X] dimension (Rejection Boundary - Exclusion Zone pair is also set up in the rostrocaudal dimension [Z],which is not shown). **C:** Each ROI volume is measured. **D:** Estimating total object counts is now performed by multiplying the mean object density by the ROI volume.

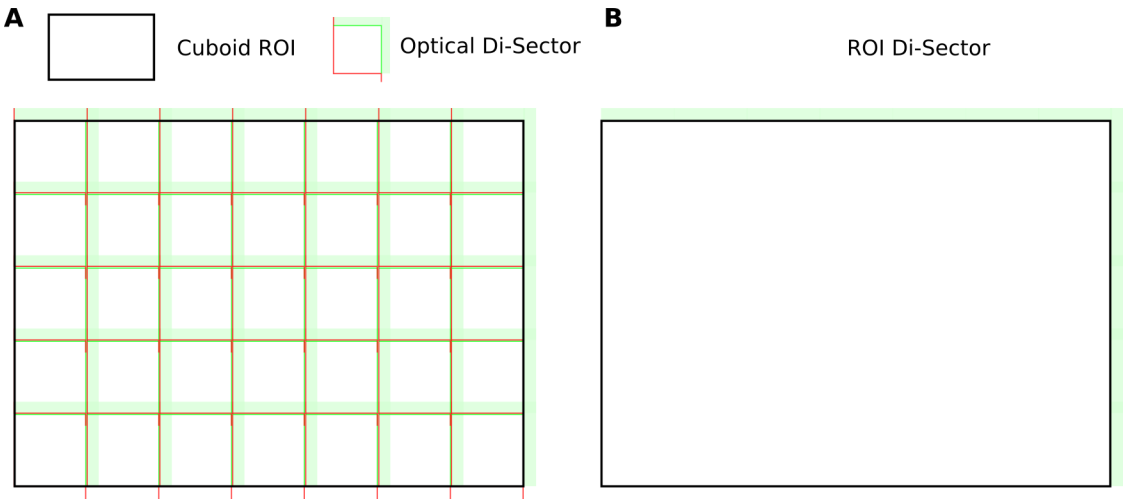

Figure 2.31: **The ROI Di-Sector and Optical Di-Sector are equivalent. A:** The Optical D-Sector placed contiguously throughout a cuboid ROI. **B:** The ROI Di-Sector applied to the same Cuboid ROI. The sum of the objects counted by the contiguous Optical Di-Sectors will always match the total objects counted by the ROI Di-Sector, due to their counting rules. Thus, the Optical Di-Sector and ROI Di-Sector are logically equivalent.

are completely contained in the image stack, no Rejection Boundary - Exclusion Zone pairs will be set up), thus giving a direct measure of total objects, and eliminating the need for a stereological estimate. Comparing this implementation to how the original Optical Di-Sector is applied, where sampling would still be performed using a rigid block of Optical Di-Sectors, the benefit of the ROI Di-Sector becomes apparent.

The ROI Di-Sector can be seen to be logically equivalent to the Optical Di-Sector if a large cuboid ROI is considered. As can be seen from Figure 2.31, the ROI Di-Sector applied to a cuboid ROI is equivalent to an array of optical Di-Sectors aligned such that their counting regions lie contiguous throughout the cuboid ROI. Following the counting rules for both Optical Di-Sector and ROI Di-Sector would result in identical object quantification for any array of objects within this ROI. By extension, the ROI Di-Sector would be equivalent to an array of contiguous Optical Di-Sectors across any shaped ROI.

The advantages of using the ROI Di-Sector results from its implementation of continuous sampling, where an imaged region has all objects quantified in a continuous fashion,

as opposed to discreet sampling (where objects are quantified in discreet and separate locations, Figure 2.32A). Continuous sampling results in an efficient means of quantifying objects, as no volume is wasted between counting frames, and regions of interest which are harder to fit counting frames to (for example, long and thin ROIs) are easily handled with the ROI Di-Sector. Measuring of object properties often requires the total reconstruction of the object, which would be limited by the size of the sampling region in discreet sampling, whereas continuous sampling tends to reconstruct and measure all objects in their entirety (assuming the region sampled is large enough, Figure 2.32A).

Furthermore, applying numerous small Optical Di-Sectors in a systematic random fashion to implement discreet sampling can be subject to Distribution Bias (Cox and Donnelly, 2011) (Figure 2.32B). It is hard to definitively prove that a periodic systematic bias has not been introduced using several Optical Di-Sectors spaced apart without quantifying the objects between Optical Di-Sectors, and thus without quantifying all the objects in a continuous fashion. This potential bias is eliminated with the ROI Di-Sector as it quantifies all objects in a continuous fashion throughout the ROI.

Thus, the ROI Di-Sector can be used as a replacement for the traditional Optical Di-Sector. It is logically equivalent to the Optical Di-Sector, and yet it possesses advantages over taking many small samples, including increased efficiency and elimination of distribution bias. The ROI Di-Sector has been used to quantify synapses throughout this Thesis.

2.3.3.3 Object Measurement

Object measurement involves extracting information from each ROI. A common characteristic to measure from a ROI is the number of objects within it (West, 1999). After labelling all objects within each ROI and applying the ROI Di-Sector to sample image

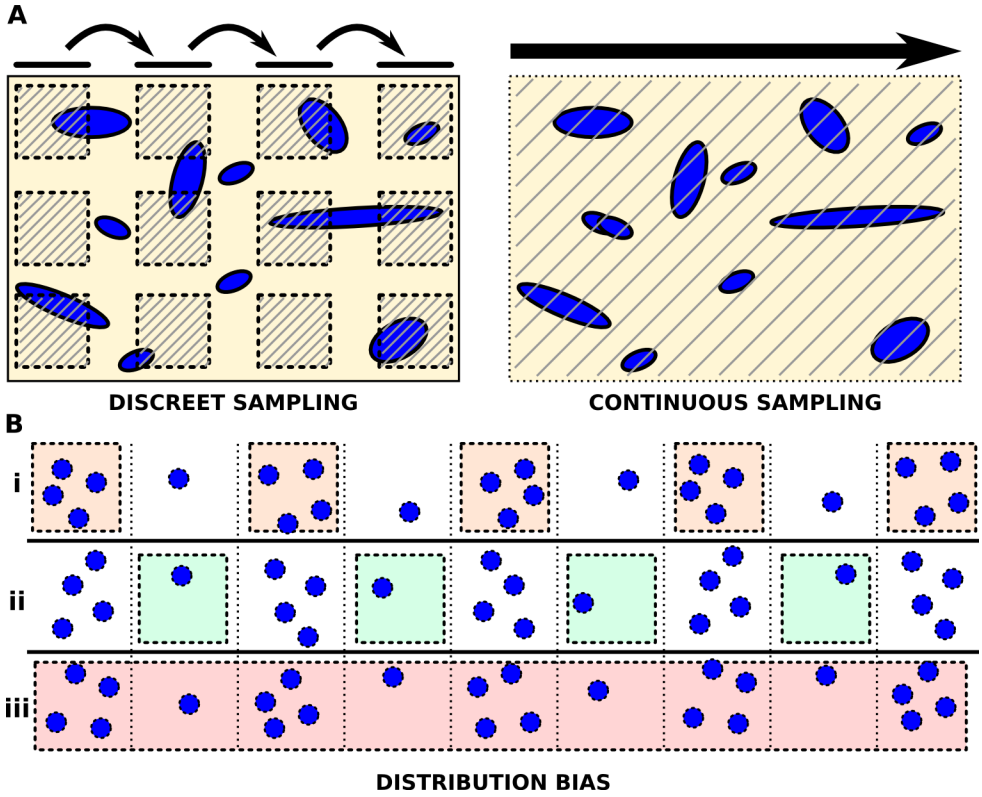

Figure 2.32: **Continuous Sampling is More Efficient and Reduces Distribution Bias. A:** Continuous sampling allows efficient quantification of image objects. With discreet sampling, quantification is less efficient due to gaps between sampling regions. Measurement of object properties (for example, object size) are constrained by whether the size of the sampling region being able to capture the entire object. Continuous sampling captures all of the objects in their entirety, producing efficient sampling and measurement of all objects. **B:** Distribution bias is not eliminated in discreet sampling. The schematic displays an extreme distribution bias with columns of densely distributed objects followed by sparsely distributed objects. If the discreet sampling scheme coincides with the width of either of these distributions(Bi or Bii), an inaccurate estimate of total object number would be measured. Continuous sampling would capture all of the objects (Biii), giving an accurate estimate of total objects, and thus eliminate distribution bias.

stack ROIs, which excludes any objects violating the ROI Di-Sector rules, the number of objects remaining within each ROI are counted (Figure 2.33). This measurement is divided by the ROI Di-Sector volume for each ROI to provide an object density estimate.

Understanding changes in object number requires this density estimate to be converted into a number that reflects an estimate of total object counts. Object density from a sample alone cannot be used to understand changes in object number in a region, as either the number of objects or the volume of the region (due, for example, to changes in other components) may have changed. In order to control for volume changes, an estimate of the total region volume must be performed. For the superficial dorsal horn, this is performed on an image of the entire cross-section of the dorsal horn. A measure of the superficial dorsal horn area is taken as a correlate for the volume of each lamina. Estimating the depth of each lamina is frustrated by the fact the tissue has been sectioned in the rostrocaudal direction. Thus, the superficial dorsal horn area is assumed to correlate to the volume of the measured dorsal horn segment (Figure 2.34).

To measure the superficial dorsal horn area, sections stained with IB4, which effectively marks the superficial dorsal horn, are used. In order to obtain an unbiased measure of the superficial dorsal horn volume, each dorsal horn is isolated and assigned a random and unique three digit identifier. All superficial dorsal horn images are then measured blindly and in a random order, to ensure no bias is introduced by the experimenter. Superficial dorsal horn regions are delineated by reference to IB4 labelling, and the area in μm^2 is measured in ImageJ (Figure 2.34).

Traditional stereological methods (i.e the Optical Di-Sector, West et al., 1991; West, 1999) would use the estimate of total region volume to derive an estimate of total object counts for that ROI. However, the accuracy in measuring synaptic puncta number is far higher than the accuracy of measuring superficial dorsal horn volume. Thus, an approach

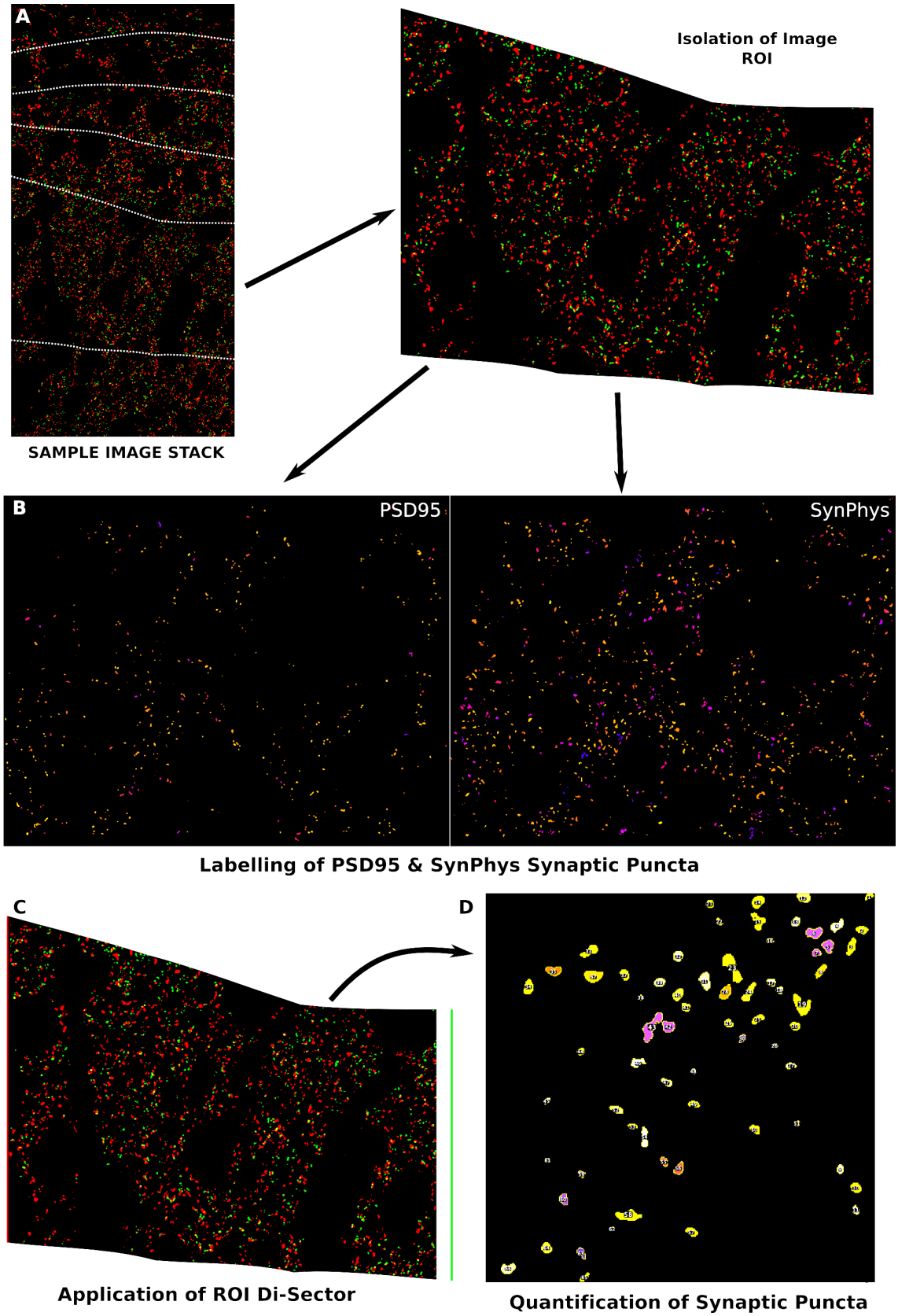

Figure 2.33: **Object Measurement.** **A:** Image ROIs are isolated from the Sample Image Stack. **B:** PSD95 and SynaptoPhysin labelling are isolated, and each channel labelled (each isolated object now appears as a separate colour). **C:** The ROI Di-Sector is applied to both PSD95 and SynaptoPhysin image stacks, excluding any objects according to ROI Di-Sector rules. **D:** Counting of labelled objects is performed. This count is divided by the ROI volume to give an object density measure.

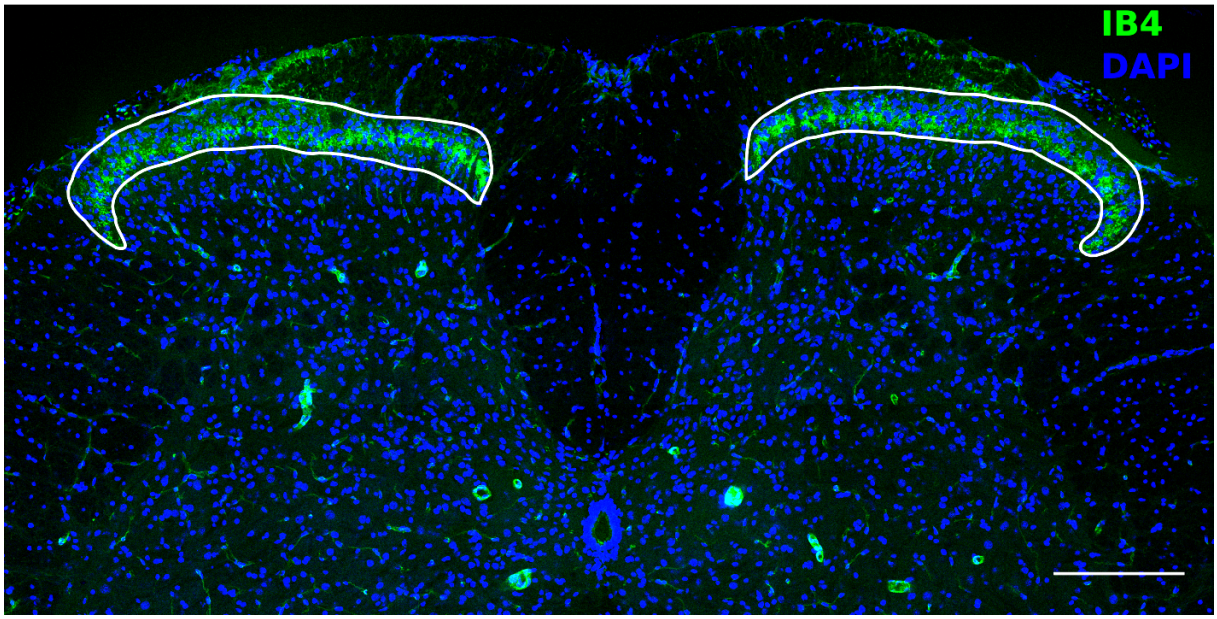

Figure 2.34: **Measurement of the superficial dorsal horn area.** IB4 is used to delineate the superficial dorsal horn, and the total superficial dorsal horn area is measured. This measurement is used to determine whether the dorsal horn volume has changed in different experimental conditions.

which allows the retention of the high quality estimate of object density, whilst still proving this measure is relevant to total object count, was utilised. This approach relies on the fact that if the total region volume can be shown to be similar between groups (i.e not significantly different), then the object density correlates to the total object count, since calculating total object count would amount to multiplying the object density by a constant factor. Thus, when no differences exist in mean superficial dorsal horn areas between groups subject to comparison, the object density can be used as a measure of total object count. If any differences exist in the mean superficial dorsal horn areas between groups, then a correction factor equal to the ratio between superficial dorsal horn areas can be applied to one set of object counts. This method retains the highly accurate synaptic density measure, and prevents the data from being corrupted by correcting the synaptic counts with the relatively inaccurate measure of total region volume.

To demonstrate the process of object measurement, the three spinal cord test sections have been taken through this process. As is shown in Figure 2.35, the three spinal cord

sections have each had the left and right dorsal horns quantified. First, ROIs are isolated from the sample image stack, and object quantification of both PSD95 and SynaptoPhysin puncta takes place (as shown in Figure 2.33). Next, overview images of the spinal cord sections are taken, and the superficial dorsal horn area is measured (as shown in Figure 2.34). Finally, the mean±SEM of each label for each ROI is plotted along with the mean±SEM of the area of left and right superficial dorsal horn.

As can be seen from the data, the superficial dorsal horn areas are not significantly different, so the synapse density per $100\mu m^3$ can be used as a measure of total synapse count in each lamina. The synapse counts show an interesting pattern, whereby PSD95 puncta significantly increase in lamina II inner, and SynaptoPhysin puncta show a steady increase from lamina I to lamina II & III. This shall be explored in greater depth in the following Chapter.

2.4 StereoMate

This Chapter has provided a detailed account of the visualisation, acquisition, data processing and analysis of synaptic puncta throughout the dorsal horn. This workflow provides an automated and efficient analysis of regions of interest in a stereological manner. Whilst synaptic puncta and the dorsal horn have been used during this account, this methodology is potentially applicable to a wide range of biologically interesting objects and regions. For example, this method could be applied to quantifying cell number, such as microglial cells (as shown in Chapter 4). Future work aims on validating the application of this work to a plethora of different regions and objects, making it a flexible and general method for automated, stereologically-consistent object quantification in selected regions of interest.

An essential component to this workflow is the high quality histological prepara-

A

PSD95

LEFT	lam1	lam2o	lam2i	lam3
01 DH	7.94	10.44	17.48	14.54
02 DH	9.29	9.21	15.56	12.57
03 DH	13.89	15.21	22.46	14.51
mean	**10.37**	**11.62**	**18.50**	**13.88**
SD	**3.12**	**3.17**	**3.56**	**1.13**
RIGHT	lam1	lam2o	lam2i	lam3
01 DH	8.20	9.47	17.95	15.21
02 DH	6.95	11.33	17.14	13.10
03 DH	10.00	13.26	21.49	17.65
mean	**8.38**	**11.36**	**18.86**	**15.32**
SD	**1.54**	**1.89**	**2.31**	**2.28**

SynPhys

LEFT	lam1	lam2o	lam2i	lam3
01 DH	12.02	13.01	19.29	20.90
02 DH	13.27	11.22	18.48	18.13
03 DH	17.37	17.86	25.11	22.29
mean	**14.22**	**14.03**	**20.96**	**20.44**
SD	**2.80**	**3.43**	**3.61**	**2.12**
RIGHT	lam1	lam2o	lam2i	lam3
01 DH	11.60	13.28	20.56	21.90
02 DH	10.07	14.17	19.48	19.21
03 DH	14.77	19.73	24.13	26.30
mean	**12.15**	**15.73**	**21.39**	**22.47**
SD	**2.40**	**3.49**	**2.44**	**3.58**

B

Superficial DH Areas

	LEFT	RIGHT
DH 01	60972	65321
DH 02	63676	60476
DH 03	67095	58478
mean	**63915**	**61425**
SD	**3068.37**	**3518.92**

C

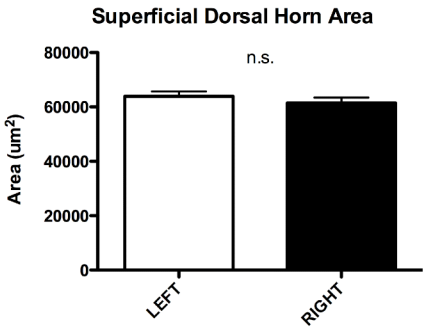

D

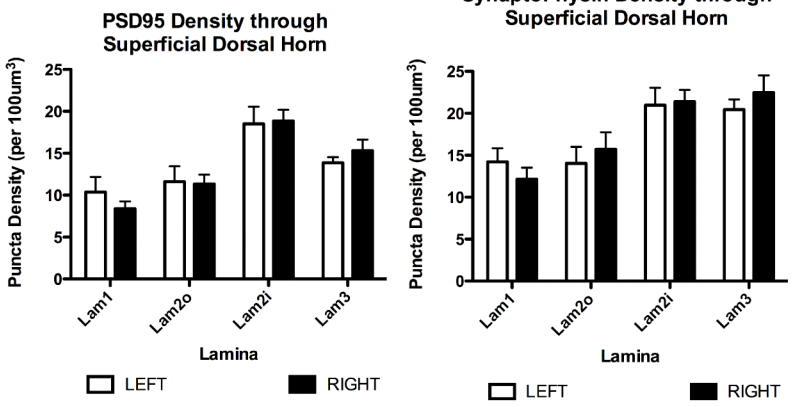

Figure 2.35: **Quantification of PSD95 and SynaptoPhysin Puncta in Three Spinal Cord Test Sections. A:** Tables showing puncta density (per $100\mu m^3$ for PSD95 and SynaptoPhysin in lamina 1, 2outer, 2inner and 3 of each dorsal horn (left and right) across three spinal cord slices. **B:** Table showing the superficial dorsal horn areas for each dorsal horn across three spinal cord slices. **C:** Graph plotting mean±SEM of superficial dorsal horn areas indicating no significant differences between left or right dorsal horns (Student's t-test, $p>0.05$). This indicates the synapse density correlates to the total synapse counts, thus synapse density can be used as a measure of synapse count. **D:** Plots of PSD95 and SynaptoPhysin synapse density in lamina 1, 2outer, 2inner and 3 in the left and right dorsal horn samples. No significant differences were seen between left and right dorsal horn laminae, as expected (two-way ANOVA, bonferroni corrected comparisons). Note an increase in density seen with PSD95 puncta in lamina 2inner compared to the other laminae, and a progressive increase in SynaptoPhysin puncta from lamina 1 to 3. These will be further explored in subsequent Chapters.

tions obtained of synaptic puncta. High quality histological preparations refers to well-maintained tissue integrity combined with high-signal immunohistochemical staining. Without a high quality histological preparation, the subsequent steps would be difficult to achieve, as image noise would be increased considerably, and thus the data quality will be severely hampered.

The importance of the histological preparation was clearly demonstrated in Schmitz et al. (2014). Here, the authors state that automated image analysis methodologies are not a sufficient replacement for manual stereological analysis. However, much of the errors cited during their analysis can be attributed to a histological preparation which does not possess sufficient signal:noise. Thus, poor segmentation is inevitable. Furthermore, little improvement in this signal:noise was achieved in any of the presented datasets with image processing, such as deconvolution.

A clear caveat between this study and the current Chapter is that Schmitz et al. is attempting to quantify large objects (whole neuronal cell bodies), and deconvolution requires very high resolution to be applied. It is possible to achieve a reasonable sampling scheme for deconvolution if a low NA objective is used, however this will almost certainly be an air-immersion objective, which will be severely compromised by spherical aberration with increased image depth. The use of deconvolution could potentially be avoided with a significant improvement in histological signal prior to image processing. Further work is required to generalise this workflow to cell counts, and some work towards this end has been achieved though optimisation of this workflow on quantification of microglia (see Chapter 4).

A key characteristic of this analysis is its automated implementation. Once Sample Image Stacks have been acquired and the ROIs delineated for them, much of the work is performed in ImageJ, utilising a number of different image processing algorithms. This

allows very large sampling that would be impractical with manual quantification, which in turn produces very robust data. For example, with the three test spinal cord sections imaged and analysed in this section (see Figure 2.35), 29,849 PSD95 puncta and 39,733 SynaptoPhysin puncta were quantified, which will be the approximate number of synaptic puncta measured per animal. In future data analysis, the animal will be the independent variable, which should result in a significant reduction in sampling variability across groups during analysis (although this does not account for biological variability).

The algorithms used to process and analyse the image datasets have been collected into an image processing suite, called StereoMate. This package provides tools for image deconvolution, segmentation and object measurement, as well as convenient utility algorithms such as ROI delineation and ROI area measurement.

Image deconvolution drastically improves object representation, and its implementation is essential when investigating objects close to the diffraction limit of visible light. A clear improvement in signal:noise, as well as dramatic reductions in image noise are apparent. Deconvolution significantly improves image segmentation, and allows the use of global thresholding methods to provide robust binary representations of diffraction-limited image objects. Global segmentation methodologies have previously been fraught with poor image segmentation. Deconvolution however has revived these methods as adequate image processing steps, and highlighted the requirement for very high signal:noise for these algorithms to work robustly and consistently.

The object measurement algorithm applies the ROI Di-Sector, which provides a highly efficient means of object quantification. It also eliminates bias due to irregular distribution of objects throughout the sample image. This method provides advantages over traditional stereological methods such as the Optical Fractionator method, where only a designated proportion of the region under analysis is quantified (West, 1999, 2012), since it allows

continuous sampling of the entire region imaged, and therefore can reconstruct larger objects for measurement as well as avoid any distribution bias.

The technical differences between the two methodologies is the automated nature in which the ROI Di-Sector is implemented, and the continuous sampling offered by the ROI Di-Sector. Whereas the Optical Fractionator is performed in a manual fashion, the ROI Di-Sector applies the stereological filter across a delineated ROI in an automated fashion, without any requirements for quantification on the experimenter. Whilst it would be technically feasible to apply the Optical Fractionator in an automated fashion, this would require breaking the ROIs into separate and discreet counting frames, which inhibits the reconstruction of large objects in their entirety. Whereas the Optical Fractionator provide unbiased counts of objects in a given region, the key difference with the ROI Di-Sector is that it provide an unbiased sample of fully reconstructed objects, which can then be measured in many ways.

Since the continuous sampling regime used in the ROI Di-Sector produces an unbiased sampling and complete reconstruction of all imaged objects, various other measures are possible, such as object size and shape parameters. Future work aims to explore these in the high-quality synaptic datasets acquired from subsequent studies.

In conclusion, this Chapter has established a rigorous image analysis workflow, taking tissue sections through histological preparation, image acquisition, processing and analysis. It produces robust object representation of synaptic puncta, and analyses them in an efficient and stereologically-consistent manner. This method will now be applied to the dorsal horn of animals subject to various experimental manipulations, including peripheral nerve injury paradigms.

Chapter 3

Synaptic Puncta Distributions Within the Dorsal Horn & their Plasticity with Peripheral Nerve Injury

3.1 Introduction

Understanding the number and distribution of synapses throughout the dorsal horn gives a broad view of circuit-level characteristics, and provides the opportunity to investigate changes to these features in different conditions. It is generally accepted that central circuit changes contributes to the hypersensitivity seen following peripheral nerve injury (Sandkühler, 2009; von Hehn et al., 2012; West et al., 2015). Thus, the aims of this Chapter are to first apply the methodologies developed in Chapter 2 to the naïve dorsal horn in order to establish the distribution patterns of synapses in the natural state, and second, to extend these methodologies to nerve injury paradigms to understand how nerve injury may impact on synaptic distributions, and thus affect circuit-level processing within the dorsal horn.

As the project has progressed, a transition from rat to mouse occurred, due to the acquisition of a transgenic mouse expressing eGFP selectively within all primary afferent neurons (a BAC transgenic driving EGFP under the Advillin promotor; Tg(Avil-EGFP)QD84Gsat, GENSAT), which allows analysis of primary afferent axonal projections. Thus, both rat and mouse tissue data will be presented throughout this thesis. Initial experiments focussing on rat tissue were conducted using the post-synaptic marker PSD95 only, since at this stage the SynaptoPhysin labelling was under optimisation. Later experiments focussed on mice using a combination of PSD95 and SynaptoPhysin.

3.2 Methods

3.2.1 Animals

Adult male Sprague Dawley rats (250-300g) used throughout this study were obtained from Harlan, UK. Adult male and female mice on a FVB/N background used throughout this study were obtained from GENSAT, and contained a transgene where eGFP protein was expressed under the Advillin promotor (Tg(Avil-EGFP)QD84Gsat, GENSAT). Animals were bred to hemi-zygosity only.

3.2.2 Behaviour & Surgery

3.2.2.1 Rhizotomy Surgery

Rhizotomy surgery was performed as previously described Li et al. (2003). Briefly, adult male Sprague-Dawley rats (˜250g) were anaesthetised with isoflurane and subjected to a unilateral laminectomy to expose the L4 and L5 dorsal roots. An incision into the dura was carefully made using a 27G hypodermic needle (SG3-2713, Terumo) to expose the dorsal roots. The L4 and L5 dorsal roots were identified and cut using spring loaded

scissors. The incision was sutured, and the animals allowed to recover in a clean and warm cage (see Figure 3.6 in Section 3.4). Seven days following surgery, the animals were sacrificed as previously described (see Section 2.2.1). The tissue was processed, imaged and analysed for PSD95 synaptic puncta as previously described (see Sections 2.2 & 3.3).

3.2.2.2 Spinal Nerve Ligation Surgery

SNL was performed using a modified version previously described (Kim and Chung, 1992). Briefly, adult male Sprague-Dawley rats (˜250g) were anaesthetised using isoflurane. A unilateral incision above the L5 & L6 DRGs was made to expose the spinal nerves. These were tightly ligated using a 2-0 suture, and transected distal to the ligation. A SHAM surgery was performed by exposing the L5 & L6 spinal nerves, but not performing a ligation or transection of these nerves. The wound was sutured, and the animals allowed to recover in a clean and warm cage (see Figure 3.9 in Section 3.5). Seven and 21 days post SNL surgery, the animals were perfused as previously described (see Section 2.2.1). The tissue was processed, imaged and analysed for PSD95 synaptic puncta as previously described (see Sections 2.2 & 3.3).

3.2.2.3 Spared Nerve Injury Surgery

SNI surgery was performed as previously described (Decosterd and Woolf, 2000; Shields et al., 2003). All mouse nerve injury experiments utilised this injury paradigm, for a number of reasons: First, the spared nerve injury is a simple nerve injury paradigm compared to the technically challenging SNL surgery, and this decreased size of mice made this an easier and thus more reproducible model; second, the model produces an injury in the medial portion of the lumbar dorsal horn, leaving intact afferents in the same spinal cord section, and therefore can allow analysis of injured as well as adjacent uninjured afferents (Shields et al., 2003; Beggs and Salter, 2007).

Briefly, mice were anaesthetised using isoflurane. A unilateral incision from the sciatic notch was made laterally to expose the biceps femoris muscle, which was bluntly dissected with scissors to expose the sciatic nerve and three branches: the common peroneal, tibial and sural nerves. The tibial and common peroneal nerves were tightly ligated using a 3-0 prolene suture, and transected distal to the ligation. A SHAM surgery was performed by exposing the sciatic nerve, but not performing a ligation or transection of the common peroneal or tibial nerves. The wound was sutured, and the animals allowed to recover in a clean and warm cage (see Figure 3.15 in Section 3.6). Seven and 21 days post SNI surgery, the animals were perfused as previously described (see Section 2.2.1). The tissue was processed, imaged and analysed for PSD95 and SynaptoPhysin synaptic puncta as previously described (see Sections 2.2 & 3.3).

3.2.2.4 von Frey Behaviour

Paw withdrawal thresholds to punctate mechanical stimuli were measured and calculated as previously described (Chaplan et al., 1994). Briefly, animals were placed into plastic boxes with an exposed and raised wire floor, to allow access to the plantar surface of the hind paws. Von Frey hairs that deliver calibrated forces were applied to the ipsilateral (and where indicated, the contralateral) paws using the "up-down" method (Chaplan et al., 1994), which was used to identify the 50% paw withdrawal threshold for each animal.

3.2.3 Histology

3.2.3.1 IB4 Staining

Staining for IB4 was performed as previously described (see Section 2.2).

3.2.3.2 Dorsal horn Area Measures

Analysis of mouse superficial dorsal horn areas for dorsal horn regions Lumbar 3 - Lumbar 5 (L3-5) were conducted, as previously described (see Section 2.3.3.3).

3.2.3.3 PSD95 and SynPhys Analysis

All experiments in this chapter followed the workflow as defined in Chapter 2. Briefly, $30\mu m$ sections were treated using the HIER-ProK-Pepsin antigen retrieval methodology, and stained for either PSD95 (rat spinal cord sections), or both PSD95 and SynaptoPhysin (mouse spinal cord sections), as well as co-labelled for IB4 for delineation of the superficial laminae. High resolution imaging of the Reference Image and Sample Image Stack were taken of the relevant dorsal horn regions, ensuring avoidance of myelin bundles in medial positions in the dorsal horn, and Sample Image Stacks were deconvolved, segmented and divided into ROIs which were first delineated on the Reference Image. Analysis of each synaptic marker was performed by quantification of the number of objects within each ROI, which provided a density measure of the synaptic marker under analysis. Finally to test whether any gross volume changes occurred in the dorsal horn, measurement of the superficial dorsal horn areas on transverse sections was performed and compared. Once any correction had been applied to the synaptic density data, the data was plotted as mean±SEM for each ROI (lamina I, II outer, II inner & III). This processed is summarised in Figure 3.1.

3.2.3.4 EGFP Analysis

Tissue was cut and stored as previously described (see Section 2.2.1). eGFP fluorescence was visualised by utilising its endogenous fluorescence. For tissue sections that had no counter-staining, slides were rehydrated in PBS and mounted using Vectashield. For

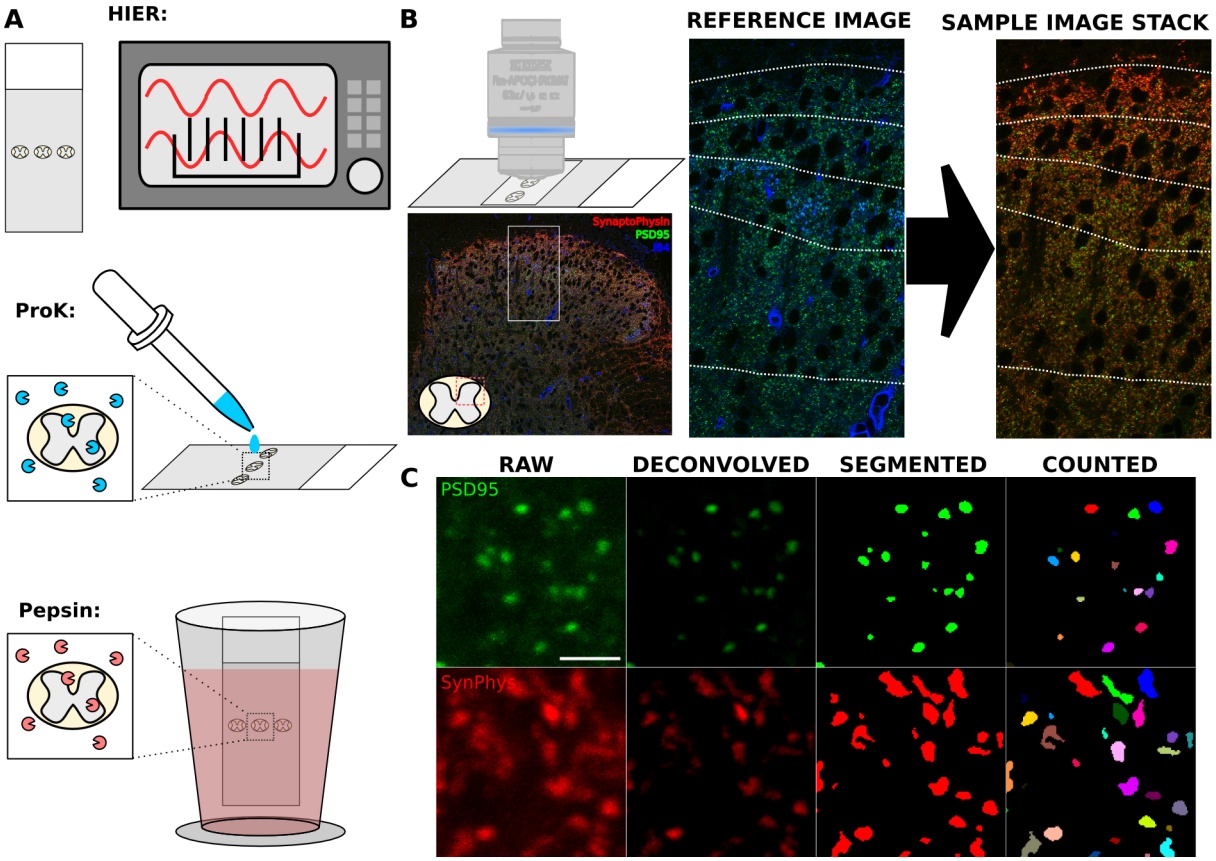

Figure 3.1: **Overview of synaptic labelling, processing and analysis. A:** 30μm sections were treated with heat induced epitope retrieval, proteinase K, and pepsin, as previously described. **B:** After immunohistochemical labelling of spinal cord sections, confocal image samples of the superficial dorsal horn were taken, including a Reference Image and Sample Image Stack, which were divided into separate laminae based on IB4 labelling, as previously described. **C:** PSD95 and SynaptoPhysin puncta were deconvolved, segmented, and counted in each ROI, using the methods previous outlined. Scale Bar: C, 2μm. HIER, heat-induced eiptope retrieval; ProK, proteinase K; SynPhys, SynaptoPhysin.

double or triple labelling, histological steps were used as outlined previously (see Section 2.2.1).

To analyse eGFP fluorescence intensity, a Zeiss LSM 700 confocal microscope was used. Imaging was always performed in the same session, and with identical imaging conditions (laser power, gain settings, identical objective lense, pinhole diameter, and image dimensions). A minimum of 3 sections were measured per slide, and a minimum N number of 3 slides were used for quantification. All images were taken at 8-bit depth.

3.3 Distribution of Synaptic Puncta within the Superficial Dorsal Horn of Naïve Animals

In order to provide baseline data for subsequent analysis, as well as explore the distribution patterns of synaptic puncta throughout the superficial dorsal horn, initial experiments focussed on the naïve animal. Few previous studies have investigated non-normalised synaptic distributions across laminae within the dorsal horn in a quantitative manner; however, unbiased stereological analysis on electron micrographs of rat sacral dorsal horn in laminae I-IV has revealed a steady increase in synapse number as the cord is traversed from lamina I to lamina IV (McNeill et al., 1988). Given the relative dearth of quantitative studies into synaptic distributions, investigating the distributions of different synaptic markers throughout the superficial dorsal horn is an essential first step to provide baseline information with which to interpret subsequent experiments.

3.3.1 PSD95 Distribution Pattern in Superficial Dorsal Horn

Initial experiments focussed on rat spinal cord, for which only PSD95 data is available. As can be seen from Figure 3.2A, PSD95 puncta distribution through the fifth lumbar

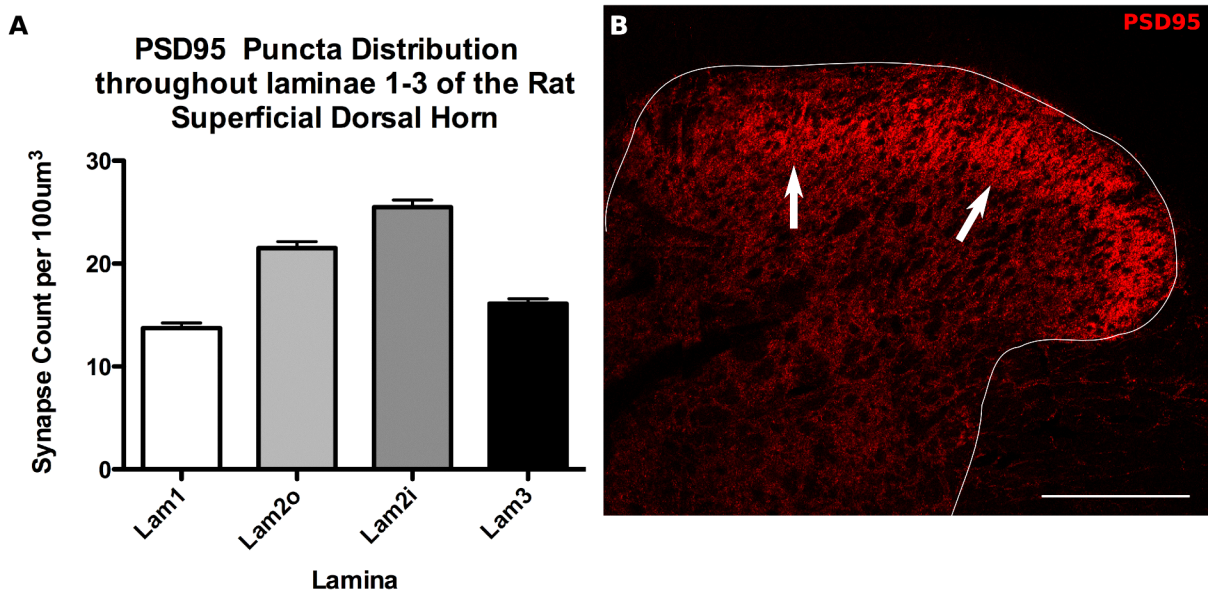

Figure 3.2: **PSD95 distribution in naïve rat dorsal horn. A:** PSD95 puncta distribution throughout laminae I-III of the rat dorsal horn. Lamina 2i and 2o both show significant increases relative to lamina 1 & lamina 3 (one-way ANOVA with bonferroni post-hoc comparisons). **B:** PSD95 staining in the superficial dorsal horn indicating the increased fluorescence intensity visible in lamina II (arrows). Scale bar: B, 200μm. Lam, lamina; 2o, II outer; 2i, II inner.

region (L5) rat dorsal horn follows a very distinctive pattern. A consistent and significant rise in PSD95 puncta is seen from lamina I, to lamina II outer and lamina II inner, which is followed by a rapid reduction in PSD95 puncta in lamina III. These data correspond to fluorescent images of PSD95 in the dorsal horn, where an intense fluorescent band is visible in lamina II (see Figure 3.2B).

Rat dorsal horn analysis was performed in the centre of the mediolateral axis of the L5 superficial dorsal horn. In order to understand whether the synaptic distributions varied in the mediolateral plane of the superficial dorsal horn, mouse spinal cord sections were imaged in the medial, middle and lateral aspects of the superficial dorsal horn. As can be seen from Figure 3.3A, the synaptic distributions are consistent throughout the mediolateral axis, with each region showing the characteristic inflection in PSD95 puncta in lamina IIi of the dorsal horn, with a significant increase seen from lamina 1 to 2i, and a reduction, which was significant for the medial region, in this density measure seen from

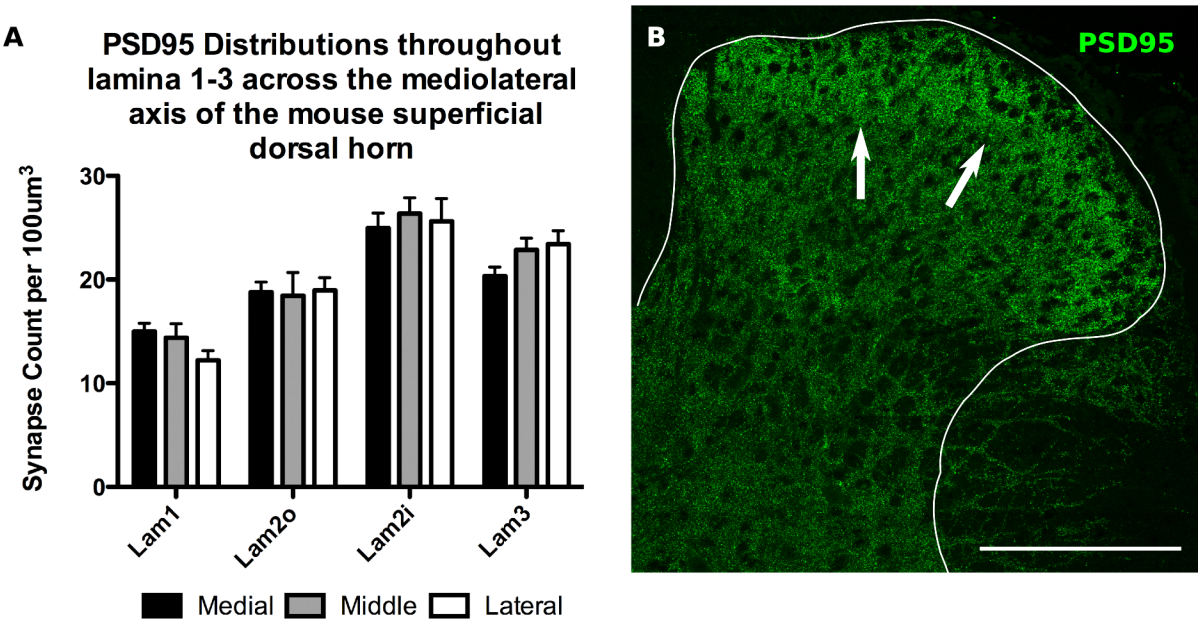

Figure 3.3: **PSD95 distribution in naïve mouse dorsal horn throughout the mediolateral axis. A:** PSD95 puncta density shows the characteristic inflection in lamina II, especially lamina II inner, in medial, middle and lateral portions of the superficial dorsal horn. No significant differences were observed between mediolateral portions in any laminae (two-way ANOVA; bonferonni-corrected selective post-hoc testing; n.s., $p>0.05$; $n=5$). A significant increase in synaptic puncta was seen for all portions of the dorsal horn between lamina 1 compared to 2i & 3, and 2o compared with 2i, whereas variable significance was seen with comparisons between 2i and 3 (one-way ANOVA performed on each region independently; bonferonni-corrected pot-hoc testing; n.s., $p>0.05$; $n=5$). **B:** Representative confocal image of the mouse superficial dorsal horn stained for PSD95, indicating an increased density in PSD95 staining in lamina II (arrows). Scale Bar: B, $200\mu m$. Lam, lamina; 2o, II outer; 2i, II inner.

lamina II inner to lamina III. This data fits well with mouse dorsal horn images, which, like rat dorsal horn, show an increase in PSD95 fluorescent signal as a band throughout the mediolateral extent of lamina II of the dorsal horn, although not as intense (Figure 3.3B). Furthermore, this data shows a close correspondence in distribution pattern between both rat and mouse PSD95 dorsal horn distributions.

3.3.2 SynaptoPhysin Distribution Pattern in Superficial Dorsal Horn

Mouse spinal cord sections were also stained for SynaptoPhysin, whose distribution pattern is shown in Figure 3.4A. The distribution pattern of SynaptoPhysin shows a steady increase in puncta number from lamina I to lamina II inner, which unlike PSD95, remains elevated in lamina III. The distributions are largely consistent throughout the medio-lateral axis, apart from lamina I, which shows a significant reduction in SynaptoPhysin puncta in the lateral aspect. In contrast to PSD95 fluorescent images, SynaptoPhysin shows an increased fluorescence intensity towards the edges of the tissue (Figure 3.4B). Whilst unclear what drives this mismatch between SynaptoPhysin puncta counts and fluorescence intensity, it demonstrates that fluorescences intensity does not always equal object density.

3.3.3 Superficial Dorsal Horn Areas Vary with Lumbar Region

Finally, since different treatments will require measurement of both synapse density and superficial dorsal horn area, analysis of mouse superficial dorsal horn areas for dorsal horn regions Lumbar 3 - Lumbar 5 (L3-5) were conducted, as previously described (see Section 2.3.3.3). As shown in Figure 3.5, L4 and L5 superficial dorsal horn areas are very consistent, whereas L3 shows a small but significant reduction in superficial dorsal horn area. Thus, to eliminate the potential for mistaken corrections to synaptic puncta densities due to changes to superficial dorsal horn areas (for example, due to oversampling L3 in one group, or mixing of L3 with L4/5 samples), only L4 and L5 dorsal horn regions were analysed for synaptic puncta throughout the remainder of the experiments.

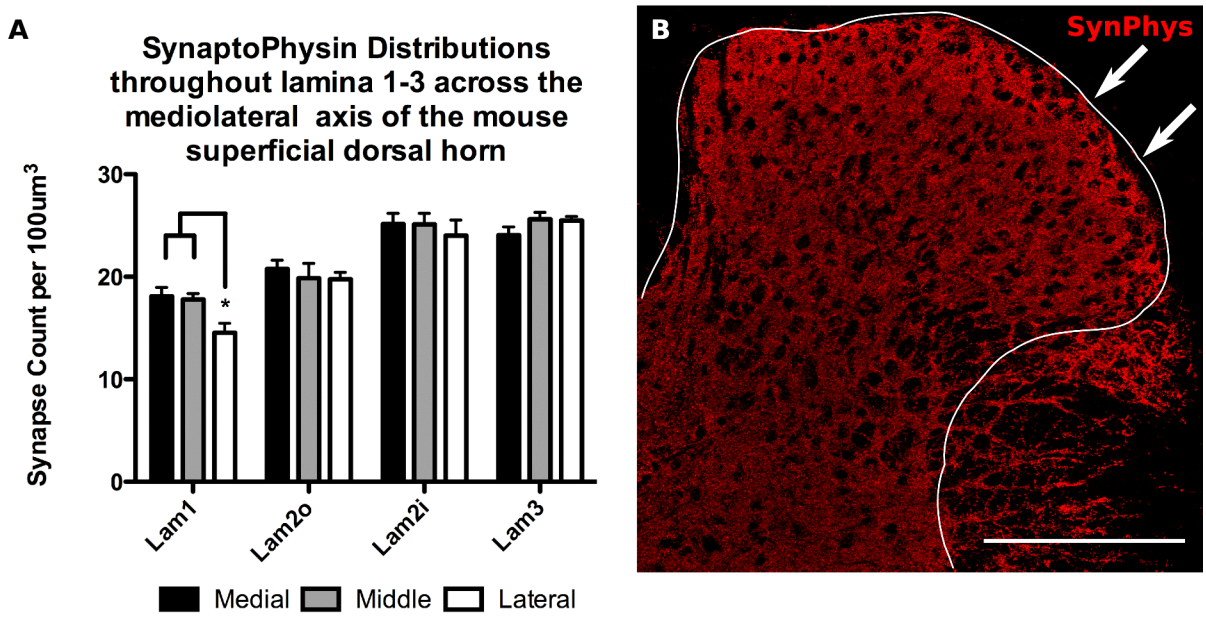

Figure 3.4: **SynaptoPhysin distribution in naïve mouse dorsal horn throughout the mediolateral axis. A:** SynaptoPhysin density distributions in the superficial dorsal horn show an increase in puncta number as the superficial dorsal horn is traversed from lamina I to lamina II inner, with a maintained elevation in SynaptoPhysin puncta in lamina III. This pattern is consistent throughout the mediolateral extent of the dorsal horn, except for a significant reduction in synaptophysin puncta in the lateral portion of lamina I relative to the middle and medial portions (two-way ANOVA; bonferonni-correct selective post-hoc testing; *, $p<0.05$; $n=5$). A significant increase in synaptic puncta was seen for some portions of the dorsal horn between lamina 1 compared to 2i & 3, and 2o compared with 2i, whereas no significance was seen with comparisons between 2i and 3 (one-way ANOVA performed on each region independently; bonferonni-corrected pot-hoc testing; n.s., $p>0.05$; $n=5$). **B:** Representative confocal image of the mouse superficial dorsal horn stained for SynaptoPhysin, which shows a higher intensity of fluorescent signal on the edge of the dorsal horn (arrows, lamina I). Scale bar: B, 200μm. Lam, lamina; 2o, II outer; 2i, II inner.

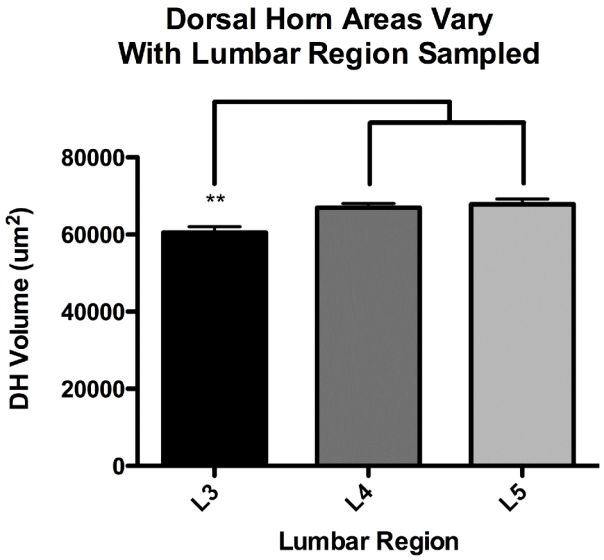

Figure 3.5: **Superficial dorsal horn area varies with lumbar region sampled.** The area of lumbar region 3 of the mouse superficial dorsal horn shows a small yet highly significant reduction relative to both lumbar regions 4 and 5 (one-way ANOVA; bonferonni-corrected post hoc testing; **, $p<0.01$; $n=20$ per group). DH, dorsal horn.

3.4 Rhizotomy Reduces the Number of Excitatory Synaptic Puncta in Superficial Dorsal Horn

Experiments exploring the naïve dorsal horn has revealed a set of stereotypical distribution patterns for both PSD95 and SynaptoPhysin. The next aim was to test the ability for the system to detect alterations to synapse distributions. In order to establish the ability of this experimental methodology to detect changes in puncta numbers, an experimental manipulation was required which would robustly alter synaptic puncta throughout the dorsal horn. In order to achieve this, a rhizotomy surgery was selected. A rhizotomy transects the dorsal roots of one or more dorsal root ganglion inputs into the spinal cord, and results in a rapid loss of primary afferent terminals within the dorsal horn (see Figure 3.6). This manipulation has been shown previously to eradicate synaptic puncta in the affected region of the dorsal horn (Kapadia and LaMotte, 1987; Chung et al., 1989; Li et al., 2003).

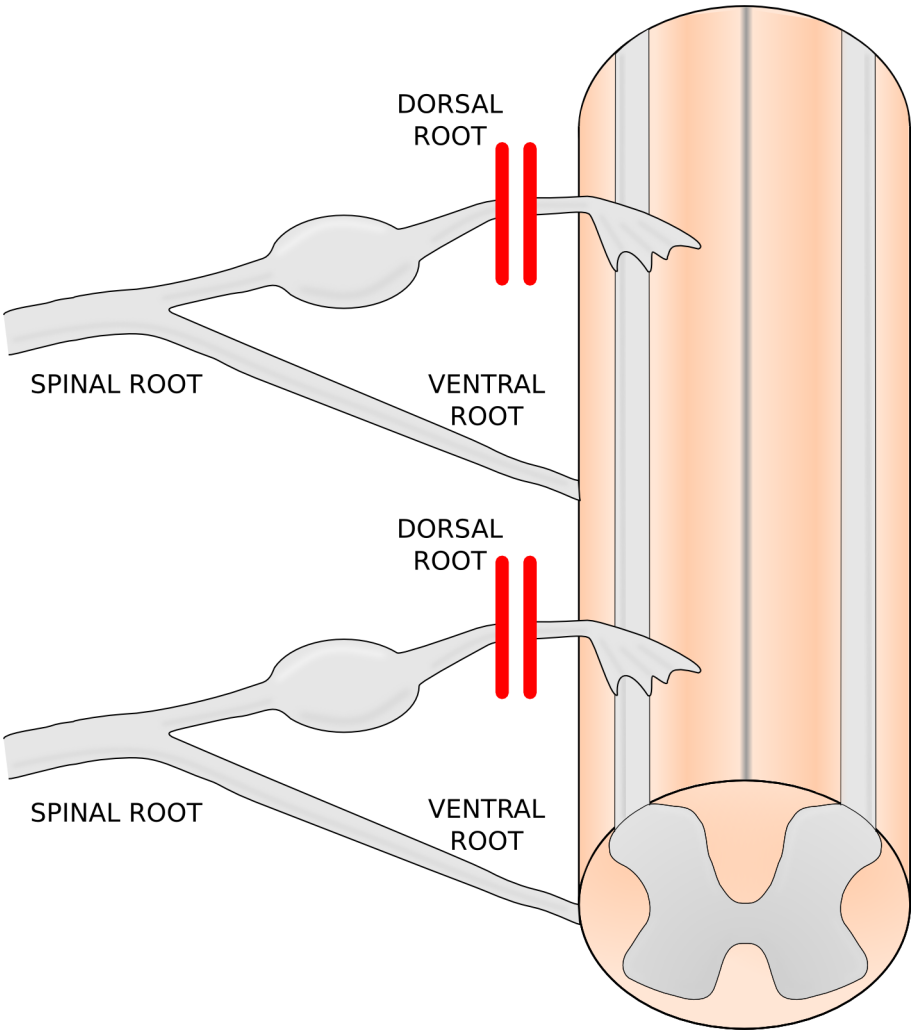

Figure 3.6: **Rhizotomy surgery in the Rat.** The dorsal roots from two dorsal root ganglia (L4 & L5) are transected to produce a dorsal rhizotomy.

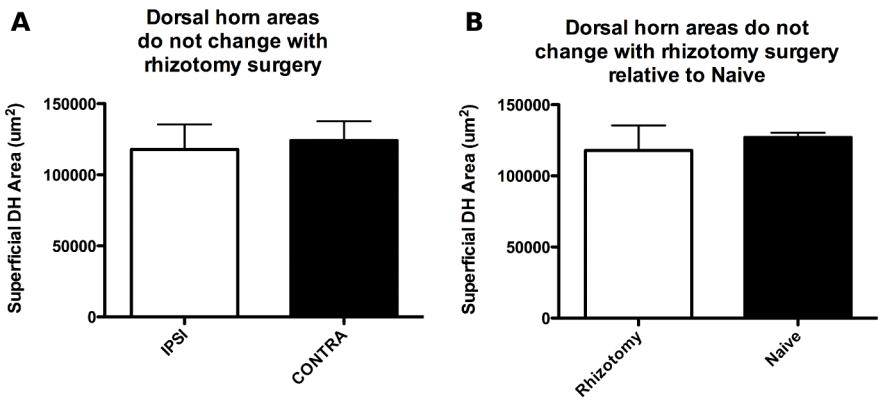

Figure 3.7: **Rhizotomy surgery does not affect dorsal horn areas. A:** Rhizotomy to the dorsal roots does not reduce the ipsilateral superficial dorsal horn area relative to the contralateral side. **B:** Rhizotomy surgery does not reduce the dorsal horn area relative to naïve animals. (Students T-Test; n.s., $p>0.05$; $n=4$). IPSI, ipsilateral; CONTRA, contralateral; DH, dorsal horn.

3.4.1 Superficial Dorsal Horn Areas Show No Changes Following Unilateral Rhizotomy

Since rhizotomy results in a loss of primary afferent input, one might expect a reduction in dorsal horn volume. Previous work suggests that rhizotomy may affect dorsal horn volume, with a non-significant trend seen towards reduced dorsal horn volumes (Chung et al., 1989). Thus, superficial dorsal horn areas were compared for ipsilateral and contralateral sides of the spinal cord. Figure 3.7A shows no significant differences in superficial dorsal horn volume between contralateral and ipsilateral regions in rhizotomised tissue. Since rhizotomy may affect the contralateral dorsal horn volume (Chung et al., 1989), the ipsilateral dorsal horn area of rhizotomy animals was compared to the areas measured from naïve rat dorsal horns. No significant differences were found, suggesting rhizotomy does not impact on dorsal horn volume. Since no evidence was found for changes in dorsal horn volume following rhizotomy, no correction was made to PSD95 synapse density measures.

3.4.2 PSD95 Puncta are Significantly Reduced in Lamina I-III of the Dorsal Horn Following Unilateral Rhizotomy

The demonstration that dorsal horn volume does not appear to significantly change following rhizotomy does not preclude a loss of synapses in this region. Thus, the distribution of PSD95 puncta throughout lamina I-III of dorsal horn sections which had received a unilateral rhizotomy was analysed. As can be seen in Figure 3.8A, a significant reduction in PSD95 puncta is observed in all four laminar regions analysed, indicating a small yet highly significant loss of PSD95 puncta from synapses in each region of the superficial dorsal horn. Comparing the ipsilateral dorsal horn PSD95 distributions following rhizotomy to the naïve rat distribution showed similar results (Figure 3.8B).

These data demonstrate the ability for this synapse imaging and analysis system to detect changes in synapse numbers following specific manipulations to the dorsal horn. This loss of PSD95 puncta likely reflects a large proportion of primary afferent derived connections within the dorsal horn. Assuming there is no compensatory synaptogenesis, and that all primary afferent axons have been effectively removed, this data suggests approximately 30% of PSD95 puncta are derived from primary afferent connections in lamina I, II outer, II inner and approximately 20% of PSD95 puncta from lamina III in the dorsal horn.

3.5 Spinal Nerve Ligation Induces a Delayed Reduction in PSD95 Puncta

So far StereoMate has revealed specific distribution patterns for PSD95 in rat and mouse superficial dorsal horn, as well as SynaptoPhysin in mouse superficial dorsal horn. Furthermore, it has shown its ability to reliably detect changes in PSD95 synapse numbers

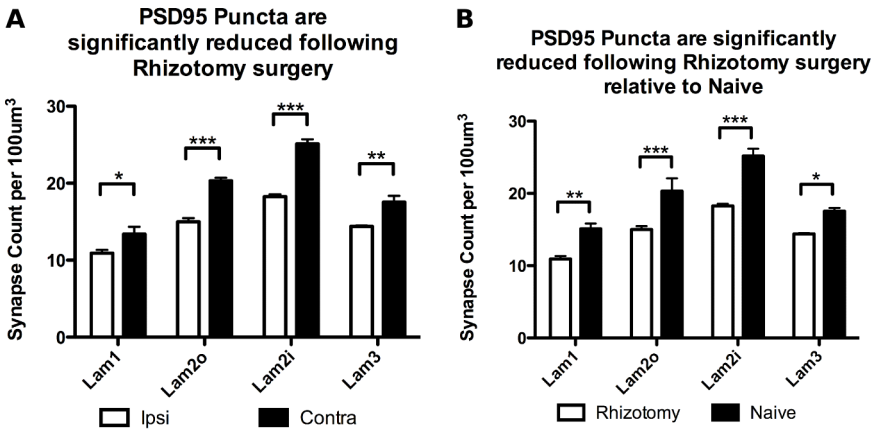

Figure 3.8: **PSD95 puncta are lost in the dorsal horn following rhizotomy surgery.** Rhizotomy surgery results in significant loss of synapses throughout the superficial dorsal horn (two-way ANOVA; bonferonni-corrected selective post-hoc testing; *, $p<0.05$; **, $p<0.01$; ***, $p<0.001$; $n=4$).

following rhizotomy, an intervention known to reduce synapse numbers in the superficial dorsal horn. The next aim was to explore the effects of peripheral nerve injury to synapse numbers in the dorsal horn.

Peripheral nerve injury is distinct from rhizotomy because it leaves the dorsal roots intact since the connection between the dorsal root ganglion (which contains the primary afferent cell bodies), dorsal root and spinal cord remains intact, whereas the link between the dorsal root ganglion and its peripheral innervation is ablated in peripheral nerve injury. This is widely accepted to result in both the sudden influx of injury-related retrograde signalling molecules as well as a loss of trophic support, which can result in profound changes in transcription and protein signalling (Michaelevski et al., 2010; Perkins et al., 2014). This is further compounded by a plethora of alterations within the dorsal horn itself (see Sandkühler, 2009; von Hehn et al., 2012; West et al., 2015, for review). Thus, although the large and robust changes in synaptic puncta seen in rhizotomy is unlikely to occur following peripheral nerve injury, there may be more subtle alterations to synapse distributions with peripheral nerve injury, which may be driven mechanistically by the complex array of changes seen in these models.

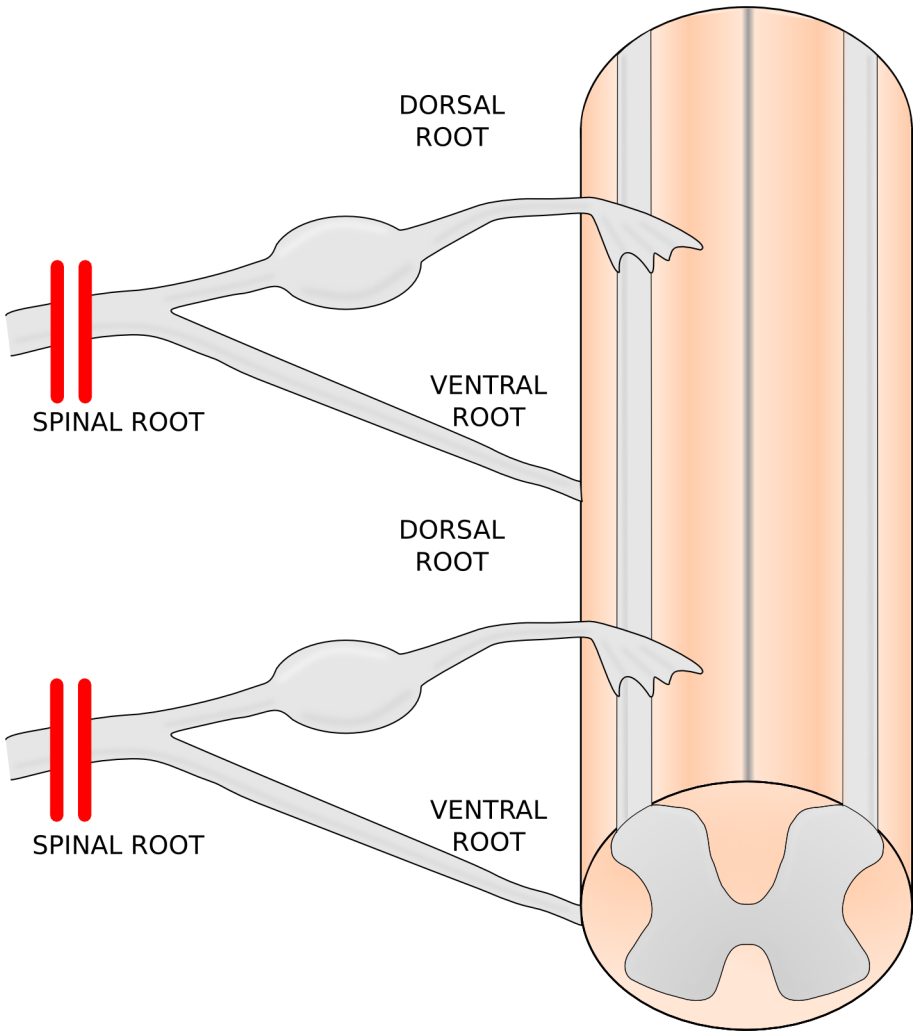

Figure 3.9: **The Spinal nerve ligation model in the Rat.** Both L5 and L6 spinal roots are transected and ligated to produce a peripheral nerve injury specific to the L5 and L6 DRGs.

In order to investigate this, initial experiments focussed on the well characterised Spinal Nerve Ligation (SNL, see Figure 3.9) model in male Sprague-Dawley rats (Kim and Chung, 1992).

3.5.1 SNL Significant Reduces Paw Withdrawal Latency

In order to assess the effects of SNL on evoked behavioural responses, animals underwent von Frey threshold testing as outlined previously (Chaplan et al., 1994, , see Methods). Von Frey testing was performed blind during two baseline sessions prior to surgery, and followed up with testing at 7, 14 and 20 days post SNL surgery.

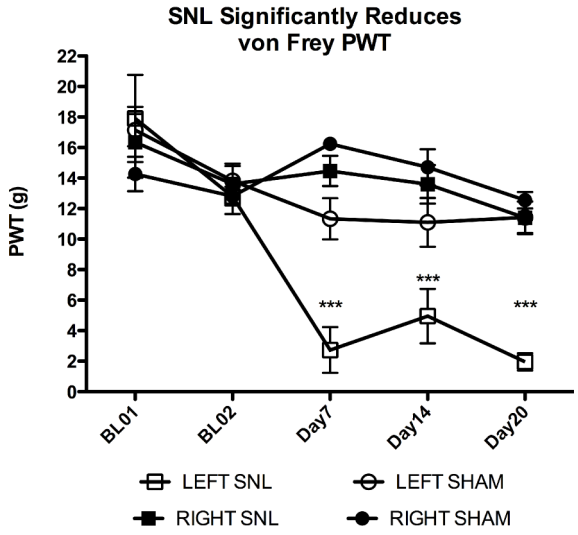

Figure 3.10: **SNL reduces paw withdrawal threshold on the ipsilateral paw.** Following SNL surgery animals display a significant reduction in ipsilateral paw withdrawal threshold relative to the contralateral paw, and to SHAM operated animals (two-way ANOVA; bonferonni-correct selective post-hoc testing; ***, $p<0.001$; n=5). PWT, paw withdrawal threshold.

Figure 3.10 shows the behavioural data obtained from this experiment, and indicates a robust reduction in paw withdrawal threshold in ipsilateral SNL paws, relative to both contralateral SNL paws, and SHAM surgery animals, consistent with previous work (Kim and Chung, 1992; Nirogi et al., 2012).

3.5.2 SNL Causes a Reduction in IB4 Labelling within the Ipsilateral Superficial Dorsal Horn

Previous studies have identified IB4 binding as a consistent marker for a subpopulation of C fibres (Streit et al., 1985; Molliver et al., 1995), which is lost by peripheral nerve injury (Molander et al., 1996; Bennett et al., 1998). It thus serves as a useful marker to identify the regions of the dorsal horn that correspond to the central projections of injured afferents. Figure 3.11 shows spinal cord sections seven and 21 days post SNL surgery stained for IB4 as previously described (see Section 2.2). Peripheral nerve injury results in a significant loss of IB4 binding to the ipsilateral dorsal horn, and therefore was

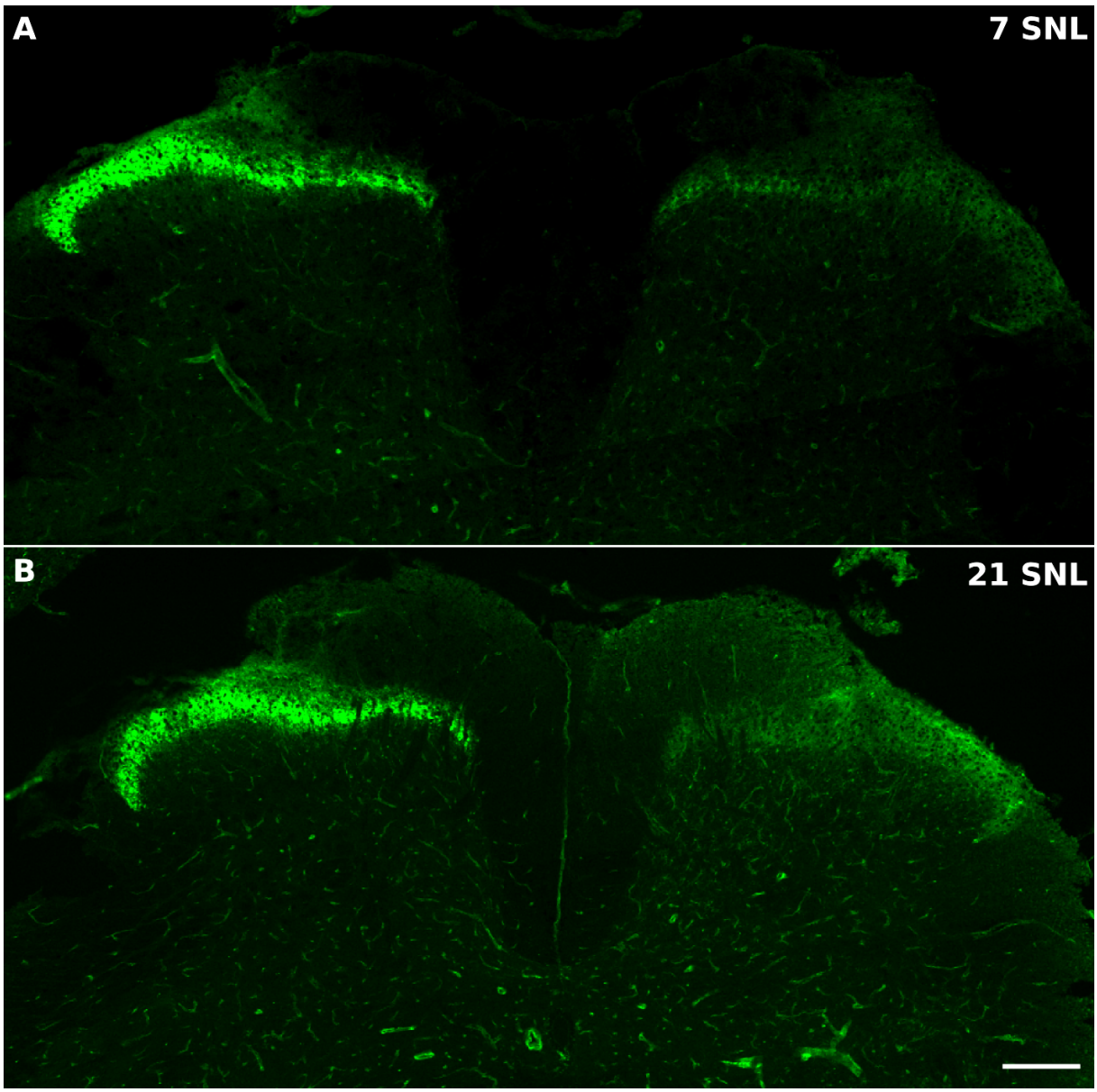

Figure 3.11: **IB4 is reduced after SNL surgery in the Rat. A:** 7 days post SNL surgery. **B:** 21 days post SNL surgery. Scale Bar: $200\mu m$.

used to identify injured central axonal projection regions in the remainder of this thesis.

3.5.3 Superficial Dorsal Horn Areas are not Altered by SNL

Injury to primary afferent axons may result in alterations to dorsal horn volumes, which could bias PSD95 synapse density data. In order to control for such changes, measures of superficial dorsal horn area were made ipsilaterally and contralaterally in both seven and 21 days post SNL surgery. As can be seen in Figure 3.12, no significant changes were observed between ipsilateral and contralateral dorsal horns in either seven or 21 day

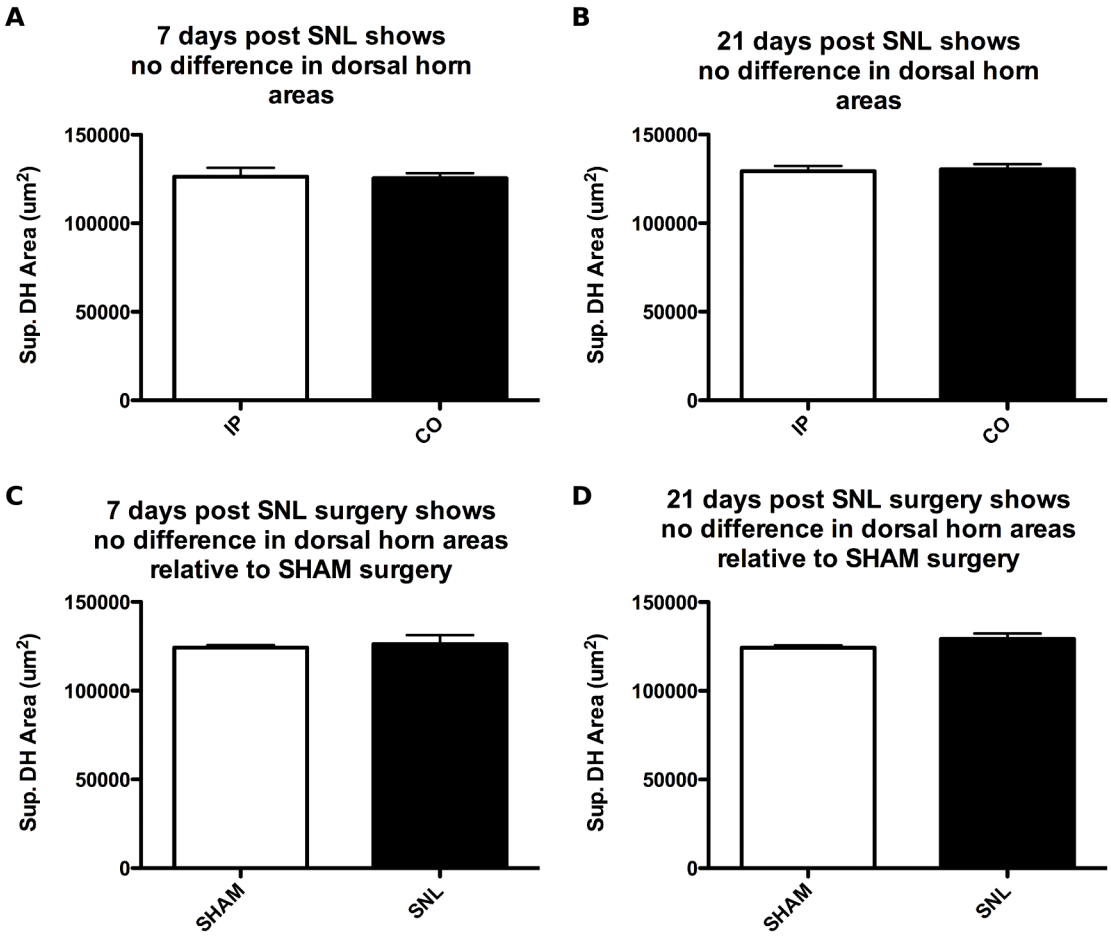

Figure 3.12: **SNL does not affect dorsal horn areas. A:** 7 days post SNL shows no change in ipsilateral dorsal horn area relative to contralateral region. **B:** 21 days post SNL shows no change in ipsilateral dorsal horn area relative to contralateral region. **C:** 7 days post SNL shows no change in ipsilateral dorsal horn area relative to SHAM control. **D:** 21 days post SNL shows no change in ipsilateral dorsal horn area relative to SHAM control. (Students T-Test; n.s., $p>0.05$; $n=4$). DH, dorsal horn.

SNL groups. SHAM surgery also had no effect on dorsal horn area, and both ipsilateral 7 and 21 day cohorts show no significant differences with the SHAM surgery group (Figure 3.12).

3.5.4 No Changes to PSD95 Synaptic Puncta Distributions Seven Days Post SNL

Initially, PSD95 synaptic puncta distributions were explored seven days post surgery, to allow a direct comparison between the effects of peripheral nerve injury and rhizotomy

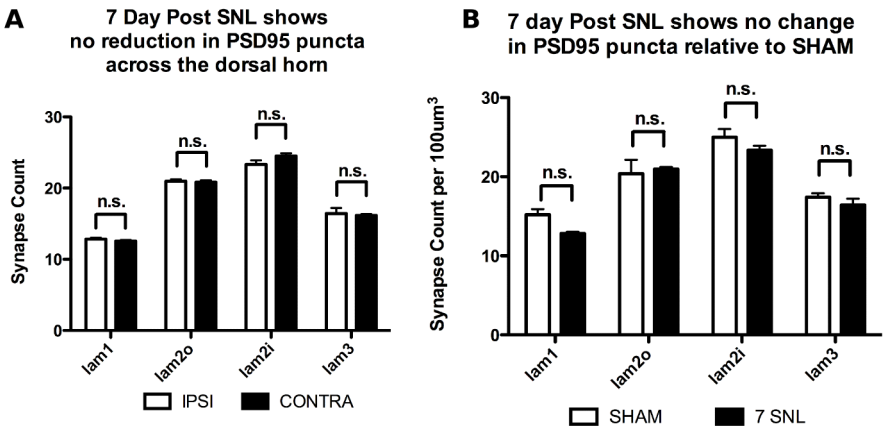

Figure 3.13: **7 days post SNL surgery does not affect PSD95 puncta distribution within the superficial dorsal horn. A:** 7 days post SNL shows no change in PSD95 density relative to the contralateral dorsal horn. **B:** 7 days post SNL show in change in PSD95 number relative to SHAM surgery (two-way ANOVA; bonferonni-corrected selective post-hoc testing; n.s., $p>0.05$; $n=4$).

surgery. Seven days post SNL revealed no alterations in PSD95 puncta number throughout lamina I-III of the ipsilateral dorsal horn when compared to the contralateral dorsal horn (Figure 3.13A) or the ipsilateral SHAM surgery cohort (Figure 3.13B).

3.5.5 PSD95 Puncta are Reduced in Lamina II Inner 21 Day Post SNL

To explore whether SNL may be having a delayed impact on the PSD95 distribution pattern within the dorsal horn, animals were assessed 21 days following peripheral nerve injury. Analysis of PSD95 synaptic puncta density revealed a small yet highly significant reduction within lamina II inner, 21 days post SNL. This reduction was specific to lamina II inner, with other laminae showing no changes (Figure 3.14). Furthermore, this reduction in lamina II inner was present when comparing the ipsilateral dorsal horn of 21 day SNL animals to the SHAM surgery group (Figure).

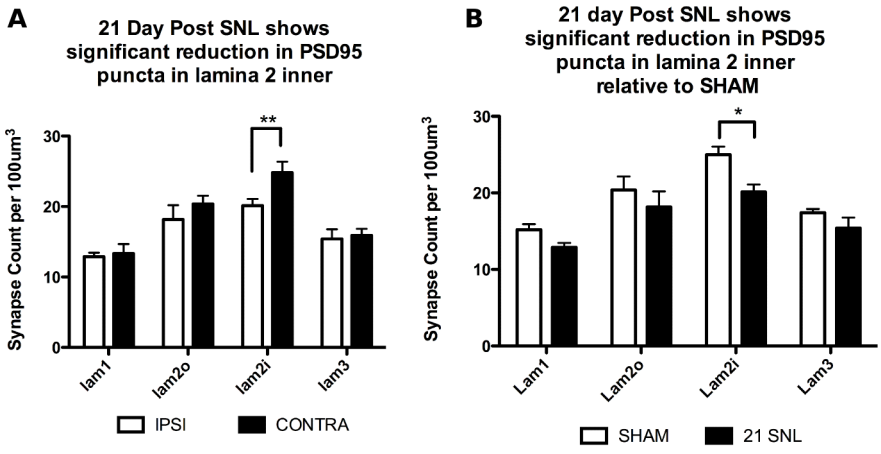

Figure 3.14: **21 days post SNL surgery shows a significant reduction in PSD95 puncta in lamina II inner. A:** 21 days post SNL show a significant reduction in PSD95 puncta in lamina II inner relative to the contralateral dorsal horn. **B:** 21 days post SNL shows a significant reduction in PSD95 puncta in lamina II inner relative to SHAM surgery (two-way ANOVA; bonferonni-corrected selective post-hoc testing; *, $p<0.05$; **, $p<0.01$; n=4).

3.6 PSD95 is Significantly Reduced in Spared Nerve Injury

To continue the exploration of peripheral nerve injury on synapse distributions within the dorsal horn, a second nerve injury paradigm was used. The spared nerve injury (SNI, Figure 3.15) model tightly ligates and transects two of the three branches from the sciatic nerve; the common peroneal and tibial nerves (Decosterd and Woolf, 2000). This leaves the third sural branch intact. This model results in a selective loss of the common peroneal and tibial nerve inputs, which innervate the medial aspect of L3-5 of the dorsal horn, and therefore allows the concomitant analysis of both injured and adjacent uninjured regions of the dorsal horn (Decosterd and Woolf, 2000; Shields et al., 2003; Beggs and Salter, 2007).

The aims of these experiments were to investigate the distributions of PSD95 in mouse dorsal horn in the context of peripheral nerve injury, to see if they mimic the previous findings in SNL, and to explore SynaptoPhysin distributions in this nerve injury paradigm.

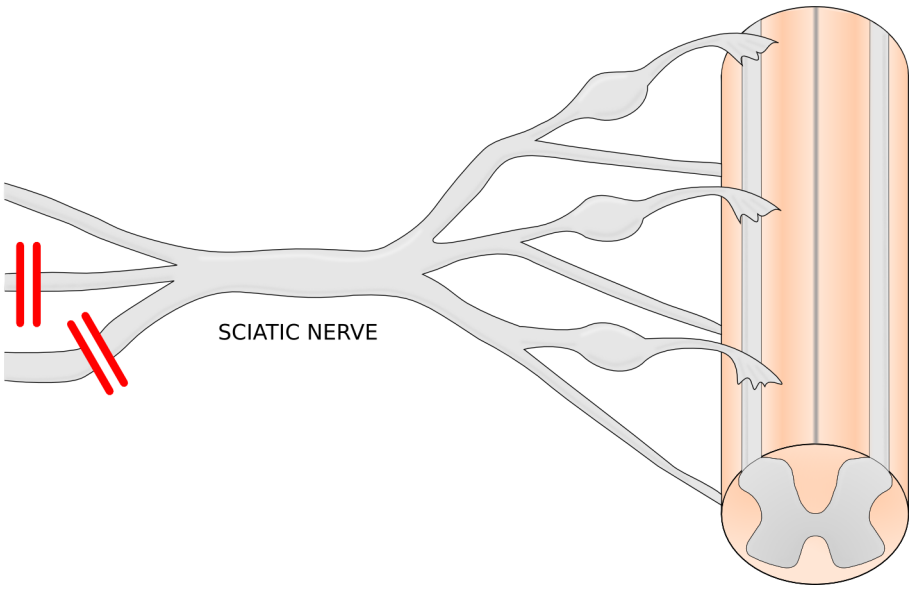

Figure 3.15: **The spared nerve injury model in the Mouse.** Two branches of the Sciatic nerve (the Tibial and Common Peroneal nerves) are ligated and transected, leaving the third branch (Sural nerve) intact.

3.6.1 Spared Nerve Injury Results in a Significant Reduction in Paw Withdrawal Threshold

In order to assess the effects of SNI on evoked behavioural responses, a number of animals underwent von Frey threshold testing as outlined previously (Chaplan et al., 1994). Von Frey testing was performed blind during two baseline sessions prior to surgery, and followed up with testing at 3, 8, 15 and 21 days post SNL surgery.

Figure 3.16 shows the behavioural data obtained from this experiment, and indicates a robust reduction in paw withdrawal threshold in ipsilateral SNI paws, relative to SHAM surgery animals, consistent with previous work (Decosterd and Woolf, 2000; Shields et al., 2003; Beggs and Salter, 2007).

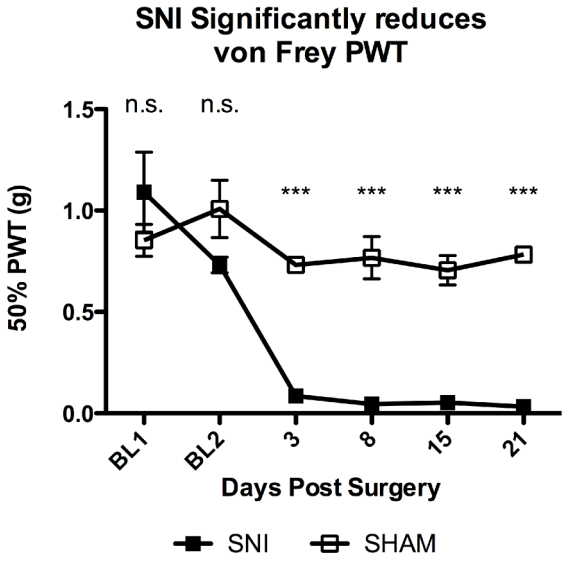

Figure 3.16: **Spared nerve injury results in a significant reduction in paw withdrawal threshold.** Following SNI surgery animals display a significant reduction in ipsilateral paw withdrawal threshold relative to SHAM operated animals (two-way ANOVA; bonferonni-correct selective post-hoc testing; ***, $p<0.001$; $n=6$). PWT, paw withdrawal threshold.

3.6.2 Isolectin B4 is Lost in Terminal Fields of Tibial and Common Peroneal Nerves

To investigate the potential loss of IB4 from injured territories within the dorsal horn, staining for IB4 was performed as previously described (see Section 2.2). Loss of IB4 was consistent with previous reports indicating a selective loss in the medial component of the ipsilateral L4 dorsal horn (Figure 3.17), areas which have previously been shown to receive input from both the tibial and common peroneal nerves (Shields et al., 2003; Beggs and Salter, 2007). Thus, medial aspects of the dorsal horn were selected for analysis of PSD95 and Synaptophysin distributions in both injured and contralateral control regions.

3.6.3 Superficial Dorsal Horn Areas are Not Affected by SNI

To determine whether the total volumes of dorsal horn regions affected by SNI were altered relative to unaffected regions, measurements of the superficial dorsal horn areas in

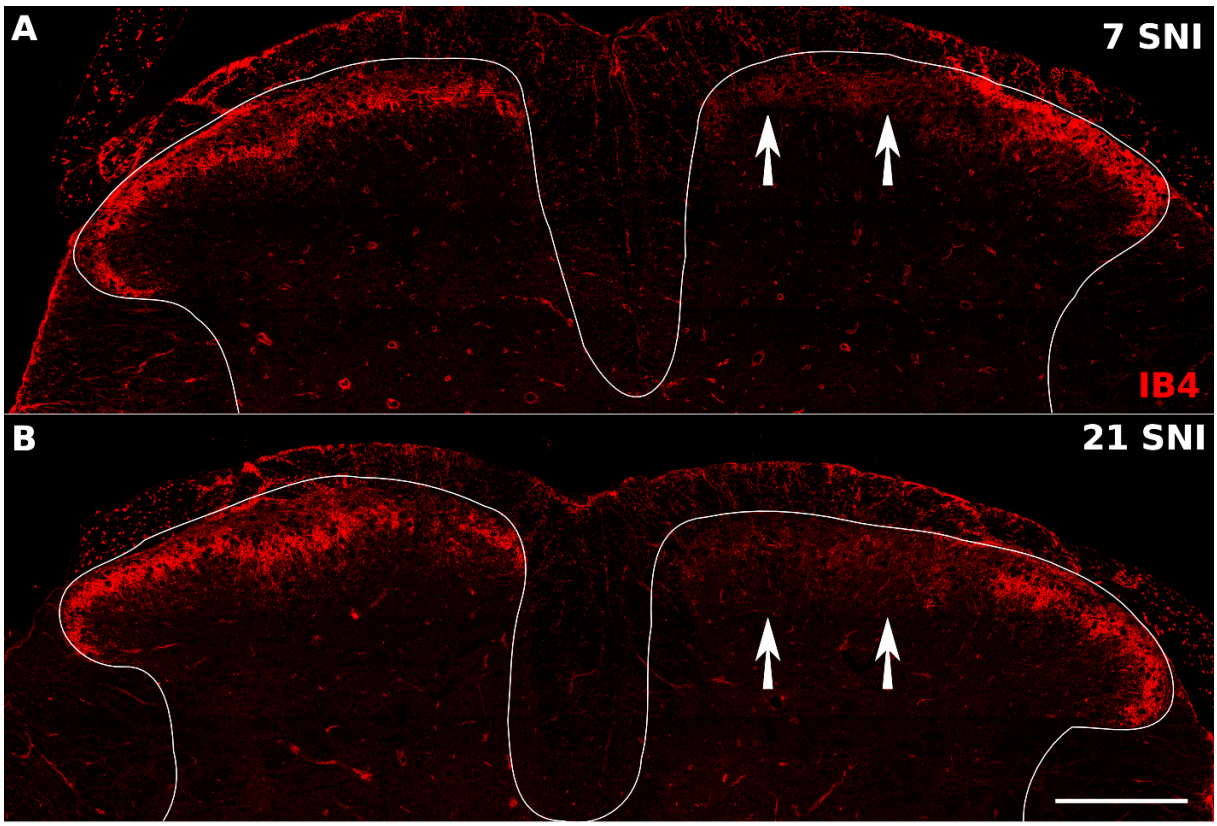

Figure 3.17: **IB4 is reduced after SNI surgery in the Mouse. A:** 7 days post SNI surgery. **B:** 21 days post SNI surgery. Arrows indicate the loss of IB4 on the ipsilateral side to injury. Scale Bar: $200\mu m$.

transverse sections were conducted. As can be see in Figure 3.18, no significant differences were seen in dorsal horn areas following SNI, relative to contralateral regions or SHAM controls. Therefore, uncorrected density measures of synaptic puncta counts can be used to compare between injured regions in SNI and other synapse distribution data.

3.6.4 Seven Days Post SNI Reveals No Change in PSD95 & SynaptoPhysin

To explore whether any changes occur to synaptic puncta by 7 days post injury, and thus allow comparisons with 7 day SNL and rhizotomy data, PSD95 and SynaptoPhysin puncta were analysed in the medial dorsal horn ipsilateral and contralateral 7 days post SNI injury. PSD95 puncta distributions showed no change throughout lamina I-III of the dorsal horn at 7 days post SNI relative to the contralateral regions, or to a SHAM control

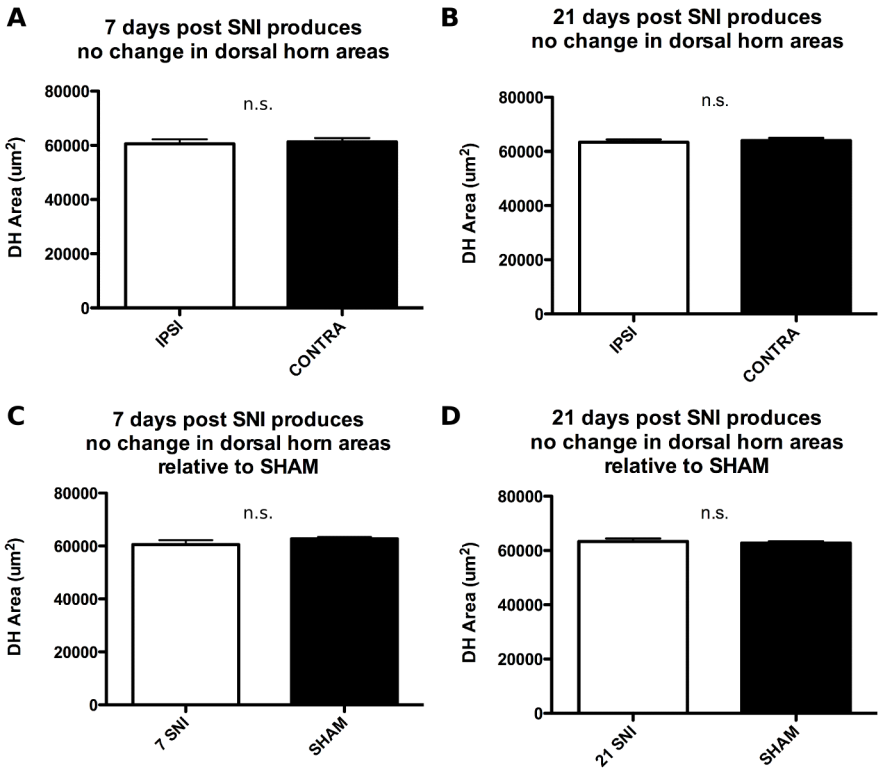

Figure 3.18: **SNI does not affect dorsal horn areas. A:** 7 days post SNI shows no change in ipsilateral dorsal horn area relative to contralateral region. **B:** 21 days post SNI shows no change in ipsilateral dorsal horn area relative to contralateral region. **C:** 7 days post SNI shows no change in ipsilateral dorsal horn area relative to SHAM control. **D:** 21 days post SNI shows no change in ipsilateral dorsal horn area relative to SHAM control. (Students T-Test; n.s., $p>0.05$; $n=4$). DH, dorsal horn.

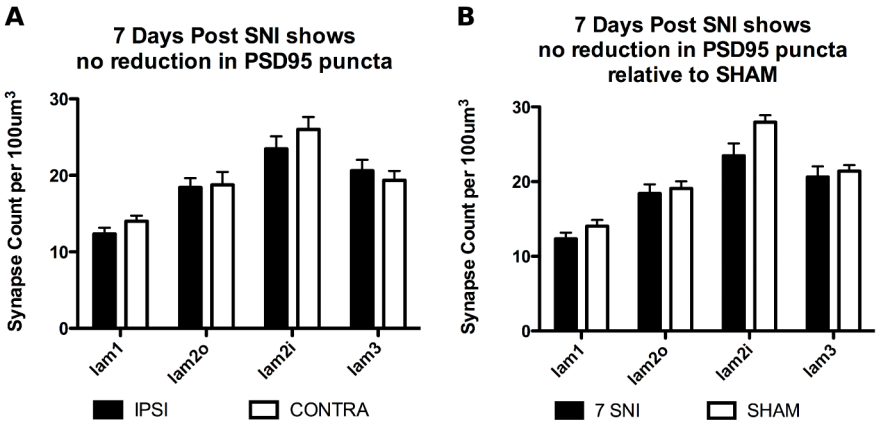

Figure 3.19: **7 days post SNI does not affect PSD95 puncta distribution within the superficial dorsal horn. A:** 7 days post SNI shows no change in PSD95 density relative to the contralateral dorsal horn. **B:** 7 days post SNI show in change in PSD95 number relative to SHAM surgery (two-way ANOVA; bonferonni-corrected selective post-hoc testing; n.s., $p>0.05$; $n=5$).

group (Figure 3.19), consistent with the previous findings in rat SNL tissue (see Figure 3.13). The PSD95 distributions observed follow the pattern previously described for both rat and mouse dorsal horn, with an increase in synapse density seen in lamina II relative to laminae I and III.

Next, the SynaptoPhysin distribution throughout the superficial dorsal horn ipsilateral to SNI injury were observed. SynaptoPhysin puncta distribution in laminae I-III of the medial ipsilateral dorsal horn 7 days post SNI injury revealed no significant alteration to the contralateral side, or a SHAM control group (Figure 3.20). This result fits with the previous data indicating no change to PSD95 puncta at 7 days post peripheral nerve injury. The synapse distribution for SynaptoPhysin follows a similar pattern to that previously described for the naïve mouse dorsal horn (see Figure 3.4), where an increased density is seen in lamina II, which is maintained in lamina III.

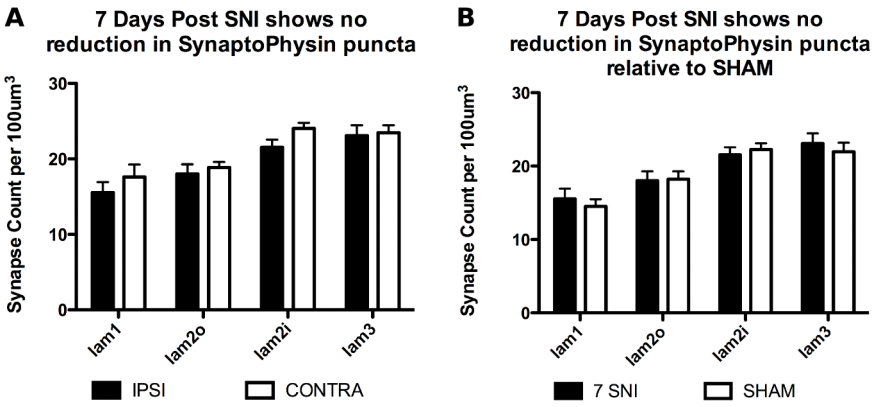

Figure 3.20: **7 days post SNI does not affect SynaptoPhysin puncta distribution within the superficial dorsal horn. A:** 7 days post SNI shows no change in SynaptoPhysin density relative to the contralateral dorsal horn. **B:** 7 days post SNI show in change in SynaptoPhysin number relative to SHAM surgery (two-way ANOVA; bonferonni-corrected selective post-hoc testing; n.s., $p>0.05$; $n=5$).

3.6.5 21 Days Post SNI Shows a Significant Reduction in Lamina II Inner PSD95 Puncta

Assessment of SNI tissue 7 days post injury revealed no change in the synaptic markers explores above (PSD95 and SynaptoPhysin), consistent with the previous data in SNL tissue. To explore whether the synaptic landscape may be modified at later time points, as has been observed in SNL tissue (see Figure 3.14), SNI tissue was analysed 21 day post injury. As can be seen in Figure 3.21A, PSD95 puncta observed on the ipsilateral medial dorsal horn at this time-point showed a small yet significant reduction in density within lamina II inner relative to the contralateral region. This reduction remained when comparing the ipsilateral data to a SHAM control group (Figure 3.21B). This data fits well with previous observations in SNL tissue indicating a reduction in lamina II inner specifically.

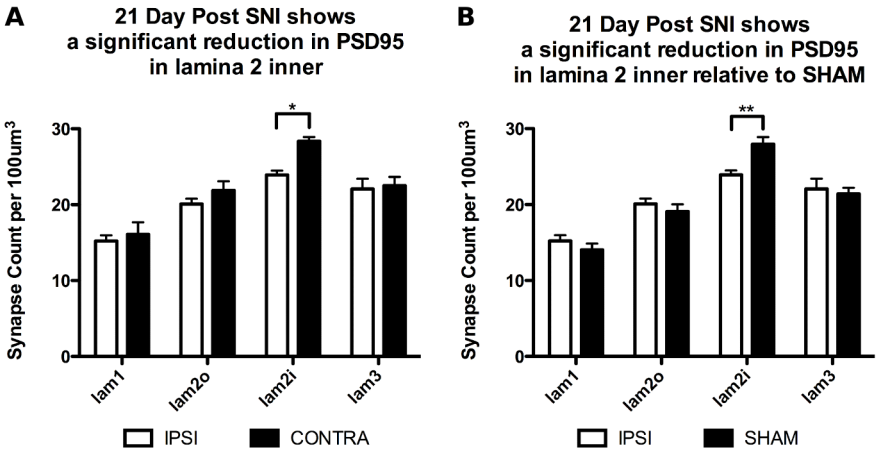

Figure 3.21: **21 days post SNI shows a significant reduction in PSD95 puncta in lamina II inner. A:** 21 days post SNI show a significant reduction in PSD95 puncta in lamina II inner relative to the contralateral dorsal horn. **B:** 21 days post SNI shows a significant reduction in PSD95 puncta in lamina II inner relative to SHAM surgery (two-way ANOVA; bonferonni-corrected selective post-hoc testing; *, $p<0.05$; **, $p<0.01$; $n=8$).

3.6.6 21 Days Post SNI Shows No Change in SynaptoPhysin

Following the confirmation of PSD95 reduction within lamina II inner in the ipsilateral dorsal horn 21 days post SNI, the distribution of SynaptoPhysin in the superficial dorsal horn 21 days post SNI was explored. As shown in Figure 3.22, there were no observed changes in SynaptoPhysin puncta density relative to the contralateral side, or a SHAM control group, and the distribution patterns fit what has been observed previously for 7 day post SNI and naïve mouse dorsal horn SynaptoPhysin distributions.

3.7 Advillin eGFP Analysis of SNI Tissue

To understand what modifications may be occurring to primary afferent axons within the dorsal horn, the Advillin-eGFP mouse from GENSAT was utilised. This transgenic mouse expresses eGFP protein in cells which express Advillin, which in the DRG & spinal cord constitutes all primary afferent neurons. Importantly, the expression of Advillin is unperturbed by axotomy, resulting in a permanent marking of primary afferents (Marks

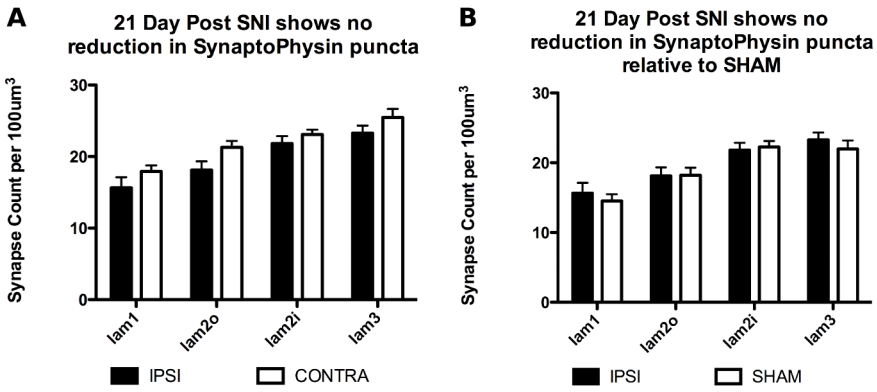

Figure 3.22: **21 days post SNI does not affect SynaptoPhysin puncta distribution within the superficial dorsal horn. A:** 21 days post SNI shows no change in SynaptoPhysin density relative to the contralateral dorsal horn. **B:** 21 days post SNI show in change in SynaptoPhysin number relative to SHAM surgery (two-way ANOVA; bonferonni-corrected selective post-hoc testing; n.s., $p>0.05$; $n=5$).

et al., 1998; Hasegawa et al., 2007; Lau et al., 2011). Thus, this transgenic line is an ideal method to understand whether primary afferent axons are truly lost after peripheral nerve injury, as many markers commonly used of primary afferents are down-regulated by nerve injury.

To characterise this transgenic, tissue was prepared for eGFP fluorescence as described in Section 3.2.3.4, and images of the DRG, sciatic nerve and spinal cord were taken of the EGFP fluorescence (Figures 3.23 & 3.24). As can be seen in Figure 3.23, all DRG cells appear to express eGFP, and sciatic nerve sections show axonal projections. Furthermore, in Figure 3.24, the spinal cord is illuminated especially on the dorsal horn, including the dorsal columns, lissauer's tract, and the superficial dorsal horn, with clearly visible large diameter axons penetrating into the dorsal horn from the medial dorsal columns, which resemble A fibre projections into the dorsal horn (Woodbury et al., 2008).

Figure 3.25A shows an example of the delineation of ROIs constituting the superficial (laminae I and II) and deep (lamina III) dorsal horn, for analysis of EGFP intensity. Using this methodology, the superficial and deep dorsal horn of naïve animals were analysed for eGFP fluorescence intensity. As can be seen in Figure 3.25B, the superficial dorsal

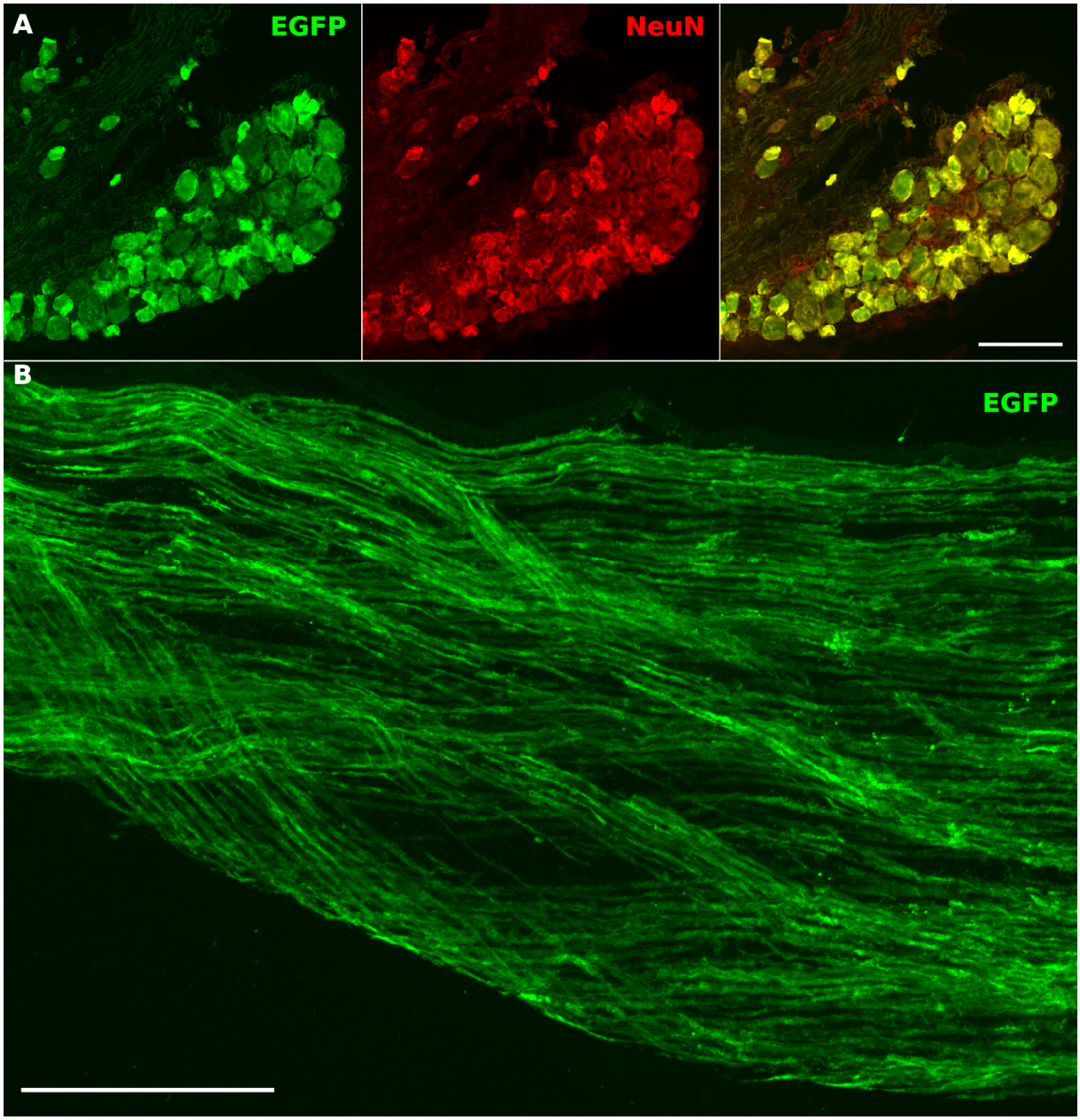

Figure 3.23: **The Advillin-eGFP mouse expresses eGFP in all primary afferent neuronal cell bodies and peripheral axons. A:** eGFP fluorescence in the DRG labels all neuronal cell bodies, as shown by NeuN double-labelling. **B:** Longitudinal section of the sciatic nerve shows labelling of all axons. Scale bars: A, B; 100μm.

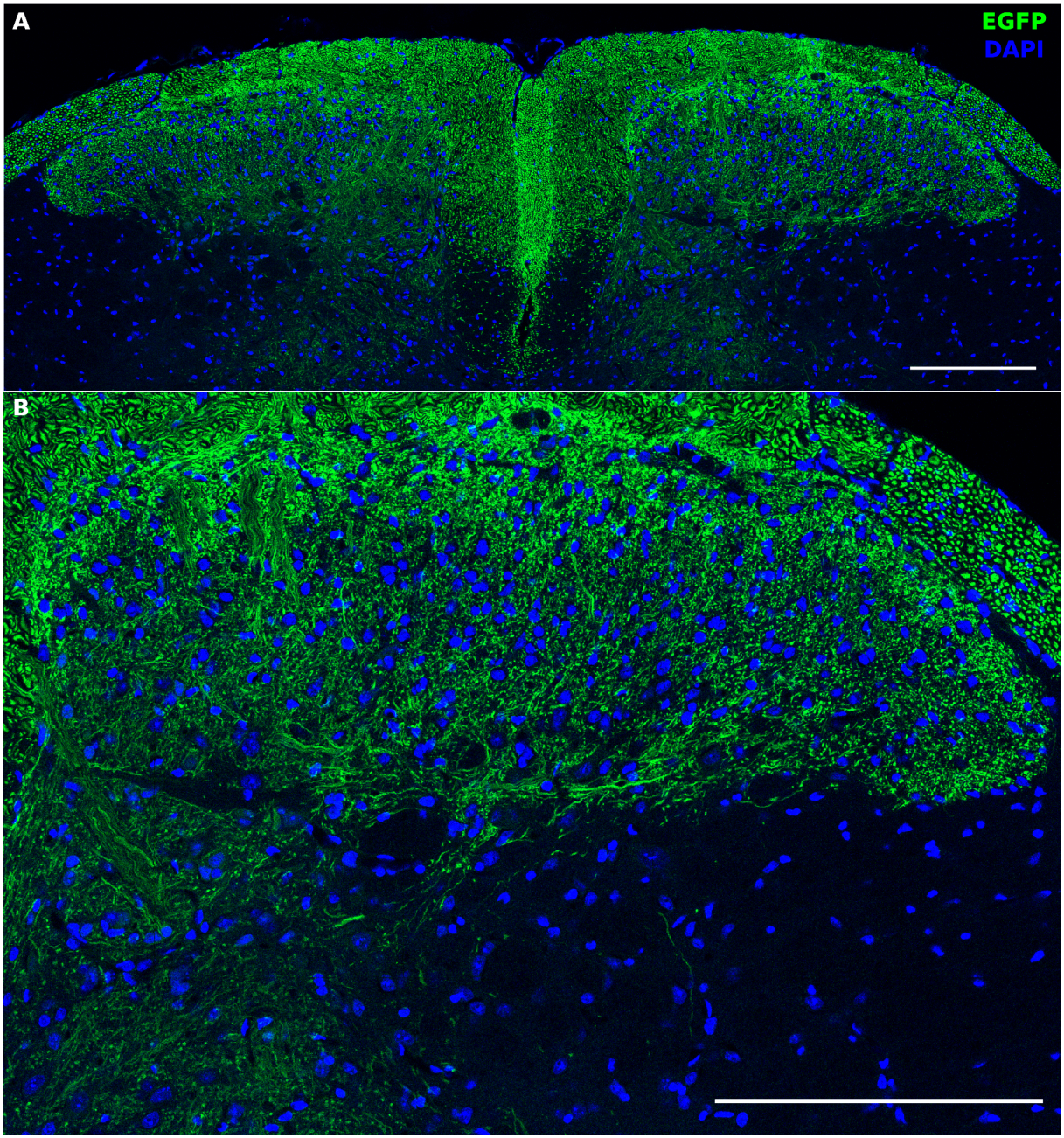

Figure 3.24: **The Advillin eGFP mouse shows eGFP axonal projections throughout the dorsal horn. A:** Overview of the lumbar dorsal horn showing eGFP labelling throughout, especially apparent in the superficial dorsal horn, the dorsal columns, and dorsal roots. **B:** Higher magnification view of the dorsal horn showing axonal projections throughout the dorsal horn. Scale Bars: A, B; 200μm.

horn displays a higher eGFP signal relative to deep dorsal horn, which reflects the larger arborisation of primary afferent C fibres in this region.

To investigate the consequences to primary afferent axons 21 days post injury, first ROIs were delineated onto the ipsilateral injured as well as the contralateral uninjured dorsal horn to derive both superficial and deep dorsal horn regions. The ipsilateral dorsal horn was divided such that only injured regions of the dorsal horn were analysed, as is shown in Figure 3.26A. Analysis of eGFP fluorescence in the delineation ROIs has been quantified and displayed in Figure 3.26B, which shows that there is no discernible different between contralateral and ipsilateral regions 21 days post SNI surgery.

To confirm the eGFP fluorescence seen in the superficial and deep regions of the dorsal horn 21 days post SNI is comparable to SHAM tissue, plots of the ipsilateral region, normalised to the corresponding contralateral region, of both 21 day SNI and SHAM tissue were measured. As is shown in Figure 3.26C, in both superficial and deep regions, 21 day SNI eGFP fluorescence is comparable to SHAM eGFP fluorescence, indicating there is no loss of eGFP 21 days post SNI surgery.

3.8 Discussion

This Chapter has applied the methodologies developed in Chapter 2 to specific laminae within the rodent spinal cord dorsal horn. This has revealed a previously undescribed stereotypical distribution pattern for two synaptic markers within the dorsal horn, the post-synaptic density marker PSD95, and the presynaptic marker SynaptoPhysin. In order to demonstrate the capacity for this technology to detect alterations in synapse number, a rhizotomy surgery was performed to ablate primary afferent input and synaptic connections. Analysis of rhizotomy tissue revealed a significant reduction in PSD95 puncta throughout the dorsal horn. Finally, the methodology was extended to peripheral nerve

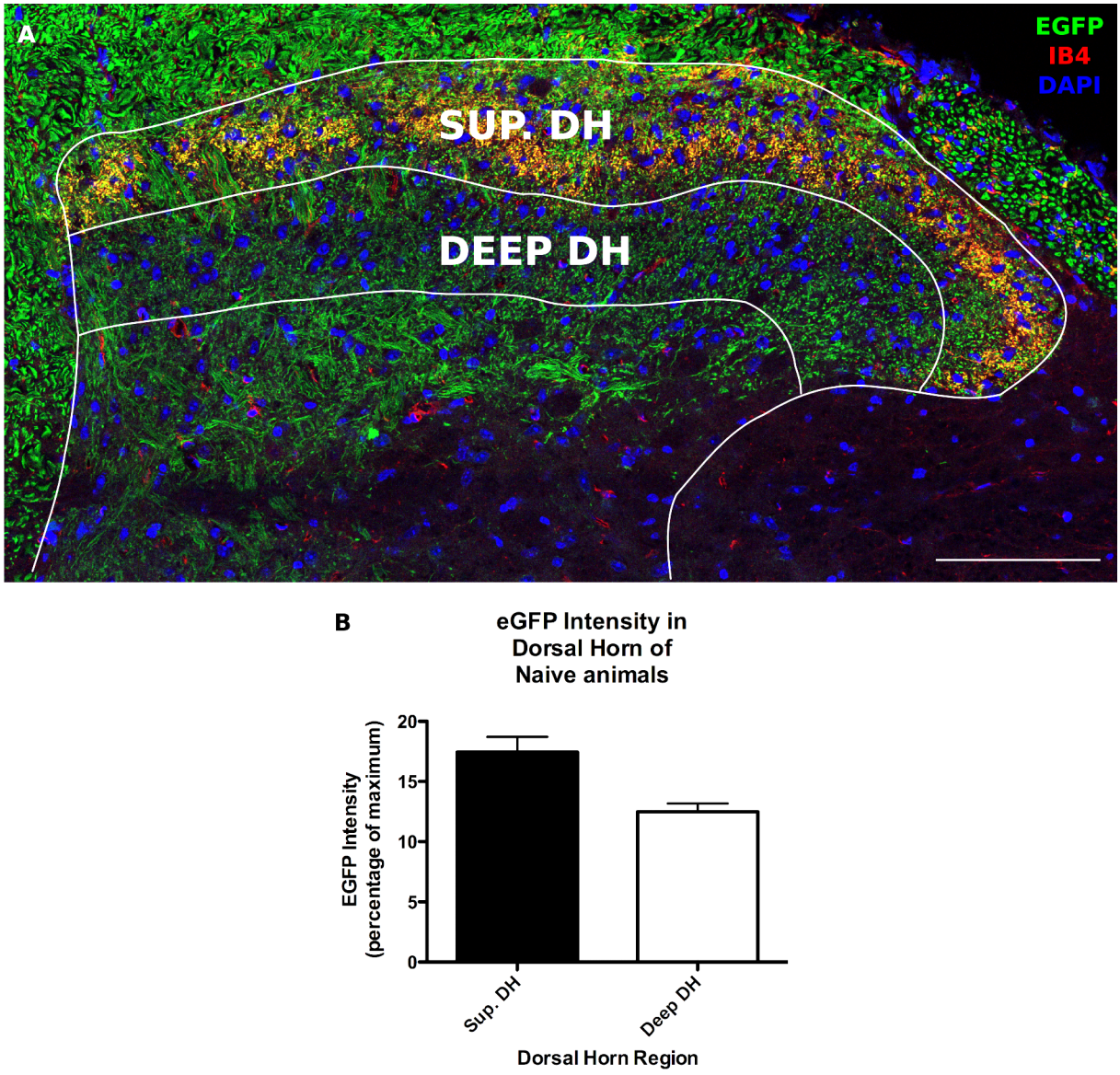

Figure 3.25: **Analysis of Advillin-eGFP projections to the dorsal horn. A:** An example of the delineation of the superficial and deep dorsal horn regions using IB4 as a marker. **B:** Recorded eGFP intensity from naïve Advillin-eGFP animals in the superficial and deep dorsal horn regions, showing a significantly higher fluorescence intensity in the superficial dorsal horn (Student's T-Test; p). Sup., superficial. Scale bar: $100\mu m$.

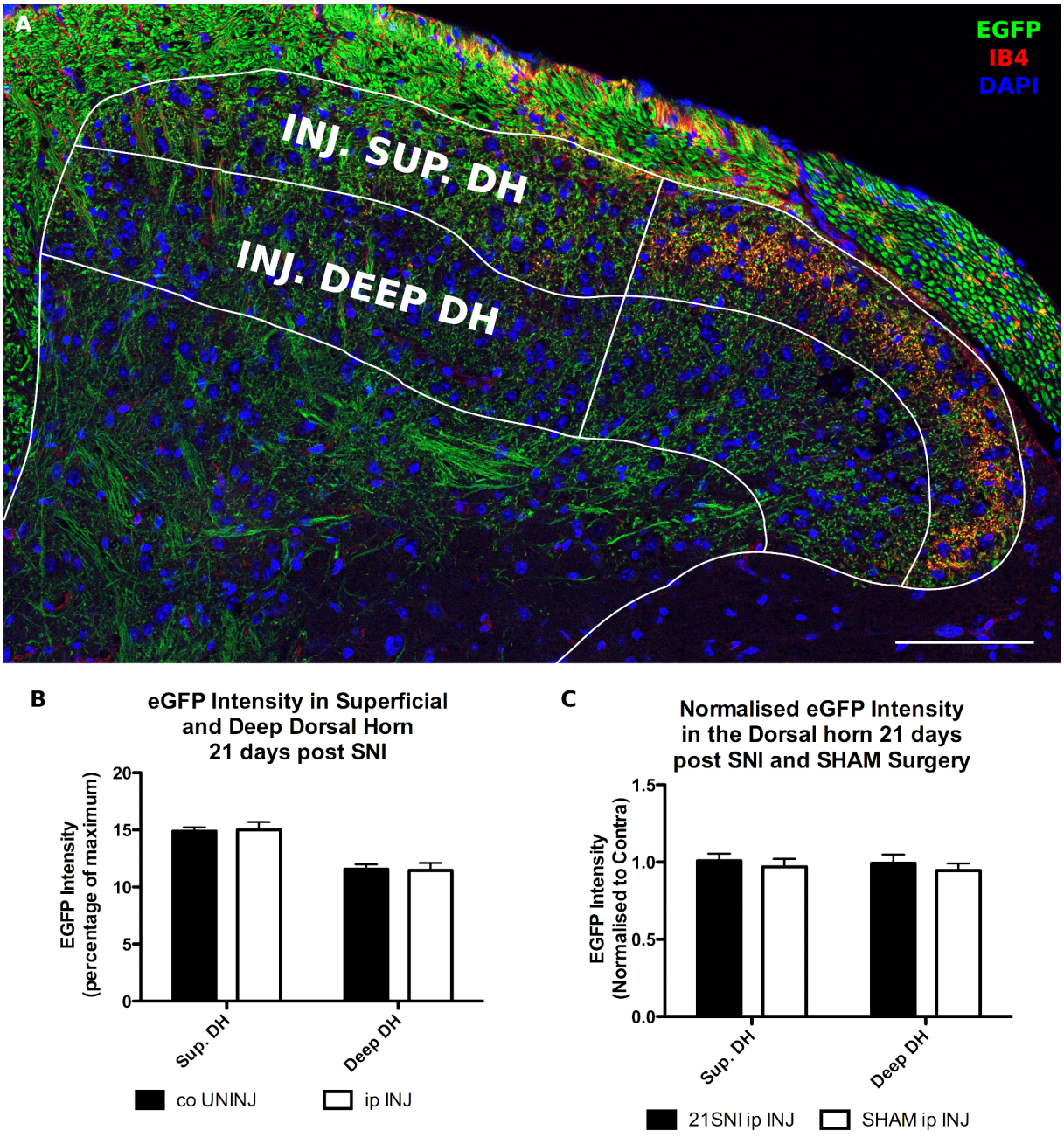

Figure 3.26: **Analysis of Advillin-eGFP projections to the dorsal horn following peripheral nerve injury. A:** An example of the delineation of the superficial and deep injured dorsal horn using IB4 as a marker. **B:** Recorded eGFP intensity from contralateral uninjured (co UNINJ) and the ipsilateral injured (ip INJ) regions in both superficial and deep dorsal horn, showing no difference between groups. **C:** Comparison of ipsilateral eGFP intensities normalised to the contralateral side of 21 day SNI (21SNI ip INJ) and SHAM surgery animals (SHAM ip INJ), showing no difference between groups. Sup., superficial. Scale bar: A, 100μm.

injury paradigms, to understand whether these conditions influence synaptic distribution patterns within the dorsal horn. A consistent finding in both nerve injury paradigms was a small yet significant reduction in PSD95 puncta specific to lamina II inner. Thus, this Chapter has demonstrated the ability for StereoMate to quantify synapse distribution patterns in selected regions of the CNS, and to detect changes in these distributions following different manipulations.

3.8.1 Synaptic Distributions - Technical Considerations

This Chapter has presented distribution patterns of PSD95 and SynaptoPhysin puncta throughout the superficial dorsal horn. These datasets were generated by initially measuring synapse density, and then proving that this density measure correlates to total object counts by measuring dorsal horn volumes, as outlined in Chapter 2.

One potential confound within the datasets is the lack of control for any potential shrinkage during tissue processing. As described in Chapter 2, all tissue sections were dried to slides prior to histological processing, to prevent tissue from detaching from the slide. To what degree this drying process shrinks tissue can potentially vary the subsequent synaptic puncta density measures, as tissue which remains more dense even after hydration and further tissue processing will display a higher density of synaptic puncta as compared tissue with the same biological distribution of synapses, but with less shrinkage. One means to control for this potential error would be to measure the thickness of all tissue sections under analysis, and to control for shrinkage observed in the Z plane. This would require an accurate measurement of the tissue thickness using an oil-immersion lens with a high NA. Any differences in tissue thickness, and therefore tissue density, could then be controlled for, which may produce even more robust data on synaptic puncta distributions.

Measurement of the dorsal horn area is another essential control to ensure object density measures directly correlate to total object counts. Dorsal horn area measurements across lumbar regions 3 to 5 revealed a significant reduction in lumbar region 3 relative to 4 and 5, which reflects a real difference in terms of lumbar spinal cord dimension (Anderson et al., 2009). This could potentially confound analyses between different animals, if a mixture of Lumbar 3 and 4 were used for synapse analysis. Since the nerve injury paradigms all affect lumbar regions 4, this region was selected for analysis. These data indicate the importance of carefully selecting regions for sampling to prevent any potential confounds from disrupting legitimate biological measurements.

3.8.2 Naïve dorsal horn

3.8.2.1 Synapse Distribution Patterns

Both PSD95 and SynaptoPhysin puncta displayed unique distribution patterns in the superficial dorsal horn. PSD95 showed a pronounced increase in puncta number in lamina II, especially lamina II inner, which diminished in lamina III. This large increase in synapse number may reflect the large input from C fibres to this lamina. It has previously been shown that C fibres outnumber A fibres by approximately 2 to 1 (Lawson, 1979; Lawson et al., 1984), and so it might be expected that the laminae where C fibres arborise may exhibit an increase in synaptic numbers. However, this assumes both C and A fibres arborise and synapse to the same degree. Furthermore, an increase would be expected in lamina I, where C fibres also arborise (Snider and McMahon, 1998). The rhizotomy data suggests this may only partially explain the difference in PSD95 puncta number, since the increase in lamina II, whilst abated following rhizotomy, does still remain (see Figure 3.8). Thus, the remaining elevated number of PSD95 puncta may be explained by a larger input from excitatory interneurons into this lamina (Kato et al., 2007, 2009).

SynaptoPhysin puncta display a similar pattern to PSD95, except the increased puncta number remained elevated in lamina III. Given this disparity with the PSD95 distribution data, this suggests the continued elevation in SynaptoPhysin puncta must represent another population of synaptic puncta. SynaptoPhysin is known to be a general pre-synaptic marker for both symmetric and asymmetric synapses (Thiel, 1993), and so the continued elevation in SynaptoPhysin may represent an increase in symmetric synapses in lamina III. It has been previously shown that the inhibitory interneurons that express glycine are present from lamina III and below (Punnakkal et al., 2014), and so this increase in SynaptoPhysin may reflect synapses contributed by these cells to this lamina.

The observed distributions across different lamina at different mediolateral locations revealed a remarkable consistency to PSD95 and SynaptoPhysin distribution densities, which suggests, at least when looking at crude synapse number distributions, that the general circuitry observed across the mediolateral axis is generally consistent. One discrepancy to this was the observed reduction in SynaptoPhysin in lamina I of the lateral portion relative to both the middle and medial portions of the dorsal horn. This was not matched by a significant reduction in PSD95 (although a trend towards a reduction was observed, see Figure 3.3), and so may reflect an altered inhibitory input to this region. It has previously been shown that neuronal sub-populations based on dendritic architecture display a regional bias in the mediolateral plane in lamina I (Lima and Coimbra, 1983, 1986), and so such a skewed distribution may reflect this fact. It is also well appreciated that dorsal horn wiring is different at different mediolateral regions (reviewed in Petkó and Antal, 2012). Another consideration is the fact lamina I on the lateral region of the dorsal horn is very narrow, which may increase the chances of error in delineating lamina I. If, for example, the outer border were to be drawn slightly beyond the true edge of the dorsal horn, this would have a larger effect on diluting synapse number in the lateral

regions than in the middle or medial regions.

An interesting observation during the course of this analysis was that PSD95 and SynaptoPhysin fluorescence intensity distributions in the dorsal horn displayed markedly different results. Whereas PSD95 fluorescence intensity was increased in lamina II, where an increase in PSD95 puncta has been observed; SynaptoPhysin consistently showed an increased fluorescence intensity in the superficial dorsal horn, in marked contrast to the observed underlying distribution of SynaptoPhysin puncta number. This highlights that fluorescence intensity does not always equal object density. The most likely explanation for the disparity between SynaptoPhysin intensity and density reflects the increased binding of the antibody to antigenic sites towards the periphery of the tissue, which antibodies washed on to the tissue will have immediate access to. This is backed up by the observation that SynaptoPhysin also displays intense fluorescence on the surface of the tissue (for example, see Figure 2.10 from Chapter 2). Why this same effect does not occur to PSD95 labelling is unclear, but may reflect the capacity for the antigen retrieval to effectively unveil post synaptic densities for antibody labelling, whereas presynaptic components remain harder for antibodies to access and label, therefore the increased time the antibody has access at the surface of the tissue creates a much higher density of SynaptoPhysin labelling than in regions within the tissue section.

3.8.3 Rhizotomy

Rhizotomy surgery results in the selective and complete loss of primary afferent input from transected dorsal roots into the dorsal horn. This has previously been shown to result in marked degeneration of primary afferent terminals, as well as dorsal horn dendritic components, and a loss of synapses in the affected dorsal horn region. Thus, rhizotomy was used as a positive control to test whether StereoMate could effectively detect a loss

in synapse numbers after injury.

3.8.3.1 Dorsal Horn Area is Not Affected by Rhizotomy

7 days post rhizotomy surgery showed no significant reduction in dorsal horn areas. This may be considered unexpected, since the loss of primary afferent fibres would be pronounced by this time point. However, this result largely correlates with previous findings (Murray and Goldberger, 1986; Chung et al., 1989). The fact no change in dorsal horn area was detected may reflect the concomitant glial response seen following rhizotomy surgery (Murray and Goldberger, 1986; Kapadia and LaMotte, 1987; Hajós et al., 1990), which may compensate for the loss of volume driven by loss of primary afferent terminals.

3.8.3.2 Synapse Loss Seen in Rhizotomy

Although no reduction in dorsal horn volume was observed after rhizotomy surgery, a dramatic loss in PSD95+ puncta was observed in all laminae 7 days post rhizotomy. This data fits with previous synaptic loss detected using electron microscopy (Chung et al., 1989). One clear disparity between Chung and the present data is the significant loss in synaptic puncta seen in the contralateral region in Chung et al. This difference may be explained by the region of the cord analysed; whereas in the present work the lumbar cord was analysed, in Chung et al. the sacral portion of the cord was analysed, which may possess more contralateral projections.

The clear reduction seen after rhizotomy surgery highlights the ability for StereoMate to effectively detect synapse number loss in the dorsal horn. By assuming that rhizotomy selectively eliminates primary afferent connections alone, that there remains no collateral inputs from adjacent dorsal roots in the sections analysed, and that no compensatory connectivity emerges, 30% of PSD95 puncta would be derived from primary afferent connections in lamina I, II outer, II inner and approximately 20% of PSD95 puncta from

lamina III in the dorsal horn. However, it has been reported that 7 days post injury some form of compensatory influence in the dorsal horn can occur, at least in cat (Basbaum and Wall, 1976; Murray and Goldberger, 1986), and so these proportions may not be completely accurate in reflecting the true number of synapses contributed by primary afferents alone in each lamina. These number are, however, assumed to roughly correspond to the contribution of primary afferents to the PSD95+ synaptic puncta number in these laminae.

3.8.4 Peripheral Nerve Injury Models

Peripheral nerve injury models are often used to model neuropathy, which is a common cause of neuropathic pain. These models are distinct from rhizotomy injuries (for example, dorsal root avulsion, or dorsal rhizotomy as performed in this Chapter) in that they leave the dorsal root intact. As the dramatic synaptic loss seen in rhizotomy is believed to reflect the sudden loss in primary afferent input, such a dramatic change might not be expected with a lesion to a peripheral nerve. Instead, a plethora of complex mechanisms are initiated at the locus of injury, affected the dorsal root ganglion, its projections to the dorsal horn, and the dorsal horn itself (Sandkühler, 2009; Michaelevski et al., 2010; von Hehn et al., 2012; Perkins et al., 2014; West et al., 2015).

The two models selected to interrogate synaptic distribution changes after nerve injury display similar behavioural, anatomical and functional changes (Sandkühler, 2009), which are typical for traumatic nerve injuries. Two reasons led to the change from SNL to SNI: the spared nerve injury results in an injury such that on one transverse section of the spinal cord, both injured and adjacent uninjured afferents can be observed (Beggs and Salter, 2007); and the SNI model is technically less challenging than the SNL model, which produces a more consistent model in mice, and makes future manipulations to the

injured nerve a simpler endeavour. Understanding any changes in uninjured afferents is important, as they may play a role in the signs and symptoms of neuropathic pain, including evoked behavioural hypersensitivity, observed following traumatic nerve injury (Wu et al., 2001; Ringkamp and Meyer, 2005; Meyer and Ringkamp, 2008).

3.8.4.1 Mechanical Paw Withdrawal Thresholds are Reduced by SNL & SNI

A consistent observation following peripheral nerve lesions is evoked hypersensitivity to different somatosensory inputs (Decosterd and Woolf, 2000; Sandkühler, 2009). In both injury paradigms, a large reduction in paw withdrawal thresholds to von Frey hairs was observed. The methodology followed that outlined by Chaplan et al. (1994), and is used to determine the 50% paw withdrawal threshold. The effects of a peripheral nerve transection model on evoked behaviour suggests that adjacent uninjured afferents and their integration with the dorsal horn is profoundly affected by injured afferents. Electrophysiological changes have been detected in uninjured afferents (Wu et al., 2001), and microglial responses observed after peripheral nerve lesion have been shown to spread to adjacent uninjured regions of the dorsal horn (Beggs and Salter, 2007, see also the next Chapter), which further implicate uninjured afferents in the presentation of neuropathic symptoms (Ringkamp and Meyer, 2005; Meyer and Ringkamp, 2008). These observations suggest that the mechanisms that drive evoked hypersensitivity are a result of nerve lesion affecting adjacent uninjured nerve territories, peripherally and/or centrally.

3.8.4.2 IB4 Labelling is Reduced by SNL & SNI

IB4 has been used to mark non-peptidergic afferents, and is known to be reduced by peripheral nerve injury (Streit et al., 1985; Molliver et al., 1995; Molander et al., 1996; Bennett et al., 1998). The loss of IB4 can pose significant problems in the delineation of laminae within the injured region of the dorsal horn, since it has been used to identify

lamina II, and divide lamina II inner from lamina II outer. To counteract this, firstly the ipsilateral and contralateral regions were taken from the same mediolateral region of the dorsal horn. This allows the laminar distribution of the contralateral side to guide the delineation for the ipsilateral side. Secondly, although IB4 is markedly reduced following peripheral nerve injury, often some labelling does still remain (as can be seen in Figure 3.11), due to innervation from separate dorsal roots into adjacent dorsal horn segments, via Lissauer's Tract (McMahon and Wall, 1985). Thus, the use of IB4, whilst not perfect, is still sufficient to delineate lamina I-III in dorsal horn regions innervated by axons affected by peripheral nerve injury, which is confirmed with the stability of the 7 day SNI & SNL data showing a similar laminar distribution of both PSD95 and SynaptoPhysin.

It may be possible to overcome this potential confound or area of confusion through the use of a more indelible marker. A plexus of neurons that express protein kinase c gamma exist within the superficial dorsal horn which stretch across the lamina II inner border in the mediolateral and rostrocaudal axes. This plexus exists just ventral to the IB4 labelling, and has been suggested to constitute a ventral region occupying lamina II inner, with IB4 labelling occupying a dorsal region of lamina II inner (Polgár et al., 1999; Zylka et al., 2005; Neumann et al., 2008). Protein Kinase C gamma is increased following peripheral nerve injury (Mao et al., 1995), and so may provide a more consistent marker for delineating the border of lamina II inner and III.

3.8.4.3 Dorsal Horn Areas are Not Affected by SNL & SNI

Peripheral nerve transection models did not show any significant change in dorsal horn areas, consistent with previous rhizotomy data. It is known that glial cells proliferate after nerve injury (Hajós et al., 1990), as well as an influx of immune cells, and since the dorsal root and thus primary afferent input remains intact, one might speculate that an

increase in dorsal horn volume may result. However, this has not been seen in either SNI or SNL models. It is unclear where the extra space for these cells comes from, but may indicate the dorsal horn in uninjured conditions contains the capacity to hold a greater density of cellular material without any significant shift in dorsal horn volume.

3.8.4.4 PSD95 and SynaptoPhysin Puncta are Not Lost 7 Days Post Injury

To directly compare peripheral nerve transection to dorsal root transection, the peripheral nerve injury models were assessed at 7 days post injury. This revealed no changes in puncta numbers across the dorsal horn, which likely reflects that primary afferent inputs remain intact after lesion to a peripheral nerve, and that these terminals do not degenerate, at least by 7 days post injury. This contrasts with rhizotomy, where a dramatic loss of primary afferent terminals is observed. The retention of primary afferent inputs 7 days post SNI and SNL may be driven by the retention of the dorsal root ganglion connection, and thus the continued supply of the central terminals with cellular signals, as well as a continued trophic signalling component to primary afferent terminals from the dorsal horn itself (Lin and Koleske, 2010). However, it should be noted that by 7 days post injury, a dramatic change in trophic support of DRG cells from the periphery will have taken place (Abe and Cavalli, 2008), but it appears this alteration is not sufficient to change the PSD95+ synaptic landscape of the dorsal horn by 7 days post injury.

3.8.4.5 PSD95 Puncta are Lost Specifically at 21 Days Post Injury in Lamina II Inner

An intriguing and consistent observation across both peripheral nerve transection paradigms is a reduction in PSD95 puncta specifically in lamina II inner by 21 days post injury. This observation is consistent with previous studies, which have observed a loss of synapses in lamina II following peripheral nerve injury (Bailey and Ribeiro-da Silva, 2006), as well

as electrophysiological evidence indicating a mean reduction in excitatory input to this lamina after nerve injury (Kohno et al., 2003). The specific loss observed in lamina II inner only occurs at later time points, with no change seen at 7 days post injury. One explanation for this loss may be a specific breaking of primary afferent synaptic contacts within this lamina of the dorsal horn, as suggested in the study by Bailey and Ribeiro-da Silva (2006). It is well known that the IB4+ primary afferent population extensively arborise within this lamina (Streit et al., 1985; Molliver et al., 1995), and so this class of primary afferent C fibre is a key candidate.

Interestingly, the loss of IB4 precedes the loss of PSD95 puncta in this lamina extensively (Molander et al., 1996; Bennett et al., 1998), and so the loss of IB4 is not a predictor of the loss of presumed primary afferent terminals. This instead likely reflects a reduction in the production of the glycoprotein which IB4 has affinity for early after peripheral nerve injury. Speculatively, this sequential loss of IB4 followed by PSD95 in the same region of the dorsal horn might indicate a progressive effect of the loss of trophic support to the IB4+ primary afferent population as a result of nerve injury. Why these neurons should be more sensitive to this loss, and why the slow degeneration of terminals is not clear, but it would suggest that peripheral trophic support is essential in maintaining IB4+ primary afferent central connections after nerve injury.

The eventual fate of these neurons after peripheral nerve injury is also of interest. Previous studies have given an ambiguous answer to the question of whether DRG cells are lost after peripheral nerve lesion (Lekan et al., 1997; Tandrup et al., 2000; Shi et al., 2001; McKay Hart et al., 2002), although the general consensus across different peripheral nerve lesions is a progressive loss of DRG neurons. However, these studies are hampered by the inability to quantify total DRG cell counts, and thus are limited to estimates derived from simple or stereological quantification. An intriguing open question is whether this

loss of synapses is the beginning of a withdrawal of the IB4+ primary afferents from the dorsal horn, and possibly their death within the DRG itself at later timepoints.

3.8.4.6 SynaptoPhysin Puncta and Advillin-eGFP are Not Lost 21 Days Post SNI

Concomitant with the loss of PSD95 in lamina II inner, studies of SNI tissue 21 days post injury revealed no changes in SynaptoPhysin puncta, nor Advillin-eGFP fluorescence intensity. The disparity of SynaptoPhysin+ puncta with the PSD95+ puncta may have one of a number of explanations. First, SynaptoPhysin is a general marker of presynaptic structures, which delineates both symmetric and asymmetric synapses. Thus, the loss seen in PSD95 puncta may be masked in the SynaptoPhysin data by the symmetric synapses these presynaptic structures contribute to. However, previous work has highlighted a loss of inhibitory interneuron presynaptic structures after peripheral nerve injury (Lorenzo et al., 2014), which contribute to the symmetric synapse population, and is inconsistent with this theory.

Secondly, the problem may be a technical issue with the use of SynaptoPhysin as a marker of synaptic contacts. SynaptoPhysin marks presynaptic structures, but it is not limited to presynaptic active zones, and instead marks vesicles throughout a much larger volume (reviewed in De Camilli et al., 2001). One issue arising from this is that one presynaptic structure may contain more than one active zone. Thus, several presynaptic active zones may become linked into one single structure due to a continuous link of SynaptoPhysin vesicles. Both of these situations would mean SynaptoPhysin puncta number would under-estimate the number of active zones within the tissue. Furthermore, a reduction in the number of active zones might not necessarily result in a reduction in the number of SynaptoPhysin puncta, since any which correspond to more than one

active zone may only reduce in size, and thus mask any loss in active zone number. This theory would, however, require the loss of presynaptic structures only from selective post-synaptic partners, which would be inconsistent with the previously proposed theory of a selective loss of IB4+ primary afferent neurons, at least at 21 days post injury.

Finally, a third explanation for the disparity in PSD95+ and SynaptoPhysin+ puncta may be that, whilst post-synaptic structures are lost after peripheral nerve injury, the pre-synaptic components remain. This idea seems most consistent with the evidence, since both SynaptoPhysin+ puncta and eGFP fluorescence intensity in Advillin-eGFP mice remain at endogenous levels 21 days post injury, suggesting no loss of presynaptic terminals or primary afferent axon loss. It is well known that the presynaptic structures such as synaptic vesicles are present at the earliest stages during the development of a new synapse (Ahmari et al., 2000; Ziv and Garner, 2004), and during degeneration of synaptic contacts, these may be the last components to be removed. Electron microscopic observations of the dorsal horn after peripheral nerve injury have revealed a phenomenon referred to as Transganglionic Degenerative Atrophy occurring at central terminals of FRAP+ (which is synonymous with the IB4+ sub-population of C fibres) in the substantia gelatinosa (lamina II) 10-14 days post injury, but a delayed loss of degenerating terminals between 30-40 days (Csillik and Knyihár-Csillik, 1981). This may reflect an early loss of PSD95+ post-synaptic structures, but the retainment of SynaptoPhysin+ presynaptic structures at day 21. This theory would predict a loss of SynaptoPhysin+ puncta at 30-40 days post injury. The extent of the loss of primary afferent axons was not fully elucidated in the Csillik and Knyihár-Csillik (1981) study, thus the consequences to primary afferent axons 30-40 day post injury would be of interest, as their retraction from the dorsal horn may have important implications for the eventual fate of the IB4+ population of C fibre primary afferents at later time points.

Some previous studies have looked at SynaptoPhysin immunohistochemistry in the dorsal horn after peripheral nerve lesions, where some studies have shown an increase in SynaptoPhysin after nerve injury (Chou et al., 2002; Lin et al., 2011), and one study shows no change in SynaptoPhysin (Sun et al., 2006). It is hard to reconcile the increase in SynaptoPhysin with the evidence presented here and the previous evidence showing a reduction of PSD95 puncta in lamina II inner, however, Sun et al. (2006) suggest the SynaptoPhysin may not mark all pre-synaptic sites, which could explain the disparity with the post synaptic marker PSD95. Furthermore, the two studies which show an increase in SynaptoPhysin after nerve lesion (Chou et al., 2002; Lin et al., 2011) have used models that constrict but do not transect the nerve, and looked at different time points. Interestingly, Chou et al. (2002) detected only a transient increase in SynaptoPhysin at 14 days, which returned to baseline by 21 days, consistent with the data presented here. Furthermore, it may be the case that increases in one sub-population of synapses, as has been observed with constriction-type injuries (Chou et al., 2002; Lin et al., 2011), are masking the possible reduction a separate population, which are reduced after nerve injury and express PSD95.

3.9 Conclusion

This Chapter has applied the methodologies from Chapter 2 to the dorsal horn in a number of different conditions. It has revealed a unique distribution pattern for both SynaptoPhysin and PSD95 puncta which has not been previously described. Furthermore, it has revealed a selective loss in PSD95 puncta in two separate models of peripheral nerve injury specifically within lamina II inner at later time points (21 days post injury). No loss of SynaptoPhysin+ puncta or Advillin-eGFP fluorescence intensity (indicating no loss of primary afferent axons) were detected. What components constitute this loss and

speculation on mechanisms have been given in the discussion. The next Chapter aims to test the hypothesis that microglia are implicated in driving the loss of synapses from lamina II inner that has been observed 21 days post peripheral nerve lesion.

Chapter 4

Experiments Exploring the Role of Microglia in Synapse Loss following Peripheral Nerve Injury

4.1 Introduction

An interesting development in the dorsal horn following peripheral nerve lesion is the reaction of microglial cells, which are recruited, proliferate and begin to alter the cellular environment within central territories of injured afferents following a lesion to the peripheral nerve (Tsuda et al., 2005; Beggs and Salter, 2013; Clark and Malcangio, 2014). A number of studies have developed the idea that microglia may be involved in modulating and sculpting neuronal circuits (Kettenmann et al., 2013): microglial stimulation can cause synaptic enhancement (Zhou et al., 2011; Clark et al., 2015), and reverse the anion gradient via BDNF signalling (Coull et al., 2005) in the dorsal horn. Microglia have been shown to contact synaptic elements in the CNS (Tremblay et al., 2010), and these cells have been recently demonstrated to remove synapses during development (Tremblay

et al., 2010; Schafer et al., 2012).

Given the suggestions that microglia are actively involved in modulating and sculpting synaptic circuits, the question emerged whether these cells may be involved in the synaptic loss observed after peripheral nerve injury in the dorsal horn. In order to explore this possibility, microglial cells were analysed after peripheral nerve injury, utilising and developing the automated stereological algorithms previously developed for use on microglial cell quantification.

To attempt to intervene with the microglial response after peripheral nerve injury, the pharmacological agent minocycline, well known for its ability to reverse a number of key molecular changes in microglia as well as the behavioural hypersensitivity seen after peripheral nerve injury (Raghavendra et al., 2003; Ledeboer et al., 2005; Mika et al., 2007; Mika, 2008), was used. Previous reports have suggested minocycline needs to be administered either prior to nerve injury, or at least during the early stages, to show efficacy (Raghavendra et al., 2003; Mei et al., 2011). Thus, chronic administration up to 21 days was performed by oral administration, as described in Section 4.2 : Methods.

Minocycline administration was used to test the idea that the microglial response may be stripping synapses after peripheral nerve injury. The effects on behavioural hypersensitivity, microglial responses, and synaptic loss in the dorsal horn were explored in animals treated with minocycline after peripheral nerve injury.

4.2 Methods

4.2.1 Animals

All work carried out conformed to UK Home Office legislation (Scientific Procedures Act 1986). Mice used in this study were on a FVB/N background. All animals were

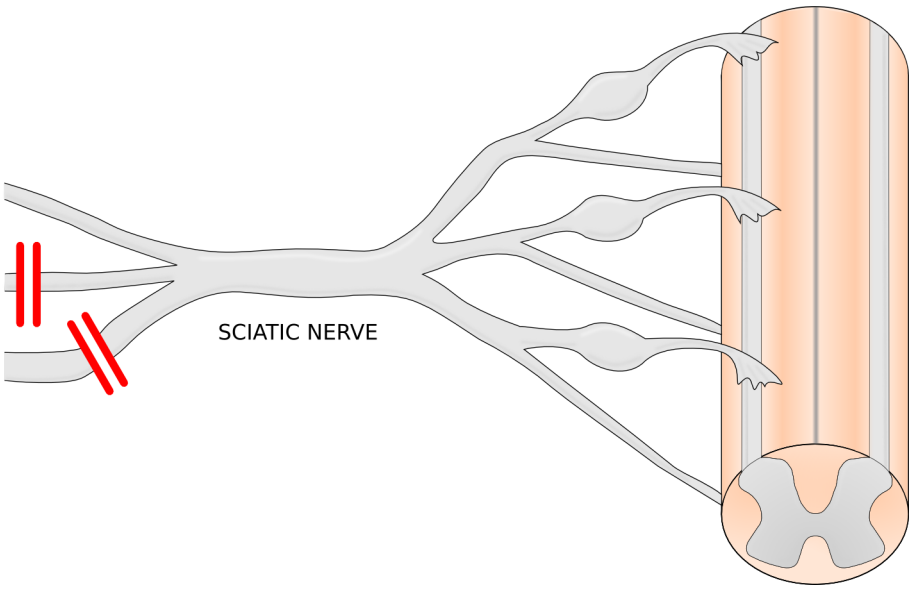

Figure 4.1: **The spared nerve injury model.** Two branches of the Sciatic nerve (the Tibial and Common Peroneal nerves) are ligated and transected, leaving the third branch (Sural nerve) intact.

young adults (12-16weeks) throughout the study. Mice were housed in groups in standard environmental conditions (12 h light/dark cycle) with *ad libitum* access to food and water.

4.2.2 Spared nerve injury surgery

The spared nerve injury (SNI) model of peripheral nerve injury was used, as previously described (Decosterd and Woolf, 2000; Shields et al., 2003). Briefly, mice were anaesthetised using isoflurane. A unilateral incision from the sciatic notch was made laterally to expose the biceps femoris muscle, which was bluntly dissected with scissors to expose the sciatic nerve and its three distal branches: the common peroneal, tibial and sural nerves (Figure 4.1). The tibial and common peroneal nerves were tightly ligated using a 3-0 prolene suture, and transected distal to the ligation. A SHAM surgery was performed by exposing the sciatic nerve, but not performing a ligation or transection of the common peroneal or tibial nerves. The wound was sutured, and the animals allowed to recover in a clean and warm cage. Behavioural assessment to determine mechanical paw withdrawal thresholds was performed as described below.

4.2.3 Mechanical paw withdrawal threshold behaviour

Behavioural assessment of 50% paw withdrawal thresholds was determined with the "up-down" method, as previous described (Chaplan et al., 1994). Briefly, animals were placed into plastic boxes with an exposed and raised wire floor, to allow access to the plantar surface of the hind paws. After a period of acclimatisation (between 15-30 minutes, and until cage exploration had ceased), von Frey hairs that deliver calibrated forces were applied to the ipsilateral plantar paw on the lateral side (since this is region is innervated by the spared sural nerve, Decosterd and Woolf (2000)), and the 50% paw withdrawal threshold was determined for each animal. This was achieved by applying consecutive von Frey hairs, and moving up the series with no response, or down the series if a positive response was noted. A positive response was assessed as a withdrawal from the test stimulus, after an application time of 3 seconds. The 50% paw withdrawal threshold was then calculated as previously described (Chaplan et al., 1994). Von Frey testing was performed blind throughout, including two baseline sessions prior to surgery, and followed up with testing at 7, 14 and 20 days post SNL surgery.

4.2.4 Drug Administration

Administration of minocycline (0.3mg/mL) was administered via the drinking water to the minocycline-treated group following SNI surgery. The control group received regular drinking water. This route of administration was chosen for several reasons: daily i.p. injections is labour-intensive, causes undue distress, and had previously caused some irritation in a pilot study to the mouse peritoneum; the half-life of minocycline is approximately 3 hours in rodent (Colovic and Caccia, 2003), compared to 18-21 hours in human (Agwuh and MacGowan, 2006), which would result in daily dosing regimens causing large fluctuations in plasma minocycline concentrations; and oral administration of

minocycline has a high bioavailability (Agwuh and MacGowan, 2006; Tynan et al., 2015) and maintains a relatively consistent plasma concentration over long periods of time, even when taking into account natural variations in mouse water consumption (Possidente and Birnbaum, 1979; Possidente et al., 1980; Minematsu et al., 1991), relative to a single daily i.p. dose.

4.2.5 Perfusion Dissection & Tissue Processing

Naive animals and animals at Seven and 21 days post SNI surgery, were perfused as previously described (see Section 2.2.1). The tissue was processed for PSD95 and SynaptoPhysin synaptic puncta as previously described (see Section 2.2). Tissue processed for microglial staining was processed in the same manner as for synaptic puncta analysis, except some naive tissue sections were taken at $60\mu m$ thickness to visualise complete microglial nuclei in the axial plane.

4.2.6 Histology & Imaging

Tissue was stained, imaged and analysed for PSD95 and SynaptoPhysin synaptic puncta as previously described (see Sections 2.2 & 3.3).

Microglia were visualised with an antibody targeting ionized calcium binding adaptor molecule 1 (Iba1, 019-19741, Wako), a protein expressed specifically in microglia in the CNS (Ito et al., 1998). The standard histological procedure progressed as follows: cryostat-sectioned and air-dried sections (see 2.2) were re-hydrated in PBS for 10 minutes at room temperature, tissue was incubated in 50% ethanol for 30 minutes to enhance antibody penetration of the tissue (Llewellyn-Smith and Minson, 1992), and tissue was incubated in a mixture of Iba1 antibody (1:1000, rabbit polyclonal, Wako), and IB4 conjugated to biotin (1:100, Sigma, L2140) in PSB containing 0.3% Triton-X100 and 0.1%

sodium Azide (PBSTx) for 3 days at room temperature. Sections were washed 4 x 5 minutes in PBSTx, and incubated in a second mixture of Cy-3 anti-rabbit (1:500; 711-166-152, Jackson ImmunoResearch), ExtrAvidin-FITC (1:500; E2761, Sigma) and DAPI (1:50,000; D8417, Sigma) in PBSTx for 1 day at room temperature. Sections were washed 4 x 5 minutes in PBSTx, mounted in VectaShield (H-1000, VectorLabs), and coverslipped (0.17±0.01mm; Hecht-Assistent, 1014).

To enhance Iba1 labelling within the dorsal horn, proteinase K antigen retrieval was used, which comprised addition of proteinase K digestion prior to ethanol treatment, consisting of a 10 minutes incubation in proteinase K diluted to $4\mu g/mL$ in PBSTx at room temperature (see 4.3.1).

Imaging of microglia was performed on a LSM 700 confocal microscope, using the x20 Plan-Apochromat (NA 0.8). Z Stacks were taken across the ipsilateral and contralateral dorsal horns to allow assessment of both sides in the same image. Z slice thickness was set to $2\mu m$, with a stack thickness of $8\mu m$.

4.2.7 Analysis of Microglia

The StereoMate algorithms previously outlined were used for analysis of microglial cell number (see Chapter 2). Results relating to this methodology development are presented in this Chapter (see Section 4.3.1). All image processing was performed in ImageJ. The segmentation of DAPI and Iba1 images was performed as described previously (Section 2.3.2.4). The boolean AND function was performed in the ImageJ plugin "Image Calculator" (available in the standard distribution of ImageJ, which isolates pixels segmented only in both images presented). ROI delineation and object measurement was performed as described in Chapter 2, except where indicated below (Section 4.3.1).

Manual quantification was compared to the automated protocol developed in this

Chapter. This was achieved by overlaying the segmented and boolean AND-treated image with the original DAPI and Iba1 images, and manually verifying whether each object was either a true microglial nucleus, or aberrant co-localisation of Iba1+ processes and other DAPI+ nuclei. This process was used to divide all objects obtained from the segmentation and boolean AND function of Iba1+ and DAPI+ images into either microglial nuclei, or to aberrant co-localisation. The differences in size between these two object populations was explored, as highlighted below, in order to determine an automated method for microglial cell quantification.

4.3 Microglia are activated following SNI model

4.3.1 Automated Microglial Quantification

To apply the automated stereological algorithms to microglial cell number, initial work focussed on deriving sufficient signal:noise from Iba1 staining in dorsal horn tissue. In order to improve Iba1 labelling, a number of different antigen retrieval methods were tested, including Proteinase K digestion. Proteinase K treatment was found to improve Iba1 signal intensity (Figure 4.2). Utilising this antigen retrieval method, accurate binary representations of both nuclear and microglial staining was achieved (Figure 4.3A-C). In order to isolate individual cells for quantification, the boolean AND function was applied to all pixels of segmented DAPI and Iba1 images, to produce a new image which retained pixels only segmented in both images (Figure 4.3D & E). This function produced a consistent representation of microglial cell bodies, which could then be quantified.

To assess the isolated microglial cell bodies in a manner consistent with stereological principles, the ROI Di-Sector must be applied. The ROIs under analysis in these images are fully delineated in both the medio-lateral and dorso-ventral planes; however, due to

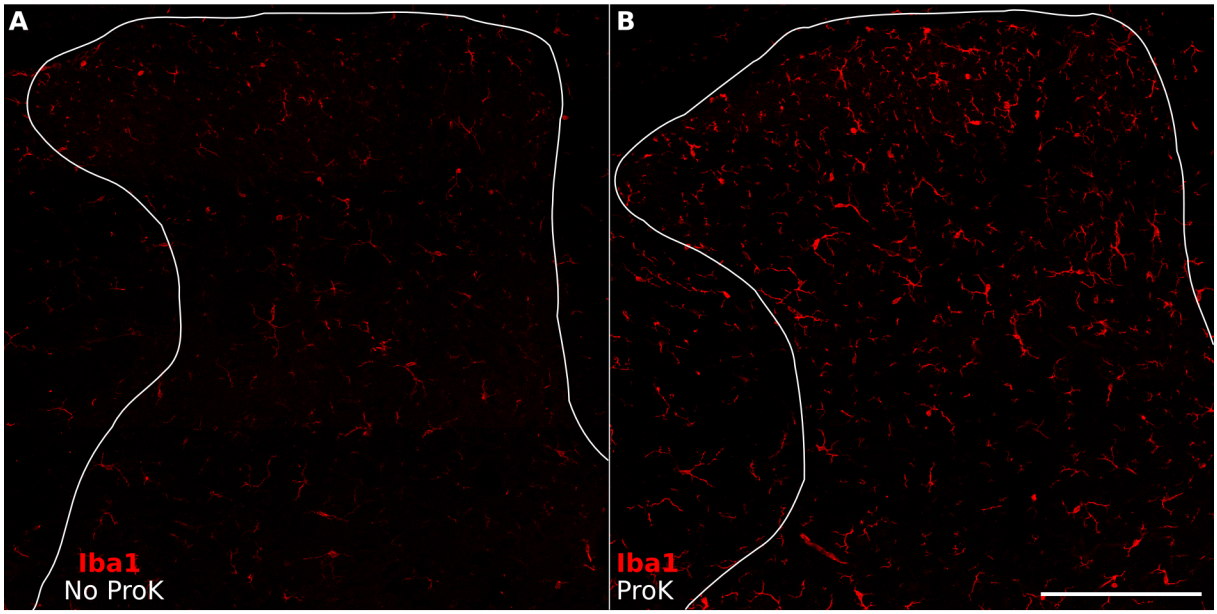

Figure 4.2: **Proteinase K treatment significantly improves Iba1 signal intensity. A:** Iba1 fluorescence without Proteinase K treatment. **B:** Iba1 fluorescence with Proteinase K treatment. Scale bar: $200\mu m$.

the physical sectioning of the dorsal horn in the transverse orientation, the dorsal horn is physically sampled in the rostro-caudal plane. Thus, a Rejection Boundary-Exclusion Zone pair must be set up in this plane (Figure 4.4A).

The microglial nuclei isolated via the AND function occupy a large proportion of the total depth of the image. This is because the image depth is limited due to the original section thickness, and shrinkage during processing. When implementing the original ROI DiSector as described in Chapter 2, the synaptic puncta quantified are reconstructed in their entirety, which allows any unique and consistent part of the particles to be used to determine whether the objects lies within the counting region, on a Rejection Boundary, or in an Exclusion Zone. With fully reconstructed objects such as synaptic puncta, the pixel on the object edge facing any rejection boundary orientations was used to reduce the puncta to a single point in each plane, and then this point was used to determine its inclusion or exclusion via the ROI DiSector rules.

It is not possible to use this methodology with the present imaging problem, since the nuclei are so large and the number of optical sections required to capture entire nuclei

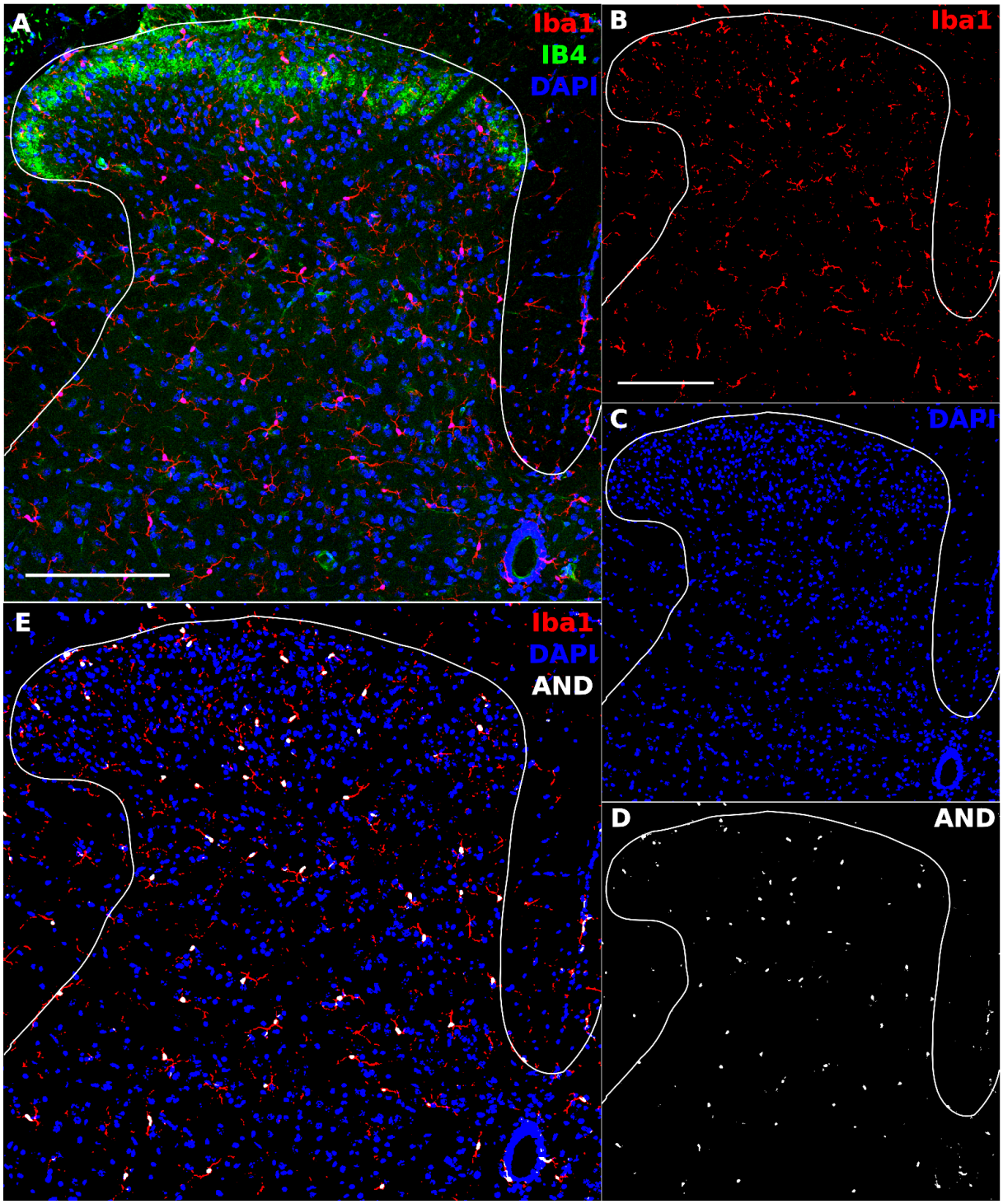

Figure 4.3: **Segmentation and isolation of microglial nuclei. A:** Original confocal image revealing Iba1+ microglial cells, DAPI+ nuclei and IB4 labelling in the superficial dorsal horn. **B:** Segmentation of Iba1+ cell bodies using a 3x3 median filter following by the OTSU method. **C:** Segmentation of DAPI+ nuclei using a 3x3 median filter following by the OTSU method. **D:** Isolation of microglial-specific nuclei by retaining pixels only thresholded in both DAPI and Iba1 segmented images (AND boolean function). **E:** Overlay of the AND boolean image with the DAPI and Iba1 segmented images, which shows a good correspondence between large microglial nuclei and microglial cell bodies. Scale bars: $200\mu m$.

so small, that few, if any, nuclei are completely reconstructed (Figure 4.4B). Thus, to improve the number of nuclei to be included in quantification, but maintain a stereological methodology of quantification, a separate method, which still identifies a unique point in the quantified objects, has been used.

Nuclei in most cells, including microglia, form a spherical or oval shape. Instead of isolating a single pixel to quantify the nucleus at the edge of the object volume (as is used for synaptic quantification), the central optical slice of the nucleus can be used. This is because the central optical slice can be uniquely identified in an automated fashion as the slice with the largest number of pixels. Thus, this new rule will now count nuclei if and only if the central optical slice of the nucleus is present *within* the image stack. This translates to testing whether any given nucleus has its thickest slice within the image stack, which implies that the thickest slice is not in the first or last slice.

This can be calculated for each nucleus by comparing the thickness of the nucleus throughout the stack; if the thickest slice is present on the first or last sections of the image, the nucleus is rejected, otherwise its central optical slice resides within the image, and the nucleus is accepted (Figure 4.4B). This method can be used to correct for objects in which it is difficult to reconstruct their entire structure, and continues to ensure an unbiased count of 3D object number is attained.

This method relies on the assumption that isolated microglial nuclei are oval in shape, and that the largest optical slice corresponds to the central portion of the nucleus. This was tested on spinal cord slices taken at $60\mu m$ and stained for Iba1 and DAPI, as described in Section 4.2.6. Three separate experiments were conducted to test the reliability of these results. The Iba1 and DAPI images were thresholded and the boolean AND function applied as previous described. All objects contained completely within the image stack, and which clearly co-localised within an Iba1+ & DAPI+ nucleus, were isolated, and their

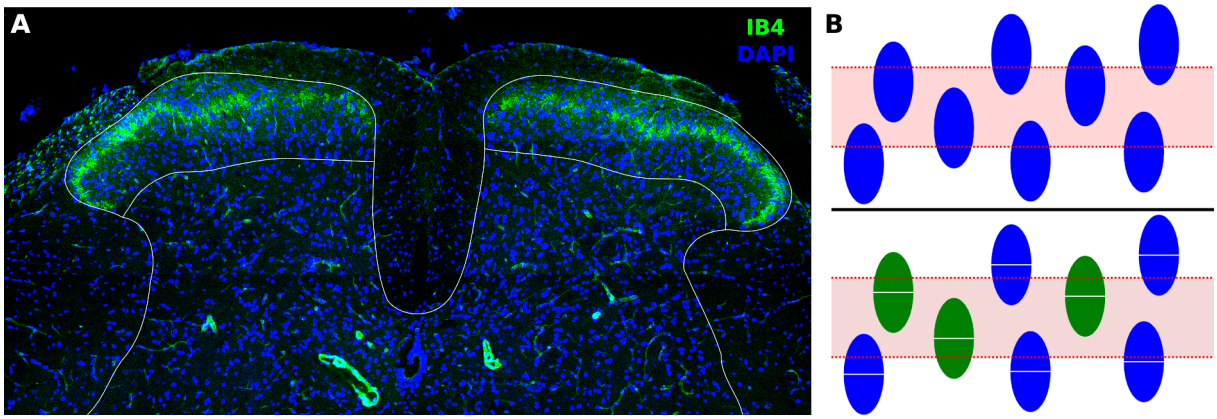

Figure 4.4: **ROI Di-Sector and Stereological Correction for Iba1 quantification. A:** Left and right superficial dorsal horn ROIs isolated, indicating the full delineation of the ROIs in the mediolateral (left-right) and dorsoventral (up-down) planes. Superficial dorsal horn was defined as a depth equal to twice the depth of IB4 from the dorsal surface of the dorsal horn. Due to physical sectioning, the dorsal horn is not fully delineated in the rostro-caudal plane,and a rejection boundary-exclusion zone pair is required in this dimension. **B:** Demonstration of the stereological correction method. Nuclei typically display an oval shape, with a central optical slice containing the largest number of pixels (top). By using this central slice to identify an individual cell (bottom), quantification can be performed consistent with stereological principles (green nuclei).

shape in the axial plane as well as the location of the optical slice with the largest number of pixels was determined.

Analysing 353 isolated Iba1+ nuclei across three separate experiments (mean: 118±17) revealed axial shapes consistent with an oval shape, and showed the average location of the largest optical slice to be at 51.6±1.0% through the object stack (n=3 experiments, Figure 4.5). These results suggest that Iba1+ cell nuclei isolated from image stacks display an oval shape and consistent with this, the slice with the maximum pixel count is, on average, at the centre of the isolated nucleus.

After manually isolating microglial nuclei described above, the next aim was to see if it was possible to automatically isolate these microglial nuclei from aberrant co-localisation between Iba1+ processes and DAPI+ nuclei from other cells. The basis for an automated separation was that microglial nuclei would correspond to a separate population of large objects, whereas aberrant co-localisation would produce a population of small objects, and that these populations could be separated with a size filter.

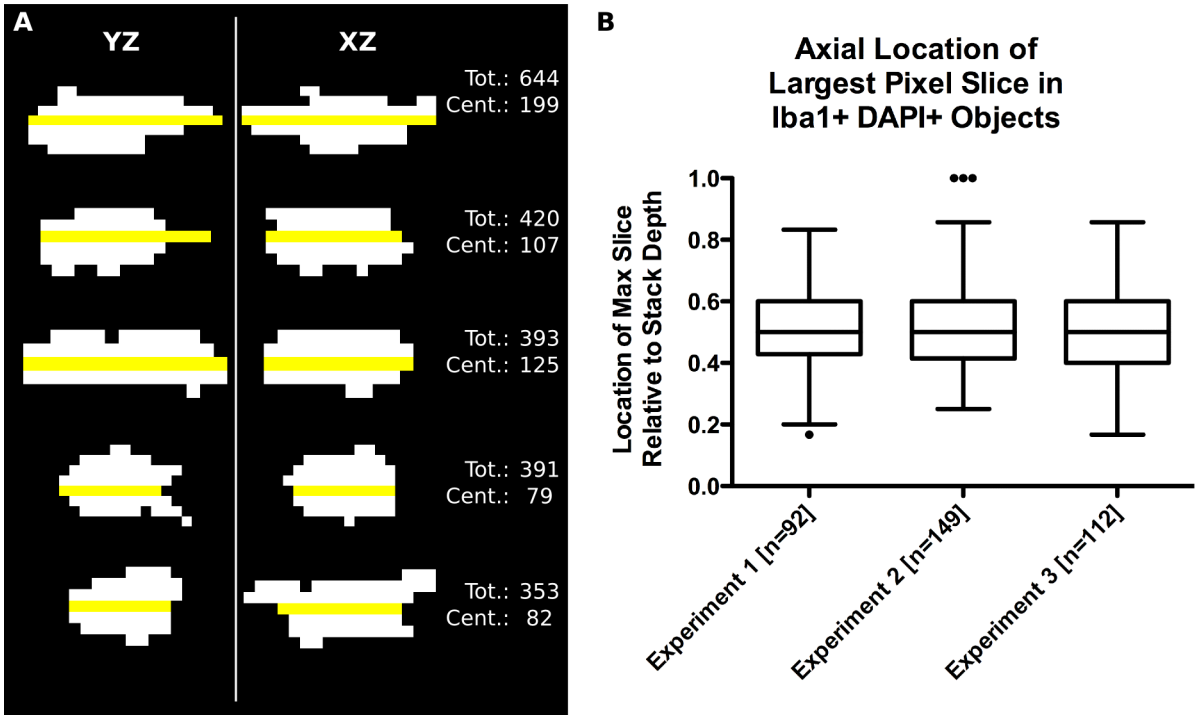

Figure 4.5: **Isolated microglial nuclei display oval-like shape characteristics. A:** Five examples of axial views of nuclei isolated from 60μm image stacks. The yellow line indicates the slice with the maximum number of pixels. Tot. and Cent. indicate the pixel numbers of the total object, and the maximum slice, respectively. **B:** Location of the slice with the maximum number of pixels relative to the axial length of the isolated microglial nuclei (n=353 across three experiments). For all three experiments, an average around 0.5 was found. Box and whiskers plot made with the Tukey method.

To investigate this possibility, every fully reconstructed Iba1+ and DAPI+ object which was isolated from the $60\mu m$ sections above were plotted onto a histogram based on size. Pooling all three independent experiments revealed a bi-modal distribution; with one small population of objects, and a second population of larger objects (Figure 4.6). These two populations seemed to be divided at approximately 200 pixels. To determine whether this bi-modal distribution consisted of a population of aberrant co-localisation and a population microglial nuclei, all objects were manually sorted by visual inspection into either aberrant co-localisation, or true microglial nuclear labelling. This analysis revealed that the bi-modal distribution does reflect these two populations, and that these two populations are separable based on size (Figure 4.7A & B).

Using 200 pixels as a divider between aberrant co-localisation and true microglial nuclear labelling showed high reliability, with a sensitivity of 94.5% and a specificity of 99.9% (pooled across three independent experiments, Figure 4.7C). Visual inspection of thresholded objects overlaid with the original Iba1-DAPI images confirms that application of a high-pass filter of 200 pixels to the AND function image allows automated quantification of microglial cell numbers of fully reconstructed microglial nuclei (Figure 4.8).

In order to adapt this automated methodology to microglial nuclei which are only partially reconstructed in thin tissue sections, first the pixel counts of the largest optical slice through verified microglial nuclei must be determined, and these numbers need to be separable from the largest optical slice through aberrant co-localised objects. Using the manually sorted datasets produced above, measures of pixel counts for the largest optical slices of all objects were determined, and manually identified microglial nuclei and aberrant co-localisation pixel counts were plotted separately onto a histogram. As can be seen from Figure 4.9, using the pixel count for only the largest optical slice of objects produces a similar delineation between microglial nuclei and aberrant colocalisation as

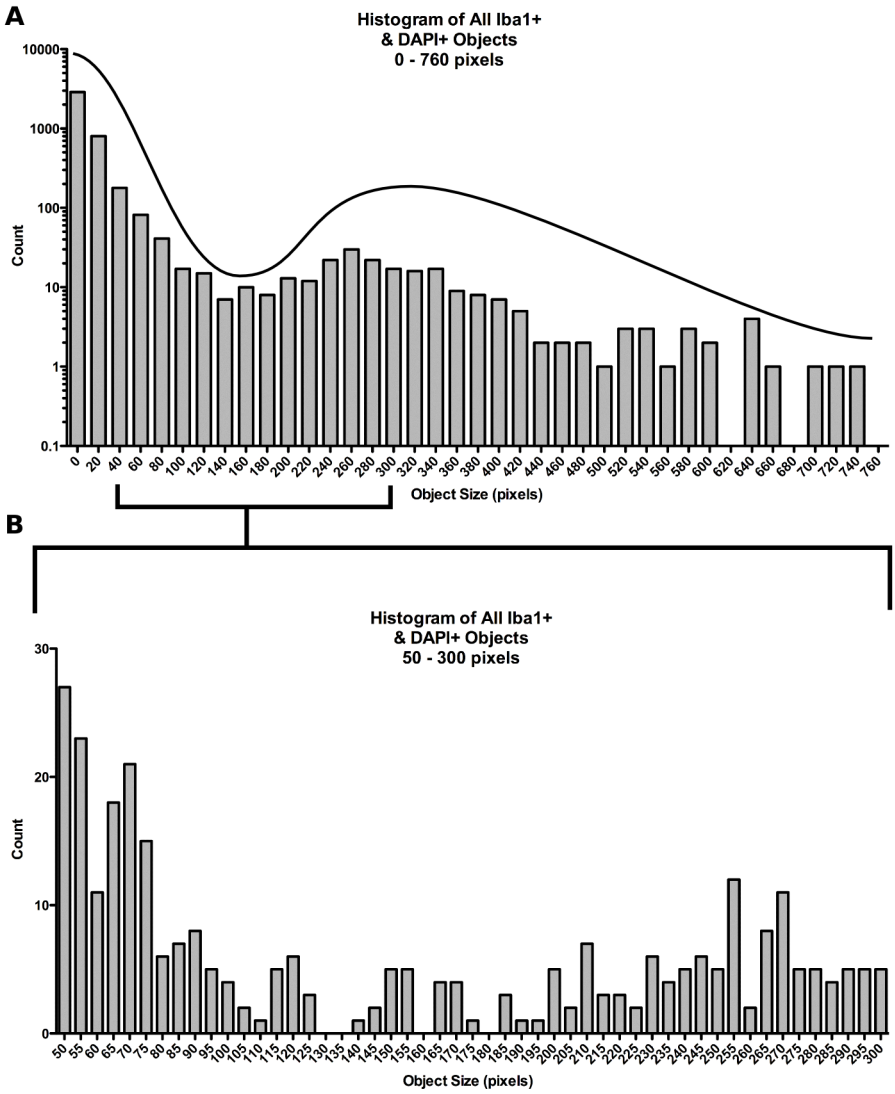

Figure 4.6: **Size histogram of isolated Iba1+ & DAPI+ objects reveals a bimodal distribution. A:** Semi-log plot of entire range of size histogram corresponding to all isolated objects from $60\mu m$ sections. The plot appears to follow a bimodal distribution. **B:** A linear plot of a section of the histogram in A with a finer bin resolution reveals a drop-off in observations at around 200 pixels in size, which then increases above 200 pixels.

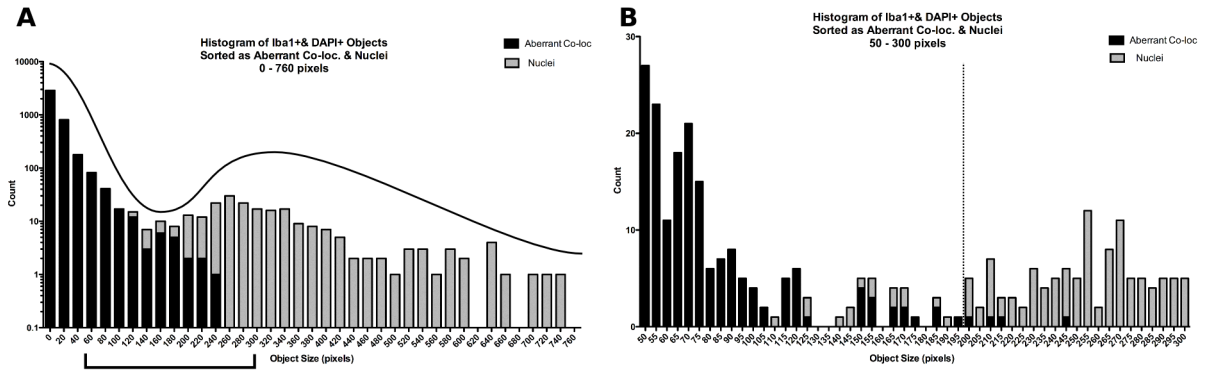

C

		GOLD STANDARD Manual		
		POSITIVE		NEGATIVE
AUTOMATED	POSITIVE	312		4
	NEGATIVE	18		5811
	TPR (Sensitivity)	0.945	False Pos. Rate	0.001
	False Neg. Rate	0.055	TNR (Specificity)	0.999

Figure 4.7: **Size histogram of sorted Iba1+ & DAPI+ objects reveals a split between nuclei and aberrant co-localisation. A:** Semi-log plot of entire range of size histogram, highlighted aberrant co-localisation and identified microglial nuclei. **B:** A linear plot of a section of the histogram in A shows a good delineation between aberrant co-localised objects and microglial nuclei. **C:** Contingency table which has been used to calculate the sensitivity, specificity, and false negative & false positive rates for the Automated method (using 200 pixels as a high-pass filter) to the manually identification of microglial nuclei. Note the high level of sensitivity and specificity demonstrated.

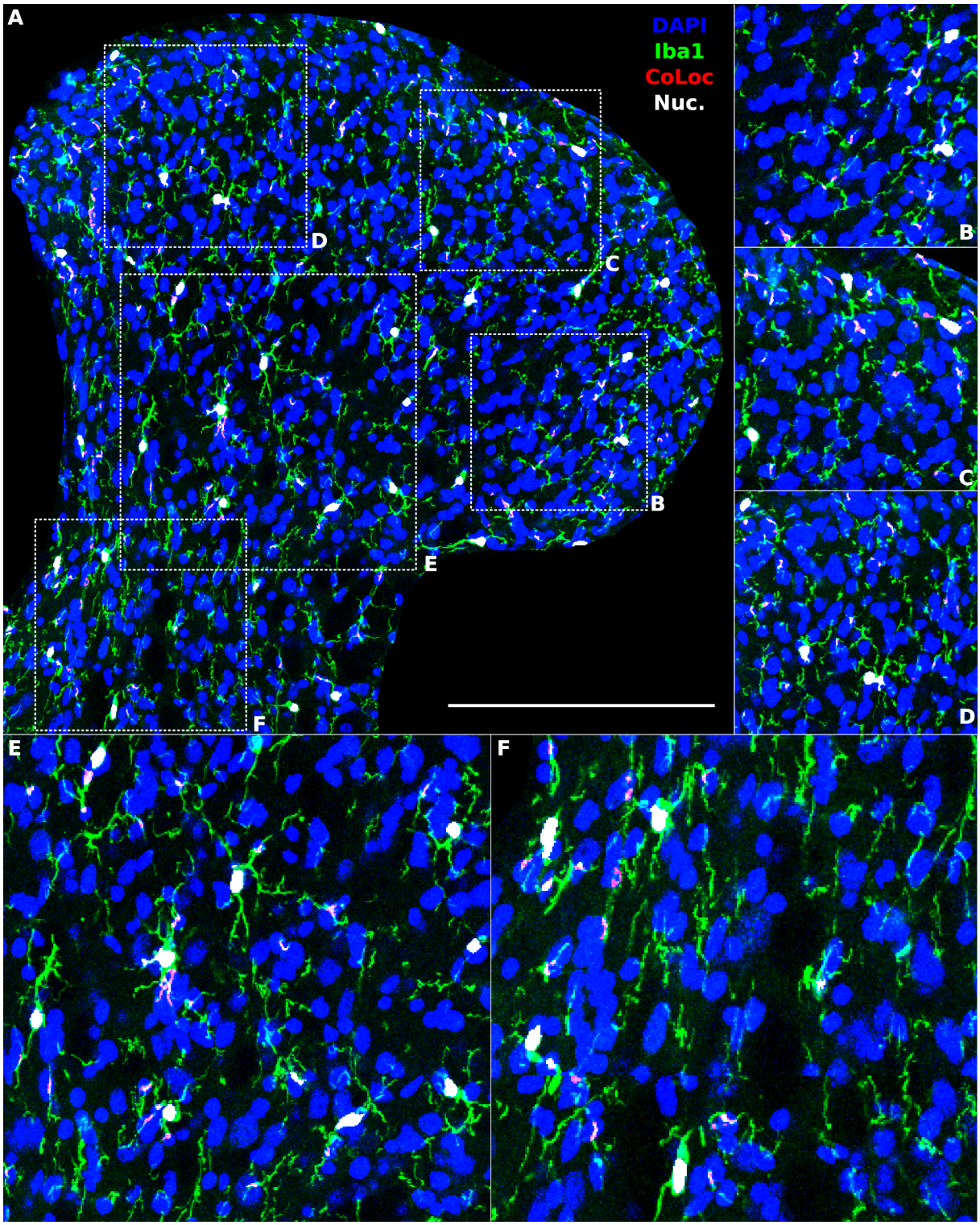

Figure 4.8: **Dorsal horn image projection of DAPI, Iba1 and thresholded objects indicates a reliable sorting of microglial nuclei based on size. A:** A maximum intensity projection of 12μm thick section of a dorsal horn, showing both the DAPI and Iba1 channels in blue and green respectively. Overlaid onto this image are objects which meet the criteria for microglial nuclei (white), and objects which were rejected and thus correspond to aberrant co-localisation (red). **B:** Magnification of highlighted region in A. **C:** Magnification of highlighted region in A. **D:** Magnification of highlighted region in A. **E:** Magnification of highlighted region in A. Scale bar: 200μm. CoLoc, co-localisation; Nuc., nucleus.

seen previously for the reconstruction of complete nuclei. Using 60 pixels as a divider between the maximum optical slice size of microglial nuclei and aberrant colocalisation showed reliable results, with a sensitivity of 95.5%, and a specificity of 99.8% (Figure 4.9C, pooled from three independent experiments).

These results reveal a method for automated quantification of microglial cell numbers within thin sections of the dorsal horn. First, dorsal horn sections are treated for Proteinase K as an antigen retrieval method. Next, the sections are stained and imaged for both Iba1 and DAPI as outlined in Section 4.2.6. These images are thresholded and colocalisation is isolated with the AND function in the ImageJ plugin Image Calculator (see Section 4.2.7). The objects are filtered first by whether the slice with the maximum number of pixels resides within the image stack (i.e that the slice with the maximum number of pixels is not in the first or last slice), and next by whether this maximum slice has 60 or more pixels (a high-pass filter). Finally, the objects remaining after filtering are quantified in ROIs which delineate the superficial dorsal horn.

This method circumvents the problems with stereological analysis on optical slices of thin tissue sections by utilising the central optical slice (which can be determined as the slice with the maximum number of pixels) as the uniquely identifying feature of the microglial nuclei. This central optical slice is also significantly larger than the largest slice from any aberrant co-localised objects, making it an ideal method for filtering true microglial cells from aberrant co-localised objects. This method is consistent with stereological methods, which means all objects are quantified in an unbiased fashion. Thus, cells of different size, shape and orientation all have the same opportunity to be quantified using this methodology, unlike methods which quantify 2D image projections of cell bodies (where, for example, larger cells have an increased chance of being counted). Importantly, this method allows supervised automated quantification of microglia, vastly

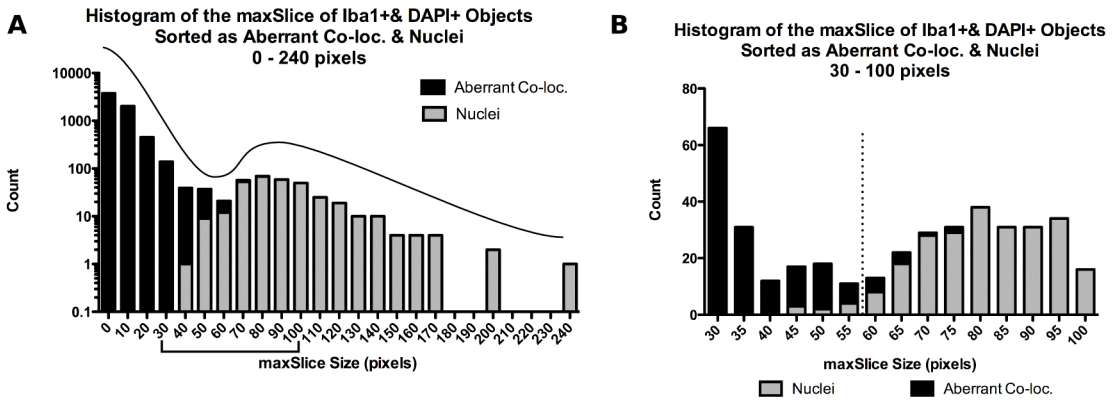

C

GOLD STANDARD

Manual

AUTOMATED	POSITIVE	NEGATIVE
POSITIVE	317	11
NEGATIVE	14	6444

TPR (Sensitivity)	**0.958**	False Pos. Rate	**0.002**
False Neg. Rate	**0.042**	TNR (Specificity)	**0.998**

Figure 4.9: **Size histogram of maximum slice pixel count of sorted Iba1+ & DAPI+ objects reveals a split between nuclei and aberrant co-localisation. A:** Semi-log plot of entire range of maximum slice size histogram, highlighted aberrant co-localisation and identified microglial nuclei. **B:** A linear plot of a section of the histogram in A shows a good delineation between the maximum slice size of aberrant co-localised objects and microglial nuclei. **C:** Contingency table which has been used to calculate the sensitivity, specificity, and false negative & false positive rates for the Automated method (using 200 pixels as a high-pass filter) to the manually identification of microglial nuclei. Note the high level of sensitivity and specificity demonstrated.

improving the speed of data processing and analysis.

Rejecting nuclei which do not have their maximum slice inside the image stack is an important component of this methodology, because otherwise application of the high-pass filter may reject not just aberrant co-localisation between nuclei and microglial processes, but also *bona fide* microglial nuclei, which are only partially within the image stack. By ensuring the central optical slice of a nucleus is in the image stack as an inclusion criteria, this method ensures that nuclei to be quantified are always larger than any aberrant co-localisation of Iba1+ processes with other DAPI+ nuclei. This method also defines the volume in which these microglia are quantified (which is the depth of the image, minus the first and last slices), which can be used to calculate microglial density within the superficial dorsal horn.

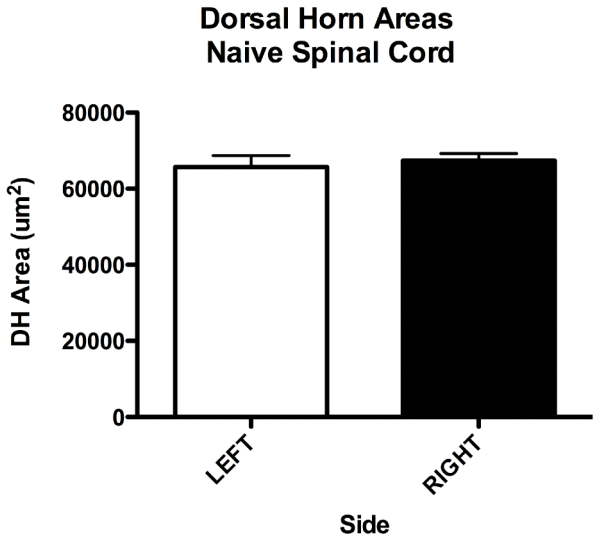

Figure 4.10: **Naive Superficial Dorsal Horn Areas display similar values.** Quantification of Left and Right superficial dorsal horn areas show no significant differences (Paired student's t-test, n=4; p>0.05).

4.3.2 Microglial Counts within the Superficial Dorsal Horn

In order to test the above workflow, microglial counts were obtained for the left and right dorsal horn in naive mice. Superficial dorsal horn ROIs were isolated as shown in Figure 4.4. As can be seen in Figures 4.10 & 4.11, the superficial dorsal horn areas & microglial counts for both left and right superficial dorsal horn sections are not significantly different from one another, respectively. These results suggest that a consistent estimate of microglial number is obtained with this method.

4.3.3 Microglial cells proliferate in the Superficial Dorsal Horn following Peripheral Nerve Injury

Quantification of microglia at 7 and 21 days post SNI surgery was performed on the superficial dorsal horn, in ROIs delineating the contralateral superficial dorsal horn, as well as injured and adjacent uninjured regions of the ipsilateral superficial dorsal horn. The injured and adjacent uninjured regions were identified by the absence and and presence,

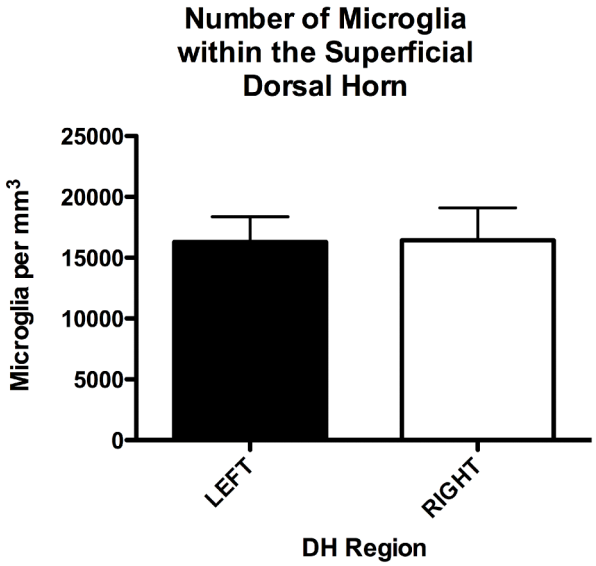

Figure 4.11: **Microglial density in the superficial dorsal horn display similar values.** Iba1 Quantification in Left and Right superficial dorsal horn show no significant differences (Paired student's t-test, n=4; $p>0.05$).

respectively, of IB4 binding. The adjacent uninjured region was defined as a region that started where IB4 binding began to return to the dorsal horn, and ended approximately 200um from this point laterally (see Figure 4.12). In order to ensure cell density measures are reflective of total cell numbers in the superficial dorsal horn, dorsal horn areas were measured as previously described (see Section 2.3.3.3). Superficial dorsal horn areas showed similar results in both 7 and 21 day post SNI, and were comparable to SHAM-treated animals (Figure 4.13).

Microglial numbers in these three defined regions are shown in Figure 4.14. As can be seen, microglial numbers are strongly upregulated in both the injured and adjacent uninjured regions at 7 days post SNI. By 21 days, this increase is still apparent, but is reduced. This data fits with dorsal horn images of Iba1 labelling at 7 and 21 days post SNI injury (Figure 4.15), and fits well with previous observations of microglial proliferation following many different peripheral nerve injury models (Narita et al., 2006; Beggs and Salter, 2007; Vega-Avelaira et al., 2007). An interesting observation is the up-regulation of microglial numbers in adjacent uninjured regions, which has been previously documented

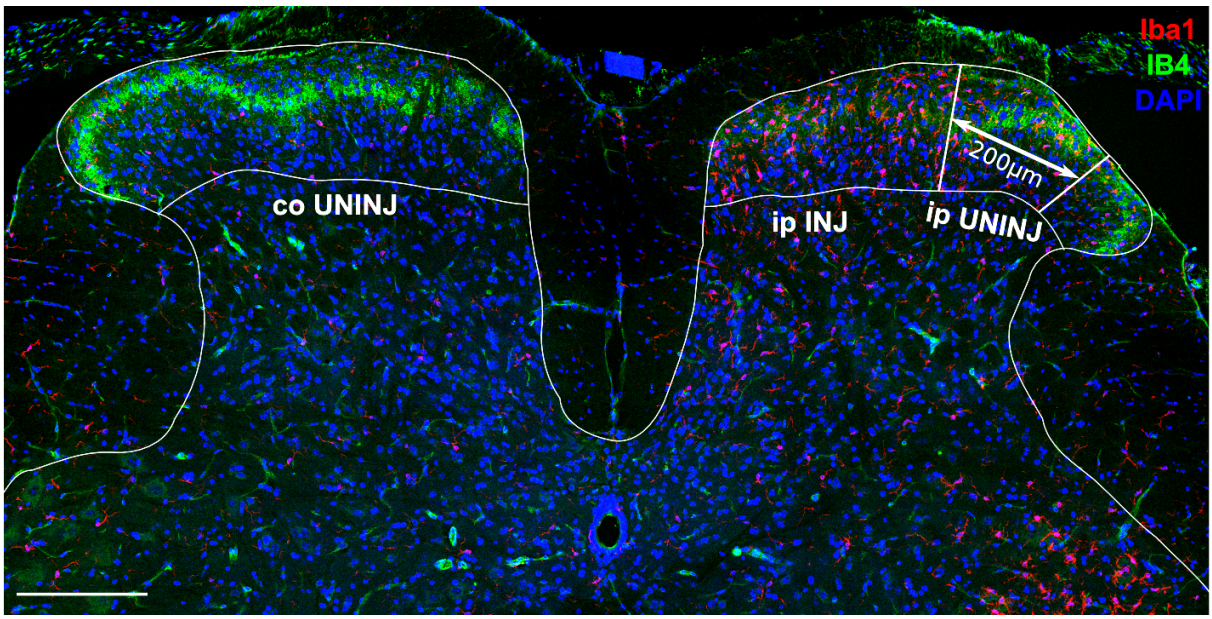

Figure 4.12: **ROI delineation on SNI injured DH for microglial quantification.** Both ipsilateral and contralateral dorsal horns were delineated as previously described. The ipsilateral dorsal horn was further divided into an injured region (ip INJ), which consisted of superficial dorsal horn regions lacking IB4 binding, and an adjacent uninjured region (ip UNINJ) measuring $200\mu m$ from the edge of the injured region laterally. Scale bar: $200\mu m$.

(Beggs and Salter, 2007).

4.4 Minocycline Treatment Does Not Rescue Synapse Loss after Peripheral Nerve Injury

Interest in microglia following peripheral nerve injury has steadily increased as they have been demonstrated to proliferate and release various molecules following injury, and that these signals are an essential part of the mechanism leading to hypersensitivity after peripheral nerve lesions (Tsuda et al., 2005; Beggs and Salter, 2013; Clark and Malcangio, 2014). Minocycline has shown good efficacy in blocking microglial signalling after peripheral nerve injury (Raghavendra et al., 2003; Mika et al., 2007; Mika, 2008), and thus to test the hypothesis that microglial responses after nerve injury may be linked to the synaptic loss previously observed in lamina 2 inner, minocycline treatment was used.

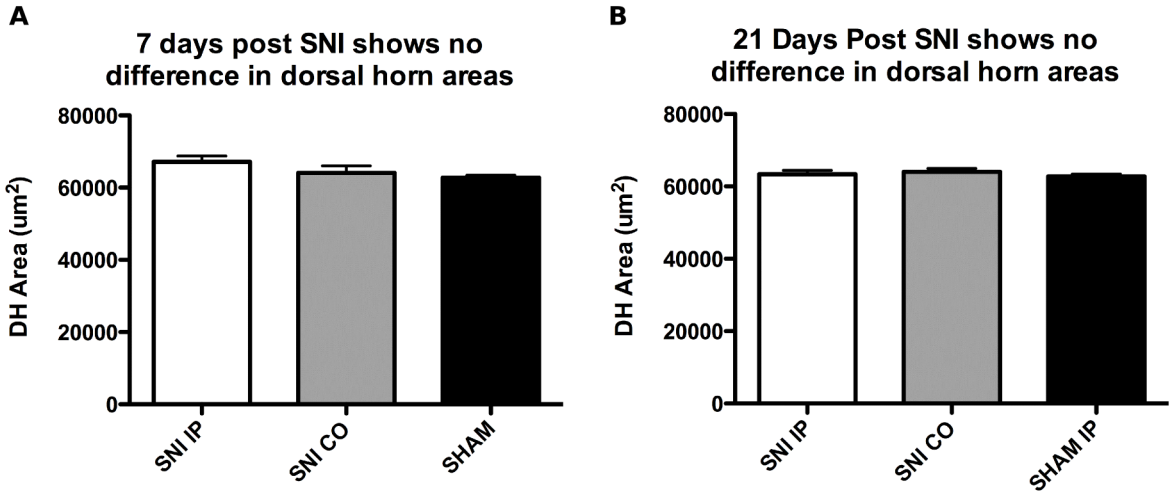

Figure 4.13: **7 and 21 days post SNI do not affect dorsal horn volume. A:** Comparison of 7 day SNI ipsilateral and contralateral superficial dorsal horn areas to SHAM surgery show no significant differences. **B:** 21 day SNI ipsilateral and contralateral superficial dorsal horn areas show no significant differences to SHAM surgery. One-way ANOVA with Tukey post-hoc corrections. DH, dorsal horn; IP, ipsilateral; CO, contralateral.

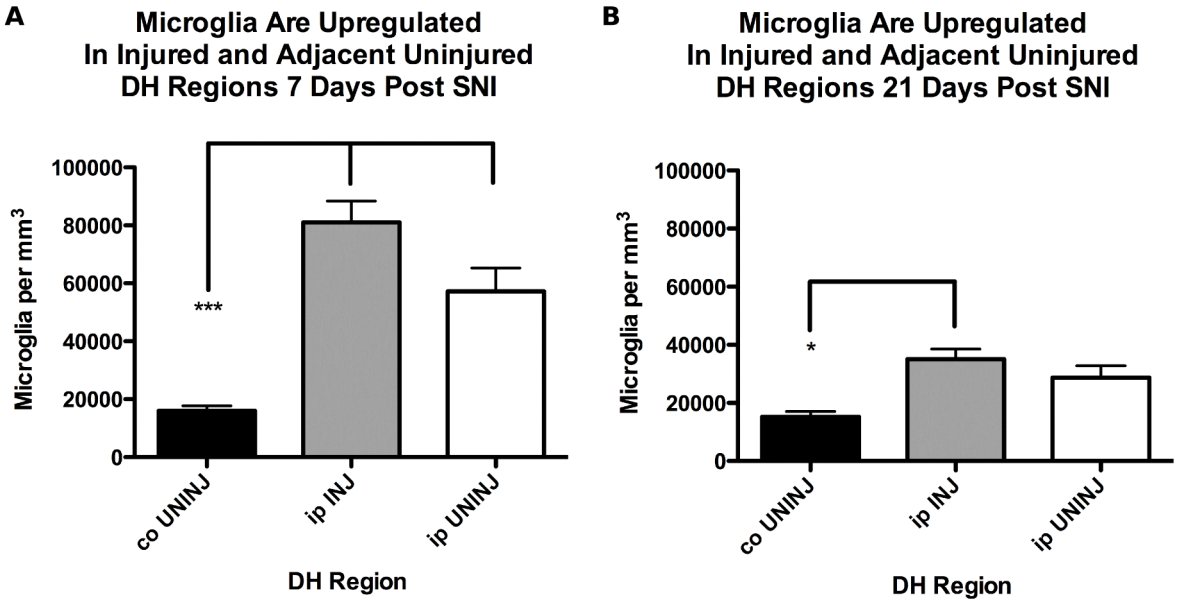

Figure 4.14: **Microglial Quantification in Injured, adjacent un-injured, and contralateral regions. A:** 7 days post SNI surgery the ipsilateral dorsal horn shows a dramatic proliferation in microglial cell numbers, especially prevalent in the injured site (ip INJ), but also in the adjacent uninjured region (ip UNINJ). **B:** 21 days post SNI surgery the ipsilateral dorsal horn shows a reduced proliferation in microglial cell numbers relative to 7 days post SNI, where only the injured site (ip INJ) shows a significant increase relative to the contralateral uninjured region. Although the adjacent uninjured region (ip UNINJ) shows an increase relative to the contralateral region, it did not reach significance. One-way ANOVA with Repeated Measures; Tukey Multiple Comparisons Test; *, $p<0.05$; ***, $p<0.001$.

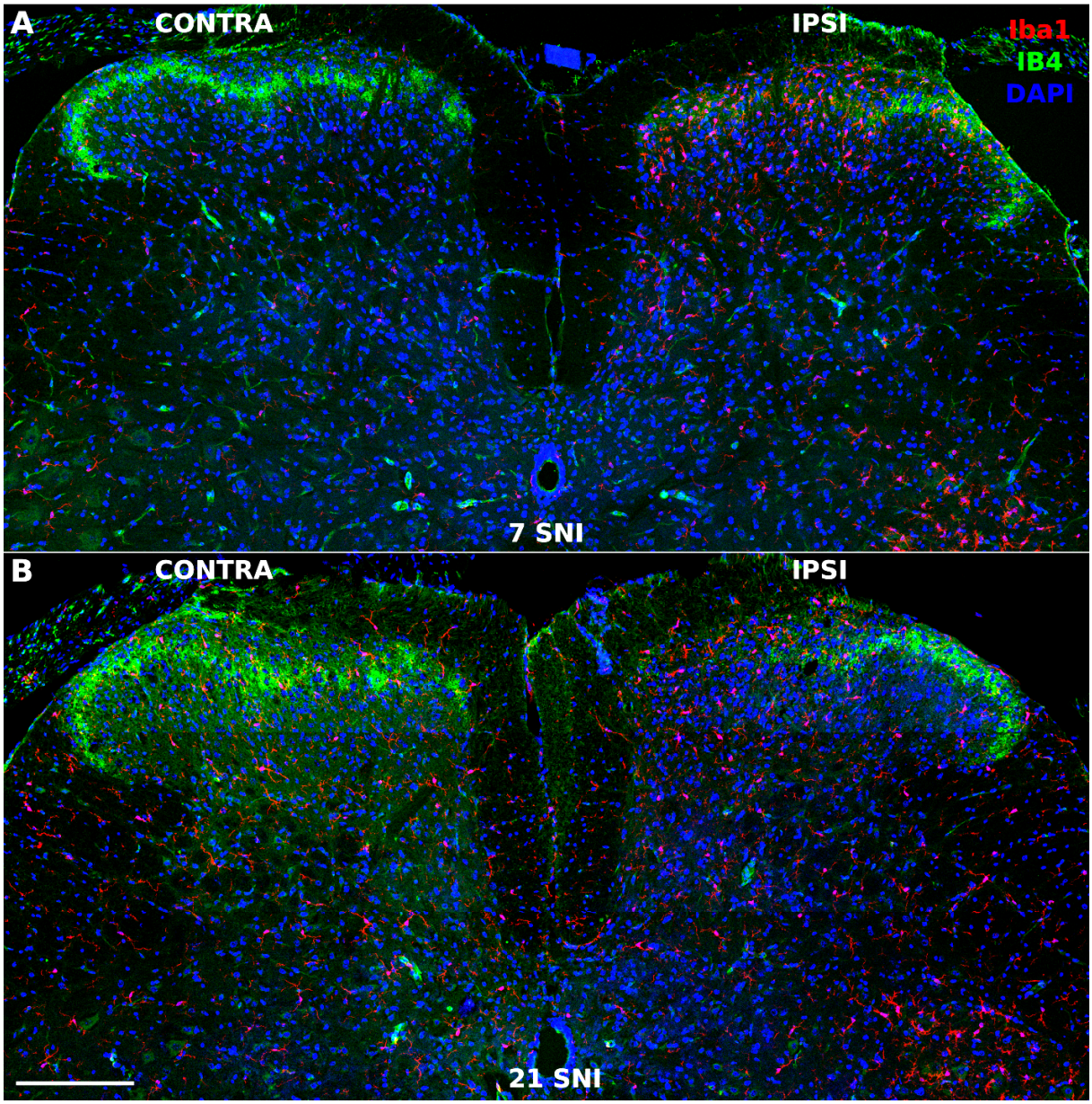

Figure 4.15: **7 & 21 SNI dorsal horn images show microgliosis. A:** 7 days post SNI surgery shows a robust increase in microglial cells the ipsilateral dorsal horn, especially in the injured region (where IB4 binding is lost). **B:** 21 days post SNI surgery shows an increase in microglial cell numbers, but reduced compared to 7 days post surgery. Scale Bar: $200\mu m$.

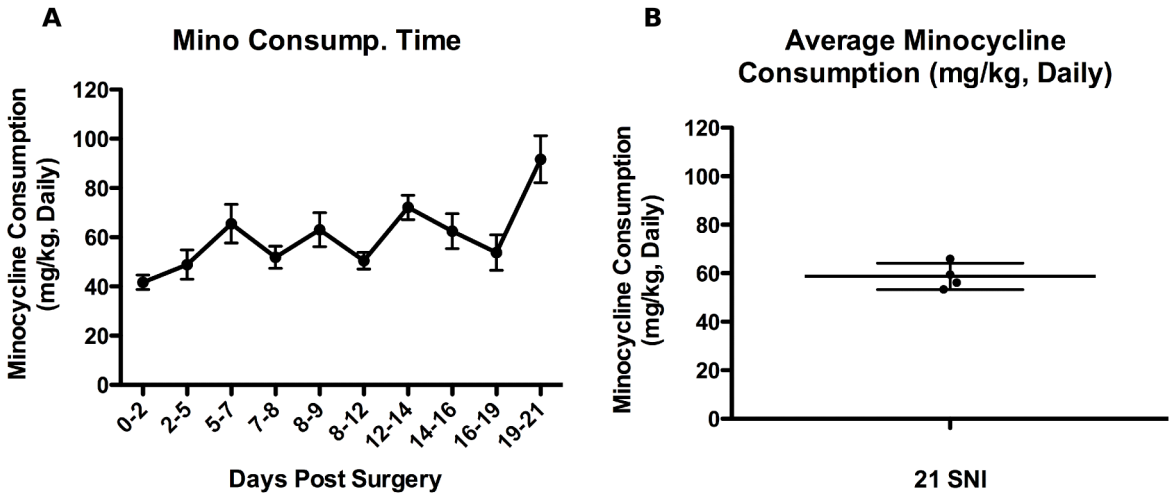

Figure 4.16: **Animals consume water containing 0.3mg/mL minocycline to a dose of approximately 60mg/kg daily. A:** Daily consumption of water containing 0.3mg/mL minocycline per cage (n=4, plotted mean±SEM). **B:** Average daily consumption of minocycline across the entire experiment (n=4, plotted mean±SD).

4.4.1 Minocycline partially reverses hypersensitive behaviour observed following SNI surgery

Minocycline dosing was performed by chronic oral administration, which was assessed over the time course of the experiment. As can be seen from Figure 4.16, animals administered minocycline in drinking water consumed, on average, 60mg/kg daily. This dose is between 2-3x higher than the effective i.p. dose which shows efficacy in nerve injury paradigms (Raghavendra et al., 2003; Ledeboer et al., 2005; Mika et al., 2007; Mika, 2008).

In order to assess the effectiveness of chronic oral administration of minocycline in ameliorating the behavioural hypersensitivity seen to mechanical paw withdrawal thresholds, behavioural testing was performed on both vehicle and minocycline treated animals. As is shown in Figure 4.17, daily oral consumption of ~60mg/kg results in a partial reversal of hypersensitivity seen following SNI surgery. This result is consistent with previous findings which show a partial reversal in nerve injury-related hypersensitivity following minocycline administration (Raghavendra et al., 2003; Ledeboer et al., 2005; Mika et al., 2007; Mika, 2008).

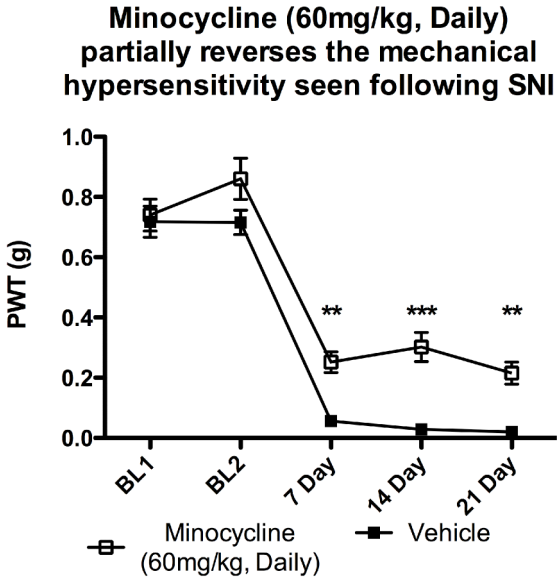

Figure 4.17: **Minocycline partially reverses the mechanical hypersensitivity seen following SNI.** Following SNI surgery animals display a significant reduction in ipsilateral paw withdrawal threshold, which is partially reversed by daily administration of minocycline. Graph plots mean±SEM, two-way ANOVA; bonferonni-corrected selective post-hoc testing; **, $p<0.01$; ***, $p<0.001$; $n=8$. PWT, paw withdrawal threshold.

4.4.2 Minocycline does not reduce the level of microglial proliferation observed following SNI

Minocycline is widely regarded to reduce behavioural hypersensitivity via its actions in microglial cells (Raghavendra et al., 2003; Mika et al., 2007; Mika, 2008). Thus, a reasonable assumption is that minocycline may reverse the microgliosis seen after peripheral nerve injury. To confirm whether minocycline inhibited microglial proliferation, widely considered a key marker in the microglial response seen after injury, an assessment of microglial number in the superficial dorsal horn of both vehicle and minocycline-treated mice was conducted, utilising the automated microglial analysis already explicated (see Section 4.3.1). To confirm microglial densities measured here reflect the total count of microglial cells for all treatments, measures of dorsal horn areas were also conducted, which all showed no significant differences (Figure 4.18).

Surprisingly, microglial numbers were found to be unchanged following chronic oral

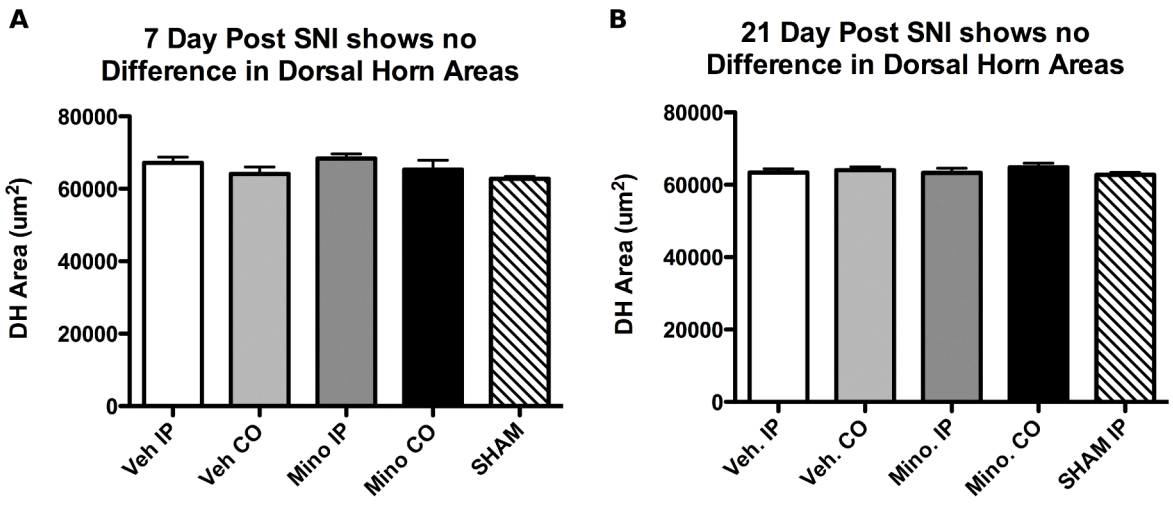

Figure 4.18: **Minocycline- and Vehicle- treated animals display similar superficial dorsal horn areas. A:** 7 days post SNI show no significant differences in dorsal horn areas between vehicle, minocycline-treated and SHAM. **B:** 21 days post SNI show no significant differences in dorsal horn area between vehicle, minocycline-treated and SHAM. One-way ANOVA with Tukey post-hoc corrections. CO, contralateral; DH, dorsal horn; IP, ipsilateral; Mino, minocycline; Veh, vehicle.

minocycline administration, which corroborated with comparisons of immunoflourescence images of the dorsal horn between vehicle- and minocycline- treated animals (Figure 4.19). This result seems to contradict the behavioural response seen with minocycline treatment, but there may be an important difference between physiologically inhibiting microglial effects that lead to mechanical hypersensitivity, and the anatomical effects to microglia due to peripheral nerve lesion (Watkins et al., 2001) (see Section 4.5 for Discussion). This conclusion has been suggested in other studies which have been unable to reverse the anatomical effects of the microglial response to nerve injury (Fendrick et al., 2005), consistent with the present results.

4.4.3 Minocycline Administration does not reverse PSD95 puncta loss after peripheral nerve injury

Previous work has highlighted the specific and significant reduction in PSD95 within lamina 2 inner of the mouse, 21 days post SNI surgery. Therefore, the next question

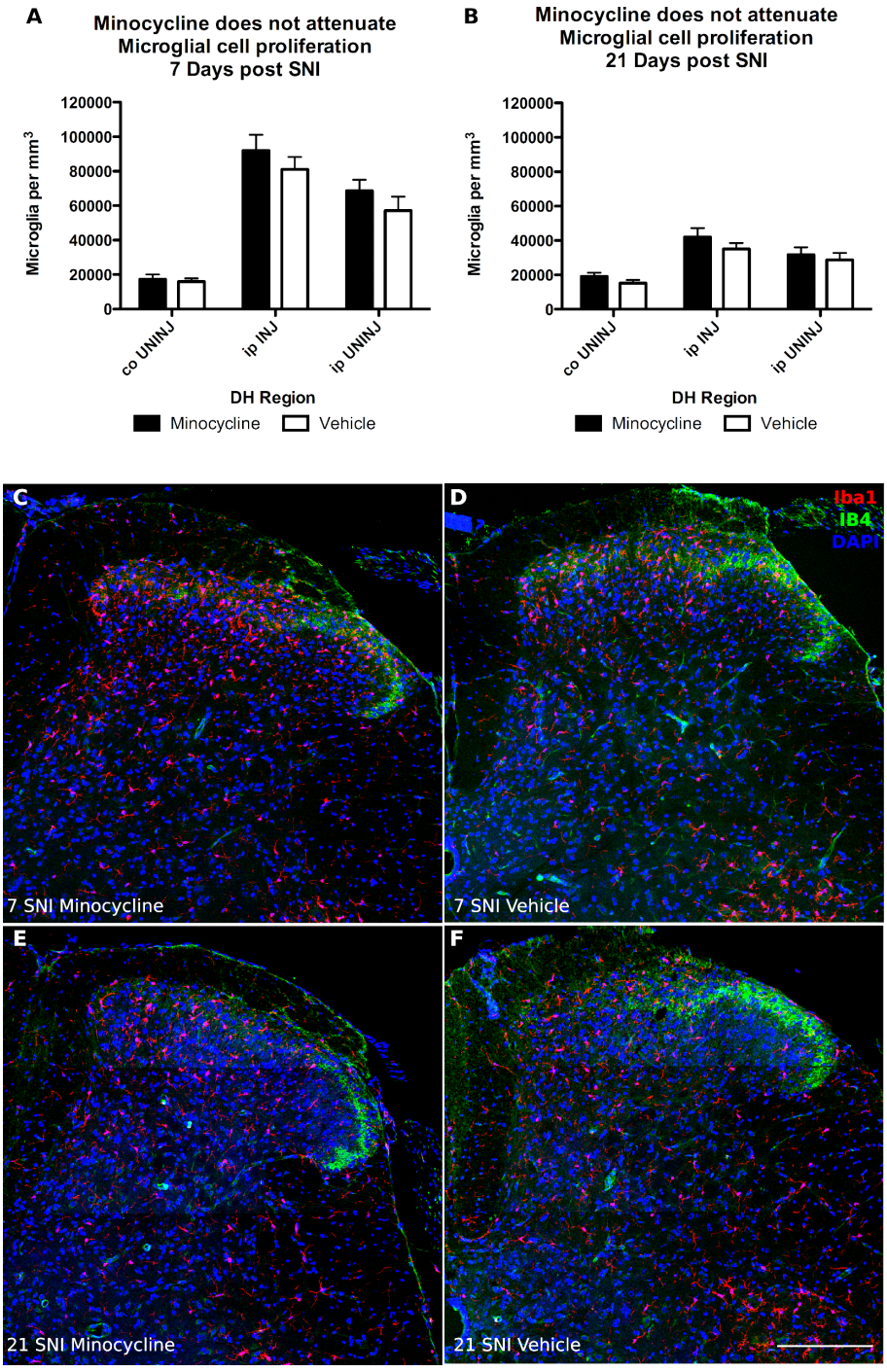

Figure 4.19: **Minocycline treatment does not attenuate the microgliosis seen after SNI. A:** 7 days post SNI quantification of microglial cells shows no differences between minocycline- and vehicle- treated animals. **B:** 21 days post SNI quantification of microglial cells shows no differences between minocycline- and vehicle- treated animals. **C-F:** 7 & 21 day post SNI treated with either minocycline or vehicle example images show no obvious differences in Iba1 labelling. Stats: two-way ANOVA; bonferonni-corrected selective post-hoc testing; n=5. Scale Bar: $200\mu m$.

to address was whether minocycline treatment was able to reverse these changes seen at 21 days post SNI surgery. To confirm that synapse density corresponds to total synapse counts in the superficial dorsal horn, measures of superficial dorsal horn areas were performed, as previously shown in Figure 4.18, which show no differences between dorsal horn areas of different treatment groups.

As can be seen from Figure 4.20, chronic administration of minocycline up to 21 days post SNI surgery has no effect on the reduction in PSD95 puncta observed at this time. A significant reduction in lamina 2 inner was still observed in the minocycline treated group relative to the contralateral side, and no difference was seen between the ipsilateral or contralateral ROIs between the minocycline-treated and vehicle-treated animals.

4.4.4 Minocycline Administration does not affect SynaptoPhysin puncta number after peripheral nerve injury

Although previous work has suggested no observed change in SynaptoPhysin puncta at 21 days post injury, in order to complete the assessment, and confirm previous findings, this analysis was also repeated. Figure 4.21 shows SynaptoPhysin puncta number are not altered in either vehicle- or minocycline-treated animals 21 days post SNI surgery.

4.4.5 Minocycline treatment does not affect eGFP intensity in the dorsal horn following SNI surgery

Finally, eGFP fluorescence intensity was compared between vehicle- and minocycline-treated animals at 21 days post SNI. Figure 4.22A shows the corresponding contralateral and ipsilateral regions assessed for eGFP fluorescence intensity. As can be seen in Figure 4.22B, comparing minocycline treated to vehicle treated animals shows no obvious differences in fluorescence intensity. Although a significant result was seen between the

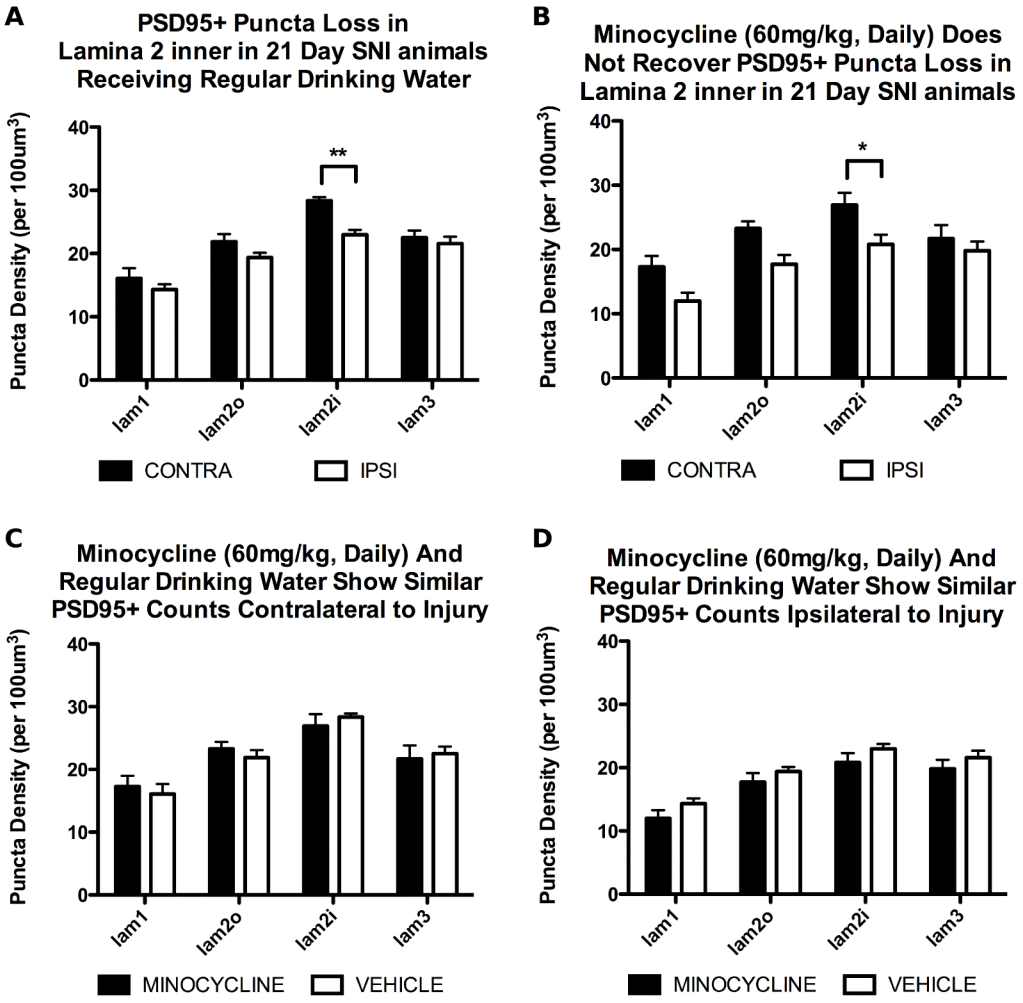

Figure 4.20: **PSD95+ puncta remain reduced in lamina 2 inner with minocycline treatment. A:** PSD95+ puncta in vehicle-treated animals show a reduction in ipsilateral lamina 2 inner relative to the contralateral region. **B:** PSD95+ puncta in minocycline-treated animals show a reduction in ipsilateral lamina 2 inner relative to the contralateral region. **C:** Comparison of minocycline- and vehicle- treated PSD95+ puncta in the contralateral dorsal horn show no significant differences. **D:** Comparison of minocycline- and vehicle- treated PSD95+ puncta in the ipsilateral dorsal horn show no significant differences. Two-Way ANOVA with bonferroni-corrected post hoc comparisons (*, $p<0.05$; **, $p<0.01$).

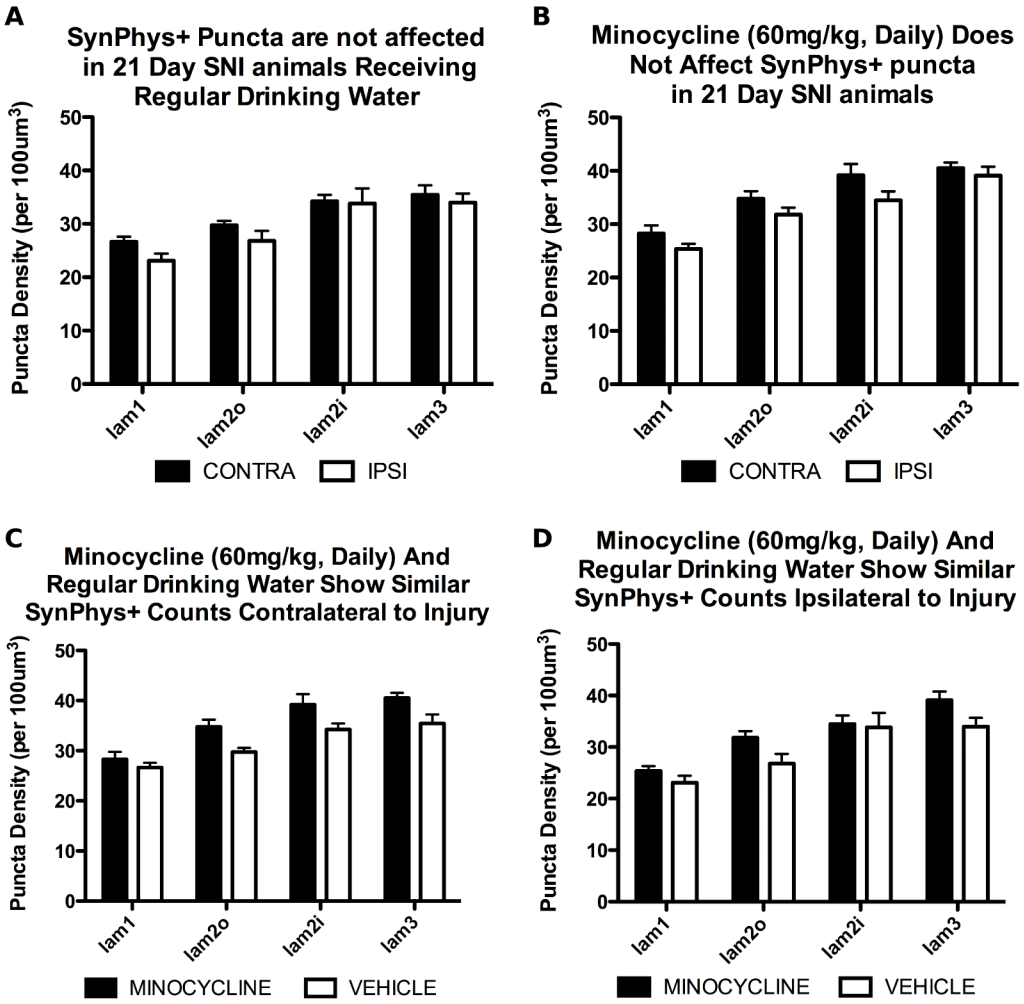

Figure 4.21: **SynaptoPhysin+ puncta show no changes with minocycline treatment. A:** SynaptoPhysin+ puncta in vehicle-treated animals show no significant differences in the ipsilateral region relative to the contralateral region. **B:** SynaptoPhysin+ puncta in minocycline animals show no significant differences in the ipsilateral region relative to the contralateral region. **C:** Comparison of minocycline- and vehicle- treated SynaptoPhysin+ puncta in the contralateral dorsal horn show no significant differences. **D:** Comparison of minocycline- and vehicle- treated SynaptoPhysin+ puncta in the ipsilateral dorsal horn show no significant differences. Two-Way ANOVA with bonferroni-corrected post hoc comparisons.

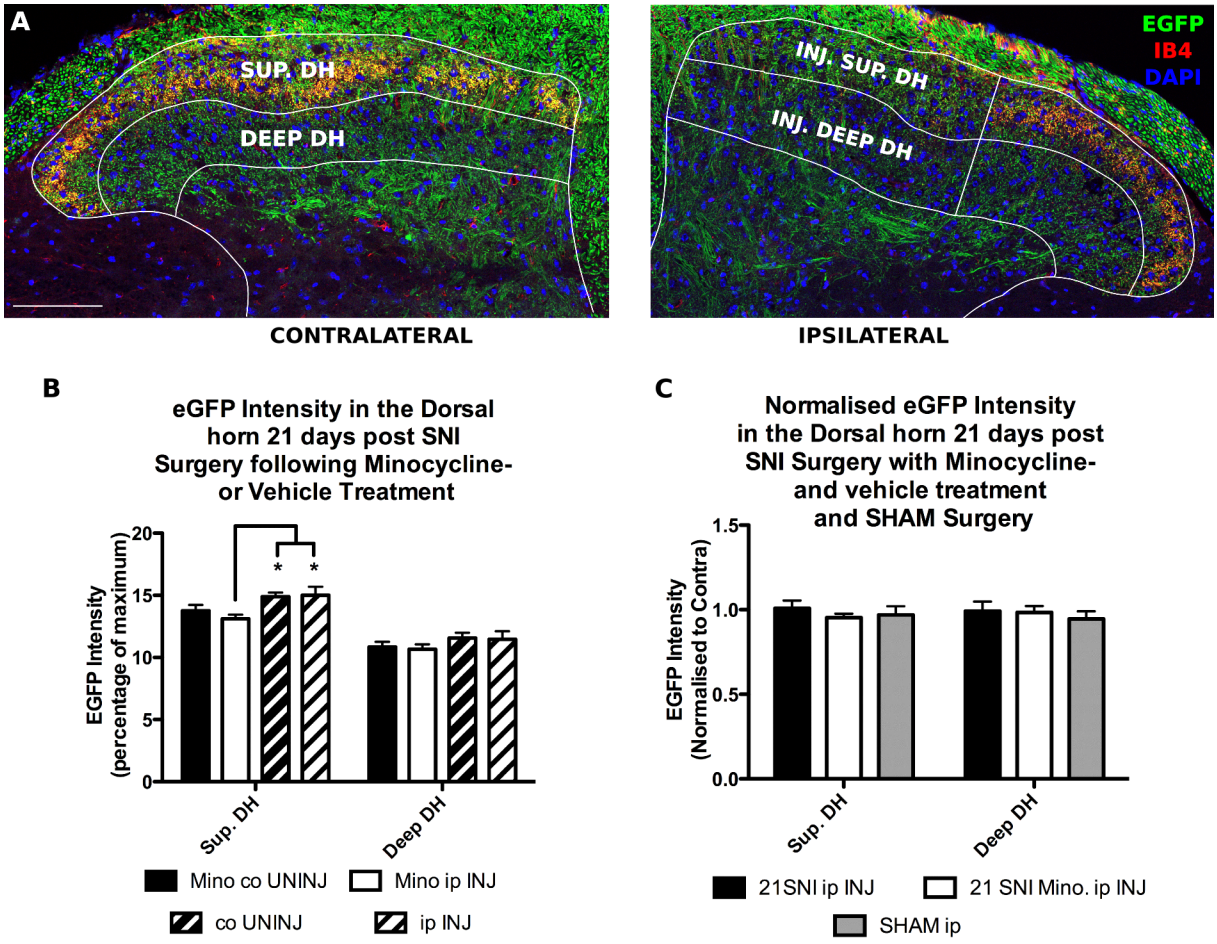

Figure 4.22: **eGFP fluorescence intensity analysis. A:** Overview of analysis scheme; **B:** ipsi injured and contra eGFP fluorescence for both mino and veh groups. **C:** ipsi injured normalised to contra values of mino and veh groups. Scale bar: $100\mu m$.

minocycline-treated ipsilateral superficial dorsal horn region relative to both ipsilateral and contralateral vehicle-treated groups, this is likely due to the fact minocycline- and vehicle- images were processed and imaged in separate experiments. To adjust for the variability between experiments, Figure 4.22C shows the ipsilateral eGFP fluorescence intensities normalised to the contralateral sides, and shows no significant differences between minocycline- or vehicle- treated animals 21 days post SNI, and neither of these results differ from a SHAM surgery group.

4.5 Discussion

This Chapter has explored the possibility that the microgliosis induced in the dorsal horn by peripheral nerve injury may be driving the PSD95+ puncta loss seen at 21 days post injury. Initially, a methodology consistent with the previously outlined automated stereological assessment of synapses was developed to quantify microglial cells within the dorsal horn. This method was used to assess microglial cell numbers after peripheral nerve injury, and revealed a significant increase in microglial cell number at 7 and 21 days post injury, consistent with previous work. Minocycline, a known inhibitor of microglia (Tikka et al., 2001; Raghavendra et al., 2003), was administered chronically to animals to inhibit microglial-associated changes to the dorsal horn. Minocycline successfully inhibited behavioural responses, yet left the microgliosis intact. Finally, chronic administration of minocycline did not result in a reversal of injured-induced dorsal horn synaptic modifications, specifically no reversal in PSD95+ puncta loss.

4.5.1 Development of Automated Microglial Quantification

A key component and advance in this Chapter was the development of the automated stereological analysis tool StereoMate to cellular structures. This relied on two key advances: Generation of a high signal to noise ratio for cellular labelling, and a stereological filter to allow stereological analysis of large and mostly incompletely reconstructed objects in limited tissue sections.

4.5.1.1 Antigen Retrieval and Utilising both Nuclear and Cellular Labelling

To facilitate the automation of cellular analysis a sufficient signal-to-noise ratio of fluorescent cellular markers is required. This signal-to-noise for synaptic markers was previously shown to be greatly improved by antigen retrieval methodologies (Chapter 2). Here,

treatment with Proteinase K was found to significantly improve fluorescent signal from Iba1 antibody binding, and was taken forward to aid in cell segmentation and automated analysis. Proteinase K has now shown good antigen retrieval properties for both synaptic markers, and for the microglial marker Iba1. This opens the possibility that Proteinase K treatment may work as a generalised antigen retrieval methodology.

The second key aspect to aid automated analysis of cellular structures was to combine the high quality cell label with a good nuclear label, and to only analyse structures which co-localised for both labels. This method ensures only nuclei which are positive for the cell of interest are present in the image for automated analysis. As has been shown, some aberrant co-localisation can also occur, but can be filtered away based on size.

4.5.1.2 Cellular Stereological Filter

The development of a cellular stereological filter emerged due to the thin sectioning and tissue shrinkage seen with sections taken for anatomical analysis. This led to very few fully reconstructed cellular nuclei for quantification, and drove the development of a cellular stereological filter. The shrinkage observed in spinal cord sections is likely driven by a number of causes. First, air drying of spinal cord sections leads to tissue shrinkage which will diminish the depth of imaging, tissue treatment such as ethanol immersion, or digestion with proteases such as Proteinase K may lead to diminished tissue thickness, and finally the use of an air-objective will lead to an apparently thinner section due to the altered light path observed as the tissue is traversed (Peterson, 2004; Egner and Hell, 2006).

In order to overcome the limitation in tissue thickness apparent following tissue drying, processing and imaging, a novel cellular stereological filter was developed. This method utilised the fact nuclei form a oval shape, and thus have a Z slice which will contain the

largest number of pixels which is roughly in the centre of the nucleus. By only counting cells at this slice, and therefore not having to fully reconstruct the nuclei, a larger number of cells can be included into the overall quantification, which improves estimates of cell number in a given volume of tissue analysed.

Stereological methods originated in the assumption-based methods where object profiles were assumed to relate to 3D objects based on an assumption on the properties of the 3D object. These methods developed into assumption-free methods, characterised by the Optical Di-Sector (Gundersen et al., 1988; West, 2001). At first glance, this new stereological filter may appear to regress to assumption-based methods. However, there are important differences between the original assumption-based methods and the stereological filter developed here. Assumption-based methods would use an assumption to calculate 3D object counts based on the 3D object size, and thus how many profiles, on average, would therefore be present in a section. These methods essentially corrected profile counts to total 3D object counts, a property which was sometimes inaccurate, and often criticised. The stereological filter here does not perform this calculation, but instead uses an assumption based on object shape to reduce a 3D object to a single Z slice for quantification. This is similar to the Optical Disector and design-based stereological methods, where each 3D object is reduced to a single point. Finally, the stereological filter developed here has established that the assumption concerning nuclear shape is true, validating the approach.

One criticism concerning the Stereological Filter might be that the number of microglial cells quantified in a given volume will be less than if simple profiles of microglia were counted. It is true that relative to counting profiles, the Stereological Filter will reduce the cell count. However, this count is firstly stereologically valid, which means objects quantified will be independent of size, shape and orientation of microglial nuclei.

For example, when quantifying cell profiles, a large cell is more likely to form a profile in a given section; whereas quantifying cells based on the thickest Z section eliminates this bias by reducing any cell to a single Z slice. Second, the Stereological Filter has been validated in an automated approach, which is largely dependent on its isolation of the Z slice containing the largest number of pixels, and dramatically speeds up data acquisition.

A second criticism might be that the time and effort required to set up the automated approach might out-weigh the benefit of automating the analysis. Whilst true that the set up required, including the manual identification of objects as either true cell nuclei or aberrant co-localisation and proving the assumption of an oval shaped nucleus, does take some time; firstly, this workflow has been highly supplemented by ImageJ macros to ease this process; and secondly, once this process has been performed once, this method can be used in an automated fashion on datasets from that point on. The overhead of conducting the initial setup is thus relatively quick in comparison to the arduous task of counting cells in numerous datasets. However, repeating the automated analysis faithfully is dependent on the objective lense, resolution, cell type, tissue type, and tissue processing & staining procedures; and the set up would need to be re-performed with each adjustment to any of these parameters.

This methodology has the potential to allow stereological quantification of any cell type in relatively thin tissue sections. This Chapter has highlighted a workflow to optimise the analysis of cells marked with fluorescence labels, where isolated and segmented objects are divided into true cell nuclei or aberrant co-localisation based on manual inspection, and finding a pixel value for a high-pass filter to allow the selective analysis of true cell nuclei. To apply stereological quantification to cells in relatively thin sections, cell nuclei must be proven to be oval in shape, and a clear delineation between aberrant co-localised objects and true cell nuclei at their thickest Z section must be demonstrated.

A number of caveats should be considered before implementing this approach. First, for good segmentation, a high quality fluorescent label is required with high signal to noise. Second, cells of a high density may be hard to separate due to nuclei from different cells conjoining during the segmentation process. This can be overcome by using high NA objective lenses, preferably oil-immersion, as well as using a sufficient image resolution to clearly delineate between cells. Third, an appropriate cell marker should be used with a high quality nuclear marker for good cell separation. If a specific nuclear marker exists for the cells of interest, then it may be possible to use only a cell-specific nuclear marker. If a combination of nuclear and cell marker is used, to minimise aberrant co-localisation, a cell marker limited to the peri-nuclear region is ideal, such as NeuN for neurons (Mullen et al., 1992). Finally, the manual identification of objects has been considered the gold standard here, yet it is well known that human error constitutes a part of the variability seen in manual quantification (Badrinath et al., 2006). Therefore, the sensitivity and specificity identified here, or with future applications, may reflect errors in manual counting as much as it might reflect errors in the automated segmentation. The only means to overcome this is to repeat the manual identification within and between observers to attempt to identify the 'ground-truth' (Badrinath et al., 2006).

4.5.2 Microglia are up-regulated after nerve injury

The data presented in this Chapter clearly shows a dramatic up-regulation in microglial cell numbers following peripheral nerve injury. This microgliosis was most pronounced at 7 days post injury, and was markedly reduced, yet still significantly higher, at 21 days post injury. These results are consistent with previous reports (Narita et al., 2006; Beggs and Salter, 2007; Vega-Avelaira et al., 2007). A second interesting observation was the "spill-over" of microglial cells into adjacent regions of the dorsal horn containing the terminals

of un-injured afferents, an observation previously highlighted (Beggs and Salter, 2007).

This observation of increased microglial numbers in regions of the dorsal horn where uninjured afferents lie opens the possibility that microglia may be affecting signalling and circuitry relating to these uninjured afferents. The evoked behavioural hypersensitivity observed after peripheral nerve injury is driven by intact & uninjured afferents, at least in transection models like the one used in this Chapter. This would imply any intervention which reduces or reverses this hypersensitivity must be somehow disrupting effects on either the intact afferents themselves, or the circuits they engage with. Use of minocycline in this study to reverse the behavioural hypersensitivity seen following SNI surgery therefore suggests that the microglial response seen in dorsal horn regions adjacent to injured afferent input may be driving, at least in part, the evoked behavioural hypersensitivity seen after peripheral nerve injury.

4.5.3 Minocycline's effects on microglia

Minocycline was selected in this study due to its known efficacy in inhibiting microglia (Tikka et al., 2001; Raghavendra et al., 2003), and its ability to reverse the behavioural hypersensitivity seen following peripheral nerve lesion (Raghavendra et al., 2003; Ledeboer et al., 2005; Mika et al., 2007; Lin et al., 2007; Mika, 2008). Consistent with these previous reports, chronic administration of minocycline resulted in a partial reversal in mechanical allodynia after peripheral nerve injury.

An interesting observation made in this Chapter is the inability for minocycline to inhibit the increase in microglial cell numbers seen after nerve injury. This was initially a surprise, given the indication in the literature showing a reduction in microglial proliferation. For example, Tikka et al. demonstrated the ability for minocycline to prevent microglial cell proliferation *in vitro* in response to glutamate excitotoxicity (Tikka et al.,

2001). Furthermore, a plethora of *in vivo* studies seem to show minocycline's ability to reduce the microgliosis after peripheral nerve injury, including reducing the increase in CD11b (Lin et al., 2007; Blackbeard et al., 2007; Ito et al., 2009; Yamamoto et al., 2015), the production of interleukin-6 (Zanjani et al., 2006; Hathway et al., 2009), phosphorylation of p38 (Ito et al., 2009; Matsui et al., 2010; Mei et al., 2011), and other glial markers (Raghavendra et al., 2003; Nutile-McMenemy et al., 2007; Padi and Kulkarni, 2008; Osikowicz et al., 2009; Nie et al., 2010). However, all of these studies have observed a reduction in either changes in expression of various proteins, or reduction in the activation of various intracellular pathways, and have not observed whether microglial proliferation after nerve injury is curbed by minocycline.

The present study observed the same number of microglial cells, as determined by the co-localisation of DAPI+ nuclei with Iba1+ microglial cells, following nerve injury in both minocycline- and vehicle- treated animals. This result can be considered consistent with the previous literature. Firstly, as already highlighted, the literature on minocycline shows effects on either the production, activation or release of various molecules by microglia into the dorsal horn. Second, the actual recruitment and proliferation of microglia is driven by injury to the peripheral nerve (Ito et al., 1998; Liu et al., 2000b; Tsuda et al., 2005). Thus, there may be a delineation between the signals arriving from the peripheral injury site which encourage microglial proliferation and activation, and the signals derived and released from microglia following their activation. It may be the case that minocycline is able to intervene with the signalling from microglia following their activation, but is not able to inhibit the signalling from injured afferents to microglia which cause their proliferation.

The fact that minocycline treatment did manage to ameliorate the paw withdrawal threshold, consistent with previous studies, suggests the minocycline dosing regimen was

effective. Furthermore, one study looking at microglial proliferation following facial nerve injury demonstrated a lack of minocycline to prevent microglial cell proliferation after nerve injury, consistent with the present results (Fendrick et al., 2005). Therefore, this theory may explain the apparent discrepancy between the results presented here and previous studies showing minocycline's ability to curb microgliosis. One way to confirm this effect is to repeat the study, and demonstrate minocycline's effects on previously identified signalling molecules and pathways, as well as the identified continued proliferation in microglial cells demonstrated here.

4.5.4 Microglial inhibition does not reverse synapse loss after injury

Previous studies have highlighted the integral role microglia can play in synaptic plasticity after nerve injury. For example, down-regulation of glial glutamate transporters has been associated with enhanced NMDA receptor signalling in at synapses in the dorsal horn after peripheral nerve injury which was reversed by minocycline (Nie et al., 2010). BDNF is an important molecule released by microglia after nerve injury which can facilitate the reversal of the chloride anion gradient in spinal neurons (Coull et al., 2005), and contribute to spinal LTP at C-fibre synapses (Zhou et al., 2011). Selective stimulation of microglia with fractalkine has also been demonstrated to affect synaptic strength by ultimately enhancing presynaptic neurotransmitter release (Clark et al., 2015).

Furthermore, microglia have also recently been demonstrated to phagocytose synapses in different regions of the CNS during development (Tremblay et al., 2010; Schafer et al., 2012). Given the large amount of evidence demonstrating minocycline as an effective agent in reversing the behavioural consequences of nerve injury, as well as elements of the microgliosis, the use of minocycline as a means of reversing the possible removal of

synapses by microglia seemed reasonable.

As shown here, administering minocycline, whilst reversing the behavioural changes, did not succeed in reversing the loss of synapses in lamina 2 inner seen after peripheral nerve injury. The majority of studies have demonstrated minocycline's capacity in reversing the activation of different intracellular signalling pathways (such as p38 and Src-family kinase) and the release of various cytokines (Zanjani et al., 2006; Matsui et al., 2010; Zhong et al., 2010; Mei et al., 2011), so this result supports the idea that microglial release of cytokines is not related to the loss of synapses seen after nerve injury.

However, whether minocycline is able to block phagocytosis after nerve injury, the key mechanism for synaptic stripping demonstrated previously (Schafer et al., 2012), is relatively unclear. Some studies observing microglia in Alzheimer's Disease have shown minocycline to be effective at reducing the inflammatory response of microglia without affecting the phagocytic potential of the cells (Familian et al., 2007; Malm et al., 2008), which suggest that minocycline, whilst reversing the release of several important molecules which may be important for hypersensitivity following peripheral nerve injury, is likely not to inhibit the phagocytotic potential of microglia.

Thus, a different approach may be more effective in determining the ability for microglia to phagocytose synapses after peripheral nerve injury. Previous work disrupted complement receptor 3 and complement component C3 signalling, which resulted in a diminished capacity for microglial phagocytosis (Schafer et al., 2012), and this method may be a more robust way of testing the hypothesis that microglia are involved in phagocytosis of synaptic elements after peripheral nerve injury.

4.5.5 Conclusions

This Chapter has explored the links between microglial responses in the dorsal horn following peripheral nerve injury, and synapse loss observed within lamina 2 inner. Microglia were found to proliferate in the injured and adjacent uninjured input regions of the dorsal horn, providing evidence for their ability to drive evoked-behavioural sensitivity. The hypothesis that microglial signalling may be involved in the loss of synaptic puncta in the dorsal horn after peripheral nerve lesion was tested by administering minocycline, which showed no reversal of synapse loss. Minocycline also showed no reversal in microglial proliferation, which may be the result of its limited mode of action. The limitation of minocycline to prevent microglial proliferation or phagocytosis means a more robust way of testing the hypothesis that microglial drive synapse loss specifically by phagocytosis needs further exploration.

Chapter 5

General Discussion

5.1 Introduction

The work presented in this Thesis has met two key objectives in the analysis of distribution patterns of synapses throughout the dorsal horn. First, it has successfully demonstrated the development of an automated stereological analysis workflow, which describes the histochemical preparation, image acquisition, processing and analysis of biological objects of interest. At each stage in the workflow, the method has been optimised to ensure an accurate representation of the biological objects of interest is produced, and its automated nature allows a large number of biological objects to be analysed per sample, and per study.

Second, this workflow has been applied to the dorsal horn to describe the distributions of different synapse-associated proteins. These synapse-associated proteins, SynaptoPhysin and PSD95, form key structural components of both the pre- and (asymmetric) post- synaptic components, respectively, and thus determining of their number provides important information on synapse number in the dorsal horn. This workflow has been applied to the dorsal horn in the naïve state, as well as to different nerve injury paradigms

at different timepoints. It has revealed a distinct distribution signature for both PSD95 and SynaptoPhysin in the naïve dorsal horn, and a selective loss of PSD95+ synaptic puncta within lamina II inner at 21 days post peripheral nerve injury.

Utilising the technique outlined in Chapter 2 gives a broad view of circuit-level characteristics, and it can be used to understand how circuitry develops, and is modified by genetics, experience, and disease states. Here is given a broad discussion of the developed workflow, its benefits over other means of analysing synapses or other biological objects of interest, and its potential applications.

This is followed with a discussion of the biological data obtained in this Thesis, the development of a working biological model of dorsal horn neural circuitry and its plasticity following peripheral nerve injury, and further work to explore this model in greater detail. Finally, a brief overview of recent developments in scientific research approaches, especially in relation to Neuroscience, and how these relate to the present work is given, along with some general remarks on how these developments may pave the way for understanding neural circuitry and its computational capacity.

5.2 StereoMate

The algorithms implemented in ImageJ to process and analyse regions of interest using an automated stereological approach has been named StereoMate (from Stereological Automated Image Analysis), but the workflow required to achieve this form of automated stereological analysis extends from the histological preparation to object data acquisition. Here, an overview of the key achievements which have enabled the workflow's implementation as an automated and stereological methodology are given, including the histological preparation, image processing, and stereological object sampling for measurement. This is concluded with the limitations of this workflow, as well as future work this method can

engage with.

5.2.1 The Histological Preparation

The histological preparation required a great deal of optimisation and work to ensure it was of sufficient quality for stereological assessment. A delicate balance had to be struck between sufficient antigen retrieval steps to unveil synaptic antigens, yet retaining a robust enough structure to maintain tissue morphology. Previous methodologies have utilised a weak fixation protocol (see Schneider Gasser et al., 2006), yet optimisation of this workflow found using a moderate fixation protocol combined with a series of antigen retrieval methods led to a robust histological preparation in terms of antigenicity and morphology.

Antigen retrieval is designed to improve the access and affinity of antibodies to their epitopes. The access and affinity of the antibody is limited by a number of factors. First, the protein target itself can prevent antibody binding by hiding epitopes within its complex 3D folded structure (Hayat, 2002). For this reason, often antibodies are targeted to amino acid sequences and epitopes present at either the N- or C- terminus of the protein; and indeed, both the PSD95 and SynaptoPhysin antibodies were produced from epitopes in the N-terminus region (Watanabe et al., 1998; Fukaya and Watanabe, 2000). Second, the extracellular & intracellular matrices, as well as the tightly bound protein structure within the biological (in this case, synaptic) components themselves (including accessory proteins bound to the protein of interest) can provide a barrier to antibody diffusion, and mask access directly to epitope sites. Finally, the fixation process further prevents antibody diffusion and epitope access by the well described cross-linking that occurs between proteins during formaldehyde fixation (Fox et al., 1985; Sompuram et al., 2004).

Antigen retrieval techniques aim to improve antibody penetration into the tissue, and to improve access of the antibody to its target epitope (Ramos-Vara, 2005; D'Amico et al., 2009). The use of heat and proteases are common methods, and form a key component of the antigen retrieval methodology used in the present workflow. By using a combination of heat, Proteinase K digestion and Pepsin digestion, the tissue becomes increasingly permeable to antibodies, and these antibodies have improved access to their epitopes, especially within dense protein structures such as synaptic components (Bayés et al., 2011, 2012).

These methods likely work through distinct mechanisms. In general, antigen retrieval methods are thought to break crosslinks originally formed during fixation, yet there may be other more important mechanisms which help antibodies reach their epitopes. Heat is well known to denature proteins, and this process may help unveil epitopes on proteins which may otherwise remain hidden. This mechanism is supported by the idea that heat treatment only retrieves antigens for a short time, and that unless the antibody is applied promptly, the improved staining intensity is diminished (Shi et al., 2001; Hayat, 2002). If the mechanism of antigen retrieval was only due to the removal of formaldehyde crosslinks on and between proteins, such a temporal effect would not be predicted to occur.

Proteases such as Proteinase K and Pepsin act on peptide sequences to cleave proteins into smaller components (Ebeling et al., 1974; Fruton, 2002). Whether these proteases can act on formaldehyde crosslinks is not known, but seems unlikely, given the different chemical structure of a peptide sequence to a crosslink. However, these proteases may aid antibody access to antigens through two other important mechanisms. Firstly, by digesting proteins in the extracellular & intracellular matrices, as well as proteins which associate with the protein of interest, the protease treatment will help the antibody diffuse through tissue and reach the target epitope. Secondly, protease effects on the target

protein itself may help to cleave and dismantle the 3D structure of the protein such that epitopes become revealed through peptide cleavage, whilst leaving crosslinks intact. These methods should provide a lasting retrieval of antigen, since the cleavage of a peptide bond should be a relatively permanent event, whilst it should still maintain a level of tissue integrity produced by the remaining crosslinks. Clearly digestion of proteins will affect tissue integrity, and thus a careful balance must be optimised to maximise antigen retrieval and therefore immunohistochemical signal, with tissue integrity.

Thus, the importance of adequate fixation to provide structural support and thus tissue integrity is of paramount importance to help maintain tissue structure during antigen retrieval, since it is likely the proteins themselves, as well as the crosslinks between them, are dramatically altered by antigen retrieval methods. This process is vastly different to simple weak fixation (Schneider Gasser et al., 2006), which does not attempt to improve access of the antibody except by minimising the vital cross-linking architecture which is so important for the retention of tissue morphology. The present method provides the high quality histological preparation required for the production of robust images suitable for automated 3D image analysis, something not achievable to simple weak fixation, and has been utilised throughout this Thesis.

Whether the antigen retrieval methods are well optimised for other synaptic antigens remains unknown. For example, will the antigen retrieval workflow work optimally for gephyrin, the key structural component of symmetric synapses? Some pilot data suggests the level of pepsin is too high for this less well-developed PSD; and that using a lower concentration of pepsin is beneficial for staining this antigen. An interesting development saw Proteinase K effectively retrieve the microglial marker Iba1 (Chapter 4). This opens the possibility of Proteinase K being a general antigen retrieval methodology.

5.2.2 Image Processing & Object Representation

The robust histological preparation allows high signal to noise images to be captured, which is the first step in achieving high-quality object representations. With large biological objects, such as microglial cells (Chapter 4), capturing images on a confocal microscope is sufficient to produce robust and realistic object representations for the subsequent image thresholding. However, synaptic puncta are very small, and the development of deconvolution methods (Sibarita, 2005) greatly improved their representation, as shown in Chapter 2. This crucial step significantly eliminated background noise, improved object signal to noise, and enhanced the resolution of the synaptic puncta.

As shown in Chapter 2, deconvolution was not perfect, with an elongation of fluorescent beads still apparent in the Z plane. This project utilised an accurate theoretical illumination point spread function model produced for the confocal microscope (Nasse and Woehl, 2010). However, it is limited by the fact it only models the illumination PSF, and not the subsequent fluorescent emission PSF. In theory a more accurate PSF can be obtained through the convolution of the illumination and emission PSFs, and this work remains to be tested for an improved theoretical PSF and subsequent object reconstruction with deconvolution.

This solid foundation of a high-quality histological preparation and improved object representation through deconvolution gives the automated thresholding algorithms a clear delineation between object signal and background, and as has been shown throughout this Thesis, leads to excellent binary representations of synaptic objects.

5.2.3 Stereological Assessment

A key breakthrough in the development of this workflow was the application of stereological principles to irregular ROIs for the efficient assessment of biological objects of

interest in an unbiased manner. The original formulation of the Di-Sector probe and other stereological tools (Sterio, 1984; Gundersen et al., 1988) were designed to infer properties of 3D objects from 2D projections. However, with the advent of modern laser-scanning microscopical techniques, where 3D image stacks can be obtained, these techniques are no longer optimal. The inadequacy for the traditional stereological techniques to measure total object number within a region that is imaged in its entirety, but only return an estimate of this measure, stimulated the formation of new stereological methods adapted for this purpose.

The ROI Di-Sector represents an improvement on the traditional Di-Sector probe since it is capable of assessing all objects within a delineated region of interest. If the region of interest encompasses the entire region under analysis, the ROI Di-Sector provides the total number of objects, and the method moves from a stereological estimate to a true count of the objects, a feat that the traditional techniques can never achieve (due to the inherent sampling required to implement the Optical Di-Sector). As the ROI Di-Sector does not further divide the ROI for sampling, it also provides an efficient means of measuring objects, since no space in the ROI between Optical Di-Sectors is wasted.

The ROI Di-Sector rules ensure maximum sampling, as the Di-Sector itself extends in all three dimensions until it reaches either the edge of the ROI or the sample image edge itself. Upon encountering the image edge, rejection boundary-exclusion zone pairs are set up to correct object counts for a stereological sampling of the objects. The exclusion zone itself does remove a portion of the sample image, yet it is essential to ensure no bias for object size, shape or orientation is introduced during the sampling of the ROIs, which is essential for fair and stereological sampling to take place.

The product of the ROI Di-Sector is an unbiased and efficiently acquired sample of fully reconstructed objects for measurement. This extends the ROI Di-Sector beyond making

simple unbiased measures on objects in regions of interest to acquiring representations of objects from a region in an unbiased manner. Thus, many different measurements can be made on the derived unbiased sample of fully reconstructed objects, and these measures will reflect the object population & provide a powerful multi-variate dataset for exploration.

5.2.3.1 Measuring Other Parameters of Synapses

The synaptic puncta sampling used in Chapters 2 & 3 resulted in complete 3D reconstructions of synaptic objects. The present work has focussed purely on counts of objects, yet the 3D reconstruction of these objects permits other measures for a more detailed analysis of synaptic puncta. An obvious measure to extend the synaptic analysis to is object size, and given that synapse size is closely correlated with both synaptic permanency and its recent activity (Cowan et al., 2001; Marrone et al., 2005), this measure has real physiological significance. A second measure may be made of the object shape. Electron microscopy has revealed PSDs of various shapes, including perforated synapses (Cowan et al., 2001), and these may be realised at the light microscope level with different shaped PSDs. The only potential limitation is the resolution limit imposed by the light microscope, yet deconvolution overcomes some of this limitation.

The capturing of information of size and shape parameters for each measured synaptic puncta would provide a rich multivariate dataset for exploration. An analysis of synaptic components in three dimensions to this level would represent a thorough examination of synaptic components and their structural alterations in relation to developmental, environmental, genetic or other manipulations. The StereoMate algorithms have been designed to collect such a multivariate dataset, and the analysis of such a dataset is the next challenge in achieving this level of comprehensive data exploration. One would

expect this multivariate dataset to display different collections of synapses based on size and shape parameters, and thus a Cluster-based analysis (García-Escudero et al., 2010) could form the initial basis of the exploration of this dataset.

5.2.3.2 Measuring Other Parameters of Cells

Similar extensions could be made with analysis of cells. For example, extending the analysis to that of average cell mass could be achieved by divided total pixel counts of the cell marker of interest by the number of cells measured using the Cellular Stereological Filter described in Chapter 4. These types of measures may reveal more subtle changes to cellular architecture which may be important indicators of changes to physiological function. However, this will require full reconstruction of cells, which depends on high image resolution coupled with imaging of a large volume of tissue - which is currently beyond the technical abilities of histological tissue analysis, although methods are becoming available for such datasets to be generated (see Section 5.4.2).

5.2.4 The Limitations and Future Goals for StereoMate

The StereoMate workflow provides high-quality biological object representation, and efficient stereological sampling of those objects for analysis. Although analysis of synaptic puncta does provide important information on synapse density, and potentially other characteristics of synapses, this approach for studying neuronal connectivity is limited. Understanding neuronal connectivity requires the identification of the pre-synaptic neuron, the post-synaptic neuron, and the actual synaptic connections between the two. Whilst the approach used here in StereoMate provides gross information on synaptic puncta distributions, information concerning pre- and post-synaptic partners is absent. In terms of analysing connectivity, this method is therefore limited.

This limitation can be met in a number of ways. A number of different viral constructs, including monosynaptic tracing methods, can be used to specifically illuminate pre- and post-synaptic partners, which combined with synaptic illumination could in theory allow the identification of connectivity motifs (Wickersham et al., 2007; Ginger et al., 2013; Ghanem and Conzelmann, 2015). A second method, which provides specific reconstruction of eGFP molecules trans-synaptically between selected pre- and post-synaptic partners (GRASP, Feinberg et al., 2008) would provide illumination only of synaptic puncta of a certain circuit, and thus allow specific identification of synaptic puncta between selective pre- and post- synaptic partners. Finally, to establish connectivity sufficient volumes of tissue must be imaged, and recent clearing methodologies such as CLARITY (Chung et al., 2013; Tomer et al., 2014), and CUBIC (Susaki et al., 2014) can provide such datasets.

Although StereoMate possesses a key limitation in the context of neural circuit mapping, in terms of standard stereological assessment, the method excels. One future goal for StereoMate includes building a user-friendly interface for the algorithms, which provides flexibility in terms of the workflow, allowing fully supervised automated image analysis or unsupervised batch processing; the capacity to check results after the application of each algorithm; and the ability to select a specific set of image processing and analysis tools to run on a given dataset, depending on its requirements. This image analysis suite must also contain instructions and tools for the optimisation of the histological preparation and image processing and analysis workflow for new imaging problems, such as for new biological objects or new regions of interest. StereoMate aims to be an open-source, fully automated, stereological analysis platform which can be applied to any general image analysis problem. This tool is more than the algorithms it contains, and the ambition is to attempt to provide methods to enhance the histological preparation for experimenters

prior to imaging, and provide general guidance on image acquisition settings for subsequent image processing and analysis.

A second goal for StereoMate is to develop optimised staining procedures for a number of other important biological structures within the central nervous system. For example, extending the histological methods to other synaptic proteins would be of interest. Gephyrin, a structural component of symmetric synapses within the CNS (Choii and Ko, 2015) is one obvious target. Furthermore, targeting proteins only present at select synapses will help to divide synaptic puncta into more functional subgroups, and understanding the biological importance of these proteins and their distributions throughout synaptomes in different environmental, genetic and disease states can provide a wealth of information in terms of their function within the CNS (O'Rourke et al., 2012).

This method is not limited to synapses, as demonstrated in Chapter 4, where the method has been extended to microglial cells. Other biological objects of interest may include axons and dendrites of selected neurons, which may help to understand how their arborisation patterns vary in different states; mitochondria and other cellular organelles, and their distributions throughout cells of interest; and the CNS cells themselves such as neurons, glia and other support cells, to understand how their distributions, morphology and expression of various molecular markers varies in different biological states. This Thesis has only focussed on the dorsal horn, but this methodology could be extended to other CNS regions, and indeed to demonstrate its general applicability, this is desirable.

A general automated stereological tool for object analysis has widespread utility, and StereoMate's potential to improve the quality and scope of quantitative neuroanatomical data, whilst doing so with little user intervention, makes it a desirable tool for the quantitative neuroanatomist. Further work is required to demonstrate StereoMate's general applicability, but the foundations laid in this Thesis are a promising start for a potentially

valuable and helpful tool.

5.3 Peripheral Nerve Injury and its Consequences on the Dorsal Horn

This Thesis has explored dorsal horn synaptic distribution patterns and the effects of peripheral nerve injury on them. A brief overview of these results is given, a working model of the effects of nerve injury to synaptic puncta is delineated, and its potential consequences for neuropathy are explored.

The naïve dorsal horn displays unique synaptic distribution patterns, where the asymmetric post synaptic density protein PSD95 shows an increased density in lamina II, especially in lamina II inner, which is reduced in lamina III; and the general presynaptic marker SynaptoPhysin displays an increased density in lamina II which is maintained in lamina III. These results suggest the excitatory synaptic circuitry present in lamina II is more developed, and that lamina III contains a stronger inhibitory or modulatory synaptic component.

Peripheral nerve injury consistently caused a loss of PSD95+ synaptic puncta specifically in lamina II inner, 21 days post injury. This reduction in PSD95+ puncta was not matched by a loss of SynaptoPhysin puncta, which remained at baseline levels. Furthermore, analysis of primary afferent axons by utilising the Advillin-eGFP mouse showed no loss of primary afferent axons at this timepoint. Initially this result seemed at odds with the convention that pre- and post- synaptic structures should disappear at the same time. Yet the formation of a synapse occurs asymmetrically, with presynaptic boutons appearing at the initial stages (Ahmari et al., 2000; Ziv and Garner, 2004); and a previous time-course study of the dorsal horn using electron microscopy revealed an apparent loss

of synaptic connections at 10-14 days post sciatic nerve injury, but a delayed loss (30-40 days) of the actual presynaptic terminals themselves (Csillik and Knyihár-Csillik, 1981). This study added to previous suspicion that the selective synaptic loss in lamina II inner was due to effects on the non-peptidergic subclass of C fibre, which expresses IB4.

A second possibility could relate to the fact SynaptoPhysin may not be expressed ubiquitously throughout all asymmetric synapses. Previous reports suggest SynaptoPhysin is not located in peptidergic primary afferent terminals, although it was reported to be present in non-peptidergic terminals (Morris et al., 2005). SynaptoPorin, a second vesicle-associated protein, has been strongly localised to the superficial dorsal horn, and so may replace SynaptoPhysin in peptidergic afferents (Sun et al., 2006). However, the current evidence suggests SynaptoPhysin is expressed in IB4-binding afferents, although it remains unclear if it labels every terminal. It is conceivable that SynaptoPhysin only marks IB4-binding afferent terminals with specific post-synaptic fibres, but not others.

In order to reconcile the data obtained in the course of Chapter 3, the following model for the effects of peripheral nerve injury on synaptic connectivity in the dorsal horn is suggested. Following peripheral nerve injury which results in a complete transection and thus complete loss of peripheral innervation, DRG neurons react with the well described chromatolysis reaction, in an attempt to re-build the damaged nerve (Hanz and Fainzilber, 2006). This is driven by positive injury signals transported along the axon, as well as negative injury signals present as a lack of neurotrophin support. These signals alter the molecular expression profile of several DRG neuronal subtypes at the early stages (Michaelevski et al., 2010), with one conspicuous change being a lack of IB4 binding to the non-peptidergic subpopulation of C fibres(Molander et al., 1996; Bennett et al., 1998). As the injury continues to prevent the re-innervation of the injured DRG neurons, the lack of neurotrophic support (likely GDNF, see Molliver et al., 1997; Bennett et al., 1998)

begins to affected the injured IB4+ subpopulation of C fibres, such that between 2-3 weeks the IB4+ subset of C fibres withdraw their synaptic contacts (observed in this Thesis as a loss of PSD95 from lamina II inner), and speculatively, at later timepoints (30-40 days, Csillik and Knyihár-Csillik, 1981), lose their presynaptic terminals to phagocytosing cells. This may eventually lead to the full retraction of axonal arbors from these injured primary afferents, and possibly even their cell death.

Although this model fits with the facts, it does make some assumptions - which also offer a number of predictions. First, if the PSD95+ puncta loss represents a progressive degeneration of the IB4 subpopulation of C fibres in injured DRGs, then the loss of SynaptoPhysin would be expected at later timepoints, with the possible loss of eGFP signal in the Advillin-eGFP mouse, and even possibly a loss of DRG neurons, if this degeneration extends as far as neuronal cell death.

Second, it suggests that intervening with neurotrophic factors may help to prevent this degeneration, and thus prevent synapse loss, and speculatively axonal degeneration and/or neuronal cell death. Previous work has indicated that GDNF is a potent neurotrophin for the IB4+ subpopulation of primary afferent (Molliver et al., 1997), and its application after nerve injury can prevent the loss of IB4 binding to these neurons (Bennett et al., 1998). If the loss of IB4 binding reflects the start of this slow degenerating process due to a lack of GDNF trophic support, it would imply that GDNF is capable of retaining these neurons after nerve injury.

Whilst this effect may not directly impact the neuropathic pain experienced after nerve injury, a loss of neurons from the DRG would mark a permanent deficit in the individual, which may be extremely hard, if not impossible, to compensate for in terms of dorsal horn circuitry alterations. The IB4+ population provide a vital function in sensing mechanical nociceptive stimuli (Cavanaugh et al., 2009), and if these neurons are lost after nerve

injury, this could have profound and permanent effects on dorsal horn circuitry, not only in terms of mechanical pain sensing, but it may also impact on other modalities, given the complexity of the wiring within the dorsal horn.

5.3.1 Microglia

The glial cell reaction after nerve injury is well known, and the requirement for both astrocytic and microglial cell gliosis for the neuropathic pain phenotype is well described (Eriksson et al., 1993; Beggs and Salter, 2007; McMahon and Malcangio, 2009; Svensson and Brodin, 2010; Beggs and Salter, 2013). Chapter 4 attempted to test the hypothesis that microglia are responsible for the loss of PSD95 puncta seen 21 days post injury. As highlighted in the discussion of that Chapter, the intervention may not be sufficient to prevent the phagocytic function of microglia, however it does partially reverse the hypersensitivity, which is likely an effect on the microglial release of various important inflammatory molecules involved in the onset and maintenance of hypersensitivity (Raghavendra et al., 2003; Nutile-McMenemy et al., 2007; Padi and Kulkarni, 2008; Osikowicz et al., 2009; Nie et al., 2010).

The above working model may also suggest that the nerve injury paradigm was not allowed to run for long enough, since phagocytic actions on presynaptic terminals was described in one study to only occur at later time points (Csillik and Knyihár-Csillik, 1981). The data presented in Chapter 4 does not preclude microglia from having a role in synapse elimination after nerve injury, although if the model described above is correct, it would suggest the phagocytosis of presynaptic terminals is really just a consequence of the progressive degeneration of IB4+ primary afferents, rather than having a direct role in the initial breaking of synaptic contact of these cells with their post-synaptic dorsal horn partners.

The idea microglia do phagocytose these presynaptic components could still be explored, either by pharmacological (propentofylline) or genetic (a complement knock-out based strategy) means (Schafer et al., 2012). Whether answering this question is truly relevant to the underlying mechanism driving the loss of synaptic contacts is debatable, and thus initial work should clarify whether the above working model correctly predicts the mechanism for synapse loss after peripheral nerve injury, by administering GDNF to injured primary afferent neurons.

5.4 Concluding Remarks

Scientific research, including neuroscience, has always been heavily impacted by technological advances. For example, computing power has revolutionised the approach to scientific research, and tissue clearing methodologies are hoped to further our understanding of neuronal connectivity in neuroscience. Therefore, some concluding remarks aim to put the work of this Thesis into the context of some important technological advances in science and neuroscience.

5.4.1 Big Data

One important advance in the way scientific research is conducted, especially apparent in the past few decades, is the concept of Big Data. Computing technology and power has advanced exponentially since the inception of computing in the 1940s and 1950s, in accordance with Moore's Law (Moore, 1998). This has had profound consequences on the sheer volume of data which can be collected and processed, and thus has had a noticeable impact on the manner in which science is conducted (Hashem et al., 2014). Instead of the classical hypothesis-driven method so revered by scholars following Karl Popper's approach to science (Popper, 1959), large consortia of scientists have teamed together, not

just for a fishing trip, but a trawling expedition which produces a plethora of multivariate datasets ripe for data-mining - perfectly suited for the ever increasing computing power available.

This has impacted biology in several important ways. The human genome project (Lander et al., 2001) is a clear and impressive example of this type of scientific endeavour, and datasets on mouse, rat, nematode, drosophila, and several other species have now been isolated (Sullivan et al., 2013). Biology is full of many complex systems composed of a very large number of components, which can interact in complex ways, and so is perfectly suited for this approach. Proteomics, transcriptomics, metabolomics, and several other '-omics' fields have developed as a direct result of this Big Data approach, and are flourishing as a result of the continued improvements in computing power, data collection and data-mining methods.

One way the Big Data approach is being used in neuroscience is to understand the connectome, or the comprehensive set of neural connections present in a complete neural network (White et al., 1986; Seung and Sümbül, 2014; Fornito et al., 2015). This information, it is hoped, will unveil the complex algorithmic potential of such neural networks, and help in understanding how cognitive functions emerge from the structure and function of the brain. This is exceptionally difficult to achieve, not only because neural circuitry is only visible at the micrometer level, but also because the circuits in question can encompass components across the entire length and breadth of the brain. This is further complicated by the huge diversity of proteins expressed within the nervous system which, individually, subtly change an individual neuron's input-output response, but collectively result in huge non-linear shifts in neuronal excitability and signalling capacity. These expression patterns are in a constant state of flux, which will have a continued impact on neuronal signalling and ultimately connectivity throughout the life of the organism.

Connectome analysis is further compounded by the practical issues associated with data capture and analysis: the tissue is fragile, the image resolution must be high, and the data captured must cover large volumes; image analysis is only feasible via automated methods; and the issues associated with translating low-level pixel data into high-level object-, or even network-, level data are still apparent (Jain et al., 2010).

StereoMate, described and developed in Chapter 2, and discussed in this Chapter, has been designed to attempt to take advantage of the increasing computational power available. The algorithms used (especially the deconvolution algorithms) would not be practically useful without the profound improvements seen in computing power over the past half century. Moving forward with this approach, the aim is to collect and analyse increasingly complex multivariate datasets of the large number of synaptic puncta obtained, which fits with the objectives of the Big Data approach to scientific research. Ultimately, building a connectome map based on statistical methods, or through brute-force methods such as attributing each synaptic puncta to a pre- and post- synaptic neuron, would lead to the elusive connectome dataset, yet this feat is far from achievable. Whilst the approach used here does solve the issue of object recognition for simple and easily separated objects such as synapses, it is unclear whether it would work in the more complex images associated with connectome mapping - including, for example, synaptic structures with neuronal structures in their entirety - which has currently only seen some limited success at the electron microscope level (White et al., 1986; Seung and Sümbül, 2014)

5.4.2 Tissue Clearing

A key technological advance seen recently in neuroscience is a movement towards clearing methodologies aimed at increasing the depth of tissue that can be scrutinised as a single block under the microscope. These methods typically work by aligning the refractive

index of the tissue to that of the proteins within it, and fortuitously, that of glass (an RI of approximately 1.5). This is achieved either by immersing the tissue into a mixture of sugars or other chemicals to render the tissue transparent (i.e give it a homogenous refractive index), or more effectively, by first removal of the lipids followed by refractive index matching (Susaki et al., 2014; Tomer et al., 2014; Yang et al., 2014).

The most effective of these methods recently described (for reasons reviewed below) is the CLARITY methodology developed by Chung et al. (2013). This method is different from most other clearing methods in that the tissue is embedded into a formaldehyde-acrylamide hydrogel which provides structural support for the subsequent removal of lipids. Lipid removal is achieved without solvents (and therefore without dehydration) using SDS micelles, and the tissue can be interrogated with antibody probes in a similar fashion to tissue sections.

This method is superior to other clearing methods because the hydrogel scaffold provides significant structural support to the tissue during the subsequent processing steps, which may otherwise result in tissue damage. This method also provides the capability of continually interrogating the same system with different probes by eluting antibody binding with SDS, and re-staining the tissue with a new set of antibodies. In this way, the complex spatial distribution patterns of proteins within the tissue could be built up, which could provide valuable information for molecular phenotyping of different cells and cellular components.

This method has been employed as a preliminary step to extend the work presented in this Thesis to clear whole DRGs. The principle aim is to obtain whole DRG neuronal cell counts, to allow a thorough characterisation of the molecular expression profile of these neurons, as well as understand how these profiles, or indeed neuronal numbers, change as a result of peripheral nerve injury.

5.4.3 Conclusions

One of the key aims of modern neuroscience is linking neuronal connectivity and network function with the behavioural responses seen in individuals. Moving beyond analysis of synaptomes or cellular architectures is required to understand the function on the level of the network. It is appreciated that connectome maps will be necessary to link the function of the network with its effects on behaviour, and that this realisation will be made through considering the computational roles of specific circuits and networks within the CNS. Clues offered by measuring synapses and individual cells give insight into the potential solution to this problem, but to fully understand the system, data relating to the emergent neural networks that form and function within the CNS is essential. This challenge produces a larger semantic gap, whereby images not only have to be correctly annotated in terms of what structures they contain, but also linking these individual structures correctly into an accurate representation of the network of interconnections between different cellular elements. The new approaches being used, such as Big Data and Tissue Clearing methods, provide valuable tools which may lead towards this level of understanding.

The tools presented in this Thesis can also fit into this puzzle, since image analysis in large regions of interest, of biological objects illuminated with high fidelity, with measurements free from systematic biases and performed in an automated fashion, are essential requirements to begin to tackle the imaging problems present in tissue clearing experiments. This form of analysis is Big Data in action, as the movement from vast arrays of pixel data to meaningful knowledge at the object level is an essential data-mining mechanism performed by the StereoMate toolkit. These tools can potentially provide a wealth of information on the neuronal circuitry involved in neuropathic pain, and help us to understand the consequences of peripheral nerve injury, and provide novels means of

addressing the challenge of chronic neuropathic pain.

References

Abe, N. and V. Cavalli: 2008, 'Nerve injury signaling.'. *Current opinion in neurobiology* **18**(3), 276–83.

Abercrombie, M.: 1946, 'Estimation of nuclear population from microtome sections.'. *The Anatomical record* **94**, 239–47.

Adrian, E. D.: 1930, 'The Effects of Injury on Mammalian Nerve Fibres'. *Proceedings of the Royal Society of London B: Biological Sciences* **106**(747), 596–618.

Afrah, A. W., A. Fiskå, J. Gjerstad, H. Gustafsson, A. Tjølsen, L. Olgart, C. O. Stiller, K. Hole, and E. Brodin: 2002, 'Spinal substance P release in vivo during the induction of long-term potentiation in dorsal horn neurons.'. *Pain* **96**(1-2), 49–55.

Agwuh, K. N. and A. MacGowan: 2006, 'Pharmacokinetics and pharmacodynamics of the tetracyclines including glycylcyclines.'. *The Journal of antimicrobial chemotherapy* **58**(2), 256–65.

Ahmari, S. E., J. Buchanan, and S. J. Smith: 2000, 'Assembly of presynaptic active zones from cytoplasmic transport packets.'. *Nature neuroscience* **3**(5), 445–51.

Ajami, B., J. L. Bennett, C. Krieger, W. Tetzlaff, and F. M. V. Rossi: 2007, 'Local self-renewal can sustain CNS microglia maintenance and function throughout adult life.'. *Nature neuroscience* **10**(12), 1538–43.

Anderson, C. R., K. W. Ashwell, H. Collewijn, A. Conta, A. Harvey, C. Heise, S. Hodgetts, G. Holstege, J. R. Keast, S. McHanwell, E. M. McLachlan, G. Plant, O. Scremin, A. Sidhu, and D. Stelzner: 2009, *The Spinal Cord: A Christopher and Dana Reeve Foundation Text and Atlas*. Elsevier.

Andres, K. H.: 1975, 'Morphological criteria for the differentiation of synapses in vertebrates.'. *Journal of neural transmission* **Suppl 12**, 1–37.

Arleo, A., T. Nieus, M. Bezzi, A. D'Errico, E. D'Angelo, and O. J.-M. D. Coenen: 2010, 'How synaptic release probability shapes neuronal transmission: information-theoretic analysis in a cerebellar granule cell.'. *Neural computation* **22**(8), 2031–58.

Azkue, J. J., X.-G. Liu, M. Zimmermann, and J. Sandkühler: 2003, 'Induction of long-term potentiation of C fibre-evoked spinal field potentials requires recruitment of group I, but not group II/III metabotropic glutamate receptors.'. *Pain* **106**(3), 373–9.

Badrinath, R., G. Lin, M.-A. Abdul-Karim, O. Al-Kofahi, K. Al-Kofahi, W. Shain, D. H. Szarowski, and J. N. Turner: 2006, 'Automated Three-Dimensional Image Analysis Methods for Confocal Microscopy'. In: *Handbook of Biological Confocal Microscopy*. pp. 316–337.

Bailey, A. L. and A. Ribeiro-da Silva: 2006, 'Transient loss of terminals from non-peptidergic nociceptive fibers in the substantia gelatinosa of spinal cord following chronic constriction injury of the sciatic nerve.'. *Neuroscience* **138**(2), 675–90.

Bannister, K., S. Sikandar, C. S. Bauer, A. C. Dolphin, F. Porreca, and A. H. Dickenson: 2011, 'Pregabalin suppresses spinal neuronal hyperexcitability and visceral hypersensitivity in the absence of peripheral pathophysiology.'. *Anesthesiology* **115**(1), 144–52.

Barclay, J., A. K. Clark, P. Ganju, C. Gentry, S. Patel, G. Wotherspoon, F. Buxton, C. Song, J. Ullah, J. Winter, A. Fox, S. Bevan, and M. Malcangio: 2007, 'Role of the cysteine protease cathepsin S in neuropathic hyperalgesia.'. *Pain* **130**(3), 225–34.

Bardoni, R., A. Ghirri, M. Zonta, C. Betelli, G. Vitale, V. Ruggieri, M. Sandrini, and G. Carmignoto: 2010, 'Glutamate-mediated astrocyte-to-neuron signalling in the rat dorsal horn.'. *The Journal of physiology* **588**(Pt 5), 831–46.

Bardoni, R., T. Takazawa, C.-K. Tong, P. Choudhury, G. Scherrer, and A. B. Macdermott: 2013, 'Pre- and postsynaptic inhibitory control in the spinal cord dorsal horn.'. *Annals of the New York Academy of Sciences* **1279**, 90–6.

Baron, R.: 2009, 'Neuropathic pain: a clinical perspective.'. *Handbook of experimental pharmacology* (194), 3–30.

Baron, R., A. Binder, and G. Wasner: 2010, 'Neuropathic pain: diagnosis, pathophysiological mechanisms, and treatment.'. *The Lancet. Neurology* **9**(8), 807–19.

Basbaum, A. I. and H. L. Fields: 1979, 'The origin of descending pathways in the dorsolateral funiculus of the spinal cord of the cat and rat: further studies on the anatomy of pain modulation.'. *The Journal of comparative neurology* **187**(3), 513–31.

Basbaum, A. I. and P. D. Wall: 1976, 'Chronic changes in the response of cells in adult cat dorsal horn following partial deafferentation: the appearance of responding cells in a previously non-responsive region.'. *Brain research* **116**(2), 181–204.

Bassand, P., A. Bernard, A. Rafiki, D. Gayet, and M. Khrestchatisky: 1999, 'Differential interaction of the tSXV motifs of the NR1 and NR2A NMDA receptor subunits with PSD-95 and SAP97.'. *The European journal of neuroscience* **11**(6), 2031–43.

Battaglia, G. and A. Rustioni: 1988, 'Coexistence of glutamate and substance P in dorsal root ganglion neurons of the rat and monkey.'. *The Journal of comparative neurology* **277**(2), 302–12.

Bayés, A., M. O. Collins, M. D. R. Croning, L. N. van de Lagemaat, J. S. Choudhary, and S. G. N. Grant: 2012, 'Comparative study of human and mouse postsynaptic proteomes finds high compositional conservation and abundance differences for key synaptic proteins.'. *PloS one* **7**(10), e46683.

Bayés, A., L. N. van de Lagemaat, M. O. Collins, M. D. R. Croning, I. R. Whittle, J. S. Choudhary, and S. G. N. Grant: 2011, 'Characterization of the proteome, diseases and evolution of the human postsynaptic density.'. *Nature neuroscience* **14**(1), 19–21.

Bee, L. A. and A. H. Dickenson: 2007, 'Rostral ventromedial medulla control of spinal sensory processing in normal and pathophysiological states.'. *Neuroscience* **147**(3), 786–93.

Beggs, S. and M. W. Salter: 2007, 'Stereological and somatotopic analysis of the spinal microglial response to peripheral nerve injury.'. *Brain, behavior, and immunity* **21**(5), 624–33.

Beggs, S. and M. W. Salter: 2013, 'The known knowns of microglia-neuronal signalling in neuropathic pain.'. *Neuroscience letters* **557 Pt A**, 37–42.

Bekkers, J. M., G. B. Richerson, and C. F. Stevens: 1990, 'Origin of variability in quantal size in cultured hippocampal neurons and hippocampal slices.'. *Proceedings of the National Academy of Sciences of the United States of America* **87**(14), 5359–62.

Bemben, M. A., S. L. Shipman, R. A. Nicoll, and K. W. Roche: 2015, 'The cellular and molecular landscape of neuroligins.'. *Trends in neurosciences* **38**(8), 496–505.

Bennett, D. L., G. J. Michael, N. Ramachandran, J. B. Munson, S. Averill, Q. Yan, S. B. McMahon, and J. V. Priestley: 1998, 'A distinct subgroup of small DRG cells express GDNF receptor components and GDNF is protective for these neurons after nerve injury.'. *The Journal of neuroscience : the official journal of the Society for Neuroscience* **18**(8), 3059–72.

Bennett, M.: 2001, *History of the Synapse*. Amsterdam: Overseas Publishers Association, first edit edition.

Bertero, M. and P. Boccacci: 1998, *Introduction to Inverse Problems in Imaging*. Bath, UK: IOP Publishing.

Binns, B. C., Y. Huang, V. M. Goettl, K. V. Hackshaw, and R. L. Stephens: 2005, 'Glutamate uptake is attenuated in spinal deep dorsal and ventral horn in the rat spinal nerve ligation model.'. *Brain research* **1041**(1), 38–47.

Blackbeard, J., K. P. O'Dea, V. C. J. Wallace, A. Segerdahl, T. Pheby, M. Takata, M. J. Field, and A. S. C. Rice: 2007, 'Quantification of the rat spinal microglial response to peripheral nerve injury as revealed by immunohistochemical image analysis and flow cytometry.'. *Journal of neuroscience methods* **164**(2), 207–17.

Blackman, A. V., T. Abrahamsson, R. P. Costa, T. Lalanne, and P. J. Sjöström: 2013, 'Target-cell-specific short-term plasticity in local circuits.'. *Frontiers in synaptic neuroscience* **5**, 11.

Bliss, T. V. and A. R. Gardner-Medwin: 1973, 'Long-lasting potentiation of synaptic transmission in the dentate area of the unanaestetized rabbit following stimulation of the perforant path.'. *The Journal of physiology* **232**(2), 357–74.

Bliss, T. V. P., G. L. Collingridge, and R. G. M. Morris: 2004, *Long-term Potentiation: Enhancing Neuroscience for 30 Years*. Oxford University Press.

Bolam, J.: 1992, *Experimental Neuroanatomy: A Practical Approach*. Oxford University Press.

Borst, J. G. G.: 2010, 'The low synaptic release probability in vivo.'. *Trends in neurosciences* **33**(6), 259–66.

Branco, T. and K. Staras: 2009, 'The probability of neurotransmitter release: variability and feedback control at single synapses.'. *Nature reviews. Neuroscience* **10**(5), 373–83.

Briggman, K. L. and W. Denk: 2006, 'Towards neural circuit reconstruction with volume electron microscopy techniques.'. *Current opinion in neurobiology* **16**(5), 562–70.

Brodin, L., L. Bakeeva, and O. Shupliakov: 1999, 'Presynaptic mitochondria and the temporal pattern of neurotransmitter release.'. *Philosophical transactions of the Royal Society of London. Series B, Biological sciences* **354**(1381), 365–72.

Burette, A., F. Collman, K. D. Micheva, S. J. Smith, and R. J. Weinberg: 2015, 'Knowing a synapse when you see one'. *Frontiers in Neuroanatomy* **9**, 100.

Burger, W. and M. J. Burge: 2008, *Digital Image Processing An algorithmic introduction using Java*, Texts in Computer Science. New York: Springer.

Burgess, S. E., L. R. Gardell, M. H. Ossipov, T. P. Malan, T. W. Vanderah, J. Lai, and F. Porreca: 2002, 'Time-dependent descending facilitation from the rostral ventromedial medulla maintains, but does not initiate, neuropathic pain.'. *The Journal of neuroscience : the official journal of the Society for Neuroscience* **22**(12), 5129–36.

Burstein, R., R. J. Dado, and G. J. Giesler: 1990, 'The cells of origin of the spinothalamic tract of the rat: a quantitative reexamination.'. *Brain research* **511**(2), 329–37.

Butovsky, O., M. P. Jedrychowski, C. S. Moore, R. Cialic, A. J. Lanser, G. Gabriely, T. Koeglsperger, B. Dake, P. M. Wu, C. E. Doykan, Z. Fanek, L. Liu, Z. Chen, J. D. Rothstein, R. M. Ransohoff, S. P. Gygi, J. P. Antel, and H. L. Weiner: 2014, 'Identification of a unique TGF-β-dependent molecular and functional signature in microglia.'. *Nature neuroscience* **17**(1), 131–43.

Cahoy, J. D., B. Emery, A. Kaushal, L. C. Foo, J. L. Zamanian, K. S. Christopherson, Y. Xing, J. L. Lubischer, P. A. Krieg, S. A. Krupenko, W. J. Thompson, and B. A. Barres: 2008, 'A transcriptome database for astrocytes, neurons, and oligodendrocytes: a new resource for understanding brain development and function.'. *The Journal of neuroscience : the official journal of the Society for Neuroscience* **28**(1), 264–78.

Cajal, S. R. Y.: 1894, 'The Croonian Lecture: La Fine Structure des Centres Nerveux'. *Proceedings of the Royal Society of London* **55**(331-335), 444–468.

Cannell, M. B., A. McMorland, and C. Soeller: 2006, 'Image Enhancement by Deconvolution'. In: J. Pawley (ed.): *Handbook of Biological Confocal Microscopy*. Springer US, pp. 488–500.

Cao, H. and Y.-Q. Zhang: 2008, 'Spinal glial activation contributes to pathological pain states.'. *Neuroscience and biobehavioral reviews* **32**(5), 972–83.

Carlin, R. K., D. J. Grab, R. S. Cohen, and P. Siekevitz: 1980, 'Isolation and characterization of postsynaptic densities from various brain regions: enrichment of different types of postsynaptic densities.'. *The Journal of cell biology* **86**(3), 831–45.

Carr, P. A., T. Yamamoto, G. Karmy, K. G. Baimbridge, and J. I. Nagy: 1989, 'Analysis of parvalbumin and calbindin D28k-immunoreactive neurons in dorsal root ganglia of rat in relation to their cytochrome oxidase and carbonic anhydrase content.'. *Neuroscience* **33**(2), 363–71.

Castro-Lopes, J. M., A. Coimbra, G. Grant, and J. Arvidsson: 1990, 'Ultrastructural changes of the central scalloped (C1) primary afferent endings of synaptic glomeruli in the substantia gelatinosa Rolandi of the rat after peripheral neurotomy.'. *Journal of neurocytology* **19**(3), 329–37.

Castro-Lopes, J. M., I. Tavares, and A. Coimbra: 1993, 'GABA decreases in the spinal cord dorsal horn after peripheral neurectomy.'. *Brain research* **620**(2), 287–91.

Cavanaugh, D. J., H. Lee, L. Lo, S. D. Shields, M. J. Zylka, A. I. Basbaum, and D. J. Anderson: 2009, 'Distinct subsets of unmyelinated primary sensory fibers mediate behavioral responses to noxious thermal and mechanical stimuli.'. *Proceedings of the National Academy of Sciences of the United States of America* **106**(22), 9075–80.

Cervero, F., J. M. A. Laird, and E. García-Nicas: 2003, 'Secondary hyperalgesia and presynaptic inhibition: an update.'. *European journal of pain (London, England)* **7**(4), 345–51.

Chaplan, S. R., F. W. Bach, J. W. Pogrel, J. M. Chung, and T. L. Yaksh: 1994, 'Quantitative assessment of tactile allodynia in the rat paw.'. *Journal of neuroscience methods* **53**(1), 55–63.

Chen, S.-R., L. Zhu, H. Chen, L. Wen, G. Laumet, and H.-L. Pan: 2014, 'Increased spinal cord Na+ K+ 2Cl- cotransporter-1 (NKCC1) activity contributes to impairment of synaptic inhibition in paclitaxel-induced neuropathic pain.'. *The Journal of biological chemistry* **289**(45), 31111–20.

Chklovskii, D. B., S. Vitaladevuni, and L. K. Scheffer: 2010, 'Semi-automated reconstruction of neural circuits using electron microscopy.'. *Current opinion in neurobiology* **20**(5), 667–75.

Cho, K. O., C. A. Hunt, and M. B. Kennedy: 1992, 'The rat brain postsynaptic density fraction contains a homolog of the Drosophila discs-large tumor suppressor protein.'. *Neuron* **9**(5), 929–42.

Choii, G. and J. Ko: 2015, 'Gephyrin: a central GABAergic synapse organizer.'. *Experimental & molecular medicine* **47**, e158.

Chou, A.-K., R. Muhammad, S.-M. Huang, J.-T. Chen, C.-L. Wu, C.-R. Lin, T.-H. Lee, S.-H. Lin, C.-Y. Lu, and L.-C. Yang: 2002, 'Altered synaptophysin expression in the rat spinal cord after chronic constriction injury of sciatic nerve.'. *Neuroscience letters* **333**(3), 155–8.

Chung, K., D. L. McNeill, C. E. Hulsebosch, and R. E. Coggeshall: 1989, 'Changes in dorsal horn synaptic disc numbers following unilateral dorsal rhizotomy.'. *The Journal of comparative neurology* **283**(4), 568–77.

Chung, K., J. Wallace, S.-Y. Kim, S. Kalyanasundaram, A. S. Andalman, T. J. Davidson, J. J. Mirzabekov, K. A. Zalocusky, J. Mattis, A. K. Denisin, S. Pak, H. Bernstein, C. Ramakrishnan, L. Grosenick, V. Gradinaru, and K. Deisseroth: 2013, 'Structural and molecular interrogation of intact biological systems.'. *Nature* **497**(7449), 332–7.

Churchland, P. S.: 2008, 'The impact of neuroscience on philosophy.'. *Neuron* **60**(3), 409–11.

Cirillo, G., C. Cavaliere, M. R. Bianco, A. De Simone, A. M. Colangelo, S. Sellitti, L. Alberghina, and M. Papa: 2010, 'Intrathecal NGF administration reduces reactive astrocytosis and changes neurotrophin receptors expression pattern in a rat model of neuropathic pain.'. *Cellular and molecular neurobiology* **30**(1), 51–62.

Clark, A. K., D. Gruber-Schoffnegger, R. Drdla-Schutting, K. J. Gerhold, M. Malcangio, and J. Sandkühler: 2015, 'Selective activation of microglia facilitates synaptic strength.'. *The Journal of neuroscience : the official journal of the Society for Neuroscience* **35**(11), 4552–70.

Clark, A. K. and M. Malcangio: 2014, 'Fractalkine/CX3CR1 signaling during neuropathic pain.'. *Frontiers in cellular neuroscience* **8**, 121.

Clark, A. K., A. A. Staniland, F. Marchand, T. K. Y. Kaan, S. B. McMahon, and M. Malcangio: 2010, 'P2X7-dependent release of interleukin-1beta and nociception in the spinal cord following lipopolysaccharide.'. *The Journal of neuroscience : the official journal of the Society for Neuroscience* **30**(2), 573–82.

Clark, A. K., P. K. Yip, J. Grist, C. Gentry, A. A. Staniland, F. Marchand, M. Dehvari, G. Wotherspoon, J. Winter, J. Ullah, S. Bevan, and M. Malcangio: 2007, 'Inhibition of spinal microglial cathepsin S for the reversal of neuropathic pain.'. *Proceedings of the National Academy of Sciences of the United States of America* **104**(25), 10655–60.

Clark, A. K., P. K. Yip, and M. Malcangio: 2009, 'The liberation of fractalkine in the dorsal horn requires microglial cathepsin S.'. *The Journal of neuroscience : the official journal of the Society for Neuroscience* **29**(21), 6945–54.

Coderre, T. J. and R. Melzack: 1992, 'The role of NMDA receptor-operated calcium channels in persistent nociception after formalin-induced tissue injury.'. *The Journal of neuroscience : the official journal of the Society for Neuroscience* **12**(9), 3671–5.

Cohen, R. S., F. Blomberg, K. Berzins, and P. Siekevitz: 1977, 'The structure of post-synaptic densities isolated from dog cerebral cortex. I. Overall morphology and protein composition.'. *The Journal of cell biology* **74**(1), 181–203.

Colangelo, A. M., M. R. Bianco, L. Vitagliano, C. Cavaliere, G. Cirillo, L. De Gioia, D. Diana, D. Colombo, C. Redaelli, L. Zaccaro, G. Morelli, M. Papa, P. Sarmientos, L. Alberghina, and E. Martegani: 2008, 'A new nerve growth factor-mimetic peptide active on neuropathic pain in rats.'. *The Journal of neuroscience : the official journal of the Society for Neuroscience* **28**(11), 2698–709.

Collman, F., J. Buchanan, K. D. Phend, K. D. Micheva, R. J. Weinberg, and S. J. Smith: 2015, 'Mapping synapses by conjugate light-electron array tomography.'. *The Journal of neuroscience : the official journal of the Society for Neuroscience* **35**(14), 5792–807.

Colovic, M. and S. Caccia: 2003, 'Liquid chromatographic determination of minocycline in brain-to-plasma distribution studies in the rat.'. *Journal of chromatography. B, Analytical technologies in the biomedical and life sciences* **791**(1-2), 337–43.

Conchello, J.-A. and J. W. Lichtman: 2005, 'Optical sectioning microscopy.'. *Nature methods* **2**(12), 920–31.

Costigan, M., K. Befort, L. Karchewski, R. S. Griffin, D. D'Urso, A. Allchorne, J. Sitarski, J. W. Mannion, R. E. Pratt, and C. J. Woolf: 2002, 'Replicate high-density rat genome oligonucleotide microarrays reveal hundreds of regulated genes in the dorsal root ganglion after peripheral nerve injury.'. *BMC neuroscience* **3**, 16.

Cotman, C. W., G. Banker, L. Churchill, and D. Taylor: 1974, 'Isolation of postsynaptic densities from rat brain.'. *The Journal of cell biology* **63**(2 Pt 1), 441–55.

Coull, J. A. M., S. Beggs, D. Boudreau, D. Boivin, M. Tsuda, K. Inoue, C. Gravel, M. W. Salter, and Y. De Koninck: 2005, 'BDNF from microglia causes the shift in neuronal anion gradient underlying neuropathic pain.'. *Nature* **438**(7070), 1017–21.

Coull, J. A. M., D. Boudreau, K. Bachand, S. A. Prescott, F. Nault, A. Sík, P. De Koninck, and Y. De Koninck: 2003, 'Trans-synaptic shift in anion gradient in spinal lamina I neurons as a mechanism of neuropathic pain.'. *Nature* **424**(6951), 938–42.

Cowan, W. and E. Kandel: 2001, 'A Brief History of Synapses and Synaptic Transmission'. In: W. Cowan, T. Sudhof, and C. Stevens (eds.): *Synapses*. Baltimore: Johns Hopkins University Press, first edition, Chapt. First Chap, pp. 1–88.

Cowan, W. M., D. H. Harter, and E. R. Kandel: 2000, 'The emergence of modern neuroscience: some implications for neurology and psychiatry.'. *Annual review of neuroscience* **23**, 343–91.

Cowan, W. M., T. C. Südhof, and C. F. Stevens: 2001, *Synapses*. JHU Press.

Cox, D. and C. Donnelly: 2011, *Principles of Applied Statistics*. Cambridge University Press.

Craig, A. D.: 2003, 'A new view of pain as a homeostatic emotion.'. *Trends in neurosciences* **26**(6), 303–7.

Craig, A. M. and Y. Kang: 2007, 'Neurexin-neuroligin signaling in synapse development.'. *Current opinion in neurobiology* **17**(1), 43–52.

Csillik, B. and E. Knyihár-Csillik: 1981, 'Regenerative synaptoneogenesis in the Mammalian spinal cord: dynamics of synaptochemical restoration in the Rolando Substance after transganglionic degenerative atrophy.'. *Journal of neural transmission* **52**(4), 303–17.

Csillik, B. and E. Knyihár-Csillik: 1982, 'Reversibility of microtubule inhibitor-induced transganglionic degenerative atrophy of central terminals of primary nociceptive neurons.'. *Neuroscience* **7**(5), 1149–54.

Dahm, R.: 2005, 'Friedrich Miescher and the discovery of DNA.'. *Developmental biology* **278**(2), 274–88.

D'Amico, F., E. Skarmoutsou, and F. Stivala: 2009, 'State of the art in antigen retrieval for immunohistochemistry.'. *Journal of immunological methods* **341**(1-2), 1–18.

Dani, A., B. Huang, J. Bergan, C. Dulac, and X. Zhuang: 2010, 'Superresolution imaging of chemical synapses in the brain.'. *Neuron* **68**(5), 843–56.

Davalos, D., J. Grutzendler, G. Yang, J. V. Kim, Y. Zuo, S. Jung, D. R. Littman, M. L. Dustin, and W.-B. Gan: 2005, 'ATP mediates rapid microglial response to local brain injury in vivo.'. *Nature neuroscience* **8**(6), 752–8.

Davenport, H. W.: 1991, 'Early history of the concept of chemical transmission of the nerve impulse.'. *The Physiologist* **34**(4), 129, 178–90.

Davidovits, P. and M. D. Egger: 1969, 'Scanning laser microscope.'. *Nature* **223**(5208), 831.

De Biasi, S. and A. Rustioni: 1988, 'Glutamate and substance P coexist in primary afferent terminals in the superficial laminae of spinal cord.'. *Proceedings of the National Academy of Sciences of the United States of America* **85**(20), 7820–4.

De Camilli, P., V. Haucke, K. Takei, and E. Mugnaini: 2001, 'The Structure of Synapses'. In: W. Cowan, T. Sudhof, and C. F. Stevens (eds.): *Synapses*. Baltimore: Johns Hopkins University Press, pp. 89–134.

De Felice, M., R. Sanoja, R. Wang, L. Vera-Portocarrero, J. Oyarzo, T. King, M. H. Ossipov, T. W. Vanderah, J. Lai, G. O. Dussor, H. L. Fields, T. J. Price, and F. Porreca: 2011, 'Engagement of descending inhibition from the rostral ventromedial medulla protects against chronic neuropathic pain.'. *Pain* **152**(12), 2701–9.

de Jong, A. P. H. and D. Fioravante: 2014, 'Translating neuronal activity at the synapse: presynaptic calcium sensors in short-term plasticity.'. *Frontiers in cellular neuroscience* **8**, 356.

De Robertis, E. D. and H. S. Bennett: 1955, 'Some features of the submicroscopic morphology of synapses in frog and earthworm.'. *The Journal of biophysical and biochemical cytology* **1**(1), 47–58.

Decosterd, I. and C. J. Woolf: 2000, 'Spared nerve injury: an animal model of persistent peripheral neuropathic pain.'. *Pain* **87**(2), 149–58.

Denk, W., J. H. Strickler, and W. W. Webb: 1990, 'Two-photon laser scanning fluorescence microscopy.'. *Science (New York, N.Y.)* **248**(4951), 73–6.

Derjean, D., S. Bertrand, G. Le Masson, M. Landry, V. Morisset, and F. Nagy: 2003, 'Dynamic balance of metabotropic inputs causes dorsal horn neurons to switch functional states.'. *Nature neuroscience* **6**(3), 274–81.

Dickenson, A. H.: 1990, 'A cure for wind up: NMDA receptor antagonists as potential analgesics.'. *Trends in pharmacological sciences* **11**(8), 307–9.

Dickenson, A. H.: 1995, 'Spinal cord pharmacology of pain.'. *British journal of anaesthesia* **75**(2), 193–200.

Dickenson, A. H. and A. F. Sullivan: 1987, 'Evidence for a role of the NMDA receptor in the frequency dependent potentiation of deep rat dorsal horn nociceptive neurones following C fibre stimulation.'. *Neuropharmacology* **26**(8), 1235–8.

Dittman, J. S., A. C. Kreitzer, and W. G. Regehr: 2000, 'Interplay between facilitation, depression, and residual calcium at three presynaptic terminals.'. *The Journal of neuroscience : the official journal of the Society for Neuroscience* **20**(4), 1374–85.

D'Mello, R. and A. H. Dickenson: 2008, 'Spinal cord mechanisms of pain.'. *British journal of anaesthesia* **101**(1), 8–16.

Dobrunz, L. E. and C. F. Stevens: 1997, 'Heterogeneity of release probability, facilitation, and depletion at central synapses.'. *Neuron* **18**(6), 995–1008.

Dostrovsky, J. and A. Craig: 2013, 'Ascending Projection Systems'. In: S. B. McMahon, I. Tracey, M. Koltzenburg, and D. Turk (eds.): *Textbook of Pain*. Elsevier Saunders, sixth edition, Chapt. 12, pp. 182–197.

Dougherty, P. M. and W. D. Willis: 1992, 'Enhanced responses of spinothalamic tract neurons to excitatory amino acids accompany capsaicin-induced sensitization in the monkey.'. *The Journal of neuroscience : the official journal of the Society for Neuroscience* **12**(3), 883–94.

Dougherty, R. P.: 2005, 'Extensions of DAMAS and Benefits and Limitations of Deconvolution in Beamforming'. *AIAA* **11th**, 2005–2961.

Drdla, R. and J. Sandkuhler: 2009, 'Long-Term Potentiation in Superficial Spinal Dorsal Horn: A Pain Amplifier'. In: M. Malcangio (ed.): *Synaptic Plasticity in Pain*. Springer New York, Chapt. nine, pp. 201–218.

Duan, B., L. Cheng, S. Bourane, O. Britz, C. Padilla, L. Garcia-Campmany, M. Krashes, W. Knowlton, T. Velasquez, X. Ren, S. E. Ross, B. B. Lowell, Y. Wang, M. Goulding, and Q. Ma: 2014, 'Identification of spinal circuits transmitting and gating mechanical pain.'. *Cell* **159**(6), 1417–32.

Dubner, R., D. R. Kenshalo, W. Maixner, M. C. Bushnell, and J. L. Oliveras: 1989, 'The correlation of monkey medullary dorsal horn neuronal activity and the perceived intensity of noxious heat stimuli.'. *Journal of neurophysiology* **62**(2), 450–7.

Dumitriu, D., S. I. Berger, C. Hamo, Y. Hara, M. Bailey, A. Hamo, Y. S. Grossman, W. G. Janssen, and J. H. Morrison: 2012, 'Vamping: stereology-based automated quantification of fluorescent puncta size and density.'. *Journal of neuroscience methods* **209**(1), 97–105.

Dworkin, R. H., A. B. O'Connor, J. Audette, R. Baron, G. K. Gourlay, M. L. Haanpää, J. L. Kent, E. J. Krane, A. A. Lebel, R. M. Levy, S. C. Mackey, J. Mayer, C. Miaskowski, S. N. Raja, A. S. C. Rice, K. E. Schmader, B. Stacey, S. Stanos, R.-D. Treede, D. C. Turk, G. A. Walco, and C. D. Wells: 2010, 'Recommendations for the pharmacological management of neuropathic pain: an overview and literature update.'. *Mayo Clinic proceedings* **85**(3 Suppl), S3–14.

Ebeling, W., N. Hennrich, M. Klockow, H. Metz, H. D. Orth, and H. Lang: 1974, 'Proteinase K from Tritirachium album Limber.'. *European journal of biochemistry / FEBS* **47**(1), 91–7.

Eccles, J. C.: 1982, 'The synapse: from electrical to chemical transmission.'. *Annual review of neuroscience* **5**, 325–39.

Eccles, J. C., R. M. Eccles, and F. Magni: 1961, 'Central inhibitory action attributable to presynaptic depolarization produced by muscle afferent volleys.'. *The Journal of physiology* **159**, 147–66.

Eccles, J. C., R. Schmidt, and W. D. Willis: 1963, 'PHARMACOLOGICAL STUDIES ON PRESYNAPTIC INHIBITION.'. *The Journal of physiology* **168**, 500–30.

Eccles, J. C., R. F. Schmidt, and W. D. Willis: 1962, 'Presynaptic inhibition of the spinal monosynaptic reflex pathway.'. *The Journal of physiology* **161**, 282–97.

Edwards, F. A., A. Konnerth, and B. Sakmann: 1990, 'Quantal analysis of inhibitory synaptic transmission in the dentate gyrus of rat hippocampal slices: a patch-clamp study.'. *The Journal of physiology* **430**, 213–49.

Egner, A. and S. Hell: 2006, 'Aberrations in Confocal and Multi-Photon Fluorescence Microscopy Induced by Refractive Index Mismatch'. In: J. Pawley (ed.): *Handbook of Biological Confocal Microscopy*. Springer US, Chapt. 20, pp. 404–413.

Erblich, B., L. Zhu, A. M. Etgen, K. Dobrenis, and J. W. Pollard: 2011, 'Absence of colony stimulation factor-1 receptor results in loss of microglia, disrupted brain development and olfactory deficits.'. *PloS one* **6**(10), e26317.

Eriksson, N. P., J. K. Persson, M. Svensson, J. Arvidsson, C. Molander, and H. Aldskogius: 1993, 'A quantitative analysis of the microglial cell reaction in central primary sensory projection territories following peripheral nerve injury in the adult rat.'. *Experimental brain research* **96**(1), 19–27.

Ernfors, P., K. F. Lee, J. Kucera, and R. Jaenisch: 1994, 'Lack of neurotrophin-3 leads to deficiencies in the peripheral nervous system and loss of limb proprioceptive afferents.'. *Cell* **77**(4), 503–12.

Familian, A., P. Eikelenboom, and R. Veerhuis: 2007, 'Minocycline does not affect amyloid beta phagocytosis by human microglial cells.'. *Neuroscience letters* **416**(1), 87–91.

Feinberg, E. H., M. K. Vanhoven, A. Bendesky, G. Wang, R. D. Fetter, K. Shen, and C. I. Bargmann: 2008, 'GFP Reconstitution Across Synaptic Partners (GRASP) defines cell contacts and synapses in living nervous systems.'. *Neuron* **57**(3), 353–63.

Fendrick, S. E., K. R. Miller, and W. J. Streit: 2005, 'Minocycline does not inhibit microglia proliferation or neuronal regeneration in the facial nucleus following crush injury.'. *Neuroscience letters* **385**(3), 220–3.

Fenselau, H., B. Heinke, and J. Sandkühler: 2011, 'Heterosynaptic long-term potentiation at GABAergic synapses of spinal lamina I neurons.'. *The Journal of neuroscience : the official journal of the Society for Neuroscience* **31**(48), 17383–91.

Fiacco, T. A. and K. D. McCarthy: 2006, 'Astrocyte calcium elevations: properties, propagation, and effects on brain signaling.'. *Glia* **54**(7), 676–90.

Finnerup, N. B., S. H. Sindrup, and T. S. Jensen: 2010, 'The evidence for pharmacological treatment of neuropathic pain.'. *Pain* **150**(3), 573–81.

Fioravante, D. and W. G. Regehr: 2011, 'Short-term forms of presynaptic plasticity.'. *Current opinion in neurobiology* **21**(2), 269–74.

Flores, J. A., F. El Banoua, B. Galán-Rodríguez, and E. Fernandez-Espejo: 2004, 'Opiate anti-nociception is attenuated following lesion of large dopamine neurons of the peri-aqueductal grey: critical role for D1 (not D2) dopamine receptors.'. *Pain* **110**(1-2), 205–14.

Fornito, A., A. Zalesky, and M. Breakspear: 2015, 'The connectomics of brain disorders'. *Nature Reviews Neuroscience* **16**(3), 159–172.

Forti, L., M. Bossi, A. Bergamaschi, A. Villa, and A. Malgaroli: 1997, 'Loose-patch recordings of single quanta at individual hippocampal synapses.'. *Nature* **388**(6645), 874–8.

Foster, M. and S. CS: 1897, *A Textbook of Physiology: Part III. The Central Nervous System.* London: Macmillan, seventh edition.

Fox, C. H., F. B. Johnson, J. Whiting, and P. P. Roller: 1985, 'Formaldehyde fixation.'. *The journal of histochemistry and cytochemistry : official journal of the Histochemistry Society* **33**(8), 845–53.

Frerking, M., S. Borges, and M. Wilson: 1995, 'Variation in GABA mini amplitude is the consequence of variation in transmitter concentration.'. *Neuron* **15**(4), 885–95.

Fritzky, L. and D. Lagunoff: 2013, 'Advanced methods in fluorescence microscopy.'. *Analytical cellular pathology (Amsterdam)* **36**(1-2), 5–17.

Fruton, J. S.: 2002, 'A history of pepsin and related enzymes.'. *The Quarterly review of biology* **77**(2), 127–47.

Fukaya, M. and M. Watanabe: 2000, 'Improved immunohistochemical detection of postsynaptically located PSD-95/SAP90 protein family by protease section pretreatment: a study in the adult mouse brain.'. *The Journal of comparative neurology* **426**(4), 572–86.

Gage, G. J., D. R. Kipke, and W. Shain: 2012, 'Whole animal perfusion fixation for rodents.'. *Journal of visualized experiments : JoVE* (65), e3564.

Gagnon, M., M. J. Bergeron, G. Lavertu, A. Castonguay, S. Tripathy, R. P. Bonin, J. Perez-Sanchez, D. Boudreau, B. Wang, L. Dumas, I. Valade, K. Bachand, M. Jacob-Wagner, C. Tardif, I. Kianicka, P. Isenring, G. Attardo, J. A. M. Coull, and Y. De Koninck: 2013, 'Chloride extrusion enhancers as novel therapeutics for neurological diseases.'. *Nature medicine* **19**(11), 1524–8.

Gallagher, J. P., H. Higashi, and S. Nishi: 1978, 'Characterization and ionic basis of GABA-induced depolarizations recorded in vitro from cat primary afferent neurones.'. *The Journal of physiology* **275**, 263–82.

García-Escudero, L. A., A. Gordaliza, C. Matrán, and A. Mayo-Iscar: 2010, 'A review of robust clustering methods'. *Advances in Data Analysis and Classification* **4**(2-3), 89–109.

Ghanem, A. and K.-K. Conzelmann: 2015, 'G gene-deficient single-round rabies viruses for neuronal circuit analysis.'. *Virus research*.

Ginger, M., M. Haberl, K.-K. Conzelmann, M. K. Schwarz, and A. Frick: 2013, 'Revealing the secrets of neuronal circuits with recombinant rabies virus technology.'. *Frontiers in neural circuits* **7**, 2.

Ginhoux, F., M. Greter, M. Leboeuf, S. Nandi, P. See, S. Gokhan, M. F. Mehler, S. J. Conway, L. G. Ng, E. R. Stanley, I. M. Samokhvalov, and M. Merad: 2010, 'Fate mapping analysis reveals that adult microglia derive from primitive macrophages.'. *Science (New York, N.Y.)* **330**(6005), 841–5.

Giuffrida, R. and A. Rustioni: 1992, 'Dorsal root ganglion neurons projecting to the dorsal column nuclei of rats.'. *The Journal of comparative neurology* **316**(2), 206–20.

Gleave, J. A., J. P. Lerch, R. M. Henkelman, and B. J. Nieman: 2013, 'A method for 3D immunostaining and optical imaging of the mouse brain demonstrated in neural progenitor cells.'. *PloS one* **8**(8), e72039.

Gold, B. G.: 1997, 'Axonal regeneration of sensory nerves is delayed by continuous intrathecal infusion of nerve growth factor.'. *Neuroscience* **76**(4), 1153–8.

Gonzalez, F. A. and E. Romero: 2010, 'From Biomedical Image Analysis to Biomedical Image Understanding Using Machine Learning'. In: F. A. Gonzalez and E. Romero (eds.): *Biomedical Image Analysis and Machine Learning Technologies: Applications and Techniques*. New York: Medical Information Science Reference, first edition, Chapt. 1, pp. 1–26.

Gordon, E. and S. Koslow: 2010, *Integrative Neuroscience and Personalized Medicine*, Vol. 19. Oxford University Press.

Govrin-Lippmann, R. and M. Devor: 1978, 'Ongoing activity in severed nerves: source and variation with time.'. *Brain research* **159**(2), 406–10.

Graham, B. and S. Redman: 1994, 'A simulation of action potentials in synaptic boutons during presynaptic inhibition.'. *Journal of neurophysiology* **71**(2), 538–49.

Gray, E. G.: 1959, 'Axo-somatic and axo-dendritic synapses of the cerebral cortex: an electron microscope study.'. *Journal of anatomy* **93**, 420–33.

Gray, E. G.: 1962, 'A morphological basis for pre-synaptic inhibition?'. *Nature* **193**, 82–3.

Gray, E. G.: 1963, 'Electron microscopy of presynaptic organelles of the spinal cord.'. *Journal of anatomy* **97**, 101–6.

Gray, E. G. and V. P. Whittaker: 1962, 'The isolation of nerve endings from brain: an electron-microscopic study of cell fragments derived by homogenization and centrifugation.'. *Journal of anatomy* **96**, 79–88.

Green, C. D., M. G. Shore, and T. Teo: 2001, *The Transformation of Psychology: Influences of 19th Century Philosophy, Technology, and Natural Science*. American Psychological Association.

Greter, M. and M. Merad: 2013, 'Regulation of microglia development and homeostasis.'. *Glia* **61**(1), 121–7.

Grudt, T. J. and E. R. Perl: 2002, 'Correlations between neuronal morphology and electrophysiological features in the rodent superficial dorsal horn.'. *The Journal of physiology* **540**(Pt 1), 189–207.

Gué, M., C. Messaoudi, J. S. Sun, and T. Boudier: 2005, 'Smart 3D-FISH: automation of distance analysis in nuclei of interphase cells by image processing.'. *Cytometry. Part A : the journal of the International Society for Analytical Cytology* **67**(1), 18–26.

Gul-Mohammed, J., I. Arganda-Carreras, P. Andrey, V. Galy, and T. Boudier: 2014, 'A generic classification-based method for segmentation of nuclei in 3D images of early embryos.'. *BMC bioinformatics* **15**, 9.

Gundersen, H. J.: 1986, 'Stereology of arbitrary particles. A review of unbiased number and size estimators and the presentation of some new ones, in memory of William R. Thompson.'. *Journal of microscopy* **143**(Pt 1), 3–45.

Gundersen, H. J., P. Bagger, T. F. Bendtsen, S. M. Evans, L. Korbo, N. Marcussen, A. Møller, K. Nielsen, J. R. Nyengaard, and B. Pakkenberg: 1988, 'The new stereological tools: disector, fractionator, nucleator and point sampled intercepts and their use in pathological research and diagnosis.'. *APMIS : acta pathologica, microbiologica, et immunologica Scandinavica* **96**(10), 857–81.

Guo, W., H. Wang, M. Watanabe, K. Shimizu, S. Zou, S. C. LaGraize, F. Wei, R. Dubner, and K. Ren: 2007, 'Glial-cytokine-neuronal interactions underlying the mechanisms of persistent pain.'. *The Journal of neuroscience : the official journal of the Society for Neuroscience* **27**(22), 6006–18.

Hajós, F., B. Csillik, and E. Knyihár-Csillik: 1990, 'Alterations in glial fibrillary acidic protein immunoreactivity in the upper dorsal horn of the rat spinal cord in the course of transganglionic degenerative atrophy and regenerative proliferation.'. *Neuroscience letters* **117**(1-2), 8–13.

Hald, A., S. Nedergaard, R. R. Hansen, M. Ding, and A.-M. Heegaard: 2009, 'Differential activation of spinal cord glial cells in murine models of neuropathic and cancer pain.'. *European journal of pain (London, England)* **13**(2), 138–45.

Hallermann, S., A. Fejtova, H. Schmidt, A. Weyhersmüller, R. A. Silver, E. D. Gundelfinger, and J. Eilers: 2010, 'Bassoon Speeds Vesicle Reloading at a Central Excitatory Synapse'. *Neuron* **68**(4), 710–723.

Hanz, S. and M. Fainzilber: 2006, 'Retrograde signaling in injured nerve ? the axon reaction revisited'. *Journal of Neurochemistry* **99**(1), 13–19.

Hanz, S., E. Perlson, D. Willis, J.-Q. Zheng, R. Massarwa, J. J. Huerta, M. Koltzenburg, M. Kohler, J. Van-Minnen, J. L. Twiss, and M. Fainzilber: 2003, 'Axoplasmic importins enable retrograde injury signaling in lesioned nerve.'. *Neuron* **40**(6), 1095–104.

Haroutounian, S., L. Nikolajsen, T. F. Bendtsen, N. B. Finnerup, A. D. Kristensen, J. B. Hasselstrøm, and T. S. Jensen: 2014, 'Primary afferent input critical for maintaining spontaneous pain in peripheral neuropathy.'. *Pain* **155**(7), 1272–9.

Harris, K. M. and J. K. Stevens: 1989, 'Dendritic spines of CA 1 pyramidal cells in the rat hippocampus: serial electron microscopy with reference to their biophysical characteristics.'. *The Journal of neuroscience : the official journal of the Society for Neuroscience* **9**(8), 2982–97.

Hasegawa, H., S. Abbott, B.-X. Han, Y. Qi, and F. Wang: 2007, 'Analyzing somatosensory axon projections with the sensory neuron-specific Advillin gene.'. *The Journal of neuroscience : the official journal of the Society for Neuroscience* **27**(52), 14404–14.

Hashem, I. A. T., I. Yaqoob, N. Badrul Anuar, S. Mokhtar, A. Gani, and S. Ullah Khan: 2014, 'The rise of "Big Data" on cloud computing: Review and open research issues'. *Information Systems* **47**, 98–115.

Hathway, G. J., D. Vega-Avelaira, A. Moss, R. Ingram, and M. Fitzgerald: 2009, 'Brief, low frequency stimulation of rat peripheral C-fibres evokes prolonged microglial-induced central sensitization in adults but not in neonates.'. *Pain* **144**(1-2), 110–8.

Hayat, M.: 2002, 'Factors Affecting Antigen Retrieval'. In: M. Hayat (ed.): *Microscopy, Immunohistochemistry, and Antigen Retrieval Methods For Light and Electron Microscopy*. New York: Kluwer Academic Publishers, Chapt. 4, p. 376.

Hebb, D. O.: 1949, *The organization of behavior: a neuropsychological theory*. Wiley.

Heck, N., M. Dos Santos, B. Amairi, M. Salery, A. Besnard, E. Herzog, T. Boudier, P. Vanhoutte, and J. Caboche: 2014, 'A new automated 3D detection of synaptic contacts reveals the formation of cortico-striatal synapses upon cocaine treatment in vivo.'. *Brain structure & function*.

Hedreen, J. C.: 1998, 'What was wrong with the Abercrombie and empirical cell counting methods? A review.'. *The Anatomical record* **250**(3), 373–80.

Heinke, B., R. Ruscheweyh, L. Forsthuber, G. Wunderbaldinger, and J. Sandkühler: 2004, 'Physiological, neurochemical and morphological properties of a subgroup of GABAergic spinal lamina II neurones identified by expression of green fluorescent protein in mice.'. *The Journal of physiology* **560**(Pt 1), 249–66.

Heinricher, M. M., M. M. Morgan, and H. L. Fields: 1992, 'Direct and indirect actions of morphine on medullary neurons that modulate nociception.'. *Neuroscience* **48**(3), 533–43.

Helmchen, F. and W. Denk: 2005, 'Deep tissue two-photon microscopy.'. *Nature methods* **2**(12), 932–40.

Helmstaedter, M., K. L. Briggman, S. C. Turaga, V. Jain, H. S. Seung, and W. Denk: 2013, 'Connectomic reconstruction of the inner plexiform layer in the mouse retina'. *Nature* **500**(7461), 168–174.

Henny, P., M. T. C. Brown, B. R. Micklem, P. J. Magill, and J. P. Bolam: 2013, 'Stereological and ultrastructural quantification of the afferent synaptome of individual neurons'. *Brain Structure and Function* **219**(2), 631–640.

Heuser, J. E. and T. S. Reese: 1973, 'Evidence for recycling of synaptic vesicle membrane during transmitter release at the frog neuromuscular junction.'. *The Journal of cell biology* **57**(2), 315–44.

Hickman, S. E., N. D. Kingery, T. K. Ohsumi, M. L. Borowsky, L.-c. Wang, T. K. Means, and J. El Khoury: 2013, 'The microglial sensome revealed by direct RNA sequencing.'. *Nature neuroscience* **16**(12), 1896–905.

Hirase, H., L. Qian, P. Barthó, and G. Buzsáki: 2004, 'Calcium dynamics of cortical astrocytic networks in vivo.'. *PLoS biology* **2**(4), E96.

Hirokawa, N., K. Sobue, K. Kanda, A. Harada, and H. Yorifuji: 1989, 'The cytoskeletal architecture of the presynaptic terminal and molecular structure of synapsin 1.'. *The Journal of cell biology* **108**(1), 111–26.

Hodgkin, A. L. and A. F. Huxley: 1990, 'A quantitative description of membrane current and its application to conduction and excitation in nerve. 1952.'. *Bulletin of mathematical biology* **52**(1-2), 25–71; discussion 5–23.

Hormuzdi, S. G., M. A. Filippov, G. Mitropoulou, H. Monyer, and R. Bruzzone: 2004, 'Electrical synapses: a dynamic signaling system that shapes the activity of neuronal networks.'. *Biochimica et biophysica acta* **1662**(1-2), 113–37.

Hulse, R., D. Wynick, and L. F. Donaldson: 2010, 'Intact cutaneous C fibre afferent properties in mechanical and cold neuropathic allodynia.'. *European journal of pain (London, England)* **14**(6), 565.e1–565.e10.

Hunt, C. A., L. J. Schenker, and M. B. Kennedy: 1996, 'PSD-95 is associated with the postsynaptic density and not with the presynaptic membrane at forebrain synapses.'. *The Journal of neuroscience : the official journal of the Society for Neuroscience* **16**(4), 1380–8.

Iannuccelli, E., F. Mompart, J. Gellin, Y. Lahbib-Mansais, M. Yerle, and T. Boudier: 2010, 'NEMO: a tool for analyzing gene and chromosome territory distributions from 3D-FISH experiments'. *Bioinformatics* **26**(5), 696–697.

Ibuki, T., A. T. Hama, X. T. Wang, G. D. Pappas, and J. Sagen: 1997, 'Loss of GABA-immunoreactivity in the spinal dorsal horn of rats with peripheral nerve injury and promotion of recovery by adrenal medullary grafts.'. *Neuroscience* **76**(3), 845–58.

Ikeda, H., J. Stark, H. Fischer, M. Wagner, R. Drdla, T. Jäger, and J. Sandkühler: 2006, 'Synaptic amplifier of inflammatory pain in the spinal dorsal horn.'. *Science (New York, N.Y.)* **312**(5780), 1659–62.

Intondi, A. B., M. N. Dahlgren, M. A. Eilers, and B. K. Taylor: 2008, 'Intrathecal neuropeptide Y reduces behavioral and molecular markers of inflammatory or neuropathic pain.'. *Pain* **137**(2), 352–65.

Irie, O., T. Kosaka, T. Ehara, F. Yokokawa, T. Kanazawa, H. Hirao, A. Iwasaki, J. Sakaki, N. Teno, Y. Hitomi, G. Iwasaki, H. Fukaya, K. Nonomura, K. Tanabe, S. Koizumi, N. Uchiyama, S. J. Bevan, M. Malcangio, C. Gentry, A. J. Fox, M. Yaqoob, A. J. Culshaw, and Allan Hallett: 2008, 'Discovery of orally bioavailable cathepsin S inhibitors for the reversal of neuropathic pain.'. *Journal of medicinal chemistry* **51**(18), 5502–5.

Ito, D., Y. Imai, K. Ohsawa, K. Nakajima, Y. Fukuuchi, and S. Kohsaka: 1998, 'Microglia-specific localisation of a novel calcium binding protein, Iba1.'. *Brain research. Molecular brain research* **57**(1), 1–9.

Ito, N., H. Obata, and S. Saito: 2009, 'Spinal microglial expression and mechanical hypersensitivity in a postoperative pain model: comparison with a neuropathic pain model.'. *Anesthesiology* **111**(3), 640–8.

Jain, V., H. S. Seung, and S. C. Turaga: 2010, 'Machines that learn to segment images: a crucial technology for connectomics.'. *Current opinion in neurobiology* **20**(5), 653–66.

Jensen, M. P., M. J. Chodroff, and R. H. Dworkin: 2007, 'The impact of neuropathic pain on health-related quality of life: review and implications.'. *Neurology* **68**(15), 1178–82.

Jensen, T. S., R. Baron, M. Haanpää, E. Kalso, J. D. Loeser, A. S. C. Rice, and R.-D. Treede: 2011, 'A new definition of neuropathic pain.'. *Pain* **152**(10), 2204–5.

Ji, R.-R., R. W. Gereau, M. Malcangio, and G. R. Strichartz: 2009, 'MAP kinase and pain.'. *Brain research reviews* **60**(1), 135–48.

Ji, R.-R., T. Kohno, K. A. Moore, and C. J. Woolf: 2003, 'Central sensitization and LTP: do pain and memory share similar mechanisms?'. *Trends in neurosciences* **26**(12), 696–705.

Jiao, Y., Z. Sun, T. Lee, F. R. Fusco, T. D. Kimble, C. A. Meade, S. Cuthbertson, and A. Reiner: 1999, 'A simple and sensitive antigen retrieval method for free-floating and slide-mounted tissue sections.'. *Journal of neuroscience methods* **93**(2), 149–62.

Jones, E. G.: 1994, 'Santiago Ramón y Cajal and the Croonian Lecture, March 1894.'. *Trends in neurosciences* **17**(5), 190–2.

Jourdain, P., L. H. Bergersen, K. Bhaukaurally, P. Bezzi, M. Santello, M. Domercq, C. Matute, F. Tonello, V. Gundersen, and A. Volterra: 2007, 'Glutamate exocytosis from astrocytes controls synaptic strength.'. *Nature neuroscience* **10**(3), 331–9.

Jung, S., J. Aliberti, P. Graemmel, M. J. Sunshine, G. W. Kreutzberg, A. Sher, and D. R. Littman: 2000, 'Analysis of fractalkine receptor CX(3)CR1 function by targeted deletion and green fluorescent protein reporter gene insertion.'. *Molecular and cellular biology* **20**(11), 4106–14.

Kandel, E.: 2013, *Principles of Neural Science, Fifth Edition*. McGraw Hill Professional.

Kandel, E. R.: 2012, 'The molecular biology of memory: cAMP, PKA, CRE, CREB-1, CREB-2, and CPEB.'. *Molecular brain* **5**, 14.

Kapadia, S. E. and C. C. LaMotte: 1987, 'Deafferentation-induced alterations in the rat dorsal horn: I. Comparison of peripheral nerve injury vs. rhizotomy effects on presynaptic, postsynaptic, and glial processes.'. *The Journal of comparative neurology* **266**(2), 183–97.

Kato, G., Y. Kawasaki, R.-R. Ji, and A. M. Strassman: 2007, 'Differential wiring of local excitatory and inhibitory synaptic inputs to islet cells in rat spinal lamina II demonstrated by laser scanning photostimulation.'. *The Journal of physiology* **580**(Pt.3), 815–33.

Kato, G., Y. Kawasaki, K. Koga, D. Uta, M. Kosugi, T. Yasaka, M. Yoshimura, R.-R. Ji, and A. M. Strassman: 2009, 'Organization of intralaminar and translaminar neuronal connectivity in the superficial spinal dorsal horn.'. *The Journal of neuroscience : the official journal of the Society for Neuroscience* **29**(16), 5088–99.

Kato, G., M. Kosugi, M. Mizuno, and A. M. Strassman: 2013, 'Three-dimensional organization of local excitatory and inhibitory inputs to neurons in laminae III-IV of the spinal dorsal horn.'. *The Journal of physiology* **591**(Pt 22), 5645–60.

Katz, B.: 1969, *The Release of Neural Transmitter Substances*. Liverpool: Liverpool University Press.

Kay, K. R., C. Smith, A. K. Wright, A. Serrano-Pozo, A. M. Pooler, R. Koffie, M. E. Bastin, T. H. Bak, S. Abrahams, K. J. Kopeikina, D. McGuone, M. P. Frosch, T. H. Gillingwater, B. T. Hyman, and T. L. Spires-Jones: 2013, 'Studying synapses in human brain with array tomography and electron microscopy.'. *Nature protocols* **8**(7), 1366–80.

Keller, A. F., S. Beggs, M. W. Salter, and Y. De Koninck: 2007, 'Transformation of the output of spinal lamina I neurons after nerve injury and microglia stimulation underlying neuropathic pain.'. *Molecular pain* **3**, 27.

Kettenmann, H., U.-K. Hanisch, M. Noda, and A. Verkhratsky: 2011, 'Physiology of microglia.'. *Physiological reviews* **91**(2), 461–553.

Kettenmann, H., F. Kirchhoff, and A. Verkhratsky: 2013, 'Microglia: new roles for the synaptic stripper.'. *Neuron* **77**(1), 10–8.

Khan, G. M., S.-R. Chen, and H.-L. Pan: 2002, 'Role of primary afferent nerves in allodynia caused by diabetic neuropathy in rats.'. *Neuroscience* **114**(2), 291–9.

Khasabov, S. G., S. D. Rogers, J. R. Ghilardi, C. M. Peters, P. W. Mantyh, and D. A. Simone: 2002, 'Spinal neurons that possess the substance P receptor are required for the development of central sensitization.'. *The Journal of neuroscience : the official journal of the Society for Neuroscience* **22**(20), 9086–98.

Kierdorf, K., D. Erny, T. Goldmann, V. Sander, C. Schulz, E. G. Perdiguero, P. Wieghofer, A. Heinrich, P. Riemke, C. Hölscher, D. N. Müller, B. Luckow, T. Brocker, K. Debowski, G. Fritz, G. Opdenakker, A. Diefenbach, K. Biber, M. Heikenwalder, F. Geissmann, F. Rosenbauer, and M. Prinz: 2013, 'Microglia emerge from erythromyeloid precursors via Pu.1- and Irf8-dependent pathways.'. *Nature neuroscience* **16**(3), 273–80.

Kim, E., K. O. Cho, A. Rothschild, and M. Sheng: 1996, 'Heteromultimerization and NMDA receptor-clustering activity of Chapsyn-110, a member of the PSD-95 family of proteins.'. *Neuron* **17**(1), 103–13.

Kim, E. and M. Sheng: 2004, 'PDZ domain proteins of synapses.'. *Nature reviews. Neuroscience* **5**(10), 771–81.

Kim, J. S., M. J. Greene, A. Zlateski, K. Lee, M. Richardson, S. C. Turaga, M. Purcaro, M. Balkam, A. Robinson, B. F. Behabadi, M. Campos, W. Denk, and H. S. Seung: 2014, 'Space-time wiring specificity supports direction selectivity in the retina.'. *Nature* **509**(7500), 331–6.

Kim, S. H. and J. M. Chung: 1992, 'An experimental model for peripheral neuropathy produced by segmental spinal nerve ligation in the rat.'. *Pain* **50**(3), 355–63.

Kirsch, J. and H. Betz: 1993, 'Widespread expression of gephyrin, a putative glycine receptor-tubulin linker protein, in rat brain.'. *Brain research* **621**(2), 301–10.

Knyihár-Csillik, E., G. W. Kreutzberg, G. Raivich, and B. Csillik: 1991, 'Vasoactive intestinal polypeptide in dorsal root terminals of the rat spinal cord is regulated by the axoplasmic transport in the peripheral nerve.'. *Neuroscience letters* **131**(1), 83–7.

Kohno, T., K. A. Moore, H. Baba, and C. J. Woolf: 2003, 'Peripheral nerve injury alters excitatory synaptic transmission in lamina II of the rat dorsal horn.'. *The Journal of physiology* **548**(Pt 1), 131–8.

Kononenko, N. L. and V. Haucke: 2015, 'Molecular mechanisms of presynaptic membrane retrieval and synaptic vesicle reformation.'. *Neuron* **85**(3), 484–96.

Kuwajima, M., J. Spacek, and K. M. Harris: 2013, 'Beyond counts and shapes: studying pathology of dendritic spines in the context of the surrounding neuropil through serial section electron microscopy.'. *Neuroscience* **251**, 75–89.

Lander, E. S., L. M. Linton, B. Birren, C. Nusbaum, M. C. Zody, J. Baldwin, K. Devon, K. Dewar, M. Doyle, W. FitzHugh, R. Funke, D. Gage, K. Harris, A. Heaford, J. Howland, L. Kann, J. Lehoczky, R. LeVine, P. McEwan, K. McKernan, J. Meldrim, J. P. Mesirov, C. Miranda, W. Morris, J. Naylor, C. Raymond, M. Rosetti, R. Santos, A. Sheridan, C. Sougnez, N. Stange-Thomann, N. Stojanovic, A. Subramanian, D. Wyman, J. Rogers, J. Sulston, R. Ainscough, S. Beck, D. Bentley, J. Burton, C. Clee, N. Carter, A. Coulson, R. Deadman, P. Deloukas, A. Dunham, I. Dunham, R. Durbin, L. French, D. Grafham, S. Gregory, T. Hubbard, S. Humphray, A. Hunt, M. Jones, C. Lloyd, A. McMurray, L. Matthews, S. Mercer, S. Milne, J. C. Mullikin, A. Mungall, R. Plumb, M. Ross, R. Shownkeen, S. Sims, R. H. Waterston, R. K. Wilson, L. W. Hillier, J. D. McPherson, M. A. Marra, E. R. Mardis, L. A. Fulton, A. T. Chinwalla, K. H. Pepin, W. R. Gish, S. L. Chissoe, M. C. Wendl, K. D. Delehaunty, T. L. Miner, A. Delehaunty, J. B. Kramer, L. L. Cook, R. S. Fulton, D. L. Johnson, P. J. Minx, S. W. Clifton, T. Hawkins, E. Branscomb, P. Predki, P. Richardson, S. Wenning, T. Slezak, N. Doggett, J. F. Cheng, A. Olsen, S. Lucas, C. Elkin, E. Uberbacher, M. Frazier, R. A.

Gibbs, D. M. Muzny, S. E. Scherer, J. B. Bouck, E. J. Sodergren, K. C. Worley, C. M. Rives, J. H. Gorrell, M. L. Metzker, S. L. Naylor, R. S. Kucherlapati, D. L. Nelson, G. M. Weinstock, Y. Sakaki, A. Fujiyama, M. Hattori, T. Yada, A. Toyoda, T. Itoh, C. Kawagoe, H. Watanabe, Y. Totoki, T. Taylor, J. Weissenbach, R. Heilig, W. Saurin, F. Artiguenave, P. Brottier, T. Bruls, E. Pelletier, C. Robert, P. Wincker, D. R. Smith, L. Doucette-Stamm, M. Rubenfield, K. Weinstock, H. M. Lee, J. Dubois, A. Rosenthal, M. Platzer, G. Nyakatura, S. Taudien, A. Rump, H. Yang, J. Yu, J. Wang, G. Huang, J. Gu, L. Hood, L. Rowen, A. Madan, S. Qin, R. W. Davis, N. A. Federspiel, A. P. Abola, M. J. Proctor, R. M. Myers, J. Schmutz, M. Dickson, J. Grimwood, D. R. Cox, M. V. Olson, R. Kaul, N. Shimizu, K. Kawasaki, S. Minoshima, G. A. Evans, M. Athanasiou, R. Schultz, B. A. Roe, F. Chen, H. Pan, J. Ramser, H. Lehrach, R. Reinhardt, W. R. McCombie, M. de la Bastide, N. Dedhia, H. Blöcker, K. Hornischer, G. Nordsiek, R. Agarwala, L. Aravind, J. A. Bailey, A. Bateman, S. Batzoglou, E. Birney, P. Bork, D. G. Brown, C. B. Burge, L. Cerutti, H. C. Chen, D. Church, M. Clamp, R. R. Copley, T. Doerks, S. R. Eddy, E. E. Eichler, T. S. Furey, J. Galagan, J. G. Gilbert, C. Harmon, Y. Hayashizaki, D. Haussler, H. Hermjakob, K. Hokamp, W. Jang, L. S. Johnson, T. A. Jones, S. Kasif, A. Kaspryzk, S. Kennedy, W. J. Kent, P. Kitts, E. V. Koonin, I. Korf, D. Kulp, D. Lancet, T. M. Lowe, A. McLysaght, T. Mikkelsen, J. V. Moran, N. Mulder, V. J. Pollara, C. P. Ponting, G. Schuler, J. Schultz, G. Slater, A. F. Smit, E. Stupka, J. Szustakowski, D. Thierry-Mieg, J. Thierry-Mieg, L. Wagner, J. Wallis, R. Wheeler, A. Williams, Y. I. Wolf, K. H. Wolfe, S. P. Yang, R. F. Yeh, F. Collins, M. S. Guyer, J. Peterson, A. Felsenfeld, K. A. Wetterstrand, A. Patrinos, M. J. Morgan, P. de Jong, J. J. Catanese, K. Osoegawa, H. Shizuya, S. Choi, Y. J. Chen, and J. Szustakowki: 2001, 'Initial sequencing and analysis of the human genome.'. *Nature* **409**(6822), 860–921.

Latremoliere, A. and C. J. Woolf: 2009, 'Central sensitization: a generator of pain hypersensitivity by central neural plasticity.'. *The journal of pain : official journal of the American Pain Society* **10**(9), 895–926.

Lau, J., M. S. Minett, J. Zhao, U. Dennehy, F. Wang, J. N. Wood, and Y. D. Bogdanov: 2011, 'Temporal control of gene deletion in sensory ganglia using a tamoxifen-inducible Advillin-Cre-ERT2 recombinase mouse.'. *Molecular pain* **7**, 100.

Lavertu, G., S. L. Côté, and Y. De Koninck: 2014, 'Enhancing K-Cl co-transport restores normal spinothalamic sensory coding in a neuropathic pain model.'. *Brain : a journal of neurology* **137**(Pt 3), 724–38.

Lawson, S. N.: 1979, 'The postnatal development of large light and small dark neurons in mouse dorsal root ganglia: a statistical analysis of cell numbers and size.'. *Journal of neurocytology* **8**(3), 275–94.

Lawson, S. N., A. A. Harper, E. I. Harper, J. A. Garson, and B. H. Anderton: 1984, 'A monoclonal antibody against neurofilament protein specifically labels a subpopulation of rat sensory neurones.'. *The Journal of comparative neurology* **228**(2), 263–72.

Lécuyer, E., N. Parthasarathy, and H. M. Krause: 2008, 'Fluorescent in situ hybridization protocols in Drosophila embryos and tissues.'. *Methods in molecular biology (Clifton, N.J.)* **420**, 289–302.

Ledeboer, A., E. M. Sloane, E. D. Milligan, M. G. Frank, J. H. Mahony, S. F. Maier, and L. R. Watkins: 2005, 'Minocycline attenuates mechanical allodynia and proinflammatory cytokine expression in rat models of pain facilitation.'. *Pain* **115**(1-2), 71–83.

Leitner, J., S. Westerholz, B. Heinke, L. Forsthuber, G. Wunderbaldinger, T. Jäger, D. Gruber-Schoffnegger, K. Braun, and J. Sandkühler: 2013, 'Impaired excitatory drive to spinal GABAergic neurons of neuropathic mice.'. *PloS one* **8**(8), e73370.

Lekan, H. A., K. Chung, Y. W. Yoon, J. M. Chung, and R. E. Coggeshall: 1997, 'Loss of dorsal root ganglion cells concomitant with dorsal root axon sprouting following segmental nerve lesions.'. *Neuroscience* **81**(2), 527–34.

Leong, M. L., M. Gu, R. Speltz-Paiz, E. I. Stahura, N. Mottey, C. J. Steer, and M. Wessendorf: 2011, 'Neuronal loss in the rostral ventromedial medulla in a rat model of neuropathic pain.'. *The Journal of neuroscience : the official journal of the Society for Neuroscience* **31**(47), 17028–39.

Leranth, C., B. Csillik, and E. Knyihar-Csillik: 1984, 'Depletion of substance P and somatostatin in the upper dorsal horn after blockade of axoplasmic transport'. *Histochemistry* **81**(4), 391–400.

Lever, I., J. Cunningham, J. Grist, P. K. Yip, and M. Malcangio: 2003, 'Release of BDNF and GABA in the dorsal horn of neuropathic rats.'. *The European journal of neuroscience* **18**(5), 1169–74.

Lever, I. J., E. J. Bradbury, J. R. Cunningham, D. W. Adelson, M. G. Jones, S. B. McMahon, J. C. Marvizón, and M. Malcangio: 2001, 'Brain-derived neurotrophic factor is released in the dorsal horn by distinctive patterns of afferent fiber stimulation.'. *The Journal of neuroscience : the official journal of the Society for Neuroscience* **21**(12), 4469–77.

Li, C.-Y., Y.-H. Song, E. S. Higuera, and Z. D. Luo: 2004, 'Spinal dorsal horn calcium channel alpha2delta-1 subunit upregulation contributes to peripheral nerve injury-induced tactile allodynia.'. *The Journal of neuroscience : the official journal of the Society for Neuroscience* **24**(39), 8494–9.

Li, J.-L., F. Fujiyama, T. Kaneko, and N. Mizuno: 2003, 'Expression of vesicular glutamate transporters, VGluT1 and VGluT2, in axon terminals of nociceptive primary afferent fibers in the superficial layers of the medullary and spinal dorsal horns of the rat.'. *The Journal of comparative neurology* **457**(3), 236–49.

Li, K.-W., Y. P. Yu, C. Zhou, D.-S. Kim, B. Lin, K. Sharp, O. Steward, and Z. D. Luo: 2014, 'Calcium channel $\alpha 2\delta 1$ proteins mediate trigeminal neuropathic pain states associated with aberrant excitatory synaptogenesis.'. *The Journal of biological chemistry* **289**(10), 7025–37.

Li, L., M. Rutlin, V. E. Abraira, C. Cassidy, L. Kus, S. Gong, M. P. Jankowski, W. Luo, N. Heintz, H. R. Koerber, C. J. Woodbury, and D. D. Ginty: 2011, 'The functional organization of cutaneous low-threshold mechanosensory neurons.'. *Cell* **147**(7), 1615–27.

Lima, D. and A. Coimbra: 1983, 'The neuronal population of the marginal zone (lamina I) of the rat spinal cord. A study based on reconstructions of serially sectioned cells.'. *Anatomy and embryology* **167**(2), 273–88.

Lima, D. and A. Coimbra: 1986, 'A Golgi study of the neuronal population of the marginal zone (lamina I) of the rat spinal cord.'. *The Journal of comparative neurology* **244**(1), 53–71.

Lin, C.-S., M.-L. Tsaur, C.-C. Chen, T.-Y. Wang, C.-F. Lin, Y.-L. Lai, T.-C. Hsu, Y.-Y. Pan, C.-H. Yang, and J.-K. Cheng: 2007, 'Chronic intrathecal infusion of minocycline prevents the development of spinal-nerve ligation-induced pain in rats.'. *Regional anesthesia and pain medicine* **32**(3), 209–16.

Lin, J.-Y., B. Peng, Z.-W. Yang, and S. Min: 2011, 'Number of synapses increased in the rat spinal dorsal horn after sciatic nerve transection: a stereological study.'. *Brain research bulletin* **84**(6), 430–3.

Lin, Y.-C. and A. J. Koleske: 2010, 'Mechanisms of synapse and dendrite maintenance and their disruption in psychiatric and neurodegenerative disorders.'. *Annual review of neuroscience* **33**, 349–78.

Linden, D. J.: 1997, 'Long-term potentiation of glial synaptic currents in cerebellar culture.'. *Neuron* **18**(6), 983–94.

Lindia, J. A., E. McGowan, N. Jochnowitz, and C. Abbadie: 2005, 'Induction of CX3CL1 expression in astrocytes and CX3CR1 in microglia in the spinal cord of a rat model of neuropathic pain.'. *The journal of pain : official journal of the American Pain Society* **6**(7), 434–8.

Lindwall, C. and M. Kanje: 2005, 'Retrograde axonal transport of JNK signaling molecules influence injury induced nuclear changes in p-c-Jun and ATF3 in adult rat sensory neurons.'. *Molecular and cellular neurosciences* **29**(2), 269–82.

Liu, C. N., P. D. Wall, E. Ben-Dor, M. Michaelis, R. Amir, and M. Devor: 2000a, 'Tactile allodynia in the absence of C-fiber activation: altered firing properties of DRG neurons following spinal nerve injury.'. *Pain* **85**(3), 503–21.

Liu, F.-Y., X.-X. Qu, J. Cai, F.-T. Wang, G.-G. Xing, and Y. Wan: 2011, 'Electrophysiological properties of spinal wide dynamic range neurons in neuropathic pain rats following spinal nerve ligation.'. *Neuroscience bulletin* **27**(1), 1–8.

Liu, G. and R. W. Tsien: 1995, 'Properties of synaptic transmission at single hippocampal synaptic boutons.'. *Nature* **375**(6530), 404–8.

Liu, L., M. Rudin, and E. N. Kozlova: 2000b, 'Glial cell proliferation in the spinal cord after dorsal rhizotomy or sciatic nerve transection in the adult rat.'. *Experimental brain research* **131**(1), 64–73.

Liu, X. G. and J. Sandkühler: 1995, 'Long-term potentiation of C-fiber-evoked potentials in the rat spinal dorsal horn is prevented by spinal N-methyl-D-aspartic acid receptor blockage.'. *Neuroscience letters* **191**(1-2), 43–6.

Llewellyn-Smith, I. J. and J. B. Minson: 1992, 'Complete penetration of antibodies into vibratome sections after glutaraldehyde fixation and ethanol treatment: light and electron microscopy for neuropeptides.'. *The journal of histochemistry and cytochemistry : official journal of the Histochemistry Society* **40**(11), 1741–9.

Lomo, T.: 2003, 'The discovery of long-term potentiation.'. *Philosophical transactions of the Royal Society of London. Series B, Biological sciences* **358**(1432), 617–20.

Lorenzo, L.-E., C. Magnussen, A. L. Bailey, M. St Louis, Y. De Koninck, and A. Ribeiro-da Silva: 2014, 'Spatial and temporal pattern of changes in the number of GAD65-immunoreactive inhibitory terminals in the rat superficial dorsal horn following peripheral nerve injury.'. *Molecular pain* **10**, 57.

Lu, Y., H. Dong, Y. Gao, Y. Gong, Y. Ren, N. Gu, S. Zhou, N. Xia, Y.-Y. Sun, R.-R. Ji, and L. Xiong: 2013, 'A feed-forward spinal cord glycinergic neural circuit gates mechanical allodynia.'. *The Journal of clinical investigation* **123**(9), 4050–62.

Lu, Y. and E. R. Perl: 2003, 'A specific inhibitory pathway between substantia gelatinosa neurons receiving direct C-fiber input.'. *The Journal of neuroscience : the official journal of the Society for Neuroscience* **23**(25), 8752–8.

Lu, Y. and E. R. Perl: 2005, 'Modular organization of excitatory circuits between neurons of the spinal superficial dorsal horn (laminae I and II).'. *The Journal of neuroscience : the official journal of the Society for Neuroscience* **25**(15), 3900–7.

Lüscher, C. and R. C. Malenka: 2012, 'NMDA receptor-dependent long-term potentiation and long-term depression (LTP/LTD).'. *Cold Spring Harbor perspectives in biology* **4**(6).

Luz, L. L., P. Szucs, and B. V. Safronov: 2014, 'Peripherally driven low-threshold inhibitory inputs to lamina I local-circuit and projection neurones: a new circuit for gating pain responses.'. *The Journal of physiology* **592**(Pt 7), 1519–34.

Ma, Q. P. and C. J. Woolf: 1995, 'Involvement of neurokinin receptors in the induction but not the maintenance of mechanical allodynia in rat flexor motoneurones.'. *The Journal of physiology* **486 (Pt 3**, 769–77.

Ma, W. and J. C. Eisenach: 2003, 'Chronic constriction injury of sciatic nerve induces the up-regulation of descending inhibitory noradrenergic innervation to the lumbar dorsal horn of mice.'. *Brain research* **970**(1-2), 110–8.

Ma, W. and R. Quirion: 2002, 'Partial sciatic nerve ligation induces increase in the phosphorylation of extracellular signal-regulated kinase (ERK) and c-Jun N-terminal kinase (JNK) in astrocytes in the lumbar spinal dorsal horn and the gracile nucleus.'. *Pain* **99**(1-2), 175–84.

Malm, T. M., J. Magga, G. F. Kuh, T. Vatanen, M. Koistinaho, and J. Koistinaho: 2008, 'Minocycline reduces engraftment and activation of bone marrow-derived cells but sustains their phagocytic activity in a mouse model of Alzheimer's disease.'. *Glia* **56**(16), 1767–79.

Mandler, G.: 2002, 'Origins of the cognitive (r)evolution.'. *Journal of the history of the behavioral sciences* **38**(4), 339–53.

Mansikka, H. and A. Pertovaara: 1995, 'The role of alpha 2-adrenoceptors of the medullary lateral reticular nucleus in spinal antinociception in rats.'. *Brain research bulletin* **37**(6), 633–8.

Mao, J., D. D. Price, L. L. Phillips, J. Lu, and D. J. Mayer: 1995, 'Increases in protein kinase C gamma immunoreactivity in the spinal cord dorsal horn of rats with painful mononeuropathy.'. *Neuroscience letters* **198**(2), 75–8.

Marks, P. W., M. Arai, J. L. Bandura, and D. J. Kwiatkowski: 1998, 'Advillin (p92): a new member of the gelsolin/villin family of actin regulatory proteins.'. *Journal of cell science* **111 (Pt 1**, 2129–36.

Marrone, D., J. LeBoutillier, and T. Petit: 2005, 'Morphological Plasticity of the Synapse'. In: P. Stanton, C. Bramham, and H. Scharfman (eds.): *Synaptic Plasticity and Transsynaptic Signaling*. Springer US, pp. 495–517.

Matsui, T., C. I. Svensson, Y. Hirata, K. Mizobata, X.-Y. Hua, and T. L. Yaksh: 2010, 'Release of prostaglandin E(2) and nitric oxide from spinal microglia is dependent on activation of p38 mitogen-activated protein kinase.'. *Anesthesia and analgesia* **111**(2), 554–60.

Matus, A. I. and D. H. Taff-Jones: 1978, 'Morphology and molecular composition of isolated postsynaptic junctional structures.'. *Proceedings of the Royal Society of London. Series B, Biological sciences* **203**(1151), 135–51.

Mayer, M. L., G. L. Westbrook, and P. B. Guthrie: 1984, 'Voltage-dependent block by Mg2+ of NMDA responses in spinal cord neurones.'. *Nature* **309**(5965), 261–3.

Mayhew, T. M. and H. J. Gundersen: 1996, 'If you assume, you can make an ass out of u and me': a decade of the disector for stereological counting of particles in 3D space.'. *Journal of anatomy* **188 (Pt 1**, 1–15.

McKay Hart, A., T. Brannstrom, M. Wiberg, and G. Terenghi: 2002, 'Primary sensory neurons and satellite cells after peripheral axotomy in the adult rat: timecourse of cell death and elimination.'. *Experimental brain research* **142**(3), 308–18.

McMahon, S. B. and M. Malcangio: 2009, 'Current challenges in glia-pain biology.'. *Neuron* **64**(1), 46–54.

McMahon, S. B. and P. D. Wall: 1985, 'The distribution and central termination of single cutaneous and muscle unmyelinated fibres in rat spinal cord.'. *Brain research* **359**(1-2), 39–48.

McNeill, D. L., K. Chung, C. E. Hulsebosch, R. P. Bolender, and R. E. Coggeshall: 1988, 'Numbers of synapses in laminae I-IV of the rat dorsal horn.'. *The Journal of comparative neurology* **278**(3), 453–60.

Mei, X.-P., H. Xu, C. Xie, J. Ren, Y. Zhou, H. Zhang, and L.-X. Xu: 2011, 'Post-injury administration of minocycline: an effective treatment for nerve-injury induced neuropathic pain.'. *Neuroscience research* **70**(3), 305–12.

Melzack, R. and P. D. Wall: 1965, 'Pain mechanisms: a new theory.'. *Science (New York, N.Y.)* **150**(3699), 971–9.

Mendell, L. M.: 1966, 'Physiological properties of unmyelinated fiber projection to the spinal cord.'. *Experimental neurology* **16**(3), 316–32.

Mendell, L. M. and P. D. Wall: 1965, 'RESPONSES OF SINGLE DORSAL CORD CELLS TO PERIPHERAL CUTANEOUS UNMYELINATED FIBRES.'. *Nature* **206**, 97–9.

Merighi, A., J. M. Polak, and D. T. Theodosis: 1991, 'Ultrastructural visualization of glutamate and aspartate immunoreactivities in the rat dorsal horn, with special reference to the co-localization of glutamate, substance P and calcitonin-gene related peptide.'. *Neuroscience* **40**(1), 67–80.

Meyer, R. A. and M. Ringkamp: 2008, 'A role for uninjured afferents in neuropathic pain.'. *Sheng li xue bao : [Acta physiologica Sinica]* **60**(5), 605–9.

Michaelevski, I., Y. Segal-Ruder, M. Rozenbaum, K. F. Medzihradszky, O. Shalem, G. Coppola, S. Horn-Saban, K. Ben-Yaakov, S. Y. Dagan, I. Rishal, D. H. Geschwind, Y. Pilpel, A. L. Burlingame, and M. Fainzilber: 2010, 'Signaling to transcription networks in the neuronal retrograde injury response.'. *Science signaling* **3**(130), ra53.

Michaelis, M., X. Liu, and W. Jänig: 2000, 'Axotomized and intact muscle afferents but no skin afferents develop ongoing discharges of dorsal root ganglion origin after peripheral nerve lesion.'. *The Journal of neuroscience : the official journal of the Society for Neuroscience* **20**(7), 2742–8.

Micheva, K. D., B. Busse, N. C. Weiler, N. O'Rourke, and S. J. Smith: 2010, 'Single-synapse analysis of a diverse synapse population: proteomic imaging methods and markers.'. *Neuron* **68**(4), 639–53.

Mika, J.: 2008, 'Modulation of microglia can attenuate neuropathic pain symptoms and enhance morphine effectiveness.'. *Pharmacological reports* **60**(3), 297–307.

Mika, J., M. Osikowicz, W. Makuch, and B. Przewlocka: 2007, 'Minocycline and pentoxifylline attenuate allodynia and hyperalgesia and potentiate the effects of morphine in rat and mouse models of neuropathic pain.'. *European journal of pharmacology* **560**(2-3), 142–9.

Millan, M. J.: 1999, 'The induction of pain: an integrative review.'. *Progress in neurobiology* **57**(1), 1–164.

Millan, M. J.: 2002, 'Descending control of pain.'. *Progress in neurobiology* **66**(6), 355–474.

Miller, G. A.: 2003, 'The cognitive revolution: a historical perspective.'. *Trends in cognitive sciences* **7**(3), 141–144.

Miller, T. M. and J. E. Heuser: 1984, 'Endocytosis of synaptic vesicle membrane at the frog neuromuscular junction.'. *The Journal of cell biology* **98**(2), 685–98.

Milligan, E., V. Zapata, D. Schoeniger, M. Chacur, P. Green, S. Poole, D. Martin, S. F. Maier, and L. R. Watkins: 2005, 'An initial investigation of spinal mechanisms underlying pain enhancement induced by fractalkine, a neuronally released chemokine.'. *The European journal of neuroscience* **22**(11), 2775–82.

Milligan, E. D., V. Zapata, M. Chacur, D. Schoeniger, J. Biedenkapp, K. A. O'Connor, G. M. Verge, G. Chapman, P. Green, A. C. Foster, G. S. Naeve, S. F. Maier, and L. R. Watkins: 2004, 'Evidence that exogenous and endogenous fractalkine can induce spinal nociceptive facilitation in rats.'. *The European journal of neuroscience* **20**(9), 2294–302.

Minematsu, S., M. Hiruta, M. Taki, Y. Fujii, and M. Aburada: 1991, 'Automatic monitoring system for the measurement of body weight, food and water consumption and spontaneous activity of a mouse.'. *The Journal of toxicological sciences* **16**(2), 61–73.

Miraucourt, L. S., R. Dallel, and D. L. Voisin: 2007, 'Glycine inhibitory dysfunction turns touch into pain through PKCgamma interneurons.'. *PloS one* **2**(11), e1116.

Miraucourt, L. S., X. Moisset, R. Dallel, and D. L. Voisin: 2009, 'Glycine inhibitory dysfunction induces a selectively dynamic, morphine-resistant, and neurokinin 1 receptor-independent mechanical allodynia.'. *The Journal of neuroscience : the official journal of the Society for Neuroscience* **29**(8), 2519–27.

Molander, C., H. F. Wang, C. Rivero-Melián, and G. Grant: 1996, 'Early decline and late restoration of spinal cord binding and transganglionic transport of isolectin B4 from Griffonia simplicifolia I after peripheral nerve transection or crush.'. *Restorative neurology and neuroscience* **10**(3), 123–33.

Molander, C., Q. Xu, and G. Grant: 1984, 'The cytoarchitectonic organization of the spinal cord in the rat. I. The lower thoracic and lumbosacral cord.'. *The Journal of comparative neurology* **230**(1), 133–41.

Molliver, D. C., M. J. Radeke, S. C. Feinstein, and W. D. Snider: 1995, 'Presence or absence of TrkA protein distinguishes subsets of small sensory neurons with unique cytochemical characteristics and dorsal horn projections.'. *The Journal of comparative neurology* **361**(3), 404–16.

Molliver, D. C., D. E. Wright, M. L. Leitner, A. S. Parsadanian, K. Doster, D. Wen, Q. Yan, and W. D. Snider: 1997, 'IB4-binding DRG neurons switch from NGF to GDNF dependence in early postnatal life.'. *Neuron* **19**(4), 849–61.

Molofsky, A. V. and B. Deneen: 2015, 'Astrocyte development: A Guide for the Perplexed.'. *Glia* **63**(8), 1320–9.

Moore, G.: 1998, 'Cramming More Components Onto Integrated Circuits'. *Proceedings of the IEEE* **86**(1), 82–85.

Moore, K. A., T. Kohno, L. A. Karchewski, J. Scholz, H. Baba, and C. J. Woolf: 2002, 'Partial peripheral nerve injury promotes a selective loss of GABAergic inhibition in the superficial dorsal horn of the spinal cord.'. *The Journal of neuroscience : the official journal of the Society for Neuroscience* **22**(15), 6724–31.

Morgan, M. M. and H. L. Fields: 1994, 'Pronounced changes in the activity of nociceptive modulatory neurons in the rostral ventromedial medulla in response to prolonged thermal noxious stimuli.'. *Journal of neurophysiology* **72**(3), 1161–70.

Morihara, K. and H. Tsuzuki: 1975, 'Specificity of Proteinase K from Tritirachium album Limber for Synthetic Peptides'. *Agricultural and Biological Chemistry* **39**, 1489–1492.

Morisset, V. and F. Nagy: 1999, 'Ionic basis for plateau potentials in deep dorsal horn neurons of the rat spinal cord.'. *The Journal of neuroscience : the official journal of the Society for Neuroscience* **19**(17), 7309–16.

Morris, J. L., P. König, T. Shimizu, P. Jobling, and I. L. Gibbins: 2005, 'Most peptide-containing sensory neurons lack proteins for exocytotic release and vesicular transport of glutamate.'. *The Journal of comparative neurology* **483**(1), 1–16.

Mullen, R. J., C. R. Buck, and A. M. Smith: 1992, 'NeuN, a neuronal specific nuclear protein in vertebrates.'. *Development (Cambridge, England)* **116**(1), 201–11.

Murray, M. and M. E. Goldberger: 1986, 'Replacement of synaptic terminals in lamina II and Clarke's nucleus after unilateral lumbosacral dorsal rhizotomy in adult cats.'. *The Journal of neuroscience : the official journal of the Society for Neuroscience* **6**(11), 3205–17.

Murthy, V. N., T. J. Sejnowski, and C. F. Stevens: 1997, 'Heterogeneous release properties of visualized individual hippocampal synapses.'. *Neuron* **18**(4), 599–612.

Nagy, G. G., M. Al-Ayyan, D. Andrew, M. Fukaya, M. Watanabe, and A. J. Todd: 2004a, 'Widespread expression of the AMPA receptor GluR2 subunit at glutamatergic synapses in the rat spinal cord and phosphorylation of GluR1 in response to noxious stimulation revealed with an antigen-unmasking method.'. *The Journal of neuroscience : the official journal of the Society for Neuroscience* **24**(25), 5766–77.

Nagy, I., C. A. Maggi, A. Dray, C. J. Woolf, and L. Urban: 1993, 'The role of neurokinin and N-methyl-D-aspartate receptors in synaptic transmission from capsaicin-sensitive primary afferents in the rat spinal cord in vitro.'. *Neuroscience* **52**(4), 1029–37.

Nagy, J. G., K. Palmer, and L. Perrone: 2004b, 'Iterative Methods for Image Deblurring: A Matlab Object-Oriented Approach'. *Numerical Algorithms* **36**(1), 73–93.

Nakagawa, T. and S. Kaneko: 2010, 'Spinal astrocytes as therapeutic targets for pathological pain.'. *Journal of pharmacological sciences* **114**(4), 347–53.

Nakaya, Y., T. Kaneko, R. Shigemoto, S. Nakanishi, and N. Mizuno: 1994, 'Immunohistochemical localization of substance P receptor in the central nervous system of the adult rat.'. *The Journal of comparative neurology* **347**(2), 249–74.

Narita, M., T. Yoshida, M. Nakajima, M. Narita, M. Miyatake, T. Takagi, Y. Yajima, and T. Suzuki: 2006, 'Direct evidence for spinal cord microglia in the development of a neuropathic pain-like state in mice.'. *Journal of neurochemistry* **97**(5), 1337–48.

Nasse, M. J. and J. C. Woehl: 2010, 'Realistic modeling of the illumination point spread function in confocal scanning optical microscopy.'. *Journal of the Optical Society of America. A, Optics, image science, and vision* **27**(2), 295–302.

Nasse, M. J., J. C. Woehl, and S. Huant: 2007, 'High-resolution mapping of the three-dimensional point spread function in the near-focus region of a confocal microscope'. *Applied Physics Letters* **90**(3), 031106.

Navlakha, S., J. Suhan, A. L. Barth, and Z. Bar-Joseph: 2013, 'A high-throughput framework to detect synapses in electron microscopy images.'. *Bioinformatics (Oxford, England)* **29**(13), i9–17.

Neumann, S., J. M. Braz, K. Skinner, I. J. Llewellyn-Smith, and A. I. Basbaum: 2008, 'Innocuous, not noxious, input activates PKCgamma interneurons of the spinal dorsal horn via myelinated afferent fibers.'. *The Journal of neuroscience : the official journal of the Society for Neuroscience* **28**(32), 7936–44.

Nicholls, D. G.: 1998, 'Presynaptic modulation of glutamate release.'. *Progress in brain research* **116**, 15–22.

Nichols, M. L., B. J. Allen, S. D. Rogers, J. R. Ghilardi, P. Honore, N. M. Luger, M. P. Finke, J. Li, D. A. Lappi, D. A. Simone, and P. W. Mantyh: 1999, 'Transmission of chronic nociception by spinal neurons expressing the substance P receptor.'. *Science (New York, N.Y.)* **286**(5444), 1558–61.

Nie, H., H. Zhang, and H. R. Weng: 2010, 'Minocycline prevents impaired glial glutamate uptake in the spinal sensory synapses of neuropathic rats.'. *Neuroscience* **170**(3), 901–12.

Nimmerjahn, A., F. Kirchhoff, and F. Helmchen: 2005, 'Resting microglial cells are highly dynamic surveillants of brain parenchyma in vivo.'. *Science (New York, N.Y.)* **308**(5726), 1314–8.

Nirogi, R., V. Goura, D. Shanmuganathan, P. Jayarajan, and R. Abraham: 2012, 'Comparison of manual and automated filaments for evaluation of neuropathic pain behavior in rats.'. *Journal of pharmacological and toxicological methods* **66**(1), 8–13.

Noakes, C. R., T. Goto, R. Keller, and A. Periasamy: 2001, 'Does digital deconvolution improve two-photon microscopy in deep tissue imaging?'. In: A. Periasamy and P. T. C. So (eds.): *BiOS 2001 The International Symposium on Biomedical Optics*. pp. 389–395, International Society for Optics and Photonics.

Nutile-McMenemy, N., A. Elfenbein, and J. A. Deleo: 2007, 'Minocycline decreases in vitro microglial motility, beta1-integrin, and Kv1.3 channel expression.'. *Journal of neurochemistry* **103**(5), 2035–46.

Obata, K., H. Yamanaka, K. Kobayashi, Y. Dai, T. Mizushima, H. Katsura, T. Fukuoka, A. Tokunaga, and K. Noguchi: 2006, 'The effect of site and type of nerve injury on the expression of brain-derived neurotrophic factor in the dorsal root ganglion and on neuropathic pain behavior.'. *Neuroscience* **137**(3), 961–70.

O'Callaghan, J. P. and D. B. Miller: 2010, 'Spinal glia and chronic pain.'. *Metabolism: clinical and experimental* **59 Suppl 1**, S21–6.

O'Connor, A. B. and R. H. Dworkin: 2009, 'Treatment of neuropathic pain: an overview of recent guidelines.'. *The American journal of medicine* **122**(10 Suppl), S22–32.

Ollion, J., J. Cochennec, F. Loll, C. Escudé, and T. Boudier: 2013, 'TANGO: a generic tool for high-throughput 3D image analysis for studying nuclear organization.'. *Bioinformatics (Oxford, England)* **29**(14), 1840–1.

O'Rourke, N. A., N. C. Weiler, K. D. Micheva, and S. J. Smith: 2012, 'Deep molecular diversity of mammalian synapses: why it matters and how to measure it.'. *Nature reviews. Neuroscience* **13**(6), 365–79.

Orstavik, K. and E. Jørum: 2010, 'Microneurographic findings of relevance to pain in patients with erythromelalgia and patients with diabetic neuropathy.'. *Neuroscience letters* **470**(3), 180–4.

Osikowicz, M., M. Skup, J. Mika, W. Makuch, J. Czarkowska-Bauch, and B. Przewlocka: 2009, 'Glial inhibitors influence the mRNA and protein levels of mGlu2/3, 5 and 7 receptors and potentiate the analgesic effects of their ligands in a mouse model of neuropathic pain.'. *Pain* **147**(1-3), 175–86.

Ossipov, M. H., G. O. Dussor, and F. Porreca: 2010, 'Central modulation of pain.'. *The Journal of clinical investigation* **120**(11), 3779–87.

Otsu, N.: 1979, 'A Threshold Selection Method from Gray-Level Histograms'. *IEEE Transactions on Systems, Man, and Cybernetics* **9**(1), 62–66.

Padi, S. S. V. and S. K. Kulkarni: 2008, 'Minocycline prevents the development of neuropathic pain, but not acute pain: possible anti-inflammatory and antioxidant mechanisms.'. *European journal of pharmacology* **601**(1-3), 79–87.

Palay, S.: 1967, 'Principles of Cellular Organization in the Nervous System'. In: G. Quarton, T. Melnechuk, and F. Schmitt (eds.): *The Neurosciences.* New York: Rockefeller University Press, pp. 24–31.

Palay, S. L.: 1956, 'Synapses in the central nervous system.'. *The Journal of biophysical and biochemical cytology* **2**(4 Suppl), 193–202.

Pappas, G. and S. Waxman: 1972, 'synaptic fine structure - morphological correlates of chemical and electrotonic transmission'. In: D. Purpura and G. Pappas (eds.): *Structure and Function of Synapses.* New York: Raven Press, Chapt. first, pp. 1–47.

Pasti, L., A. Volterra, T. Pozzan, and G. Carmignoto: 1997, 'Intracellular calcium oscillations in astrocytes: a highly plastic, bidirectional form of communication between neurons and astrocytes in situ.'. *The Journal of neuroscience : the official journal of the Society for Neuroscience* **17**(20), 7817–30.

Percie du Sert, N. and A. S. C. Rice: 2014, 'Improving the translation of analgesic drugs to the clinic: animal models of neuropathic pain.'. *British journal of pharmacology* **171**(12), 2951–63.

Perea, G. and A. Araque: 2005, 'Properties of synaptically evoked astrocyte calcium signal reveal synaptic information processing by astrocytes.'. *The Journal of neuroscience : the official journal of the Society for Neuroscience* **25**(9), 2192–203.

Perea, G. and A. Araque: 2007, 'Astrocytes potentiate transmitter release at single hippocampal synapses.'. *Science (New York, N.Y.)* **317**(5841), 1083–6.

Pereda, A. E.: 2014, 'Electrical synapses and their functional interactions with chemical synapses.'. *Nature reviews. Neuroscience* **15**(4), 250–63.

Perkins, J. R., A. Antunes-Martins, M. Calvo, J. Grist, W. Rust, R. Schmid, T. Hildebrandt, M. Kohl, C. Orengo, S. B. McMahon, and D. L. H. Bennett: 2014, 'A comparison of RNA-seq and exon arrays for whole genome transcription profiling of the L5 spinal nerve transection model of neuropathic pain in the rat.'. *Molecular pain* **10**, 7.

Peters, A., S. Palay, and H. d. F. Webster: 1976, *The Fine Structure of the Nervous System: The Neurons and Supporting Cells.* Philadelphia: W. B. Saunders, 2nd edition.

Peterson, D.: 2004, 'The Use of Fluorescent Probes in Cell-Counting Procedures'. In: S. Evans, A. Janson, and NyengaardJens (eds.): *Quantitative Methods in Neuroscience.* Oxford University Press, Chapt. 4, pp. 86–110.

Petkó, M. and M. Antal: 2012, 'Propriospinal pathways in the dorsal horn (laminae I-IV) of the rat lumbar spinal cord.'. *Brain research bulletin* **89**(1-2), 41–9.

Petralia, R. S., Y.-X. Wang, M. P. Mattson, and P. J. Yao: 2015, 'Structure, Distribution, and Function of Neuronal/Synaptic Spinules and Related Invaginating Projections.'. *Neuromolecular medicine* **17**(3), 211–40.

Pieraut, S., V. Laurent-Matha, C. Sar, T. Hubert, I. Méchaly, C. Hilaire, M. Mersel, E. Delpire, J. Valmier, and F. Scamps: 2007, 'NKCC1 phosphorylation stimulates neurite growth of injured adult sensory neurons.'. *The Journal of neuroscience : the official journal of the Society for Neuroscience* **27**(25), 6751–9.

Piette, D., M. Hendrickx, E. Willems, C. R. Kemp, and L. Leyns: 2008, 'An optimized procedure for whole-mount in situ hybridization on mouse embryos and embryoid bodies'. *Nature Protocols* **3**(7), 1194–1201.

Polgár, E., J. H. Fowler, M. M. McGill, and A. J. Todd: 1999, 'The types of neuron which contain protein kinase C gamma in rat spinal cord.'. *Brain research* **833**(1), 71–80.

Polgár, E., S. Gray, J. S. Riddell, and A. J. Todd: 2004, 'Lack of evidence for significant neuronal loss in laminae I-III of the spinal dorsal horn of the rat in the chronic constriction injury model.'. *Pain* **111**(1-2), 144–50.

Polgár, E., D. I. Hughes, A. Z. Arham, and A. J. Todd: 2005, 'Loss of neurons from laminas I-III of the spinal dorsal horn is not required for development of tactile allodynia in the spared nerve injury model of neuropathic pain.'. *The Journal of neuroscience : the official journal of the Society for Neuroscience* **25**(28), 6658–66.

Polgár, E., D. I. Hughes, J. S. Riddell, D. J. Maxwell, Z. Puskár, and A. J. Todd: 2003, 'Selective loss of spinal GABAergic or glycinergic neurons is not necessary for development of thermal hyperalgesia in the chronic constriction injury model of neuropathic pain.'. *Pain* **104**(1-2), 229–39.

Polgár, E. and A. J. Todd: 2008, 'Tactile allodynia can occur in the spared nerve injury model in the rat without selective loss of GABA or GABA(A) receptors from synapses in laminae I-II of the ipsilateral spinal dorsal horn.'. *Neuroscience* **156**(1), 193–202.

Popper, K.: 1959, *The Logic of Scientific Discovery*. London: Hutchinson & Co.

Porreca, F., M. H. Ossipov, and G. F. Gebhart: 2002, 'Chronic pain and medullary descending facilitation.'. *Trends in neurosciences* **25**(6), 319–25.

Possidente, B. and S. Birnbaum: 1979, 'Circadian rhythms for food and water consumption in the mouse, Mus musculus'. *Physiology & Behavior* **22**(4), 657–660.

Possidente, B., J. P. Hegmann, B. Elder, and L. Carlson: 1980, 'Dissociation of circadian rhythms for food and water consumption in mice.'. *Physiology & behavior* **25**(2), 279–81.

Pozzan, T., R. Rizzuto, P. Volpe, and J. Meldolesi: 1994, 'Molecular and cellular physiology of intracellular calcium stores.'. *Physiological reviews* **74**(3), 595–636.

Price, T. J., F. Cervero, M. S. Gold, D. L. Hammond, and S. A. Prescott: 2009, 'Chloride regulation in the pain pathway.'. *Brain research reviews* **60**(1), 149–70.

Prodanov, D. and K. Verstreken: 2012, 'Automated Segmentation and Morphometry of Cell and Tissue Structures. Selected Algorithms in ImageJ'. In: B. Schaller (ed.): *Molecular Imaging*. InTech, Chapt. 8, pp. 183–208.

Punnakkal, P., C. von Schoultz, K. Haenraets, H. Wildner, and H. U. Zeilhofer: 2014, 'Morphological, biophysical and synaptic properties of glutamatergic neurons of the mouse spinal dorsal horn.'. *The Journal of physiology* **592**(Pt 4), 759–76.

Raghavendra, V., F. Tanga, and J. A. DeLeo: 2003, 'Inhibition of microglial activation attenuates the development but not existing hypersensitivity in a rat model of neuropathy.'. *The Journal of pharmacology and experimental therapeutics* **306**(2), 624–30.

Rahman, W., C. S. Bauer, K. Bannister, J.-L. Vonsy, A. C. Dolphin, and A. H. Dickenson: 2009, 'Descending serotonergic facilitation and the antinociceptive effects of pregabalin in a rat model of osteoarthritic pain.'. *Molecular pain* **5**, 45.

Rahman, W., R. D'Mello, and A. H. Dickenson: 2008, 'Peripheral nerve injury-induced changes in spinal alpha(2)-adrenoceptor-mediated modulation of mechanically evoked dorsal horn neuronal responses.'. *The journal of pain : official journal of the American Pain Society* **9**(4), 350–9.

Raivich, G., R. Hellweg, and G. W. Kreutzberg: 1991, 'NGF receptor-mediated reduction in axonal NGF uptake and retrograde transport following sciatic nerve injury and during regeneration.'. *Neuron* **7**(1), 151–64.

Ramon y Cajal, S.: 1989, *Recollections of my life*. The MIT Press.

Ramos-Vara, J. A.: 2005, 'Technical aspects of immunohistochemistry.'. *Veterinary pathology* **42**(4), 405–26.

Regehr, W. and C. Stevens: 2001, 'Physiology of Synaptic Transmission and Short-Term Plasticity'. In: W. Cowan, T. C. Sudhof, and C. Stevens (eds.): *Synapses*. Baltimore: Johns Hopkins University Press, first edition, Chapt. third, pp. 135–176.

Regehr, W. G.: 2012, 'Short-term presynaptic plasticity.'. *Cold Spring Harbor perspectives in biology* **4**(7), a005702.

Rexed, B.: 1952, 'The cytoarchitectonic organization of the spinal cord in the cat.'. *The Journal of comparative neurology* **96**(3), 414–95.

Ribeiro-Da-Silva, A., J. M. Castro-Lopes, and A. Coimbra: 1986, 'Distribution of glomeruli with fluoride-resistant acid phosphatase (FRAP)-containing terminals in the substantia gelatinosa of the rat.'. *Brain research* **377**(2), 323–9.

Ribeiro-da Silva, A. and A. Coimbra: 1982, 'Two types of synaptic glomeruli and their distribution in laminae I-III of the rat spinal cord.'. *The Journal of comparative neurology* **209**(2), 176–86.

Ribeiro-da Silva, A., D. Pignatelli, and A. Coimbra: 1985, 'Synaptic architecture of glomeruli in superficial dorsal horn of rat spinal cord, as shown in serial reconstructions.'. *Journal of neurocytology* **14**(2), 203–220.

Ribeiro-da Silva, A., P. Tagari, and A. C. Cuello: 1989, 'Morphological characterization of substance P-like immunoreactive glomeruli in the superficial dorsal horn of the rat spinal cord and trigeminal subnucleus caudalis: a quantitative study.'. *The Journal of comparative neurology* **281**(4), 497–15.

Rigaud, M., G. Gemes, M.-E. Barabas, D. I. Chernoff, S. E. Abram, C. L. Stucky, and Q. H. Hogan: 2008, 'Species and strain differences in rodent sciatic nerve anatomy: implications for studies of neuropathic pain.'. *Pain* **136**(1-2), 188–201.

Ringkamp, M. and R. A. Meyer: 2005, 'Injured versus uninjured afferents: Who is to blame for neuropathic pain?'. *Anesthesiology* **103**(2), 221–3.

Rizzoli, S. O.: 2014, 'Synaptic vesicle recycling: steps and principles'. *The EMBO Journal* **33**(8), 788–822.

Rizzoli, S. O. and W. J. Betz: 2005, 'Synaptic vesicle pools.'. *Nature reviews. Neuroscience* **6**(1), 57–69.

Rudolph, S., M.-C. Tsai, H. von Gersdorff, and J. I. Wadiche: 2015, 'The ubiquitous nature of multivesicular release.'. *Trends in neurosciences* **38**(7), 428–38.

Rudomin, P. and R. F. Schmidt: 1999, 'Presynaptic inhibition in the vertebrate spinal cord revisited.'. *Experimental brain research* **129**(1), 1–37.

Russell, R. A., N. M. Adams, D. A. Stephens, E. Batty, K. Jensen, and P. S. Freemont: 2009, 'Segmentation of fluorescence microscopy images for quantitative analysis of cell nuclear architecture.'. *Biophysical journal* **96**(8), 3379–89.

Sahoo, P., S. Soltani, and A. Wong: 1988, 'A survey of thresholding techniques'. *Computer Vision, Graphics, and Image Processing* **41**(2), 233–260.

Salter, M. W. and S. Beggs: 2014, 'Sublime microglia: expanding roles for the guardians of the CNS.'. *Cell* **158**(1), 15–24.

Sandkühler, J.: 2009, 'Models and mechanisms of hyperalgesia and allodynia.'. *Physiological reviews* **89**(2), 707–58.

Satoh, O. and K. Omote: 1996, 'Roles of monoaminergic, glycinergic and GABAergic inhibitory systems in the spinal cord in rats with peripheral mononeuropathy.'. *Brain research* **728**(1), 27–36.

Schafer, D. P., E. K. Lehrman, A. G. Kautzman, R. Koyama, A. R. Mardinly, R. Yamasaki, R. M. Ransohoff, M. E. Greenberg, B. A. Barres, and B. Stevens: 2012, 'Microglia sculpt postnatal neural circuits in an activity and complement-dependent manner.'. *Neuron* **74**(4), 691–705.

Schmitz, C., B. S. Eastwood, S. J. Tappan, J. R. Glaser, D. A. Peterson, and P. R. Hof: 2014, 'Current automated 3D cell detection methods are not a suitable replacement for manual stereologic cell counting.'. *Frontiers in neuroanatomy* **8**, 27.

Schmitz, C. and P. R. Hof: 2005, 'Design-based stereology in neuroscience.'. *Neuroscience* **130**(4), 813–31.

Schneider, S. P.: 1992, 'Functional properties and axon terminations of interneurons in laminae III-V of the mammalian spinal dorsal horn in vitro.'. *Journal of neurophysiology* **68**(5), 1746–59.

Schneider Gasser, E. M., C. J. Straub, P. Panzanelli, O. Weinmann, M. Sassoè-Pognetto, and J.-M. Fritschy: 2006, 'Immunofluorescence in brain sections: simultaneous detection of presynaptic and postsynaptic proteins in identified neurons.'. *Nature protocols* **1**(4), 1887–97.

Schoch, S. and E. D. Gundelfinger: 2006, 'Molecular organization of the presynaptic active zone.'. *Cell and tissue research* **326**(2), 379–91.

Scholz, J., D. C. Broom, D.-H. Youn, C. D. Mills, T. Kohno, M. R. Suter, K. A. Moore, I. Decosterd, R. E. Coggeshall, and C. J. Woolf: 2005, 'Blocking caspase activity prevents transsynaptic neuronal apoptosis and the loss of inhibition in lamina II of the dorsal horn after peripheral nerve injury.'. *The Journal of neuroscience : the official journal of the Society for Neuroscience* **25**(32), 7317–23.

Schulz, C., E. Gomez Perdiguero, L. Chorro, H. Szabo-Rogers, N. Cagnard, K. Kierdorf, M. Prinz, B. Wu, S. E. W. Jacobsen, J. W. Pollard, J. Frampton, K. J. Liu, and F. Geissmann: 2012, 'A lineage of myeloid cells independent of Myb and hematopoietic stem cells.'. *Science (New York, N.Y.)* **336**(6077), 86–90.

Schummers, J., H. Yu, and M. Sur: 2008, 'Tuned responses of astrocytes and their influence on hemodynamic signals in the visual cortex.'. *Science (New York, N.Y.)* **320**(5883), 1638–43.

Seth, P. and N. Koul: 2008, 'Astrocyte, the star avatar: redefined.'. *Journal of biosciences* **33**(3), 405–21.

Seung, H. S. and U. Sümbül: 2014, 'Neuronal cell types and connectivity: lessons from the retina.'. *Neuron* **83**(6), 1262–72.

Sezgin, M. and B. Sankur: 2004, 'Survey over image thresholding techniques and quantitative performance evaluation'.

Shadiack, A. M., Y. Sun, and R. E. Zigmond: 2001, 'Nerve growth factor antiserum induces axotomy-like changes in neuropeptide expression in intact sympathetic and sensory neurons.'. *The Journal of neuroscience : the official journal of the Society for Neuroscience* **21**(2), 363–71.

Shehab, S. A. and M. E. Atkinson: 1986, 'Vasoactive intestinal polypeptide (VIP) increases in the spinal cord after peripheral axotomy of the sciatic nerve originate from primary afferent neurons.'. *Brain research* **372**(1), 37–44.

Shehab, S. A. S., R. C. Spike, and A. J. Todd: 2003, 'Evidence against cholera toxin B subunit as a reliable tracer for sprouting of primary afferents following peripheral nerve injury.'. *Brain research* **964**(2), 218–27.

Shehab, S. A. S., R. C. Spike, and A. J. Todd: 2004, 'Do central terminals of intact myelinated primary afferents sprout into the superficial dorsal horn of rat spinal cord after injury to a neighboring peripheral nerve?'. *The Journal of comparative neurology* **474**(3), 427–37.

Sheng, M.: 2001, 'The Postsynaptic Specialization'. In: W. Cowan, T. C. Sudhof, and C. F. Stevens (eds.): *Synapses*. Baltimore: Johns Hopkins University Press, first edition, Chapt. seventh, pp. 315–356.

Sheng, M. and E. Kim: 2011, 'The postsynaptic organization of synapses.'. *Cold Spring Harbor perspectives in biology* **3**(12), a005678–.

Shepherd, G.: 2009, *Creating Modern Neuroscience: The Revolutionary 1950s*. Oxford University Press, USA.

Shi, T. J., T. Tandrup, E. Bergman, Z. Q. Xu, B. Ulfhake, and T. Hökfelt: 2001, 'Effect of peripheral nerve injury on dorsal root ganglion neurons in the C57 BL/6J mouse: marked changes both in cell numbers and neuropeptide expression.'. *Neuroscience* **105**(1), 249–63.

Shields, S. D., W. A. Eckert, and A. I. Basbaum: 2003, 'Spared nerve injury model of neuropathic pain in the mouse: a behavioral and anatomic analysis.'. *The journal of pain : official journal of the American Pain Society* **4**(8), 465–70.

Shupliakov, O., V. Haucke, and A. Pechstein: 2011, 'How synapsin I may cluster synaptic vesicles.'. *Seminars in cell & developmental biology* **22**(4), 393–9.

Sibarita, J.-B.: 2005, 'Deconvolution microscopy.'. *Advances in biochemical engineering/biotechnology* **95**, 201–43.

Sikandar, S., I. Ronga, G. D. Iannetti, and A. H. Dickenson: 2013, 'Neural coding of nociceptive stimuli-from rat spinal neurones to human perception.'. *Pain* **154**(8), 1263–73.

Simone, D. A., L. S. Sorkin, U. Oh, J. M. Chung, C. Owens, R. H. LaMotte, and W. D. Willis: 1991, 'Neurogenic hyperalgesia: central neural correlates in responses of spinothalamic tract neurons.'. *Journal of neurophysiology* **66**(1), 228–46.

Sivilotti, L. G., G. Gerber, B. Rawat, and C. J. Woolf: 1995, 'Morphine selectively depresses the slowest, NMDA-independent component of C-fibre-evoked synaptic activity in the rat spinal cord in vitro.'. *The European journal of neuroscience* **7**(1), 12–8.

Sivilotti, L. G., S. W. Thompson, and C. J. Woolf: 1993, 'Rate of rise of the cumulative depolarization evoked by repetitive stimulation of small-caliber afferents is a predictor of action potential windup in rat spinal neurons in vitro.'. *Journal of neurophysiology* **69**(5), 1621–31.

Sloan, S. A. and B. A. Barres: 2014, 'Mechanisms of astrocyte development and their contributions to neurodevelopmental disorders.'. *Current opinion in neurobiology* **27**, 75–81.

Smith, B. H. and N. Torrance: 2012, 'Epidemiology of neuropathic pain and its impact on quality of life.'. *Current pain and headache reports* **16**(3), 191–8.

Smith, B. H., N. Torrance, M. I. Bennett, and A. J. Lee: 2007, 'Health and quality of life associated with chronic pain of predominantly neuropathic origin in the community.'. *The Clinical journal of pain* **23**(2), 143–9.

Smith, S. J. and G. J. Augustine: 1988, 'Calcium ions, active zones and synaptic transmitter release.'. *Trends in neurosciences* **11**(10), 458–64.

Snider, W. D. and S. B. McMahon: 1998, 'Tackling pain at the source: new ideas about nociceptors.'. *Neuron* **20**(4), 629–32.

Solway, B., S. C. Bose, G. Corder, R. R. Donahue, and B. K. Taylor: 2011, 'Tonic inhibition of chronic pain by neuropeptide Y.'. *Proceedings of the National Academy of Sciences of the United States of America* **108**(17), 7224–9.

Somogyi, J., A. Baude, Y. Omori, H. Shimizu, S. El Mestikawy, M. Fukaya, R. Shigemoto, M. Watanabe, and P. Somogyi: 2004, 'GABAergic basket cells expressing cholecystokinin contain vesicular glutamate transporter type 3 (VGLUT3) in their synaptic terminals in hippocampus and isocortex of the rat.'. *The European journal of neuroscience* **19**(3), 552–69.

Sompuram, S. R., K. Vani, E. Messana, and S. A. Bogen: 2004, 'A molecular mechanism of formalin fixation and antigen retrieval.'. *American journal of clinical pathology* **121**(2), 190–9.

Sonka, M., V. Hlavac, and R. Boyle: 2013, *Image Processing, Analysis, and Machine Vision*. Stamford: Cengage Learning, fourth edition.

Spacek, J. and K. M. Harris: 2004, 'Trans-endocytosis via spinules in adult rat hippocampus.'. *The Journal of neuroscience : the official journal of the Society for Neuroscience* **24**(17), 4233–41.

Staniland, A. A., A. K. Clark, R. Wodarski, O. Sasso, F. Maione, F. D'Acquisto, and M. Malcangio: 2010, 'Reduced inflammatory and neuropathic pain and decreased spinal microglial response in fractalkine receptor (CX3CR1) knockout mice.'. *Journal of neurochemistry* **114**(4), 1143–57.

Sterio, D. C.: 1984, 'The unbiased estimation of number and sizes of arbitrary particles using the disector.'. *Journal of microscopy* **134**(Pt 2), 127–36.

Stevens, B., N. J. Allen, L. E. Vazquez, G. R. Howell, K. S. Christopherson, N. Nouri, K. D. Micheva, A. K. Mehalow, A. D. Huberman, B. Stafford, A. Sher, A. M. Litke, J. D. Lambris, S. J. Smith, S. W. M. John, and B. A. Barres: 2007, 'The classical complement cascade mediates CNS synapse elimination.'. *Cell* **131**(6), 1164–78.

Stevens, C. F. and Y. Wang: 1995, 'Facilitation and depression at single central synapses.'. *Neuron* **14**(4), 795–802.

Stjärne, L.: 1999, 'Catecholaminergic neurotransmission: flagship of all neurobiology.'. *Acta physiologica Scandinavica* **166**(4), 251–9.

Streit, W. J., B. A. Schulte, D. J. Balentine, and S. S. Spicer: 1985, 'Histochemical localization of galactose-containing glycoconjugates in sensory neurons and their processes in the central and peripheral nervous system of the rat.'. *The journal of histochemistry and cytochemistry : official journal of the Histochemistry Society* **33**(10), 1042–52.

Sudhof, T. C.: 2001, 'The Synaptic Cleft and Synaptic Cell Adhesion'. In: W. Cowan, T. C. Sudhof, and C. Stevens (eds.): *Synapses*. Baltimore: Johns Hopkins University Press, first edition, Chapt. sixth, pp. 275–314.

Sudhof, T. C.: 2004, 'The synaptic vesicle cycle.'. *Annual review of neuroscience* **27**, 509–47.

Südhof, T. C.: 2012, 'The presynaptic active zone.'. *Neuron* **75**(1), 11–25.

Südhof, T. C.: 2014, 'The molecular machinery of neurotransmitter release (nobel lecture).'. *Angewandte Chemie (International ed. in English)* **53**(47), 12696–717.

Südhof, T. C. and J. E. Rothman: 2009, 'Membrane fusion: grappling with SNARE and SM proteins.'. *Science (New York, N.Y.)* **323**(5913), 474–7.

Sullivan, J., K. Karra, S. A. T. Moxon, A. Vallejos, H. Motenko, J. D. Wong, J. Aleksic, R. Balakrishnan, G. Binkley, T. Harris, B. Hitz, P. Jayaraman, R. Lyne, S. Neuhauser, C. Pich, R. N. Smith, Q. Trinh, J. M. Cherry, J. Richardson, L. Stein, S. Twigger, M. Westerfield, E. Worthey, and G. Micklem: 2013, 'InterMOD: integrated data and tools for the unification of model organism research.'. *Scientific reports* **3**, 1802.

Sun, R.-Q., N. B. Lawand, and W. D. Willis: 2003, 'The role of calcitonin gene-related peptide (CGRP) in the generation and maintenance of mechanical allodynia and hyperalgesia in rats after intradermal injection of capsaicin.'. *Pain* **104**(1-2), 201–8.

Sun, T., H.-S. Xiao, P.-B. Zhou, Y.-J. Lu, L. Bao, and X. Zhang: 2006, 'Differential expression of synaptoporin and synaptophysin in primary sensory neurons and up-regulation of synaptoporin after peripheral nerve injury.'. *Neuroscience* **141**(3), 1233–45.

Susaki, E. A., K. Tainaka, D. Perrin, F. Kishino, T. Tawara, T. M. Watanabe, C. Yokoyama, H. Onoe, M. Eguchi, S. Yamaguchi, T. Abe, H. Kiyonari, Y. Shimizu, A. Miyawaki, H. Yokota, and H. R. Ueda: 2014, 'Whole-brain imaging with single-cell resolution using chemical cocktails and computational analysis.'. *Cell* **157**(3), 726–39.

Suzuki, R., S. Morcuende, M. Webber, S. P. Hunt, and A. H. Dickenson: 2002, 'Superficial NK1-expressing neurons control spinal excitability through activation of descending pathways.'. *Nature neuroscience* **5**(12), 1319–26.

Suzuki, R., W. Rahman, S. P. Hunt, and A. H. Dickenson: 2004, 'Descending facilitatory control of mechanically evoked responses is enhanced in deep dorsal horn neurones following peripheral nerve injury.'. *Brain research* **1019**(1-2), 68–76.

Suzuki, R., W. Rahman, L. J. Rygh, M. Webber, S. P. Hunt, and A. H. Dickenson: 2005, 'Spinal-supraspinal serotonergic circuits regulating neuropathic pain and its treatment with gabapentin.'. *Pain* **117**(3), 292–303.

Svensson, C. I. and E. Brodin: 2010, 'Spinal astrocytes in pain processing: non-neuronal cells as therapeutic targets.'. *Molecular interventions* **10**(1), 25–38.

Szabolcs, M. J., M. Kopp, and G. E. Schaden: 1989, 'Carbonic anhydrase activity in the peripheral nervous system of rat: the enzyme as a marker for muscle afferents.'. *Brain research* **492**(1-2), 129–38.

Tajti, J., J. Fischer, E. Knyihár-Csillik, and B. Csillik: 1988, 'Transganglionic regulation and fine structural localization of lectin-reactive carbohydrate epitopes in primary sensory neurons of the rat.'. *Histochemistry* **88**(3-6), 213–8.

Takahashi, Y., Y. Nakajima, and T. Sakamoto: 1994, 'Dermatome mapping in the rat hindlimb by electrical stimulation of the spinal nerves'. *Neuroscience Letters* **168**(1-2), 85–88.

Takei, K., O. Mundigl, L. Daniell, and P. De Camilli: 1996, 'The synaptic vesicle cycle: a single vesicle budding step involving clathrin and dynamin.'. *The Journal of cell biology* **133**(6), 1237–50.

Takeuchi, T., A. J. Duszkiewicz, and R. G. M. Morris: 2014, 'The synaptic plasticity and memory hypothesis: encoding, storage and persistence.'. *Philosophical transactions of the Royal Society of London. Series B, Biological sciences* **369**(1633), 20130288.

Tan, A. M., Y.-W. Chang, P. Zhao, B. C. Hains, and S. G. Waxman: 2011, 'Rac1-regulated dendritic spine remodeling contributes to neuropathic pain after peripheral nerve injury.'. *Experimental neurology* **232**(2), 222–33.

Tan, A. M., O. A. Samad, T. Z. Fischer, P. Zhao, A.-K. Persson, and S. G. Waxman: 2012, 'Maladaptive dendritic spine remodeling contributes to diabetic neuropathic pain.'. *The Journal of neuroscience : the official journal of the Society for Neuroscience* **32**(20), 6795–807.

Tandrup, T., C. J. Woolf, and R. E. Coggeshall: 2000, 'Delayed loss of small dorsal root ganglion cells after transection of the rat sciatic nerve.'. *The Journal of comparative neurology* **422**(2), 172–80.

Tawfik, V. L., M. R. Regan, C. Haenggeli, M. L. Lacroix-Fralish, N. Nutile-McMenemy, N. Perez, J. D. Rothstein, and J. A. DeLeo: 2008, 'Propentofylline-induced astrocyte modulation leads to alterations in glial glutamate promoter activation following spinal nerve transection.'. *Neuroscience* **152**(4), 1086–92.

Thiel, G.: 1993, 'Synapsin I, synapsin II, and synaptophysin: marker proteins of synaptic vesicles.'. *Brain pathology (Zurich, Switzerland)* **3**(1), 87–95.

Thompson, S. W., A. E. King, and C. J. Woolf: 1990, 'Activity-Dependent Changes in Rat Ventral Horn Neurons in vitro; Summation of Prolonged Afferent Evoked Postsynaptic Depolarizations Produce a d-2-Amino-5-Phosphonovaleric Acid Sensitive Windup.'. *The European journal of neuroscience* **2**(7), 638–49.

Thureson-Klein, A. K. and R. L. Klein: 1990, 'Exocytosis from neuronal large dense-cored vesicles.'. *International review of cytology* **121**, 67–126.

Tikka, T., B. L. Fiebich, G. Goldsteins, R. Keinanen, and J. Koistinaho: 2001, 'Minocycline, a tetracycline derivative, is neuroprotective against excitotoxicity by inhibiting activation and proliferation of microglia.'. *The Journal of neuroscience : the official journal of the Society for Neuroscience* **21**(8), 2580–8.

Todd, A. J.: 2002, 'Anatomy of primary afferents and projection neurones in the rat spinal dorsal horn with particular emphasis on substance P and the neurokinin 1 receptor.'. *Experimental physiology* **87**(2), 245–9.

Todd, A. J.: 2010, 'Neuronal circuitry for pain processing in the dorsal horn.'. *Nature reviews. Neuroscience* **11**(12), 823–36.

Todd, A. J., M. M. McGill, and S. A. Shehab: 2000, 'Neurokinin 1 receptor expression by neurons in laminae I, III and IV of the rat spinal dorsal horn that project to the brainstem.'. *The European journal of neuroscience* **12**(2), 689–700.

Todd, A. J. and A. C. Sullivan: 1990, 'Light microscope study of the coexistence of GABA-like and glycine-like immunoreactivities in the spinal cord of the rat.'. *The Journal of comparative neurology* **296**(3), 496–505.

Tomer, R., L. Ye, B. Hsueh, and K. Deisseroth: 2014, 'Advanced CLARITY for rapid and high-resolution imaging of intact tissues.'. *Nature protocols* **9**(7), 1682–97.

Tonegawa, S., X. Liu, S. Ramirez, and R. Redondo: 2015, 'Memory Engram Cells Have Come of Age'. *Neuron* **87**(5), 918–931.

Tønnesen, J. and U. V. Nägerl: 2013, 'Superresolution imaging for neuroscience.'. *Experimental neurology* **242**, 33–40.

Tracey, I.: 2010, 'Getting the pain you expect: mechanisms of placebo, nocebo and reappraisal effects in humans.'. *Nature medicine* **16**(11), 1277–83.

Tracey, I. and P. W. Mantyh: 2007, 'The cerebral signature for pain perception and its modulation.'. *Neuron* **55**(3), 377–91.

Trang, T., S. Beggs, X. Wan, and M. W. Salter: 2009, 'P2X4-receptor-mediated synthesis and release of brain-derived neurotrophic factor in microglia is dependent on calcium and p38-mitogen-activated protein kinase activation.'. *The Journal of neuroscience : the official journal of the Society for Neuroscience* **29**(11), 3518–28.

Tremblay, M.-È., R. L. Lowery, and A. K. Majewska: 2010, 'Microglial interactions with synapses are modulated by visual experience.'. *PLoS biology* **8**(11), e1000527.

Tsuda, M., K. Inoue, and M. W. Salter: 2005, 'Neuropathic pain and spinal microglia: a big problem from molecules in "small" glia.'. *Trends in neurosciences* **28**(2), 101–7.

Tsuda, M., K. Kuboyama, T. Inoue, K. Nagata, H. Tozaki-Saitoh, and K. Inoue: 2009, 'Behavioral phenotypes of mice lacking purinergic P2X4 receptors in acute and chronic pain assays.'. *Molecular pain* **5**, 28.

Tsuda, M., Y. Shigemoto-Mogami, S. Koizumi, A. Mizokoshi, S. Kohsaka, M. W. Salter, and K. Inoue: 2003, 'P2X4 receptors induced in spinal microglia gate tactile allodynia after nerve injury.'. *Nature* **424**(6950), 778–83.

Tsuruoka, M., K. Matsutani, and T. Inoue: 2003, 'Coeruleospinal inhibition of nociceptive processing in the dorsal horn during unilateral hindpaw inflammation in the rat.'. *Pain* **104**(1-2), 353–61.

Tyagarajan, S. K. and J.-M. Fritschy: 2014, 'Gephyrin: a master regulator of neuronal function?'. *Nature reviews. Neuroscience* **15**(3), 141–56.

Tynan, B. E., M. G. Papich, M. E. Kerl, and L. A. Cohn: 2015, 'Pharmacokinetics of minocycline in domestic cats.'. *Journal of feline medicine and surgery*.

Ulmann, L., J. P. Hatcher, J. P. Hughes, S. Chaumont, P. J. Green, F. Conquet, G. N. Buell, A. J. Reeve, I. P. Chessell, and F. Rassendren: 2008, 'Up-regulation of P2X4 receptors in spinal microglia after peripheral nerve injury mediates BDNF release and neuropathic pain.'. *The Journal of neuroscience : the official journal of the Society for Neuroscience* **28**(44), 11263–8.

Urban, M. O. and G. F. Gebhart: 1997, 'Characterization of biphasic modulation of spinal nociceptive transmission by neurotensin in the rat rostral ventromedial medulla.'. *Journal of neurophysiology* **78**(3), 1550–62.

Urban, M. O. and G. F. Gebhart: 1999, 'Supraspinal contributions to hyperalgesia.'. *Proceedings of the National Academy of Sciences of the United States of America* **96**(14), 7687–92.

Usoskin, D., A. Furlan, S. Islam, H. Abdo, P. Lönnerberg, D. Lou, J. Hjerling-Leffler, J. Haeggström, O. Kharchenko, P. V. Kharchenko, S. Linnarsson, and P. Ernfors: 2014, 'Unbiased classification of sensory neuron types by large-scale single-cell RNA sequencing'. *Nature Neuroscience* **18**(1), 145–53.

Valenstein, E.: 2006, *The War of The Soups And The Sparks*. Columbia University Press, first edit edition.

Valtschanoff, J. G., A. Burette, R. J. Wenthold, and R. J. Weinberg: 1999, 'Expression of NR2 receptor subunit in rat somatic sensory cortex: synaptic distribution and colocalization with NR1 and PSD-95.'. *The Journal of comparative neurology* **410**(4), 599–611.

Vega-Avelaira, D., A. Moss, and M. Fitzgerald: 2007, 'Age-related changes in the spinal cord microglial and astrocytic response profile to nerve injury.'. *Brain, behavior, and immunity* **21**(5), 617–23.

Vera-Portocarrero, L. P., J. Y. Xie, J. X. Yie, J. Kowal, M. H. Ossipov, T. King, and F. Porreca: 2006, 'Descending facilitation from the rostral ventromedial medulla maintains visceral pain in rats with experimental pancreatitis.'. *Gastroenterology* **130**(7), 2155–64.

Verge, G. M., E. D. Milligan, S. F. Maier, L. R. Watkins, G. S. Naeve, and A. C. Foster: 2004, 'Fractalkine (CX3CL1) and fractalkine receptor (CX3CR1) distribution in spinal cord and dorsal root ganglia under basal and neuropathic pain conditions.'. *The European journal of neuroscience* **20**(5), 1150–60.

Vogels, T. P., R. C. Froemke, N. Doyon, M. Gilson, J. S. Haas, R. Liu, A. Maffei, P. Miller, C. J. Wierenga, M. A. Woodin, F. Zenke, and H. Sprekeler: 2013, 'Inhibitory synaptic plasticity: spike timing-dependence and putative network function.'. *Frontiers in neural circuits* **7**, 119.

Volterra, A., N. Liaudet, and I. Savtchouk: 2014, 'Astrocyte Ca2+ signalling: an unexpected complexity'. *Nature reviews. Neuroscience* **15**(5), 327–35.

von Hehn, C. A., R. Baron, and C. J. Woolf: 2012, 'Deconstructing the neuropathic pain phenotype to reveal neural mechanisms.'. *Neuron* **73**(4), 638–52.

Wake, H., A. J. Moorhouse, S. Jinno, S. Kohsaka, and J. Nabekura: 2009, 'Resting microglia directly monitor the functional state of synapses in vivo and determine the fate of ischemic terminals.'. *The Journal of neuroscience : the official journal of the Society for Neuroscience* **29**(13), 3974–80.

Wakisaka, S., K. C. Kajander, and G. J. Bennett: 1992, 'Effects of peripheral nerve injuries and tissue inflammation on the levels of neuropeptide Y-like immunoreactivity in rat primary afferent neurons.'. *Brain research* **598**(1-2), 349–52.

Wall, P. D. and M. Gutnick: 1974, 'Properties of afferent nerve impulses originating from a neuroma.'. *Nature* **248**(5451), 740–3.

Wall, P. D., S. Waxman, and A. I. Basbaum: 1974, 'Ongoing activity in peripheral nerve: injury discharge.'. *Experimental neurology* **45**(3), 576–89.

Wang, D. D. and A. Bordey: 2008, 'The astrocyte odyssey.'. *Progress in neurobiology* **86**(4), 342–67.

Wang, X., N. Lou, Q. Xu, G.-F. Tian, W. G. Peng, X. Han, J. Kang, T. Takano, and M. Nedergaard: 2006, 'Astrocytic Ca2+ signaling evoked by sensory stimulation in vivo.'. *Nature neuroscience* **9**(6), 816–23.

Wang, X., J. Zhang, D. Eberhart, R. Urban, K. Meda, C. Solorzano, H. Yamanaka, D. Rice, and A. Basbaum: 2013, 'Excitatory superficial dorsal horn interneurons are functionally heterogeneous and required for the full behavioral expression of pain and itch.'. *Neuron* **78**(2), 312–24.

Watanabe, M., M. Fukaya, K. Sakimura, T. Manabe, M. Mishina, and Y. Inoue: 1998, 'Selective scarcity of NMDA receptor channel subunits in the stratum lucidum (mossy fibre-recipient layer) of the mouse hippocampal CA3 subfield.'. *The European journal of neuroscience* **10**(2), 478–87.

Watkins, J. C. and R. H. Evans: 1981, 'Excitatory amino acid transmitters.'. *Annual review of pharmacology and toxicology* **21**, 165–204.

Watkins, L. R., E. D. Milligan, and S. F. Maier: 2001, 'Spinal cord glia: new players in pain.'. *Pain* **93**(3), 201–5.

Wei, B., T. Kumada, T. Furukawa, K. Inoue, M. Watanabe, K. Sato, and A. Fukuda: 2013, 'Pre- and post-synaptic switches of GABA actions associated with Cl- homeostatic changes are induced in the spinal nucleus of the trigeminal nerve in a rat model of trigeminal neuropathic pain.'. *Neuroscience* **228**, 334–48.

Wendykier, P. and J. G. Nagy: 2010, 'Parallel Colt: A High-Performance Java Library for Scientific Computing and Image Processing'. *ACM Transactions on Mathematical Software* **37**(3), 31.

West, M. J.: 1993, 'New stereological methods for counting neurons.'. *Neurobiology of aging* **14**(4), 275–85.

West, M. J.: 1999, 'Stereological methods for estimating the total number of neurons and synapses: issues of precision and bias.'. *Trends in neurosciences* **22**(2), 51–61.

West, M. J.: 2001, 'Design based stereological methods for estimating the total number of objects in histological material.'. *Folia morphologica* **60**(1), 11–9.

West, M. J.: 2012, 'Introduction to stereology.'. *Cold Spring Harbor protocols* **2012**(8).

West, M. J.: 2013, 'Optimizing the sampling scheme for a stereological study: how many individuals, sections, and probes should be used.'. *Cold Spring Harbor protocols* **2013**(6), 521–32.

West, M. J., L. Slomianka, and H. J. Gundersen: 1991, 'Unbiased stereological estimation of the total number of neurons in thesubdivisions of the rat hippocampus using the optical fractionator.'. *The Anatomical record* **231**(4), 482–97.

West, S. J., K. Bannister, A. H. Dickenson, and D. L. Bennett: 2015, 'Circuitry and plasticity of the dorsal horn - Toward a better understanding of neuropathic pain.'. *Neuroscience* **300**, 254–75.

White, J. G., E. Southgate, J. N. Thomson, and S. Brenner: 1986, 'The Structure of the Nervous System of the Nematode Caenorhabditis elegans'. *Philosophical Transactions of the Royal Society B: Biological Sciences* **314**(1165), 1–340.

Wickersham, I. R., S. Finke, K.-K. Conzelmann, and E. M. Callaway: 2007, 'Retrograde neuronal tracing with a deletion-mutant rabies virus.'. *Nature methods* **4**(1), 47–9.

Willis, W. D.: 1999, 'Dorsal root potentials and dorsal root reflexes: a double-edged sword.'. *Experimental brain research* **124**(4), 395–421.

Winkler, H.: 1997, 'Membrane composition of adrenergic large and small dense cored vesicles and of synaptic vesicles: consequences for their biogenesis.'. *Neurochemical research* **22**(8), 921–32.

Winship, I. R., N. Plaa, and T. H. Murphy: 2007, 'Rapid astrocyte calcium signals correlate with neuronal activity and onset of the hemodynamic response in vivo.'. *The Journal of neuroscience : the official journal of the Society for Neuroscience* **27**(23), 6268–72.

Woodbury, C. J., F. A. Kullmann, S. L. McIlwrath, and H. R. Koerber: 2008, 'Identity of myelinated cutaneous sensory neurons projecting to nocireceptive laminae following nerve injury in adult mice.'. *The Journal of comparative neurology* **508**(3), 500–9.

Woodruff, G. N., A. C. Foster, R. Gill, J. A. Kemp, E. H. Wong, and L. L. Iversen: 1987, 'The interaction between MK-801 and receptors for N-methyl-D-aspartate: functional consequences.'. *Neuropharmacology* **26**(7B), 903–9.

Woolf, C. and Z. Wiesenfeld-Hallin: 1986, 'Substance P and calcitonin gene-related peptide synergistically modulate the gain of the nociceptive flexor withdrawal reflex in the rat.'. *Neuroscience letters* **66**(2), 226–30.

Woolf, C. J.: 1983, 'Evidence for a central component of post-injury pain hypersensitivity.'. *Nature* **306**(5944), 686–8.

Woolf, C. J. and M. W. Salter: 2000, 'Neuronal plasticity: increasing the gain in pain.'. *Science (New York, N.Y.)* **288**(5472), 1765–9.

Woolf, C. J., P. Shortland, and R. E. Coggeshall: 1992, 'Peripheral nerve injury triggers central sprouting of myelinated afferents.'. *Nature* **355**(6355), 75–8.

Woolf, C. J. and S. W. Thompson: 1991, 'The induction and maintenance of central sensitization is dependent on N-methyl-D-aspartic acid receptor activation; implications for the treatment of post-injury pain hypersensitivity states.'. *Pain* **44**(3), 293–9.

Wouterlood, F. G., T. Böckers, and M. P. Witter: 2003, 'Synaptic contacts between identified neurons visualized in the confocal laser scanning microscope. Neuroanatomical tracing combined with immunofluorescence detection of post-synaptic density proteins and target neuron-markers.'. *Journal of neuroscience methods* **128**(1-2), 129–42.

Wu, G., M. Ringkamp, T. V. Hartke, B. B. Murinson, J. N. Campbell, J. W. Griffin, and R. A. Meyer: 2001, 'Early onset of spontaneous activity in uninjured C-fiber nociceptors after injury to neighboring nerve fibers.'. *The Journal of neuroscience : the official journal of the Society for Neuroscience* **21**(8), RC140.

Xiao, H.-S., Q.-H. Huang, F.-X. Zhang, L. Bao, Y.-J. Lu, C. Guo, L. Yang, W.-J. Huang, G. Fu, S.-H. Xu, X.-P. Cheng, Q. Yan, Z.-D. Zhu, X. Zhang, Z. Chen, Z.-G. Han, and X. Zhang: 2002, 'Identification of gene expression profile of dorsal root ganglion in the rat peripheral axotomy model of neuropathic pain.'. *Proceedings of the National Academy of Sciences of the United States of America* **99**(12), 8360–5.

Xiao, W. H. and G. J. Bennett: 2008, 'Chemotherapy-evoked neuropathic pain: Abnormal spontaneous discharge in A-fiber and C-fiber primary afferent neurons and its suppression by acetyl-L-carnitine.'. *Pain* **135**(3), 262–70.

Xin, W.-J., H.-R. Weng, and P. M. Dougherty: 2009, 'Plasticity in expression of the glutamate transporters GLT-1 and GLAST in spinal dorsal horn glial cells following partial sciatic nerve ligation.'. *Molecular pain* **5**, 15.

Yamada, K., M. Fukaya, H. Shimizu, K. Sakimura, and M. Watanabe: 2001, 'NMDA receptor subunits GluRepsilon1, GluRepsilon3 and GluRzeta1 are enriched at the mossy fibre-granule cell synapse in the adult mouse cerebellum.'. *The European journal of neuroscience* **13**(11), 2025–36.

Yamamoto, Y., R. Terayama, N. Kishimoto, K. Maruhama, M. Mizutani, S. Iida, and T. Sugimoto: 2015, 'Activated microglia contribute to convergent nociceptive inputs to spinal dorsal horn neurons and the development of neuropathic pain.'. *Neurochemical research* **40**(5), 1000–12.

Yan, X. and H.-R. Weng: 2013, 'Endogenous interleukin-1β in neuropathic rats enhances glutamate release from the primary afferents in the spinal dorsal horn through coupling with presynaptic N-methyl-D-aspartic acid receptors.'. *The Journal of biological chemistry* **288**(42), 30544–57.

Yan, X., R. Yadav, M. Gao, and H.-R. Weng: 2014, 'Interleukin-1 beta enhances endocytosis of glial glutamate transporters in the spinal dorsal horn through activating protein kinase C.'. *Glia* **62**(7), 1093–109.

Yang, B., J. Treweek, R. Kulkarni, B. Deverman, C.-K. Chen, E. Lubeck, S. Shah, L. Cai, and V. Gradinaru: 2014, 'Single-Cell Phenotyping within Transparent Intact Tissue through Whole-Body Clearing'. *Cell* **158**(4), 945–958.

Yasaka, T., D. I. Hughes, E. Polgár, G. G. Nagy, M. Watanabe, J. S. Riddell, and A. J. Todd: 2009, 'Evidence against AMPA receptor-lacking glutamatergic synapses in the superficial dorsal horn of the rat spinal cord.'. *The Journal of neuroscience : the official journal of the Society for Neuroscience* **29**(42), 13401–9.

Yasaka, T., G. Kato, H. Furue, M. H. Rashid, M. Sonohata, A. Tamae, Y. Murata, S. Masuko, and M. Yoshimura: 2007, 'Cell-type-specific excitatory and inhibitory circuits involving primary afferents in the substantia gelatinosa of the rat spinal dorsal horn in vitro.'. *The Journal of physiology* **581**(Pt 2), 603–18.

Yasaka, T., S. Y. Tiong, E. Polgár, M. Watanabe, E. Kumamoto, J. S. Riddell, and A. J. Todd: 2014, 'A putative relay circuit providing low-threshold mechanoreceptive input to lamina I projection neurons via vertical cells in lamina II of the rat dorsal horn.'. *Molecular pain* **10**, 3.

Yasaka, T., S. Y. X. Tiong, D. I. Hughes, J. S. Riddell, and A. J. Todd: 2010, 'Populations of inhibitory and excitatory interneurons in lamina II of the adult rat spinal dorsal horn revealed by a combined electrophysiological and anatomical approach.'. *Pain* **151**(2), 475–88.

Yoshimura, M. and T. M. Jessell: 1989, 'Primary afferent-evoked synaptic responses and slow potential generation in rat substantia gelatinosa neurons in vitro.'. *Journal of neurophysiology* **62**(1), 96–108.

Zanjani, T. M., M. Sabetkasaei, N. Mosaffa, H. Manaheji, F. Labibi, and B. Farokhi: 2006, 'Suppression of interleukin-6 by minocycline in a rat model of neuropathic pain.'. *European journal of pharmacology* **538**(1-3), 66–72.

Zhang, X., Z. Wu, Y. Hayashi, R. Okada, and H. Nakanishi: 2014a, 'Peripheral role of cathepsin S in Th1 cell-dependent transition of nerve injury-induced acute pain to a chronic pain state.'. *The Journal of neuroscience : the official journal of the Society for Neuroscience* **34**(8), 3013–22.

Zhang, Y., K. Chen, S. A. Sloan, M. L. Bennett, A. R. Scholze, S. O'Keeffe, H. P. Phatnani, P. Guarnieri, C. Caneda, N. Ruderisch, S. Deng, S. A. Liddelow, C. Zhang, R.

Daneman, T. Maniatis, B. A. Barres, and J. Q. Wu: 2014b, 'An RNA-Sequencing Transcriptome and Splicing Database of Glia, Neurons, and Vascular Cells of the Cerebral Cortex.'. *The Journal of neuroscience : the official journal of the Society for Neuroscience* **34**(36), 11929–47.

Zhong, Y., L.-J. Zhou, W.-J. Ren, W.-J. Xin, Y.-Y. Li, T. Zhang, and X.-G. Liu: 2010, 'The direction of synaptic plasticity mediated by C-fibers in spinal dorsal horn is decided by Src-family kinases in microglia: the role of tumor necrosis factor-alpha.'. *Brain, behavior, and immunity* **24**(6), 874–80.

Zhou, L.-J., T. Yang, X. Wei, Y. Liu, W.-J. Xin, Y. Chen, R.-P. Pang, Y. Zang, Y.-Y. Li, and X.-G. Liu: 2011, 'Brain-derived neurotrophic factor contributes to spinal long-term potentiation and mechanical hypersensitivity by activation of spinal microglia in rat.'. *Brain, behavior, and immunity* **25**(2), 322–34.

Zhuang, Z.-Y., Y. Kawasaki, P.-H. Tan, Y.-R. Wen, J. Huang, and R.-R. Ji: 2007, 'Role of the CX3CR1/p38 MAPK pathway in spinal microglia for the development of neuropathic pain following nerve injury-induced cleavage of fractalkine.'. *Brain, behavior, and immunity* **21**(5), 642–51.

Zhuang, Z.-Y., Y.-R. Wen, D.-R. Zhang, T. Borsello, C. Bonny, G. R. Strichartz, I. Decosterd, and R.-R. Ji: 2006, 'A peptide c-Jun N-terminal kinase (JNK) inhibitor blocks mechanical allodynia after spinal nerve ligation: respective roles of JNK activation in primary sensory neurons and spinal astrocytes for neuropathic pain development and maintenance.'. *The Journal of neuroscience : the official journal of the Society for Neuroscience* **26**(13), 3551–60.

Ziv, N. E. and C. C. Garner: 2004, 'Cellular and molecular mechanisms of presynaptic assembly.'. *Nature reviews. Neuroscience* **5**(5), 385–99.

Zrouri, H., C. Le Goascogne, W. W. Li, M. Pierre, and F. Courtin: 2004, 'The role of MAP kinases in rapid gene induction after lesioning of the rat sciatic nerve.'. *The European journal of neuroscience* **20**(7), 1811–8.

Zylka, M. J., F. L. Rice, and D. J. Anderson: 2005, 'Topographically distinct epidermal nociceptive circuits revealed by axonal tracers targeted to Mrgprd.'. *Neuron* **45**(1), 17–25.

Zylka, M. J., N. A. Sowa, B. Taylor-Blake, M. A. Twomey, A. Herrala, V. Voikar, and P. Vihko: 2008, 'Prostatic acid phosphatase is an ectonucleotidase and suppresses pain by generating adenosine.'. *Neuron* **60**(1), 111–22.